Engineering Geological Evaluation of Bowa Dayole Dam Site and its Reservoir Area, North Shewa Zone, Oromia, Ethiopia

Ashu Fekadu Terefe

A Thesis Submitted to the Department of Applied Geology

School of Applied Natural Science

Presented in Partial Fulfillment of the Requirement for the Degree of Master of Science in Applied Geology

Office of Graduate Studies

Adama Science and Technology University

July, 2023

Adama, Ethiopia

Engineering Geological Evaluation of Bowa Dayole Dam Site and its Reservoir Area, North Shewa Zone, Oromia, Ethiopia

Ashu Fekadu Terefe

Major Advisor:

Endalu Tadele (Ph.D.)

Co-Advisor:

Yadeta Chemdesa (Ph.D.)

A Thesis Submitted to the Department of

Applied Geology

School of Applied Natural Science

Presented in Partial Fulfillment of the Requirement for the Degree of Master of Science in Applied Geology

Office of Graduate Studies

Adama Science and Technology University

July, 2023

Adama, Ethiopia

Declaration

I hereby declare that this Master Thesis entitled "Engineering Geological Evaluation of Bowa Dayole Dam Site and its Reservoir Area, North Shewa Zone, Oromia, Ethiopia" is my original work. That is, it has not been submitted for the award of any academic degree, diploma, or certificate in any other university. All sources of materials used for this thesis have been duly acknowledged through the citation.

Name of the Student:	Signature	Date

Recommendation

We, the advisors of this thesis, hereby certify that we have read the revised version of the thesis entitled **"Engineering Geological Evaluation of Bowa Dayole Dam Site and its Reservoir Area, North Shewa Zone, Oromia, Ethiopia"** prepared under our guidance by Ashu Fekadu Terefe submitted in partial fulfillment of the requirements for the degree of Master of Science in Applied Geology. Therefore, we recommend the submission of revised version of the thesis to the department following the applicable procedures.

Major Advisor:	Signature	Date
Co-advisor:	Signature	Date

Approval Page

We, the advisors of the thesis entitled **"Engineering Geological Evaluation of Bowa Dayole Dam Site and its Reservoir Area, North Shewa Zone, Oromia, Ethiopia"** and developed by Ashu Fekadu Terefe, hereby certify that the recommendation and suggestions made by the board of examiners are appropriately incorporated into the final version of the thesis.

Major Advisor:	Signature	Date
Co-advisor:	Signature	Date

We, the undersigned, members of the Board of Examiners of the thesis by Ashu Fekadu Terefe have read and evaluated his thesis entitled **"Engineering Geological Evaluation of Bowa Dayole Dam Site and its Reservoir Area, North Shewa Zone, Oromia, Ethiopia"** and examined the candidate during open defense. This is, therefore, to certify that the thesis has been accepted in partial fulfillment of the requirement of the Degree of Master of Science applied Geology.

Chairperson:	Signature	Date
Internal Examiner:	Signature	Date
External Examiner:	Signature	Date

Finally, approval and acceptance of the thesis is contingent upon submission of its final copy to the Office of Postgraduate Studies (OPGS) through the Department Graduate Council (DGC) and School Graduate Committee (SGC).

Department Head:	Signature	Date
School Dean:	Signature	Date
Office of Postgraduate Studies, Dean:	Signature	Date

ACKNOWLEDGEMENT

First and foremost, praises and honor be to the Almighty God who has been my guide, my comforter, and my fortress throughout my life and academic journey. My deepest gratitude goes to my loving Family, whose unwavering love, prayers, and sacrifices have sustained and uplifted me throughout my life and academic pursuit.

With a humble spirit, I would like to express my sincere gratitude to my thesis advisors, Dr. Endalu Tadele and Dr. Yadeta Chemdesa, for their unceasing guidance, encouragement, and support. Their wisdom, patience, and commitment to my success have been indispensable and have inspired me to strive for excellence both in this research endeavor. I extend my heartfelt appreciation to Adama Science and Technology University and especially our Department Chairperson, Mr. Tola Garo, who generously offered his time, expertise, and valuable suggestions to improve the quality of this thesis. His intellectual contributions have immeasurably enriched this work and my academic development. I would like also to express my deepest thanks to all others who have contributed to the successful completion of this study, including Dr. Shankar Karuppannan, Mr. Tesfaye Fita, and Mr. Chali Kejela.

TABLE OF CONTENTS

Contents **Pages**

LIST OF FIGURES

Figures **Pages**

LIST OF TABLES

Tables **Pages**

LIST OF ACRONYMS AND ABBREVIATIONS

ASTU	Adama Science and Technology University
ASTM	American Society of Testing and Materials
DEM	Digital Elevation Model
EBCS	Ethiopian Building Code Standard
ECDSWC	Ethiopian Construction Design & Supervision Works Corporation.
ECO	Engineering Corporation of Oromia
FAO	Food and Agriculture Organizations
FOS	Factor of Safety
GDP	Gross Domestic Product
GIS	Geographical Information System
GSI	Geological Strength Index
GPS	Global Positioning System
ISRM	International Society of Rock Mechanics
JCS	Joint Compressive Strength
JRC	Joint Roughness Coefficient
LEM	Limit Equilibrium Method
LL	Liquid limit
MER	Main Ethiopian Rift
MMS	Moment Magnitude Scale
MoWR	Ministry of Water Resources
PI	Plasticity Index
PL	Plastic Limit
RMC	Rock Mass Classification
RMR	Rock Mass Rating
RQD	Rock Quality Designation
UCS	Uniaxial Compressive Strength
USBR	United States Bureau of Reclamation
UTM	Universal Transverse Mercator

ABSTRACT

Food security is a crucial challenge for developing countries like Ethiopia, where weather variations and droughts threaten food and water supply. The Bowa Dayole dam site is a masonry gravity dam which is mainly planned to irrigate the farmland downstream. In spite of this, the dam site is subjected to engineering geological issues due to the presence of highly fractured and weathered aphanitic basaltic rock and weak unwelded to welded tuff rock mass at the dam foundation. To address these issues, engineering geological evaluation of the dam site and its reservoir area was conducted on the rocks and soils of the site. In order to achieve these aims, the geological mapping, discontinuity surveying, in-situ strength test analysis, core drilling, in-situ permeability test and sampling and laboratory analysis of the samples were carried out. From geological mapping, the main lithological unit of the study area were colluvial and alluvial soil deposits, aphanitic basaltic rock, and tuff unit with various degree of fracturing and weathering. The unconfined compressive strength of these rocks' ranges from 0.16MPa to 146.88MPa and 22.13MPa to 194MPa as determined from the point load index test and Schmidt hammer rebound values which indicated very low to high strength. The Rock Quality Designation of subsurface indicated poor to excellent rock mass quality. The packer test results revealed that the hydraulic conductivity with representative Lu values of less than 1 indicated that excessive leakage at the dam foundation and abutments would not be expected. The soils found at the reservoir area were mostly covered by clayey silt soils with plasticity index values ranging from 13.84% to 26.1% with medium to high plasticity of soil and hydraulic conductivity values ranging from 1.055×10^{-3} *cm/sec to* 9.0343×10^{-6} *cm/sec indicated semi-permeable to impermeable of soil mass. The allowable bearing capacity of aphanitic basaltic rock at the dam abutment and dam foundation ranges from 0.1MPa to 22.19MPa and 0.54MPa to 6.77MPa respectively. The allowable bearing capacity of tuff rock at the dam foundation ranges from 0.037MPa to 0.11MPa. Due to the lower bearing capacity of tuff rock unit under the dam foundation, the total settlement along the dam foundation was expected but this issue can be compensated by the even load distribution by the aphanitic basaltic rock and proper foundation design. The slope stability analysis revealed that the slope sections were unstable during the fully saturated static and dynamic condition. This research recommends further detailed study of soils at the reservoir area, proper load distribution, and dam foundation design, additional evaluation of design and implementation of remedial measures such as rock bolts and shotcrete.*

Keywords*:* *Bowa Dayole Dam site, Lugeon value, Allowable bearing capacity, slope stability analysis.*

CHAPTER ONE

1. INTRODUCTION

1.1. Background of the Study

Dams are essential infrastructure for human civilization, providing a range of benefits such as flood control, irrigation, sediment control, domestic and industrial water supply, groundwater recharge, water diversion, fish farming, and recreational facilities (Umoren et al., 2016; Sissakian et al., 2020). According to the Research (USBR, 1976), Individual dams vary in kind and design based on various variables, including the amount of water available, the topography, the geology, and the type and availability of local building materials. They vary in size and structural complexity and are tailored to the river's topography, stability, and hydrological regime. According to (USBR, 1977), the major types of dams are gravity dams, arch dams, embankment dams, and buttress dams. From these categories of dams, a gravity dam is a massive structure that holds backwater in a reservoir by its sheer weight. The stability of gravity dams is derived from their weight and geometry, which resists the hydrostatic forces exerted by the impounded water (USBR, 1977). Different types of gravity dams are based on the construction materials used in their construction, encompassing Masonry, Concrete, and RCC (Roller Compacted Concrete) gravity dams. A masonry gravity dam is constructed using individually cut and shaped stones or bricks placed in a cementitious mortar to create the dam structure. Masonry gravity dams offer durability, longevity, and lesser cement usage but are labor-intensive. These dams have existed for centuries, and some ancient masonry dams still stand today (Lane, 1935).

Dam construction is vital for development in Ethiopia due to its significant water resources, serving various purposes such as electricity generation, flood mitigation, and irrigation (McCartney and Girma, 2012; Sissakian et al., 2020). This is especially important for agriculture, which dominates the nation's economy and needs water access for dry and semi-arid regions. Food security is a crucial challenge for developing countries like Ethiopia, where weather variations and droughts threaten food and water supply (De Hamer et al., 2008). Although the agricultural sector employs 80% of the workforce and contributes 47% of the GDP (World Bank, 2008), over 80% of the population depends on rain-fed agriculture with uneven rainfall distribution. Despite having 12 major drainage basins and 3.7 million ha of irrigable land (MoWR, 2001; WSDP 2002), only 4.3% of this land is utilized for irrigation (FAO, 2002), demonstrating that the country's irrigation production is far from satisfactory, and highlighting the need for improved irrigation and dam construction.

Many dams in Ethiopia have faced issues due to geological and geotechnical factors. Micro dams, built since the 1970s to combat drought and improve food security, have also experienced failures and operational problems (Tiruneh, 2005; Berhane et al., 2017). Studies show they have not performed as expected due to seepage or water leakage, slope instability, and other challenges (Berhane et al., 2013). Building dams on unsuitable terrains, like the sedimentary terrain of the Mekelle Outlier, has resulted in leakage, sedimentation, and hydrological issues. Engineering geological investigations are crucial to ensure dams function safely and effectively. Similar to other terrains, dams constructed on volcanic terrains face significant geological and engineering geological challenges, including seepage, bearing capacity, and slope stability issues. Igneous rocks have primary and secondary porosity, joints, fractures, and fault lines that increase the risk of seepage, leading to water loss from the reservoir, slope instability, and deformation.

Furthermore, volcanic basalt is highly weathered, affecting the rock's bearing capacity (Cabria, 2015; Chala and Rao, 2021). Weathering weakens the mechanical properties of the rocks, potentially causing failures or significant settlements in numerous rock-engineering structures (Gupta and Seshagiri, 2000). These challenges infer that constructing a dam requires thorough engineering geological investigations in the country for its operational longevity and overall safety of dams.

To ensure that the dam will last its intended lifespan, the main goal of the engineering geological investigation for the dam project is to give accurate data and information. In order to guarantee that the dam will last its intended lifespan, the main goal of this study is that the engineering geological evaluation is to provide comprehensive knowledge and information about the dams by the characterization and classification of soils, geomechanical characterization of rocks, determining the bearing capacity of foundation rocks, deformability of rock masses, permeability of foundation rocks or seepage analysis, slope stability analysis for both abutments and also determining whether the reservoir is watertight or not. These can be accomplished by a site-specific geological and engineering geological investigation involving outcrop (geological) mapping, geophysical testing, geotechnical drilling, joint (discontinuity) survey, in situ testing, rock and soil sampling, and sample testing in a laboratory.

The Bowa Dayole Gravity Dam site is one of the rainwater-harvesting hydraulic structures that the Ethiopian government planned to recently build on some of these drainage basins to promote irrigation and increase food security. As a result, this research aimed to address engineering geological issues by conducting a thorough analysis and providing remedial strategies for the dam site to ensure the long-term safety and sustainability of the dam.

1.2. Statement of Problem

Inadequate engineering geological investigation causes most of dam failures and geological evaluation before dam construction is initiated. The geological setting of dam sites and related geotechnical issues vary from location to location, where any dam site could have unfavorable geological conditions. An in-depth understanding of the geological conditions and their impact on the anticipated dam must be understood by adequate engineering geological assessment, and necessary corrective measures must be provided.

The Bowa Dayole dam project is a masonry gravity dam, mainly anticipated to irrigate the farmland downstream. The dam project's safe and operational longevity determines the project's success in meeting the irrigational need of the present study area. One of the most essential components of a dam safety study is a proper assessment of the site's geological and geotechnical state. The dam site abutments, foundation, and reservoir must all have been sufficiently inspected, explored, and studied to thoroughly understand the engineering geological state of the area; where for the dam site to sustain the loads exerted on the dam, it must be stable and watertight. This is necessary to evaluate the safety of the new dam, among other things.

According to ECDSWC (2022), the foundation of the dam site is highly challenging due to the presence of thick weak rock mass formation, which is slightly welded to welded tuff in the foundation area, which could cause water loss from the dam foundation and failure of the foundation. Geotechnical drilling along the left and right abutments of the dam also revealed that the rock mass is slightly weathered and highly fractured aphanitic basaltic rock masses with increasing weakening toward the river center, which could cause the failure of the abutments.

Furthermore, the dam site is located on the western margin of the main Ethiopian rift. This could increase the vulnerability of the dam site to earthquake seismicity.

Therefore, this study intends to perform an engineering geological evaluation regarding the watertightness analysis, rock mass bearing capacity, and the foundation's stability, abutments, and overall water tightness of the dam reservoirs to avoid possible failures.

1.3. Research Question

This study is expected to answer the following research questions:

- What is the lithological exposure, geological structures, and influences of geology and geological structures of the dam site on the overall stability of the dam and its reservoir?
- What engineering geological issues are anticipated depending on the data obtained from the investigation?
- Is the planned reservoir area watertight?
- Based on site-specific physical parameters, what is the most efficient corrective action for those engineering geological challenges for the slope instability of abutments and seepage problems in the foundation and reservoir areas?

1.4. Objectives of the Study

1.4.1. The General Objectives of the Study

The main objective of this study is to carry out the geological and engineering geological evaluation of geological material conditions at the Bowa Dayole masonry gravity dam and reservoir sites.

1.4.2. The Specific objectives of the study

The specific objectives of this study are:

- To study the dam site's geological setting and produce a geological map with a detailed scale of 1:10,000.
- To study the index and engineering properties of rocks and soil of the dam site and reservoir area.
- To evaluate the watertightness and the bearing capacity of rock masses at the dam site.

- To carry out the abutment slope stability analysis.
- To provide possible effective countermeasures for engineering geological problems of the dam.

1.5. Significance of the Study

The dam is an engineering structure requiring detailed engineering geological investigation on the dam construction site. The goal of this study is to provide a detailed engineering geological characterization of geological materials of the dam site where this dam is anticipated to be built in order to address issues with seepage/leakage problems foundation and reservoir area and slope stability from the dam's abutment.

The outcome of this study will provide some mechanisms for ensuring a long-term impoundment of water in the dam's reservoir based on data collected from the investigation of slope stability and seepage conditions of the dam foundation and reservoir. This study will evaluate the condition of the foundation in order to indicate the suitability of the rocks and provides some early data on the need for grouting. This is expected by forwarding and examining geological questions that must be resolved before the dam's construction.

This study offers reasonable recommendations to ensure the proposed dam achieves its fundamental goals. Additionally, the findings from this study will Also, the findings of this study will serve as a guide for engineering projects and academics interested in working on related research projects of a similar nature that will be built on the same terrain.

CHAPTER TWO

2. LITERATURE REVIEW

2.1. Gravity Dam Failure Modes

Failures in gravity dams can be classified into three primary types: sliding failures, overturning failures, and structural failures.

A sliding failure transpires when the dam moves across its base, or when a part of the dam glides over another segment of the dam (Ellingwood and Tekie, 2001). This occurs when the frictional resistance generated between the dam's body and its foundation exceeds the net horizontal forces applied to the gravity dam. The resistance may arise from friction only, or a mixture of friction and shear strength, depending on the dam's construction. The resistance to motion is usually calculated by dividing the horizontal forces acting on the dam by the resistance to motion. Although its value may vary depending on the loading conditions, it typically ranges between 1.3 and 1.5 (ASDSO, 2022).

A gravity dam may be toppled or turned due to horizontal and vertical forces, including those exerted by water pressure, waves, silt, ice, and uplift (Martt et al., 2005; Baylosis and Bennett, 1989; Su et al., 2013). The sufficient weight of the structure stops it from rotating. A dam is at risk of rotating and flipping over if the entire force exerted on it acts through or beyond its downstream toe. While a structure has the potential to rotate around its toe, it is more likely to fail if the forces causing overturning raise the stress levels at the dam's toe to an unsafe extent (ASDSO, 2022).

Structural failure in a dam takes place when the tension or compression forces acting on it surpass the strength of the materials that make up the dam (Hariri and Saouma, 2014). Concrete and masonry have low tensile strength, thus the design of concrete and masonry gravity dams aims to reduce tension within the structure (Zhang et al., 2014; Asthana and Khare, 2022). During construction, steel bars, also known as rebar, are embedded within the concrete to withstand expected tensile forces. Over time, the rebar may corrode or deteriorate, leading to the development of tensile forces in areas where the rebar is absent or weakened (ASDSO, 2022).

2.2. Engineering Geological Evaluation of Dam Sites and Reservoir Areas

Dam is a hydraulic structure that creates a water reservoir for irrigation or household use, flood mitigation, and electric power generation. It requires a meticulous geotechnical investigation and analysis of the dam site to ensure the structure's longevity, stability, and safety (Wahlstrom, 2012; Fell, 2005). Engineering geological investigations incorporate collecting and interpreting geological data through surface feature investigations, subsurface explorations, rock discontinuities, and identifying geological issues, all required to design, construct, and maintain dam sites and reservoir areas. The purpose of these inquiries is to determine the appropriateness of a site for constructing the dam and retaining water in the reservoir area, taking into account the geological, geotechnical, engineering geological, and hydrogeological factors. It involves collecting and interpreting geological data by assessing surface features, subsurface explorations, rock discontinuities, and identifying geological hazards (Fell, 2005; USBR, 1977; Lancellotta, 2008; Ljubomir, 2014).

A thorough engineering geological investigation helps ensure a dam project's safety, sustainability, and economic feasibility. It provides crucial information on the bedrock of the foundation, geological structure, slopes, and geological material properties in terms of the physical and mechanical properties of geological materials required for designing the foundation, the dam body, and the reservoir area (USBR, 1977; Bowles et al., 2007; Wahlstrom, 2012).

Numerous studies have stated that in order to attain a better understanding of the geology of the dam's foundation, reservoir area, and abutments, engineering geological investigations should utilize integrated surface geological surveying, core drilling, discontinuity surveying, test pit excavations, in-situ and laboratory testing, and geophysical methods (Özsan and Akın, 2002; Haile and Atsbaha, 2014; Abay and Meisina, 2015; Garo and Meten, 2021; Asfaw et al., 2022).

2.2.1. Watertightness Assessment of Dams

Dam site engineering geological evaluation is vital in dam design and construction. The water tightness of dam foundations, abutments, and reservoir areas, which might jeopardize their functioning and structural integrity, is one of the most critical aspects of this investigation. The geological parameters of the dam site are analyzed to guarantee that the foundation is impermeable and can prevent water from seeping and leaking through the dam foundation, abutments, and reservoir areas (Zaruba and Mencl, 1976; Qureshi et al., 2013; Qi and Dashui, 2019; Garo and Meten, 2021).

According to Fell et al.(2014), one of the primary goals of engineering geological investigation for seepage issues in the dam is to identify any potential geological hazards and the analysis of soil and rock properties that could affect the permeability of the foundation. These hazards can include faults, fractures, the presence of weak geological formations, and other geological features that could lead to seepage or other forms of water infiltration (Asfaw et al., 2022). To identify these hazards, engineers must carefully analyze the geological characteristics of the site and use appropriate techniques to map and characterize the subsurface geology. The process of geological material analysis at the dam site and reservoir area includes geotechnical drilling combined with in-situ tests, sampling of soils and rocks, and laboratory testing. These methods are used to ascertain the index and engineering properties of the materials involved. Understanding the engineering geological conditions is crucial for safe dam design considering each dam site is unique (Uromeihy and Barzegari, 2007; Barzegari, 2017).

According to the research work by Asfaw (2020), Dam reservoir might fail because of excessive leakage or water seepage triggered by swift sedimentation and slope instability. Water loss, known as leakage, is linked to primary geological defects like solution channels, geological structures like fractures, joints, fault zones, or buried channels, which enable significant localized flow of water. These water losses subsequently generate streams downstream. In contrast, seepage is a smaller-scale flow that occurs over a larger area, with seepage failure occurring due to saturation of the foundation materials or a weakening of the rock towards a sliding failure (Alonso et al., 2010; García et al., 2012). While investigating the seepage and leakage issues from the reservoir, two distinctive elements must be considered: the basin's water tightness and reservoir bank stability. As a result, once the groundwater conditions and geological characteristics have been examined, an assessment of water tightness may be done, and any necessary groundwater control measures can be designed. A certain amount of leakage or seepage is acceptable if it does not jeopardize the dam's safety or appurtenant hydraulic structures (Fell et al., 2014; Asfaw, 2020).

One of the most critical aspects of seepage analysis is the utilization of engineering geological investigation to ensure the water-tightness of the dam, which involves analyzing the geological characteristics of the site to ensure that the dam foundation and its surrounding is impermeable and can prevent water from seeping through the dam body and foundation. Implementing a seepage control system is a popular way of improving the water-tightness of the dam site. This might entail installing a grout curtain, which is a series of closely spaced drill holes filled with cement or another low-permeability material to provide a barrier against seepage along the foundation, similar to a slurry trench or concrete cut-off (Malkawi and Al-Sheriadeh, 2000; Uromeihy and Barzegari, 2007; Gurocak and Alemdag, 2012; Azimian and Ajalloeian, 2014; Fell et al., 2014; Hailu, 2020; Asfaw et al., 2022).

The permeability of the dam foundation and its surrounding is determined from the permeability investigation of in-situ permeability test of geological materials that make up the dam environment with respect to depth by the Packer test, the estimation of permeability of rock mass from discontinuity characteristics during the field investigation, and evaluation of permeability test of soil masses in the laboratory. According to the study by Vaskou et al.(2019), we can conclude that the relative change in permeability values in Lu which is a valuable tool for hydro stratigraphical characterization of lithological units with depth. The Lugeon test assesses the water absorption capacity of a rock mass and estimates the equivalent isotropic coefficient of permeability/hydraulic conductivity around a specific test borehole. This information helps determine the required amount of grouting for dam foundations, abutments, or underground rock excavations by measuring the variable hydraulic behavior of the rock mass based on depth and location. Additionally, the test can identify the most suitable grouting materials and injection pressures for pre-grouting applications.

2.2.2. Stability Analysis of Slopes

Slope instabilities are complex problems that primarily influence civil engineering structures including highways, tunnels, dams, open pit mines, and the ground itself. Rotational, translational, and wedge modes of failure can occur, each of which has a particular effect on the environment, human life, and the flow of traffic (Hoek and Bray, 1981; Pantelidis, 2009; Cheng and Lau, 2014). The fragile character of the soil and rock slope is disturbed by slope instability issues caused by humans and nature (Abramson et al., 2001). Owing to the excavation of hills and roadsides, most of the northern, southern, and western parts of the Ethiopian plateau have experienced slope instability historically, due to the surface materials and the underlying bedrock (Ayalew, 1999). According to Hoek and Bray (1981), slope instability governs the connection between shear stress and shear strength forces. A range of methodologies and procedures can be employed to perform the analysis of slope stability. These methods encompass kinematic analysis, limit equilibrium, numerical modeling, and empirical approaches (Gurocak et al., 2008; Abramson et al., 2001; Cheng and Lau, 2014). In this section, kinematic analysis and limit equilibrium method are discussed below.

2.2.2.1. Kinematic Analysis Method

The existence of unfavorably positioned discontinuities along the abutment, road, hill, and pit slope may lead to the potential for rock slope failures (plane, wedge, and toppling failures). These failures can happen on both current and proposed rock slopes (Hoek and Bray, 1981; Hocking, 1976; Yoon et al., 2002; Wyllie and Mah, 2004; Raghuvanshi, 2019). Without referencing the forces that drive them, cohesiveness, or unit weight, kinematic analysis method portrays how bodies move (Hoek and Bray, 1981; ZainAlabideen and Helal, 2016). According to Norrish and Wyllie (1996) In kinematic analysis, the interpretation of the analysis of slope stability using stereographic projections in 2D utilizes the orientation of the joints and slope face. In order to identify potential failure scenarios and methods, angular relationships between discontinuities and the slope surfaces are used (Alade and Abdulazeez, 2014). The kinematic analysis of rock slope stability analysis method includes the collection of two input parameters (friction angle and slope and joint orientation), the data analysis using the manual method of the stereo net, or the utilization of dips software with input parameters such as angle of friction, dip amount, and dip direction of both discontinuities and slope faces. Manual interpretation and analysis of the kinematic approach utilizing stereo net could be tedious, according to (Richards, 1992; Maurenbrecher and Hack, 2007), when large orientations are used. Using the Dips software makes the kinematic analysis easier and simple.

2.2.2.2. Limit Equilibrium Methods (LEM)

This approach assesses the various forces responsible for driving the rock mass and opposing forces on separate failure surfaces. The factor of safety (FOS) is determined by the proportion of resisting forces to driving forces when equilibrium is achieved (Abramson et al., 2001).

According to (Karaman et al. (2013), slope failure via convoluted and complex modes of failure causes inconsistency in the results from this method. These systems take into account the shear strength along a failure surface, the pressure of pore water, and the effects of external forces such as reinforcing mechanisms or seismic accelerations. The factor of safety is directly proportional to the shear strength of the possible failure plane, which is established by the cohesion (c) and friction angle (ϕ) (Raghuvanshi, 2017).

After identifying the type of rock slope failure through kinematic analysis, the safety factor is calculated by considering both the force causing the rock mass to fail along the failure surface and the force preventing the rock mass from failing (Aprilia and Indrawan, 2015). In the stability assessment of soil slopes, there isn't a predetermined failure surface like in rock slope failures, and the soil typically exhibits a circular-shaped failure (Norrish and Wyllie, 1996; Wyllie and Mah, 2004).

The factor of safety for planar failure mode can be determined by breaking down the forces acting on the failure surface into perpendicular and parallel components, as explained by Hoek and Bray (1981) and Wyllie and Norrish (1996). The general formula for calculating the safety factor for this mode of failure, based on the ratio of resisting, and driving components of the forces mentioned above, was provided by Hoek and Bray (1981). The conditions for determining the safety factor usually depend on the saturation and seismic conditions, as well as the geometric configuration of the slope, such as the existence or nonexistence of a tension crack and its position within the slope (Hoek and Bray, 1981; Wyllie and Norrish, 1996). As a result, the stability analysis for this mode of failure can be carried out under conditions where seismic acceleration is either present or absent, and where a tension crack is either present or absent within the slope, considering whether this tension crack is dry or water-saturated.

The stability analysis of the wedge mode of failure necessitates determining the geometry and orientation of various wedge elements, such as two discontinuities, the slope face, the upper slope face, and, if present, the plane representing the tension crack (Wyllie and Norrish, 1996). To assess the stability of the wedge, the factor of safety can be calculated by examining the forces acting perpendicular to the discontinuities and parallel to the intersection line. Similar to the planar mode of rock slope stability analysis, a comprehensive general formula for calculating the wedge stability safety factor was provided by Hoek and Bray (1981), which includes forces like the weight of the wedge, external forces such as foundation loads, seismic acceleration, tension reinforcement elements, water pressure-induced forces acting on surfaces, and shear strength developed along the failure plane.

The stability of a slope can be determined by calculating the ratio of shear strength to shear stress, considering the safety factor for a circular failure mode in soil. According to (Abramson et al., 2001 ;Shukla and Hossain, 2011), The stability of a slope is ascertained by the factor of safety. A stable slope has a factor of safety value greater than one, while an unstable slope has a value less than one. If the factor of safety is exactly one, it indicates that the slope is in a critical state of equilibrium. According to Abramson et al. (2001) and Krahn (2004), Limit equilibrium methods involve dividing the soil mass into several segments and calculating the normal and shear forces between the segments, as well as their balance. The Slice limit equilibrium methods such as Swedish Circle, The ordinary method (Fellenius, 1927), Bishop's modified method (Bishop, 1955), Janbu's generalized method of a slice (1968) as cited in (Manna et al., 2014), Spencer's method (Spencer, 1967), and Morgenstern and Price's method (Morgenstern and Price, 1965) are utilized to assess the factor of safety concerning circular failure modes.

2.2.3. Rock Mass Characterization and Classifications

In the society of rock mechanics, the expressions "classify" and "characterize" are employed to "describe" the distinctive characteristics of the rock mass. In the real world, there is little practical significance to the divergence between categorizing and describing the rock mass procedures. The following description is based on Palmström (1995) and Stille and Palmström, (2003). Rock mass characterization entails characterizing the rock while concentrating on its color, type (origin formation), texture, and other properties. Different rock mass characteristics are categorized by grouping them into specific groups using a preset system. The descriptive terms serve as the main distinguishing boundary between characterization and categorization.

Rock engineering classification systems are essential for the characterization and design of engineering structures, according to Bieniawski (1989). Additionally, these techniques for classifying rock masses may be used to determine a rock mass's composition and characteristics, which aid in determining an initial estimate of the rock mass's support needs and strength and deformation characteristics (Hoek et al., 1998). A "rock mass classification" refers to a system that classifies and organizes rock masses into different categories based on established relationships. This classification not only offers insights into strength, and deformation characteristics of the rock mass, but also highlights the vital factors that significantly influence its behavior (Bieniawski, 1989). Rock mass classification methods are employed as an experimental approach to evaluate rock mass quality or rock slope stability, according to researchers like (Bieniawski, 1973; Haines et al., 1991; Jordá-Bordehore, 2017).

According to Liu and Chen (2007, the primary goal of rock mass classification is to provide scientists and engineers with the quantitative knowledge as well as guidelines that can be used to define geological formations and assess the stability of rock-cut slopes using geological structural data. Kirkaldie (1988) states that the classification of a rock mass depends on the individual rock mass and joint parameters, including strength of the rock mass, rock quality designation, joint orientation, roughness and spacing, moisture conditions, weathering, and other significant factors.

In 1879, Ritter began developing a system for classifying rock masses to create an empirical method for determining support needs in tunnel construction. This system, as mentioned in Jordá-Bordehore's 2017 study, laid the foundation for later rock mass classification systems such as Rock Load Strength (Terzaghi, 1946) as cited in Bieniawski (1989); Rock Quality Designation (Deere, 1967; Deere and Deere, 1989); Rock Structure Rating (RSR) (Wickham et al., 1972); Rock Mass Rating (RMR) (Bieniawski, 1989); Rock Mass Quality (Q) (Barton et al., 1974); Rock Mass Index (RMI) (Palmström, 1996); Geological Strength Index (GSI) (Marinos et al., 2007) were developed.

There are several methods available for categorizing rock masses, but the most frequently utilized techniques are the rock mass rating (RMR) and the rock quality designation (RQD) (Bieniawski, 1979). These classification methods are necessary for recognizing, defining, and differentiating rock mass formation in specific zones where engineering constructions are to be built. Furthermore, rock mass classification systems attempt to assess the properties of the rock mass by considering the factors affecting its properties and quality (Tzamos and Sofianos, 2007).

In conclusion, an adequate RMC system must be implemented for engineering projects to be successful. For projects in areas with massive, well-jointed, and weathered rock formations, precise RMC applications are needed to determine rock mass quality. Rock mass classification makes it easier to choose the best excavation method, reduce possible risks during construction, and predict deformations or instability problems that may occur in the structure's operational life. Classification methods take into factors that are considered to influence stability rock mass. As a result, the parameters are frequently connected to discontinuities such as the number of joint sets, joint persistence/distance, roughness, joint alteration and filling, groundwater conditions, and, in some cases, the strength of the intact rock and the stress magnitude. The classification procedure assists in predicting the stability of the rock mass and determining if it requires any support. A rock mass's stability is often graded in subjective terms as 'poor,' 'fair,' 'good,' 'very good,' and 'excellent'. According to Kirkaldie(1988) Continuous updates may be performed throughout excavation to change the classification, which measures the rock mass strength. The outcome may then be compared to a failure criterion to assess whether the rock mass is stable.

2.2.3.1. Rock Quality Designation (RQD)

In large-scale engineering projects, particularly those involving tunneling, mining, and geotechnical and civil engineering like dams, Rock Quality Designation (RQD) is essential in determining the quality and integrity of rock masses. In the practice of rock engineering, the parameter quantifies the degree of rock mass fracturing. Despite being the primary parameter in use for rock mass engineering today (Hoek and Bray, 1981), the RQD index is affected by a wide range of well-known factors, including fracture frequency, core size, joint orientation, and joint roughness (Azimian, 2016). Two distinctive methods to estimate rock quality designation (RQD) are direct and indirect. The table below illustrates the rock mass quality classification using the RQD values.

Table 2. 1. Engineering classification of rock mass quality according to Deere and Deere (1988).

RQD	90 - 100	75 - 90	50 - 75	25 - 50	< 25
Rock mass quality	Excellent	Good	Fair	Poor	Very poor

The degree of jointing can be described from the Jv values by using the following According to Palmstrom (2005).

Table 2. 2. Engineering classification of degree of jointing according to Palmstrom (2005).

	Degree Of Jointing					
	Very Low	Low	Moderate	High	Very High	Crushed
Jv Values	<1	1-3	3-10	10-30	30-60	>60

2.2.3.1.1. Direct Methods: Rock Quality Designation

The direct method of estimating when core drill samples are available from geotechnical drilling (core logging). Rock quality designation (RQD), a quantitative index to evaluate rock quality, was developed by D. U. Deere and was first released in 1964. The RQD is a core recovery percentage that is in part determined by the number of fractures and degree of rock mass softening seen in the drill cores. The length of the core run is added up, and only the unbroken sections with lengths larger than 100 mm (4 in.) are split by it (Deere and Deere, 1989). The RQD is presented as a percentage, with a greater percentage implying better-grade rock mass.

$$\mathbf{RQD} = \frac{\sum \textbf{Length of core pieces>10cm}}{\textbf{Total core length}} \mathbf{x100} \qquad \textbf{(2.1)}$$

Generally, The RQD index is calculated by measuring the length of intact rock cores (core recovery) in a borehole or tunnel and expressing that length as a percentage of the total length of the borehole or tunnel.

2.2.3.1.2. Indirect Methods: Rock Quality Designation

When no cores are available, we can also estimate RQD from, for instance, joint spacing (Brady et al., 1985 as cited in Hanekom, 2003). The RQD can also be estimated using the volumetric count method proposed by Palmström (1982) utilizing the correlation between RQD and volumetric discontinuity frequency Jv (Palmstrom, 1982):

$$\mathbf{RQD = 115 - 3.3Jv} \qquad \textbf{(2.2)}$$

Where Jv is the total of the number of discontinuities per unit length for all discontinuity sets, which can be generated from the joint set spacings within a volume of rock outcrop (Palmström, 1982):

$$\mathbf{Jv} = \left(\frac{\mathbf{1}}{\mathbf{s1}}\right) + \left(\frac{\mathbf{1}}{\mathbf{s2}}\right) + \left(\frac{\mathbf{1}}{\mathbf{s3}}\right) + \cdots + \left(\frac{\mathbf{1}}{\mathbf{sn}}\right) \qquad \textbf{(2.3)}$$

where s1, s2 and s3 are the mean discontinuity set spacings. Disruptions in the rock mass can be taken into account by assuming a random gap (sr) for each. According to Palmstrom (2005), Sr = 5m can be assumed. So, the volumetric discontinuity frequency lv can be generally expressed as:

$$\mathbf{Jv} = \left(\frac{\mathbf{1}}{\mathbf{s1}}\right) + \left(\frac{\mathbf{1}}{\mathbf{s2}}\right) + \left(\frac{\mathbf{1}}{\mathbf{s3}}\right) + \cdots + \left(\frac{\mathbf{1}}{\mathbf{sn}}\right) + \frac{\mathbf{Nr}}{\mathbf{5}} \qquad \textbf{(2.4)}$$

Where s1, s2 and s3…sn is the average spacing for the joint sets, Nr is the number of random joints in the actual location. For Jv < 4.5, RQD = 100.

2.2.3.2. Rock Mass Rating (RMR)

The Rock Mass Rating (RMR) system is an integral and widely used tool in geological engineering for categorizing rock masses based on mechanical and geological properties (Bieniawski, 1979). The RMR, or geomechanics classification system, was developed at South African Council for Scientific and Industrial Research (CSIR) by Prof. Z.T. Bieniawski in 1976 and later modified in 1989. It changed over time as additional case histories became available and corresponded to international standards and procedures (Bieniawski, 1979). The benefit of this system lies in the fact that it necessitates only a small number of fundamental parameters, which pertain to the geometric and mechanical characteristics of the rock mass.

The original RMR (1976) has eight parameters, including the rock quality designation (RQD). Degree of weathering, uniaxial compressive strength (UCS), joint and bedding spacing, strike and dip direction, joint separation, joint continuity, and groundwater inflow are all factors to consider. Bieniawski introduced the improved approach in 1989, removing the state of weathering because UCS accounts for its influence and combining two factors, separation of joints and continuity of joints, into the condition of joints. Furthermore, after the fundamental characteristics have been evaluated, joints' striking and dip orientations are eliminated, and their impacts are adjusted into the rating.

Discontinuity characteristics, which are used as a parameter of the fundamental rock mass rating (RMR), include spacing between discontinuities and conditions of discontinuities (aperture, persistence, roughness, infilling, and alteration/weathering), which have a direct impact on the characteristics of the rock mass by weakening it (Bieniawski, 1989). Furthermore, the behavior of rock masses can be significantly impacted by groundwater conditions. According to the circumstances, the groundwater rating can be classified as completely dry, moist, wet, dripping, or flowing, with a completely dry rock mass assigned as a higher rating (Bieniawski, 1989).

Finally, RMR (1989) considers the six parameters listed below (Bieniawski, 1989).

1. **Uniaxial Compressive Strength (UCS)** in MPa is an essential parameter for determining the rock's ability to withstand compressive loads.
2. **Spacing of discontinuities**
3. **Groundwater conditions**: The presence of groundwater can cause a reduction in rock mass strength and increase the chances of instability.
4. **Rock Quality Designation (RQD)**
5. **Condition of discontinuities**: The surface characteristics of discontinuities (such as persistence (length), roughness, separation, presence of infilling, and degree of weathering) have an essential effect on the stability of rock masses. Rough and uneven surfaces are less susceptible to failure than smooth and plane discontinuities (Hudson and Priest, 1979).
6. **Orientation of discontinuities**: The orientation of discontinuities to the engineering project's plane can significantly influence the rock mass's stability. For example, discontinuities parallel to a tunnel's axis or a slope's surface and discontinuities dipping towards the dam's downstream side may be more vulnerable to failure.

The first five parameters in the categorization scheme indicate the fundamental (basic) parameters (RMR basic). Because the impact of discontinuity orientations varies depending on the engineering applications, the final parameter joint orientation is considered independently.

The overall rating of the classification system is given as follows:

$$\mathbf{RMR_{basic}} = \sum \boldsymbol{The\ Six\ Parameters}(\boldsymbol{I} + \boldsymbol{II} + \boldsymbol{III} + \boldsymbol{IV} + \boldsymbol{V}) \quad \textbf{(2.5)}$$

RMR = (RMR $_{basic}$) + adjustment for joint orientation

One of the six factors used to determine the Rock Mass Rating involved the uniaxial compressive strength (UCS) of unbroken rock material, which was acquired from laboratory testing or calculated based on the point load index outcome. The RQD, joint spacing, joint condition (length/persistence, separation, roughness, infilling, and weathering), discontinuity orientation, and groundwater conditions were gathered and evaluated during field investigations. All of these data were used to create the RMR system.

Table 2. 3. Rock mass classification based on RMR-value (After Bieniawski, 1989).

Rock Mass Rating	100 - 81	80 – 61	60 - 41	40 - 21	20 - 0
Rock Class	I	II	III	IV	V
Classification	Very good	Good	Fair	Poor	Very poor

Bieniawski (1989) suggested employing multiple classification systems to enable comparison of results and assess their reliability. Additionally, the RMR specifies the range for cohesion and friction angle of a rock mass. For this purpose, (Bieniawski, 1979) suggested the following relationships in order to determine the cohesion (eq. 2.4) and angle of friction (2.5) for specific RMR values as follows.

$$\mathbf{C = 0.05RMR} \quad \textbf{(2.6)}$$

$$\mathbf{\Phi = 0.5RMR + 5} \quad \textbf{(2.7)}$$

Where **Φ** = angle of internal friction (degree) **C** = cohesion (MPa)

In conclusion, rock mass classification systems like RMR and others are essential in assessing rock mass stability in various engineering applications. These systems consider determining several parameters, such as rock mass strength and deformation modulus. These systems are crucial in ensuring the safety of workers and equipment in underground excavations.

2.2.3.3. Geological Strength Index (GSI)

The Geological Strength Index (GSI) is a system of classification used to characterize the mechanical properties of heavily jointed rock masses (Hoek et al., 1998). In recent years, GSI has become an essential tool in various engineering disciplines, including tunneling, mining, and the design of underground structures, highlighting its significance in ensuring the safety, efficiency, and cost-effectiveness of numerous engineering projects (Marinos and Hoek, 2000b). It comprises an essentially important assessment method for estimating the quality of a rock mass in terms of its strength, deformation characteristics, and overall performance (Cai et al., 2004). Wyllie and Mah (2004) suggested that the GSI value could be ascertained by examining the weathering state of the discontinuity surface, the structure of the rock mass, and the interlocking nature of rock blocks in particular rock outcrops. To determine the rock mass strength parameters that describe the rock's properties, one must first estimate the Geological Strength Index and mi, and then utilize the subsequent equation.

$$\boldsymbol{\sigma_1 = \sigma_3 + \sigma_c \left(mb\ \frac{\sigma_3}{\sigma_c} + S \right)^{a}} \tag{2.12}$$

Where mb is the reduced value of the material constant mi and is given by:

$$\boldsymbol{mb = m_i \exp\left(\frac{GSI-100}{28-14D}\right)} \tag{2.13}$$

mi for intact rock is determined from the laboratory triaxial test or the tabulated data proposed by Hoek et al. (2000) for different rock types.

S and a are the constants for the rock mass given by the following expression.

$$\boldsymbol{S = \exp\left(\frac{GSI-100}{9-3D}\right)} \tag{2.14}$$

$$\boldsymbol{a = \frac{1}{2} + \frac{1}{6}\left(e^{\frac{-GSI}{15}} - e^{\frac{-20}{3}}\right)} \tag{2.15}$$

D is a variable that depends on the level of blasting damage and stress relaxation that the rock mass has experienced. It ranges from 0 for in situ rock mass that hasn't been disturbed to 1 for highly disturbed rock mass.

Marinos et al., (2007) created an empirical method for assessing the strength of jointed rock masses and established a failure criterion for these rock masses. This criterion has been revised based on findings from various projects, initially by Hoek and Brown (1988) and subsequently by Hoek et al., (1992). Additionally, the GSI (Geological Strength Index) of rock masses can be approximated through visual inspection of the outcrop. The chart of the basic GSI is presented in the figure below (Marinos and Hoek, 2000).

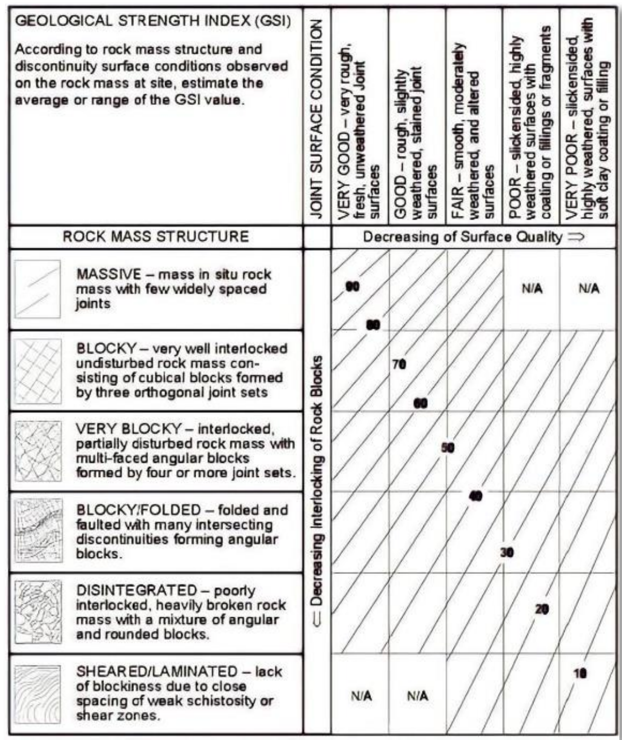

Figure 2.1.The chart of the basic GSI for field estimation (Marinos and Hoek, 2000).

In 1998, Hoek and his other colleagues employed Bieniawiski's RMR (Rock Mass Rating) System to calculate the material constants using this empirical approach. The method proved effective for rock masses with an RMR greater than 25. Nonetheless, it was unsuccessful for those with an RMR of less than 25.

For RMR76 > 18 **GSI = RMR$_{76}$** **(2.16)**

RMR89 >23 **GSI = RMR$_{89}$ – 5** **(2.17)**

Despite its widespread applications, the primary limitation of the GSI system is its qualitative nature, which can result in subjective evaluations (Morelli, 2015; Yang and Elmo, 2022). It relies on visual descriptions and manual interpretations of rock mass features, which might generate varying estimations based on their experience and perception. Consequently, this subjectivity can lead to potential inconsistencies and inaccuracies in the predicted rock mass properties.

2.2.4. Determination of Uniaxial Compressive Strength (UCS) of Rocks

The uniaxial compressive strength of the intact rock material can be obtained from rock cores in the laboratory test. However, direct determination of the UCS is relatively expensive, and it can be estimated from point load strength index $Is_{(50)}$ using empirical formula (Broch and Franklin, 1972) and Schmidt hammer rebound hardness value (R) measurements both in the laboratory and in situ tests (Aydin and Basu, 2005).

2.2.4.1. The Point Load Index test

Using correlation equations, the Point Load Index test provides beneficial parameters for evaluating rock samples' uniaxial compressive strength (UCS) (Singh et al., 2011). This information is crucial for engineering structures that need rock mass stability appraisals, such as dams, tunnels, slopes, and foundations (Hoek and Bray, 1981; Broch and Franklin, 1972). UCS values are additionally employed in geomechanical rock mass classification, such as the rock quality designation (RQD), rock mass rating (RMR), and Q system, which are used in the design and planning of underground operations (Barton et al., 1974; Bieniawski, 1979) and correlated with a sonic velocity of rocks in order to determine the dynamic properties of rocks (Yaşar and Erdoğan, 2004).

The International Society of Rock Mechanics (ISRM, 1985) established the standard for conducting the testing and accompanying computations for the Point Load Strength Index. The point load test (PLT) applies a point load on a cylindrical, prismatic, or irregularly shaped rock sample, often through a steel or carbide sphere. The test intends to determine the rock sample's response to a concentrated load until a failure. The point load index can be computed by measuring the load at failure, dividing by the square of the distance between loading points, and multiplying by a correction factor for sample size and shape (Broch and Franklin, 1972; Cargill and Shakoor, 1990; Rusnak and Mark, 2000).

According to Broch and Franklin (1972), the value for the Point load test index (Is_{50}) (in psi) is determined by the following equation:

$$Is_{50} = \frac{P}{D_e^2} \qquad \textbf{(2.18)}$$

Where P is failure load (M.N./m$^{2)}$; De is Equivalent core diameter (m)

Numerous investigations have been conducted to investigate the relationship between uniaxial compressive strength (UCS) and point load index (Is) for hard, strong rocks (Singh et al., 2011). As stated by Mark and Rusnak (2000), Broch and Franklin (1972) described the relationship between uniaxial compressive strength (UCS) and point load test index as follows:

$$\boldsymbol{UCS = Is_{50}(K) = 24.Is_{50}} \qquad \textbf{(2.19)}$$

Where K is the "conversion factor” which is 24.

2.2.4.2. The Schmidt Hammer Rebound Values

Estimating rock strength during fieldwork is crucial in estimating the uniaxial compressive strength (UCS) and young modulus in terms of determining the mechanical properties of rocks (deformability and strength), an essential aspect of various engineering fields, particularly in civil engineering and mining projects (Katz et al., 2000; Aydin and Basu, 2005; Yagiz, 2008; Wang and Wan, 2019). The Schmidt hammer, developed in 1948 by Swiss engineer Ernest Schmidt, is a portable, affordable piece of equipment capable of assessing intact rock strength with unique benefits above typical laboratory testing (Schmidt, 1951, as cited in Haramy and DeMarco, 1985). It has been subsequently used to measure rocks' compressive strength. Schmidt hammer models are created with different levels of impact energy, with types L and N being the most widely used for assessing rock mass characteristics. The L-type Schmidt hammer has an impact energy of 0.735 Nm and is typically used for rock testing, whereas the N-type hammer has an impact energy of 2.207 Nm and is used for concrete testing (Aydin and Basu, 2005). The International Society for Rock Mechanics (ISRM) and the American Society for Testing and Materials (ASTM) recognized the Schmidt hammer technique due to its widespread use in rock mechanics.

Barton and Choubey (1977) stated that the uniaxial compressive strength (σc) of the rock can be determined by correlating the rebound number with the rock's dry density through multiplication, as demonstrated in the following equation.

$$\boldsymbol{\log_{10} \sigma_c = 0.00088\gamma R + 1.01} \qquad \textbf{(2.20)}$$

Where, σ_c is the uniaxial compressive strength in M.N./m^2, γ is the dry rock densities in K.N./m^{3,} and R is the average Schmidt rebound value.

2.2.5. Rock Mass Permeability Characteristics

According to Baghbanan and Jing (2007), the permeability of a rock mass refers to the capacity of a rock formation that allows fluids like water or hydrocarbons to flow via its interconnected pore spaces or fractures. It is a crucial characteristic of rock masses in several engineering fields, such as groundwater management, civil engineering, petroleum engineering, and environmental engineering. Rock type, porosity, grain size, and fissures or cracks in the rock formation with advantageous characteristics are some variables that affect permeability.

2.2.5.1. Packer Permeability Test

Rock mass permeability is a critical parameter in several fields, including hydrogeology, civil and mining engineering, and dam reservoir management. It is defined as the ability of a porous geological material to allow fluids to flow via its interconnected pores or cracks. High permeability suggests fluid may move relatively easily, whereas low permeability means fluid movement is difficult. The Lugeon test was developed in 1933 by French geologist Maurice Lugeon, who worked in Switzerland, and the name of this test is after the geologist. Maurice Lugeon offered his test to create a straightforward tool for describing and contrasting prior dam foundation zones in various locations (Vaskou et al., 2019).

The most common field in-situ test used to establish the adequate hydraulic conductivity of rock masses is the water pressure test, also called the Lugeon or "packer" test (Vaskou et al., 2019). The test's main purpose is to determine whether water can pass through cracks in rocks. In addition to the packer test, boreholes may be employed in areas with geological defects, including faults, bedding planes, joints, fissures, and fractures to determine the rock mass permeability (Foyo et al., 2005). The test is conducted in five phases. The first stage is completed with low water pressure, and the subsequent stages increase the pressure until the maximum pressure is reached. The same pressure stages used to increase pressure are employed to decrease tensions after reaching their maximum. Every minute of the test, measurements for the flow rate (q) and water pressure (P) are recorded. The hydraulic conductivity result of the test is described in terms of Lugeon value. The Lugeon value (Rozo, 1933), which is defined as the hydraulic conductivity required to establish a flow rate of 1 liter/minute/meter of test interval at a reference water pressure (P_0) of 1MPa (equation 2.21), is used to calculate the hydraulic conductivity of rock mass. One liter of water flows per minute per meter at a single Lugeon value.

$$Lu = a\ x\ \frac{q}{L} x \frac{P_o}{P} \tag{2.21}$$

Where q is the flow rate in liters per minute, L is the length of the testing section in meters, P is the pressure necessary for the test in mega Pascals, and *a* is a dimensionless factor with a value of 1 when the S.I. units' system is employed (q (L/min), L (m), and P (MPa). The Lugeon value results are then used to express the discontinuity characteristics and rock mass types in the dam foundation and impoundment reservoirs, and the packer test information is used to determine the water/cement ration and grout injection pressure used during grouting (Azimian and Ajalloeian, 2013).

2.2.5.2. Permeability of Rock Mass from Discontinuity features

According to the study by Duan and Yang (2014), Fractures and discontinuities within rock masses significantly influence the permeability characteristics of the rock mass itself. This infers that high permeability zones are often associated with fractured rock masses, as the larger discontinuity spacing, and interconnected pathways facilitate fluid flow. Conversely, intact rock masses with fewer fractures possess lower permeability.

According to Öge (2017), The fracture characteristics such as geometry, spacing, apertures, fracture density, continuity, roughness, infilling material, degree of weathering, and the stress applied to fractures primarily control and influence the permeability of rock mass. The equivalent hydraulic conductivity, k, of rock mass for a parallel array of discontinuities with varied apertures and spacing is particularly sensitive to stress, and as stress increases, the fractures close and the hydraulic conductivity decreases.

In addition to the discontinuity features of the rock mass, the groundwater substantially influences rock engineering structures in terms of construction operations life, rock mass deformation, and overall stability. Hydraulic conductivity, pore water pressure, and water pressure acting along joints are all critical, as is the water sensitivity of the rock material. Groundwater conditions must be understood through surface structures on rock masses, foundations, and slopes (Hoek and Bray, 1981; Rastegar et al., 2017; Aksoy, 2008). Groundwater pressure and water input rate information are crucial for underground rock structures, as they significantly impact operational difficulties, structural integrity, and support stability. Pump selection, infrastructure design for water outflow, and the need for grouting and water sealing may be operational problems. Surface engineering works such as dams and foundations are affected by ground permeability (Gurocak and Alemdag, 2012).

The size and characteristics of the joints generally determine the permeability of jointed rocks. The higher the permeability, the closer the spacing and the broader the aperture. The hydraulic conductivity (k) of rock mass may be calculated using the fracture aperture and spacing, and the relation between the hydraulic conductivity (k) and fracture parameters is given in the equation below (Snow, 1968; Louis, 1974). The fractures are considered to be parallel and smooth fractures. However, rough fractures have a hydraulic conductivity that is 25% of smooth fractures (Qureshi et al., 2014). Field observations confirmed this assumption.

$$\boldsymbol{K = \frac{ge3}{12\mu S}} \quad \textbf{(2.22)}$$

Where g is the gravitational acceleration (9.81m/s^2), e is the average fracture aperture (m), μ is the fluid's coefficient of kinematic viscosity (1x10-6m^2/s for water at 20^{o}C), and S is the average fracture spacing (m). On the other hand, the reciprocal of fracture spacing equals the fracture frequency (λ). As a result, the above equation may be expressed as follows.

$$\boldsymbol{K = \frac{\lambda ge3}{12\mu}} \quad \textbf{(2.23)}$$

2.2.6. Rock Mass Failure Criteria

Rock mass failure criteria are often based on rock mass classification or characterization systems in the fields of rock mechanics and rock engineering. The Hoek-Brown failure criterion describes the strength and properties of rock masses. The Hoek-Brown failure criterion is the best known and most widely used (Hoek and Brown, 1980). In various engineering applications, this empirical criterion is widely used to evaluate the failure behavior of fractured rocks. The Hoek-Brown criterion enables prediction of the strength and stability of rock structures in the design and analysis of underground excavations, tunnels, foundations, and embankments by evaluating the complex interplay between the strength of the rock, the quality of the rock mass, and the effects of stresses in geologic materials (Hoek and Brown, 1980). The Hoek-Brown failure criterion is a method for estimating the strength and deformation of rock masses. It was originally developed in 1980 and has been updated several times since then (1983, 1988, 1992, 1995, 1997, 2001, and 2002).

The generalized expression is used in the Hoek-Brown failure criterion's 2002 version but with modifications to the m_b, s, and *a* value.

$$m_b = m_i \exp^{\left(\frac{GSI-100}{24-14D}\right)} \quad \textbf{(2.24)}$$

$$s = exp^{\left(\frac{GSI-100}{9-3D}\right)} \quad \textbf{(2.25)}$$

$$a = \frac{1}{2} + \frac{1}{6}\left(e^{\frac{-GSI}{15}} - e^{-\frac{20}{3}}\right) \quad \textbf{(2.26)}$$

where D is a variable based on the disturbance's intensity. It should result in a smooth, continuous transition for the whole range of GSI values because the switch at GSI = 25 is eliminated for the coefficients s and a. D = 0 for in situ rock masses that have not been disturbed and D = 1 for disturbed rock mass characteristics are the suggested values for the disturbance factor.

2.2.7. Bearing Capacity of the Rock Mass

According to the study by Shirzad and Nikkhah (2021), a reliable estimate of rock mass strength and deformation properties are required to design rock structures. In addition, the settlement and stress caused by the structure loading should not exceed the allowable bearing capacity and settlement of the soil and medium. Bearing capacity is no longer an issue for rock foundations because the rocks are generally stronger than the concrete used for construction (Duncan and Hancock, 1966; Wyllie and Mah, 2004). Nevertheless, the bearing capacity of rock masses is directly related to the quality of the rock masses, and discontinuities can significantly reduce the bearing capacity. When a structure is built on rock, conditions differ from when it is built on earth. There are two significant differences between rock and soil media: the strength of the rock at higher loads and the occurrence of discontinuities in rock masses that result in a different strength level than the entire rock (Carter and Kulhawy, 1992). As a result, the engineering performance of the subsurface strata and their bearing capacity influence foundation design. The bearing capacity was calculated using the Hoek-Brown empirical failure criterion from several equations.

According to Carter and Kulhawy (1992), the equation for calculating the ultimate bearing capacity of a rock mass can be suggested as the following:

$$q_u = UCS[S^a + (m_b S^a + S)^a] \quad \textbf{(2.26)}$$

Where UCS is the uniaxial compressive strength of intact rock (MPa), m_b, S, and *a* are the rock mass Hoek–Brown constants.

For tightly fractured and weak rocks lying on a relatively horizontal surface, Wyllie (1992) developed the following equation to obtain the allowable bearing capacity (qa) based on the Hoek-Brown strength criteria:

$$q_a = \frac{C_{f1} S^{0.5} UCS[1 + (m_b S^{-0.5} + 1)^{0.5}]}{FOS} \quad \textbf{(2.27)}$$

Where UCS is the uniaxial compressive strength of the intact rock, FOS is the safety factor.

Suppose the foundation is on a sloped surface. In that case, the bearing capacity factors must be modified to account for the lower lateral resistance created by the smaller rock mass on the downslope side of the foundation Bell (2007) as cited in Wyllie (1992). For shallow slopes with an angle of repose less than ϕ/2, the allowable working load of the foundation is usually determined by the bearing capacity or settlement. For slope angles greater than ϕ/2, it is seldom necessary to check the bearing capacity since the stability of the slope is the determining factor (Shen, 1998). For foundations on sloped surfaces, the allowable bearing pressure is calculated as follows:

$$q_a = \frac{Cf_1 C N_{cq} + Cf_2 \left(\frac{B\gamma}{2}\right) N_{\gamma q}}{FOS} \quad \textbf{(2.28)}$$

Cf1 and Cf2 are correction factors, Ncq and Nγq are bearing capacity factors and depend on the slope angle (β), C is the cohesion, B is the width of the foundation, FOS is the factor of safety, and γ is the unit weight of the rock. H is the slope height and No is the stability number, which is calculated as follows:

$$N_o = \frac{\gamma * H}{C} \quad \textbf{(2.29)}$$

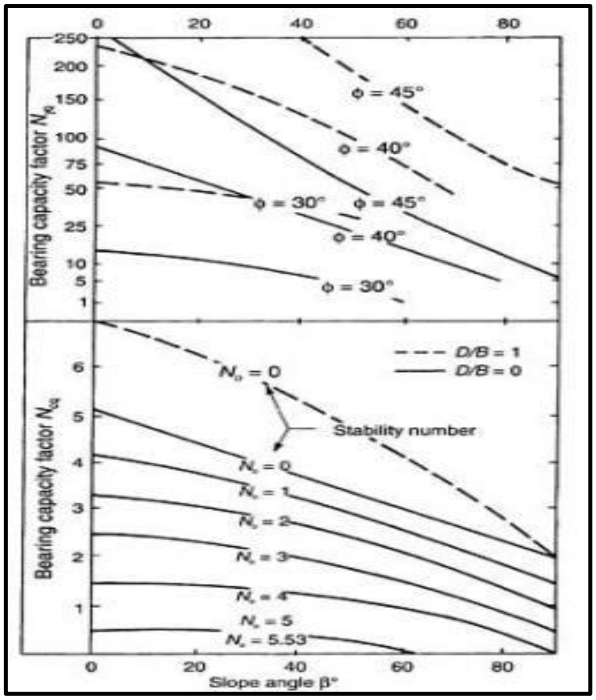

Figure 2.2. Bearing capacity considerations for sloping ground surface footings (US Department of the Navy, 1982)

Engineering considerations for designing a foundation include the engineering performance of the subsurface layers and their bearing capacity. Bowles (1996) utilizes the following equation to calculate a rock mass's ultimate bearing capacity (Q_{ult}) and acceptable bearing capacity value (Q_{all}).

$$\boldsymbol{Q_{ult} = UCS_{av}\left(\frac{RQD_{av}}{100}\right)^2} \quad \textbf{(2.30)}$$

$$\boldsymbol{Q_{all} = \frac{Q_{ult}}{FOS}} \quad \textbf{(2.31)}$$

Qult is the ultimate bearing capacity, Qall is the allowed bearing capacity, FOS is the safety factor, RQD_{av} is the average rock quality designation, and UCS_{av} is the average uniaxial compressive strength.

2.2.8. Soil Mass Engineering Characterization and Classification

Soils are naturally occurring, unconsolidated or loosely compacted mineral and organic constituents that form the top layer of the earth's crust in engineering practice, especially in soil mechanics. Buildings, highways, bridges, and retaining walls are just a few examples of the many structures that rely on these materials. In other words, soil is often used as a critical component in the construction of earthen structures such as highways and dams. In the construction of dams, soils can be used as embankment fill for the dam body or as cover material for permeable impoundment areas (Arora, 2008; Budhu, 2011).

The classification of soils into different categories and subgroups based on their engineering behavior is called soil classification. There are several different categories for classifying soils. Examples include the Unified Soil Classification System (USCS), the American Association of State Highway and Transportation Officials (AASHTO), and classification based on soil texture. The engineering classification has nothing to do with the textural classification because it only considers texture and excludes plasticity. The AASHTO does consider texture and plasticity but is more relevant to the classification of road soils. The USCS is most relevant for all purposes and, like the AASHTO, emphasizes texture and plasticity in soil classification. ASTM, the American Society for Testing Materials, also supports this methodology. The system is most commonly used for all types of soil mechanics problems (Arora, 2008; Budhu, 2011). Engineering and index properties are usually used to describe soil properties. Index parameters of soil are soil properties such as specific gravity, water content, particle size distribution, and consistency limits used for identification and classification. The engineering properties of soils are their permeability, shear strength, and compressibility.

2.2.8.1. Permeability of soil masses

Since soils comprise discrete particles, the spaces between them are linked and can be envisioned as a highly complex network of asymmetric tubes. In a two-phase solid-liquid system, the liquid, in most soil engineering issues water, fills these spaces. When a potential difference in soil mass is formed, the water in these tubes can flow freely. From zones with higher potential to those with lesser potential, water flows. Flow resistance increases when pores are smaller, and pore channels are disorganized (Ranjan and Rao, 2005).

On the contrary, when soils have more significant voids or more or less regular flow channels, the resistance to flow is significantly lower. Consequently, despite all soils being permeable, there are differences in the degree of perviousness. Sands are more permeable than silts, silts are more permeable than clays, and gravels are even more permeable than sand. Furthermore, a soil's degree of perviousness can vary depending on its composition. Loose sand is substantially more permeable than thick sand. Compared to the same clay soil with a dispersed structure, one with a flocculated structure is more permeable (Ranjan and Rao, 2005; Arora, 2008).

Water movement through the soil is called soil permeability, directly affecting engineering structures' performance. The evaluation of soil permeability is one of the vital components in establishing structural stability and integrity. The appropriateness of soils for various projects is mainly determined through laboratory permeability studies. Since the permeability of soil is directly related to the rate of water flow in soil, it has a significant impact on issues with open-cut excavations in sands below the water table, seepage through the dam body and below dam foundations, and the overall integrity of engineering structures foundation (Ranjan and Rao, 2005; Arora, 2008). Permeability tests of soils are categorized into two tests: constant head and falling head permeability of soils where the constant head test is mainly used for determining the permeability of coarse-grained soils like sand and gravels, and the falling head permeability test of soil is commonly used for fine-grained soils (Das, 2002).

2.2.8.1.1. The Constant-Head Permeability Test

The constant-head permeability test is commonly utilized for determining the hydraulic coefficient of permeability of a significantly more permeable soil with a value of $k > 10^{-4}$ cm/s (primarily for coarse-grained soils, such as sands and gravels) (Arora, 2008; Budhu, 2011). Constant-head permeameter is the instrument used for the test. According to I.S.: 2720 (Part XVII), it consists of a metallic mould with an internal diameter of 100 mm, an effective height of 127.3 mm, and a capacity of 1000 ml. A removable extension collar 100 mm in diameter and 60 mm in height are included with the mould and is necessary for soil compaction. A drainage base plate with a recess for porous stone is bundled with the mould. A drainage cap with an air release valve and an inlet valve is attached to the mould. There are fittings on the drainage base and cap for fastening them to the mould. In the mould, the soil sample is placed between two porous discs. At least 10 times more permeable than the soil should be porous discs. Before inserting the porous discs into the mould, they must be de-aired. Deairing the water tubes is also necessary. The soil can also be poured into the permeameter, which can then be compacted to the necessary density to prepare the sample or utilize the soil sample remoulded, and compacted by a standard proctor to get the same density as they do in nature (Murthy, 2003). When the sample is compacted in the mould, a dummy plate measuring 12 mm thick and 108 mm in diameter is built into the base.

The sample must be completely saturated. This is accomplished by putting the soil into a permeameter filled with water, submerging it, and then allowing water to flow through the soil into the mould from the base to the top. The constant-head reservoir is connected to the drainage base to accomplish this. When all the air has been expelled, the upward flow is maintained long enough (Arora, 2008; Budhu, 2011).

The sample's length, L, and cross-sectional area, A, are exposed to a constant head, h, while the test progresses. Allowing water to pass through the sample and measuring the amount of discharge Q in time t represents the test. The permeability coefficient (k), which measures the soil's capacity to transfer water, may be determined using Darcy's Law.

$$\boldsymbol{Q = k\frac{h}{L}At} \tag{2.33}$$

By computing for a value of k, we will get:

$$\boldsymbol{k = \frac{QL}{hAt}} \tag{2.34}$$

Where k is the hydraulic conductivity, Q is the discharge (volume flow rate) in m^3/sec, L is the length of the soil specimen in meters, A is the cross-sectional area of the soil specimen in m^2 h is the head difference in meters, and t is the time in seconds.

2.2.8.1.2. Falling Head Permeability Test

The falling head permeability test is predominantly employed for fine-grained soils like silts and clays, which possess low permeability (Budhu, 2011). The test works for soil samples with permeability values between 10^{-2} to 10^{-6} cm/s and features a similar set-up to the constant head test, except the head difference is permitted to drop as water passes through the soil specimen rather than being held constant (Murthy, 2003; Arora, 2008).

The amount of water collected in the graduated jar of the constant-head permeability test is relatively minuscule. It cannot be determined precisely for considerably less permeable soils requiring the falling-head permeability test. The permeameter mould used in the constant-head permeability test is the same one. The permeameter's top has a vertical, graduated standpipe with a specified diameter. The sample is sandwiched between two porous discs. At the beginning of the test, the entire assembly is put in a constant head chamber filled with water. Before placing the sample, the water tubes and porous discs must be de-aired. If an in-situ, undisturbed sample is available, it can be utilized; if not, the soil is taken and compacted to the necessary density in a mould. In order to remove air from the soil, the valve at the drainage base is closed, and gradual vacuum pressure is exerted through the drainage cap. Vacuum pressure is raised to 700 mm of mercury and kept at that level for around 15 minutes. While under vacuum, de-aired water is allowed to flow upward from the drainage base, saturating the sample. Both the top and bottom outlets close when the soil is saturated. Water is poured into the standpipe until it reaches the desired height (Murthy, 2003; Arora, 2008; Budhu, 2011).

To begin the test, the water in the standpipe is allowed to pass through the sample and into the constant-head chamber, where it overflows and spills out. The water level in the standpipe decreases as the water percolates through the soil. It is calculated how long it will take for the water level to drop from a known beginning head (h_1) to a known final head (h_2) (Arora, 2008). The amount of water in the constant-head chamber determines the head. The permeability can be calculated using the following equation by monitoring the changes in the head and timing how long it takes the head to decrease from an initial to a final value (Das, 2010):

$$\boldsymbol{k = 2.303\ x\ \frac{a(L)}{A(t_f - t_i)}\ x\ \log_{10}(\frac{h_1}{h_2})} \qquad \textbf{(2.35)}$$

Where A is the sample's cross-sectional area, a is the standpipe's cross-sectional area, L is the specimen's length, tf and ti are the time interval (T) final and initial, respectively, h_1 is the initial head, and h_2 is the final head.

2.2.9. Common Dam Site Treatment Methods

The common issues challenging the dam construction's structural integrity, stability, and operational life are leakage and seepage problems at the dam foundation and reservoir area and slope instabilities in the dam abutments and rims. Therefore, these challenging issues must be treated in terms of their related issues, as discussed below.

2.2.9.1. Dam Foundation Treatment Methods

Despite adverse geological conditions under varied geological set-up, numerous dams have been constructed, and others are planned to be constructed. Proper foundation treatment involving grouting methods, deep soil mixing, trench excavation and backfilling with an engineered material can stabilize composite cut-off walls and upstream or downstream buttress structures in embankment dams (Bruce et al., 2012). A clay blanket is an impervious layer upstream of a dam to control the seepage from the dam foundation (Hedayati et al., 2015). Replacing the top layer of a riverbed of higher permeability is the most economical way of controlling seepage/leakage. In addition, clay blanketing is used mainly in alluvial soil when cement grouts are not applicable.

Foundation treatment using rock-mass grouting has been utilized frequently (Warner, 2004; Bruce and Dreese, 2010). This method should be carried out with care to achieve the contradictory technical goals of maximizing the filling of voids and deteriorated areas and at the same time minimizing the potential risks of harmful hydraulic fracturing or weakening of earthen cores (Weaver, 1991; Park and Oh, 2018; Kanik and Ersoy, 2019; Nield, 2018). Grouting is the process in which fluid material is injected and flows into fractures or cracks within the rock mass (Houlsby, 1991; Barani et al., 2014). The execution of grouting largely depends on the result of the permeability (water pressure) test to delimit the foundation rock mass into zones of different rock mass quality requiring different levels of treatment (Sadeghiyeh et al., 2013). The permeability (q, expressed in Lugeon/Lu) of the grout curtain and the relatively impervious rock strata shall meet the following criteria (USBR, 1977):

- For dams over 100m high, q is between 1Lu and 3Lu.
- For dams between 100m and 50m high, q is between 3Lu and 5Lu.
- For dams below 50m high, q is 5Lu.
- The lower limit of the above ranges shall be adopted for pumped-storage power stations or reservoirs in areas of shortage in water resources.

Thus, grouting is carried out to (USBR, 1977):

- Reduce leakage through the dam foundation through the defects.
- Reduce uplift pressures (under concrete gravity dams when used in conjunction with drain holes).

- Reduce settlements in the foundation (for concrete gravity, buttress, and arch dams).

2.2.9.2. Abutment Slope Stabilization Methods

Remedial measures, as their name suggests, are slope stabilization techniques carried out after a slope failure event or when excessive deformation is reported which may trigger instability. In many scenarios, dams are constructed without prior investigation of rock mass strength and slope stability analysis; this can result in slope instability due to slope angle modification and disintegration of rock mass by excavation; hence slope stabilization is needed to avoid abutments slope failure, which can cause property and life loss in dams as a mass of earth material falls into the reservoir and causing in the topping of the reservoir water failing the dam. To assess the appropriate slope stabilization technique that can be used to stabilize an unsafe slope, one has to know the factors contributing to slope failure and the geological material of the slope (Abramson et al., 2001).

General reviews on different remedial measures are available in many works (Hutchinson, 1977; Zaruba and Mencl, 2014; Holtz and Schuster, 1996; Popescu, 2002). According to these scholars, modification of slope geometry, retaining structures, internal slope reinforcement and drainage are some remedial measures generally considered to stabilize unstable slopes. According to Abramson (2001), the stability of any slope will be improved if specific actions are carried out. A soil and rocks mass has different properties, so the remedial measures of slope stabilization are separately implemented.

Generally, the slope becomes stable by performing stabilization methods for rock and soil slopes. Slope stabilization methods generally increase the factor of safety through reducing driving force by excavating material from the unstable ground, installing appropriate drainage methods, and increasing resistive force by building retaining structures or support, and chemical treatment to harden the soil (Abramson et al., 2002).

CHAPTER THREE

3. METHODS AND MATERIALS

3.1. Methods

The Methods used for this research to achieve the research objectives can be summarized as follows: desk work; data collection (including primary data collected from detailed fieldwork, discontinuity surveying, in-situ testing, geological mapping, and sampling (soils and rocks), and laboratory testing); and secondary data such as borehole drilling results, packer test results, and laboratory analysis of soil and rock samples from core logging (specific gravity, water absorption, unit weight, strength test (point load index test, UCS), and slake durability); data processing and analysis. Primary and secondary data were used to evaluate, summarize, and present the findings.

3.2. Desk Work

Throughout this stage of the research, existing data from the study area, such as topographic maps (from the Ethiopian Space Science and Geospatial Information Institute), regional geology reports and maps (from the Geological Survey of Ethiopia), aerial photographs, satellite imagery such as Digital Elevation Model (DEM), and aerial photographs were collected and thoroughly reviewed to obtain information about the physiography, structure, and geological setup of the study area. Consequently, the study area's location and accessibility, geomorphological setting, and drainage map were created using Arc-GIS 10.8, and Surfer 21 software. Additionally, topographic maps were utilized to create a base map for geological and engineering geological mapping. Literature review of published journals and unpublished reports related to gravity dam failure modes, characterization, and classification of soils and rock masses, engineering geological evaluation of dam sites and reservoir areas like water tightness of evaluation of dam sites and reservoir area, and slope stability analysis methods were carried out to have the comprehensive understanding of engineering geological condition of the study area. Essential data for the current investigation were gathered from secondary and primary sources. Secondary data, including borehole drilling results, packer test findings, and laboratory examination of core samples (specific gravity, water absorption, unit weight, strength test (point load index test and UCS), and slake durability), and the hydrological aspects of the study area was provided by the

Engineering Corporation of Oromia (ECO). Meteorological data such as precipitation(monthly and annual precipitation data) and temperature(monthly and annual temperature data) were gathered from the National Meteorological Agency of Ethiopia (NMAE). The primary data were generated from detailed fieldwork and laboratory investigations from the samples collected from the dam site and reservoir areas.

3.3. Field Survey and Data Collection

The second approach to this research work was detailed fieldwork and sample collection. Primary data were obtained from the study area, and a detailed geological and engineering geological evaluation was carried out at the dam site and reservoir areas. This step includes extensive discontinuity surveying, digging test pits and soil sampling for laboratory tests, in-situ strength tests, field descriptions of soils and rocks, and mapping. Potential modes of slope instabilities were identified during the field investigation based on the factors influencing failure mechanisms; either structurally controlled failures or non-structurally controlled failures (rock mass-controlled failures).

All field survey data and sample collections are compiled to make up the method of primary data collection referred to as Geological Mapping. This method is critical to determine if the dam site and its surroundings are suitable for the construction of dam projects in terms of stability, operational longevity, and overall structural integrity of the dam. The abovementioned approach was used to precisely determine the foundation's geological formation, abutments, and reservoir areas. Different rock types were classified based on their genetic type and degree of weathering. The lithology's thickness and the geological structure's orientation were measured in the field at different study area outcrops. To carry out extensive geologic mapping, representative traverse lines connected several lithological units and notable geological structures. Field methods were used to detect crucial slope sections from dam abutments and reservoir rims of the study areas, including identifying stress fracture development on the upper slope face, slope face tilting, and discontinuity orientation, favouring rock slope failures.

During the fieldwork, testing such as in-situ strength tests on rocks using a Schmidt hammer, field descriptions of soils and rocks, mapping and sampling for laboratory analysis, and adequate discontinuity survey parameters were carried out. Visual observation was used to determine the engineering properties of rocks and soils. The rock type, spacing, roughness, orientation, aperture, persistency, degree of weathering, infilling materials, and groundwater condition of the dam abutments were all noted on the rocky outcrops. Topographic features, surface soil deposit type, and depth were recorded in the field.

3.3.1. Discontinuity Survey (Surface Mapping of Geological Structures)

A discontinuity survey of rock outcrops conveys essential data on the geological structure and mechanical characteristics of rocks, which help evaluate the stability of rock slopes, estimate rock mass quality, and predict the rock mass response to excavation and other construction activities. To comprehensively understand the influence of discontinuities on rock mass behavior, such as permeability, deformability, and strength, the relevant discontinuity survey must be characterized and quantified. Therefore, surface mapping of geological structures assists in understanding their behaviour in response to different natural and human-induced forces. It entails systematically mapping and measuring fractures, joints, bedding planes, and other discontinuities within rock masses in terms of measuring and determining the spacing, orientation (dip amount and direction), condition of discontinuities (length/persistence, separation/aperture, roughness, infilling materials, and weathering), and groundwater conditions of dam site rock masses and also including measurement of the slope height and orientation (Hoek and Bray, 1981; Wyllie and Mah, 2004).

Discontinuity surveys were primarily conducted on both the dam abutments and the dam's downstream side. Potentially unstable slopes were identified during the field investigation based on the factors affecting the failure mechanism, either structurally or non-structurally controlled failures (rock mass-controlled failures). Structurally controlled and non-structurally controlled instabilities are mainly related to the discontinuity orientation of geological structures and the degree of rock mass weathering, respectively (Wyllie and Mah, 2004). Those discontinuity sets with favourable orientations for rock slope instability were given specific attention throughout the field measurement. This evaluation was primarily conducted along the excavation area. This discontinuity survey provided the critical input parameters for rock mass classification and characterization, which were then used for slope stability analysis (Hoek and Bray, 1981).

The clinometer compass was used to determine the orientations of discontinuities and the dam site's slope face. Similarly, a tape meter was used to measure the spacing of discontinuities, aperture, and persistence of discontinuity sets, and other discontinuity parameters such as surface roughness, infill material, weathering condition, and associated groundwater condition were observed and estimated visually during the fieldwork at the dam site. using International Society of Rock Mechanics (ISRM, 1978) standard method. The degree of weathering of the rock outcrops was assessed using geological hammer blows following the International Society of Rock Mechanics (ISRM, 1978).

3.3.2. The Sampling of Soils and Rocks

Soil and rock sampling provides comprehensive and critical information about a site's subsurface properties and significantly impacts the design and construction of numerous engineering projects. Because of the wide variety of soils and rocks in depth, location, and formation processes, thorough and representative sampling is required for effective classification. Sampling soils and rocks during fieldwork is critical to providing essential information on the index and engineering properties of soils and rocks. Prior to the start of construction of the dam, the Engineering Corporation of Oromia (ECO) collected and analyzed three soil samples to study the soil around the dam reservoir area.

For this study, test pits were excavated to obtain soil samples in the reservoir area (one test pit on the right bank and one test pit on the left bank of the reservoir), and three representative soil samples were collected to determine the index and engineering properties of the soil samples. The soil samples were packed in plastic bags to preserve their natural moisture content. In addition, the rocks that make up the dam and reservoir were described in terms of their engineering properties. Subsequently, three rock samples (one from the left abutment, one from the right abutment, and one from the reservoir area) were collected from the surface area for laboratory testing. Based on visual observation techniques, the soils encountered during fieldwork in the study area can be described in terms of color as brownish-black and yellowish-light.

Figure 3.1. Test pit digging process and soil sampling from the test pit (LBSS-1, LBSS-2, and RBSS-1).

Table 3. 1. Location of test pits with depth.

Location		Soil Sample Code	UTM Coordinates (Adindan Zone 37N)		Depth (m)
			Easting	Northing	
Reservoir Area	Left side of the riverbank	LBSS-1	39º 18’ 59.742”	9º 34’ 04.709”	0.0-1.0
		LBSS-2	39º 18’ 59.742”	9º 34’ 04.709”	1.0-1.70
		SO/77/99	39º 17’ 53.676”	9º 33’ 53.461”	0.0-1.0
	Right side of the riverbank	RBSS-1	39º 18’ 08.273”	9º 33’ 53.448”	0.0-1.0
		SO/75/99	39º 17’ 51.201”	9º 34’ 04.871”	0.0-1.0
		SO/76/99	39º 17’ 49.75”	9º 33’ 55.777”	0.0-1.0

3.3.3. In-situ Strength Estimation (Schmidt Hammer Test)

This study measured the uniaxial compressive strength (UCS) of representative fresh and weathered rock outcrops in situ using a portable instrument, the Schmidt hammer. The purpose of using the Schmidt hammer is to determine the uniaxial compressive strength of rock masses and further this value is used as an input parameter in the determination of shear strength parameters of joints. In-situ rock strength was estimated using a Schmidt hammer at the right and left abutments and in the reservoir area. The test was conducted per the (Aydin, 2009). ASTM (2001) recommends taking at least ten (10) individual impact readings, excluding those that deviate from the average by more than seven (7) units, and averaging those that remain. The. The rebound value, often referred to as the rebound number, corresponds to the strength of the rock. The procedures followed during the utilization of the Schmidt hammer to estimate the in-situ strength rock mass include as:

1. Specimen Preparation: The rock surface must be petrographically homogenous and representative of the rock mass domain to ensure accurate measurements. Smooth, clean, and dry; if not, note the degree of moistness of the surface and the specimen as wet, moist, or damp.
2. Testing: While holding the hammer perpendicular to the test surface, the plunger is pressed forcefully against the rock until the impact is triggered. Multiple readings (typically 10-12) are taken at different positions and orientations across the surface to account for variability. Then, lock the Schmidt hammer by pressing the button after the impact and read the gauged rebound values from the instrument. Maintaining constant

pressure on the rock during testing is crucial to obtain consistent results as shown in the figure below (Figure 3.2).

Finally, using Equation **(2.20)**, the rock's uniaxial compression strength (UCS) was determined by averaging the results of distinctive rebound values.

Figure 3.2. In-situ rock strength estimation test using Schmidt hammer.

3.3.4. Soil Laboratory Test

After the test pits from the right bank and left bank of the dam reservoir areas are dug up and soil samples are collected, they are brought to the laboratory for testing and determining the index and engineering properties of the soil samples. The laboratory tests conducted on soil samples include water content, the specific gravity of solid soils, particle size distribution tests (sieve and hydrometer analysis), consistency of soils (liquid and plastic limit), compaction test (standard proctor test), and permeability test. The tests were conducted at the Engineering Corporation of Oromia (ECO) Geotechnical Laboratory.

Table 3. 2. Laboratory test standard applied for the soil samples.

<table>
<tr><th>S.No.</th><th colspan="2">Soil Laboratory tests</th><th>Standard Test Method</th></tr>
<tr><td>1.</td><td colspan="2">Water Content Determination</td><td>ASTM D2216 (1998)</td></tr>
<tr><td>2.</td><td colspan="2">Specific Gravity</td><td>ASTM D854 (1998)</td></tr>
<tr><td rowspan="2">3.</td><td rowspan="2">Grain Size Analysis</td><td>Sieve Analysis</td><td rowspan="2">ASTM D422 (1998)</td></tr>
<tr><td>Hydrometer Analysis</td></tr>
<tr><td>4.</td><td colspan="2">Atterberg Limits (Consistency Limits)</td><td>ASTM D4318 (1998)</td></tr>
<tr><td>5.</td><td colspan="2">Standard compaction test</td><td>ASTM D698 (1998)</td></tr>
<tr><td>6.</td><td colspan="2">Permeability test: Falling Head permeability test</td><td>ASTM D2434 (1994)</td></tr>
</table>

The Procedures followed for each soil laboratory test are elaborated on in the sections below.

3.3.4.1. Water Content Determination

The ASTM D 2216 (1998) standard was utilized to conduct the test, which used the oven-drying method, one of the most extensively used methods in laboratories for assessing soil water content due to its simplicity and accuracy. The process involves drying a weighed damp soil sample for 24 hours at a controlled temperature (105–110°C) (Das, 2002). First the mass of the container with lid was measured on the weight balance (M_1) as shown in Figure 3.3e. Then add the soil sample to the container and the mass of the container, lid and soil sample was weighed (M_2). Furthermore, the soil sample in the container with lid was placed in the oven and dried in an oven for 24 hours at temperatures ranging from 105 to 110°C. The dried soil sample with container is weighed (M_3).

The water content of the soil sample is calculated from the following equation:

$$w = \frac{M_w}{M_s} = \frac{M_2 - M_3}{M_3 - M_1} x\ 100 \qquad \textbf{(3.1)}$$

Where M_1 is the mass of the container with lid, M_2 is the mass of the container, lid and wet soil, and M_3 is the mass of the container, lid and dry soil.

3.3.4.2. Specific Gravity of soil test

According to ASTM D 854 (1998) standard, the test was conducted. By utilizing a pycnometer, this test technique involves figuring out the specific gravity of soils. In the pycnometer method, according to ASTM D 854 (1998), a clean and dry pycnometer was weighed, and its weight was recorded as M_1. A representative soil sample was then oven-dried at a temperature of around 110°C for 24 hours to eliminate any water content. The dry soil was placed in the pycnometer, and its weight was again recorded as M_2. The pycnometer was then carefully filled with water until it overflowed, ensuring no air bubbles were trapped in the soil sample. The weight of the pycnometer filled with soil and water was recorded as M_3, and the weight of the pycnometer filled with water alone was measured as M_4 as shown in Figure 3.3c. The following formula can determine the specific gravity of the soil:

$$\boldsymbol{G_s = \frac{(M_2 - M_1)}{(M_4 - M_1) - (M_3 - M_4)}} \qquad \textbf{(3.2)}$$

Where M_1 is mass of empty pycnometer, M_2 is the pycnometer with dry soil M_3 is mass of the Pycnometer and soil and water, M_4 is the pycnometer filled with water only. Gs is Specific gravity of soils.

3.3.4.3. Grain Size Analysis of Soils

The sieve analysis was used to determine the distribution of particle sizes bigger than 75 µm (retained on the No. 200 sieve), whereas sedimentation using a hydrometer analysis determines the distribution of particle sizes lower than 75 µm.

The sieve analysis was carried out according to ASTM D 422 and the procedure involves several steps to ensure the accurate determination of soil particle size distribution. The samples are oven-dried at 110±5°C for at least 24 hours to remove all moisture content. The agglutinated/clumped/conglomerated parts of the soil samples were crushed to the correct size using a crushing device such as a pestle. The dry samples were then weighed and the notation of the initial soil mass. The next stage of the procedure involves selecting an appropriate series of sieves. A standard set of sieves specified by the American Society for Testing and Materials (ASTM) is typically employed, ranging in size from 75µm to 75mm. The sieves are stacked in descending order, with the largest openings at the top and the smallest at the bottom, with a receiving pan at the bottom as shown in Figure 3.3f. The prepared soil sample was placed on the top sieve, and the entire stack was mounted on a sieve shaker, which mechanically agitates the sieves for a predetermined period (typically 10 to 30 minutes). The shaking process separates soil particles according to size through the sieve openings. Upon completion of the shaking process, each sieve was carefully removed, and the soil retained on the sieve was weighed. The cumulative weight retained on each sieve and the receiving pan was recorded. The soil samples that passed through 75μm diameter size were further taken for hydrometer analysis as shown in Figure 3.3a and Figure 3.3b. Finally, the gradation curve was plotted from the analysis result.

3.3.4.4. Atterberg Limits (Consistency Limits)

The test was conducted according to ASTM D 4318 (1998) standard. To determine the liquid limit of the soil sample the following procedures are considered.

First, a 30g sample of soil passing through a 425 micron IS sieve was mixed with water to form a paste. Then, a portion of the paste was placed in the cup of a Casagrande device, and a vertical groove was created with a standard grooving tool. The device was rotated at 2 revolutions per second while counting the number of blows required for a 12 mm closure of the groove at the bottom as shown in Figure 3.3d. A representative slice of the soil was collected with a spatula for water content determination. This procedure was repeated for different numbers of blows ranging from 15 to 35, with the consistency of the paste being adjusted accordingly. The moisture content of each sample collected was determined and plotted on semi-log paper, with the number of blows on the X-axis (using a log scale) and the water content on the Y-axis (using an arithmetic scale). The liquid limit was then calculated by finding the water content for 25 blows from the resulting graph.

To determine the plastic limit of a soil sample, an 8g portion was taken and formed into a ball. The ball was then rolled on a glass plate with sufficient pressure to create a thread of uniform diameter. Rolling continued until the thread began to crumble, which was noted when the diameter reached 3 mm or larger. At this point, a small amount of water was added to the sample, and the kneading and rolling process resumed until the thread crumbled at 3 mm diameter. This process was repeated two or three times to obtain an average value for the plastic limit (PL). The plasticity index (PI) is the difference between liquid limit and plastic limit (PI = LL – PL).

3.3.4.5. Compaction Test: Standard Proctor test

The test was carried out according to ASTM D 698 (1998) standard. In general, compaction is removing air from soil to make it denser, which takes mechanical effort. The dry unit weight of the soil is used to determine the degree of compaction. The procedure comprises applying varied compaction efforts at various moisture levels to compact a soil sample in layers inside a cylindrical mould. A typical compaction effort with a specific energy of 592kN-m/m^3 compacts the soil. Engineers can establish the optimal compaction parameters by using the results of tests to construct a graph showing the relationship between dry density and moisture. The soil is compacted in a mold with a volume of 943.3 cm3 in the Standard proctor test. The mold has a diameter of 101.6 mm. The soil is combined with variable quantities of water before being crushed in three equal levels using a hammer that strikes each layer 25 times. The hammer has a drop of 304.8 mm and weighs 24.4 N (mass =2.5 kg) as shown in Figure 3.3f and Figure 3.3g. The wet unit weight of compaction and dry unit weight may be estimated for each test as follows:

$$\boldsymbol{\gamma = \frac{W}{V} \quad , \quad \gamma_d = \frac{\gamma}{1+w}} \qquad \textbf{(3.3)}$$

Where, W = weight of the compacted soil in the mold V= volume of the mold 944 cm^3. The values of γd determined from the above equation can be then plotted against the corresponding moisture contents to obtain the maximum dry unit weight and the optimum moisture content for the soil.

3.3.4.6. Soil Permeability Test

The test was carried out in accordance with the ASTM D 2434 (1994) standard. The falling head method is used in this test procedure for measuring the coefficient of permeability. The soil sample was compacted in a standard mold and to begin the test, the water in the standpipe is allowed to pass through the sample and into the constant-head chamber, where it overflows and spills out. The water level in the standpipe decreases as the water percolates through the soil as shown in Figure 3.3h. To calculate the coefficient of permeability of the soils for the A is the sample's cross-sectional area, a is the standpipe's cross-sectional area, L is the specimen's length, tf and ti are the time interval (T) final and initial, respectively, h1 is the initial head, and h2 is the final head, the equation **(2.35)** was used for the course of the test.

Figure 3.3. Soil laboratory tests (water content, specific gravity test, grain size analysis (sieve and hydrometer analysis), Atterberg limit test, compaction test, falling head permeability.)

3.3.5. Rock Laboratory Test

The rock samples collected during the field investigation are brought to the laboratory for test and analyzed accordingly. Laboratory tests on rock samples are the determination of the unit weight, point load index test, and water absorption test. The tests were conducted at the Gia Engineering Pvt. Ltd. Co.

Table 3.3. Rock laboratory tests with the corresponding applied standard.

S.No.	The Conducted Rock Laboratory Test Types	Standard Followed
1.	Point Load Index Strength test	ASTM D5731 (1995)
2.	Unit Weight	ISRM (1978)
3.	Water Absorption	ASTM D6473-10 (2010)

The procedures followed to test the rock in the laboratory are described in the following section.

3.3.5.1. Unit Weight Test of Rock Samples

The unit weight test of a rock sample is a conventional laboratory test used to evaluate the density of a rock sample for determining the slope stability analysis and evaluation of the strength of the rocks. The following are the fundamental test procedures according to the standard suggested by ISRM (1978).

Firstly, the sample must be free of visible fractures or other structural flaws that might compromise the accuracy of the test findings. The sample must be typical of the rock formation under consideration. The next stage in the technique was to determine the mass of the rock sample after it has been oven-dried for 24 hours at 105° C and recorded as (Md) as illustrated in Figure (3.4C) below. After the mass of the rock samples were determined, the method moved on to determine its volume and saturated weight. The next procedure was filling a container (typically a graduated cylinder) with a predetermined amount of water, a rock sample was immersed in the water to saturate it with water and recording the saturated weight (Ms). The subsequent rise in water level was measured, which corresponds to the rock sample volume (V_1 and V_2 in ml). The density of the rock samples (ρ) was computed using the formula: ρ = mass/volume. The result was then stated in quantities such as Kg/m^3. The final stage in determining the unit weight test was computing by multiplying the value of the dry and saturated density of the samples and the acceleration due to gravity to determine its unit weight (γ).

$$\gamma = \rho x \ g \quad \textbf{(3.4)}$$

Where γ is the unit weight of the rock sample (KN/m^3), ρ is the density of the sample g/cm^3), and g is the acceleration due to gravity (m/s^2).

3.3.5.2. Point Load Index Test

The test was carried out in accordance with ASTM D 5731 (1995) specifications to measure the strength of irregular rock samples collected from the field investigations, and it was also carried out on an irregular rock sample with natural moisture content. The procedure of the point load index test is described as the follow (as shown in figure 3.4B below).

The PLI test technique begins with collecting a representative rock from the fieldwork, often in the shape of an irregular lump. It is crucial to ensure that the specimen is free of visible weaknesses such as bedding planes or fractures. Irregular rock samples were broken down into an appropriate shape and size as the scale of the point load testing apparatus using a geological hammer and chisel. Before beginning the test, the irregular rock samples' height (H), length (W1), and width (W2) were measured, and it is placed into the Point Load Testing Machine between two conical loading platens. Conical platens apply a force to the specimen perpendicular to the loading axis until failure occurs, resulting in a pair of fragments. Upon the occurrence of this failure, the failure load (P) was recorded, whereas the equivalent core diameter (D) obtained from sample dimension during the test. Then, uncorrected point load index (Is) was determined from failure load (P). The data is then used to calculate the Point Load Strength Index ($Is_{(50)}$) and consequently, the Uniaxial compressive strength (UCS) of the rock samples from the equation **(2.18)** and **(2.19)** respectively.

3.3.5.3. Water Absorption Test for Rocks

The test was conducted according to the standard by American Society for Testing and Materials (ASTM D6473-10, 2010). In the test, the weight of the basket in air is measured and noted as $\mathbf{W_1}$. A 2-kilogram sample of irregularly broken rock is properly cleaned to eliminate fines, then drained, put in a wire basket, and submerged in distilled water for at least 5 cm above the top of the basket at a temperature between 22 and 32 ^oC as shown in figure (3.4A) below. After immersion, the sample's trapped air is evacuated by raising the basket holding it 25 mm above the tank's bottom, and letting it fall at a rate of roughly one drop per second. For the following 24 hours, the basket and rock sample must be entirely submerged in water.

A temperature range of 22° to 32°C is used to weigh the basket and the sample while they are submerged in water. It is noted that the weight when suspended in water **= W_2.** The rock samples are transferred to the dry absorbent fabrics once the basket and rock samples have been removed from the water and have allowed enough time to drain. The empty basket is then jolted 25 times in the water tank before being weighed there = **W_3 .** The rock samples applied to the absorbent clothing are surface dried until the cloth is unable to absorb any more moisture. The rock samples are then moved to a second dry cloth and spread out in a single layer, where they are left to dry for at least 10 minutes or until the surface is totally dry. After that, the aggregate is weighted = **W_4 .** The irregularly broken rock sample is placed in a shallow pan and kept in a 110° C-maintained oven for 24 hours. Once it has finished cooling in an airtight container, the oven is turned off = **W_5** .

Where weights of saturated and basket irregularly broken rock suspended in water are W_2 and W_3, respectively. The weights of saturated surface dry irregularly broken rock suspended in air and the weight of oven-dry aggregate are W_4 and W_5, respectively. Weight of the saturated aggregate in water = $W_2 – W_3$, Volume of the aggregate in water = W_4 - ($W_2 – W_3$). The Water absorption, bulk specific gravity, bulk specific gravity (SSD), and apparent specific gravity are determined by using the following equation:

$$\text{Water Absorption} = \frac{W_3-W_1-W_5}{W_5}\, x\ 100 \quad \textbf{(3.5)}$$

$$\text{Bulk Specific Gravity(SSD)} = \frac{W_3-W_1}{(W_3-W_1)-(W_4-W_2)} \quad \textbf{(3.6)}$$

$$\text{Bulk Specific Gravity} = \frac{W_5}{(W_3-W_1)-(W_4-W_2)} \quad \textbf{(3.7)}$$

$$\text{Apparent Specific Gravity} = \frac{W_5}{W_5-(W_4-W_2)} \quad \textbf{(3.8)}$$

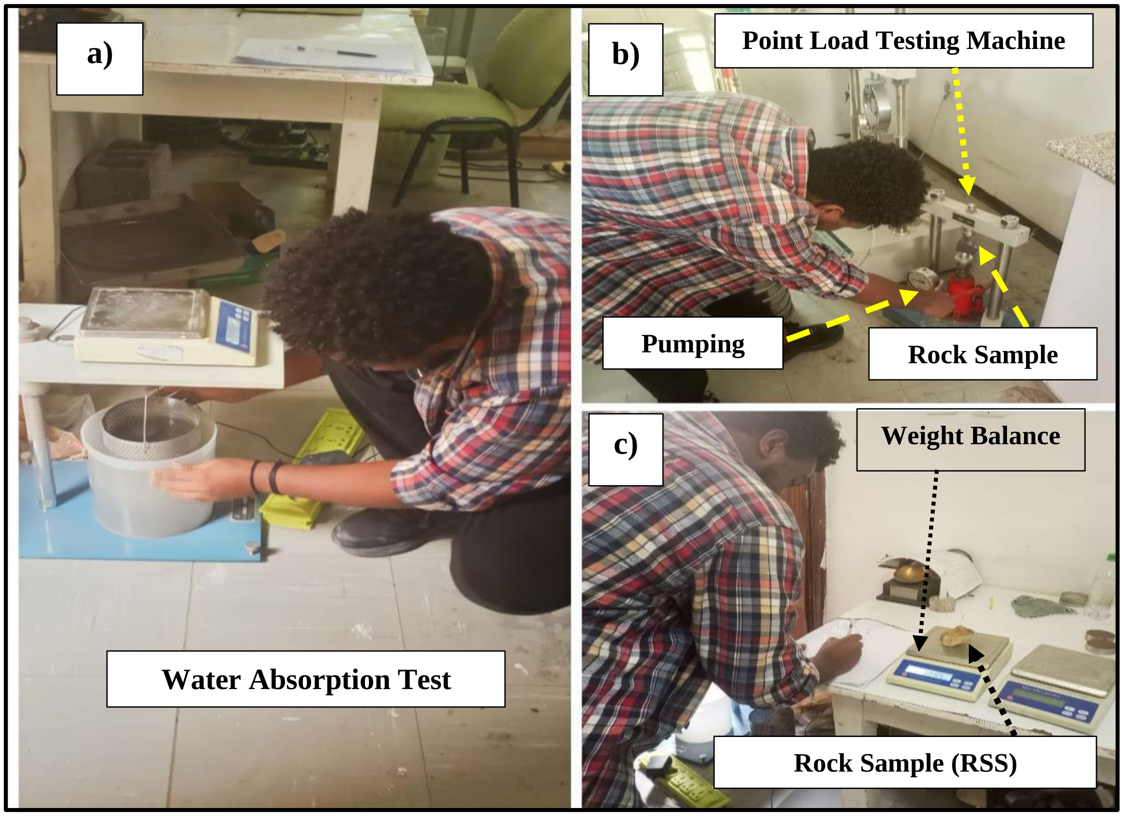

Figure 3.4. Rock laboratory tests. a) water absorption tests, b) point load index tests, and c) unit weight determination.

3.4. Secondary Data Collection

Secondary data from the dam site's subsurface investigation, including borehole logging and core sampling performed during the geotechnical drilling process, permeability data (packer test results and falling head permeability test), and laboratory investigation results such as specific gravity, water absorption, unit weight, strength test (point load index test), and slake durability, were collected from the Engineering Corporation of Oromia (ECO). As a result, three boreholes of various depths were drilled for direct exploration of the subsurface condition using section logging and permeability testing. The location and depth of boreholes are shown in Table 3.4. Consequently, core logging, RQD, and geological data for each borehole were extracted from the relevant project's borehole geological log data. These boreholes' falling head permeability and water pressure tests were also utilized to investigate the dam site's water-tightness condition. The packer test was used for generally competent rock formations, whereas the falling head permeability test was employed for highly weathered and fractured rock formations and soils.

In addition to the subsurface investigation, the secondary data of surface investigation of the reservoir area including the Atterberg limits, compaction test, and permeability test.

Table 3.4. Location and depth of drilled boreholes at the dam site.

Borehole Site	Location	BH-ID	UTM coordinates (Adindan Zone 37N)		Depth(m)
			Easting	Northing	
Dam Axis	Left abutment	BH3	532534	1057807	25
	River Center	BH2	532589	1057833	23
	Right Abutment	BH1	532641	1057860	25

3.5. Rock Mass Classification Methods

Although there are other ways to classify surface rock outcrops in the study area, this research will employ the rock quality designation (RQD) from the volumetric joint count method, rock mass rating (RMR), and geological strength index (GSI) approach to characterize the rocks at the dam site and reservoir area. In order to determine the surface rock exposure quality in terms of RQD, the indirect method volumetric joint count method was used (Palmström, 1982; Bieniawski, 1989). In determining the RQD of rock outcrops using the volumetric joint count method (Jv), the number of joints as joint sets by counting and joint spacings were determined using a ruler and tape meter. Then the Jv values were calculated using equation (2.4), and the RQD values were estimated using equation (2.2).

After determining the RQD values of the rock mass, the following rock mass classification is the rock mass rating (RMR). During the field investigations, the Schmidt hammer rebound values were used to determine the uniaxial compressive strength of rock mass. The point load index test on rock samples was conducted to determine the uniaxial compressive strength of intact rocks in the laboratory. In the case of utilizing the UCS values of the rocks for rock mass classifications, the UCS values obtained from the point load index test were used as the input parameter for the rock mass rating (RMR) classification system since the UCS values estimated from the Schmidt hammer rebound values can be compromised by the influences of the discontinuity conditions beneath the tested surface of the rock masses. The discontinuity survey data such as spacing, orientation (dip amount and direction), condition of discontinuities (length/persistence, separation/aperture, roughness, infilling materials, and weathering), and groundwater condition that were collected during the fieldwork were used as the input parameters for rock mass classification of rock outcrops at the dam site (Bieniawski, 1989).

Consequently, the data such as RQD, discontinuity survey data, and UCS from the point load index test are then changed into the rated parameters. The RMR basic was calculated using the equation (2.5).

According to Hoek and Marinos (2000), visual observation and assessment of the surface rock quality can be used for the characterization of rock masses in terms of geological strength index (GSI) using the GSI basic chart. GSI can also be determined by using the equation (2.17). Further, GSI value can be used in determining the shear strength parameters in the RocData software.

3.6. Determination of Shear Strength and Deformation Modulus Parameters

Depending on the rock materials' strength and the discontinuities' features, shear strength parameters are the most significant factors that influence the stability of the rock slope. RocData software was used to evaluate the shear strength and modulus of deformation of dam site rock masses using Generalized Hoek-Brown Failure criteria (Hoek et al., 2002). This software employs GSI, material constant of intact rock (mi), UCS of intact rock, and disturbance of factor (D) to determine the geo-mechanical properties of the rock mass. As a result, in this case, GSI was estimated from field observation, and the UCS of intact rock was calculated using the point load index as input data. Similarly, the material constant of intact rock (mi) was taken from the RocData software's standard table. The disturbance factor value (D) is determined by the degree of disturbance in the rock mass caused by the excavation method. Its values range from 0 to 1 for undisturbed in situ rock masses and 1 for extremely disturbed rock masses, as built into the RocData software. In this study, the disturbance factor used is 0.7.

RocData software (Rocscience, 2004b) was also used to calculate the rock joints' shear strength parameters (cohesion and friction angle) along the discontinuity failure plane for structurally controlled slope sections, based upon the empirically derived correlation described by (Barton, 1973) which has already been integrated into RocData software given in the equation below.

$$\boldsymbol{\tau = \sigma_n \tan\left[JRC\log_{10}\left(\frac{JCS}{\sigma_n}\right) + \emptyset_r\right]} \qquad \textbf{(3.10)}$$

Where JRC is the joint roughness coefficient, JCS is the joint wall compressive strength, and τ is the peak shear strength (in MPa), σn is the effective normal stress (in MPa), and ϕ_r is residual frictional angle.

According to the shear strength criteria for rock joints (Barton and Bandis, 1990), the basic input parameters of the RocData software (Rocscience, 2004b) include the residual friction angle (ϕr), the joint roughness coefficient profile (JRC) profile, the joint wall compressive strength (JCS), the slope height, and the unit weight of the rock. The uniaxial compressive strength (UCS), determined from the Schmidt rebound value (R) on an un-weathered rock surface with unit weight (γ), represents the joint wall compressive strength of the rock (JCS) (Barton and Bandis, 1990). According to Sharma et al. (1999), the joint wall compressive strength becomes a fraction of the uniaxial rock compressive strength of approximately equal to UCS, 0.75UCS, 0.5UCS and 0.25UCS for unweathered, slightly weathered, moderately, and highly weathered joint wall of rocks. In this case, JCS was determined considering all the rock joint wall condition of moderately weathered joint walls with value of 0.5UCS. The JRC value was determined visually during fieldwork by comparing the appearance of the discontinuity surface to the standard joint roughness profile developed by (Barton and Choubey, 1977). The base friction angle value (ϕb) for basalt ranges from 35º to 38º for most smooth and un-weathered rock surfaces (Barton and Choubey, 1977).

3.7. Evaluation of Bearing Capacity of Rock Mass

In this research work, around four empirical equations were used to determine the bearing capacity of the rock masses at the dam site. In case of the determining the bearing capacity of rock mass using empirical equations (equation 2.26) forwarded by Carter and Kulwahy(1992) were calculated using the input parameters like shear strength parameters (cohesion and frictional angle and Hoek-Brown failure criteria constants (mb, S, and *a*). Using the parameters such as Hoek-Brown constant (mb), UCS and Cf1 with value of 1, were used in the equation (equation 2.27) forwarded by Wyllie (1992). Similarly, for the equation (equation 2.28) suggested by Bell (2007) the bearing capacity factors (No, Ncq and Nγq) which were determined using the chart shown in Figure 2.2 (which in turn depends on the slope angle and height, width of foundation, unit weight of rock, and cohesion), and correction factors (Cf1 and Cf2) with value of 1. From borehole at the dam site, one lithological unit was identified at the right abutment borehole BH-1 with the same degree weathering and strength. At the left abutment borehole, one rock unit with wide variation in strength and degree of weathering was identified. Therefore, the bearing capacity of rock mass at the left abutment was calculated as two rock units. Similarly, the bearing capacity of rock mass was also calculated for 5 geotechnical units were also calculated at the river center. The geotechnical rock unit identified at the dam site from the drilled boreholes varies with depth in terms of strength and degree of weathering and fracturing. Using the equation (equation 2.30 and 2.31) given by Bowles (1996), The ultimate and allowable bearing capacity of these geotechnical units were calculated by using the input parameters of average RQD and UCS of each rock unit and the bearing capacity factors are determined using charts as given in Appendix 20.

3.8. Water tightness Assessment Methods

The soil sample from the reservoir area was subjected to laboratory permeability testing. This was followed by packer tests from the in-situ test and surface hydraulic conductivity estimation from discontinuity aperture and spacing. Six (6) representative soil samples collected from the test pits were subjected to a laboratory permeability test to ascertain the soil deposits' permeability of coefficient. Equation (2.22) was derived by Snow (1968) and Louis (1974) to determine the hydraulic conductivity of rock mass in both dam abutments. It relates hydraulic conductivity (K) with fracture properties (spacing, S, and aperture, e). Special attention was devoted during the discontinuity surveying data collecting to the orientation of joints conducive to leakage issues. ECDSWC (2022) also conducted packer or water pressure tests in the three boreholes at the dam axis to evaluate dam site water tightness.

3.9. Slope Stability Analysis Methods

Kinematic analysis, and limit equilibrium method were used to analyze the stability of the rock slope for this study. The factor of safety and deformation of the slope sections were established for both dry and saturated situations following the collection of essential data from fieldwork, laboratory, and correlation. When the situation is dry, stability analysis is carried out for this condition under static and dynamic circumstances, considering that the slope section is entirely dry, and that water has no impact on the instability of the slope. The slope was considered saturated, and when water forces formed within the slope, the material determines the safety factor in wet conditions. This water significantly impacts the condition of the slope's instability.

3.9.1. Kinematic Analysis Method

In this study, kinematic analysis of the abutment slopes was carried out for rock slope sections with distinctive discontinuity orientation and strength where possible failure modes were assessed during the fieldwork. Regarding analyzing the rock slope of the abutments in terms of mode of failures, Dips 6.0 software (Rocscience, 2004a) was utilized by inputting the discontinuity data like the orientation of discontinuity and slope faces, and the friction angle, which was measured and collected from the field.

3.9.2. Limit Equilibrium Method

Since the slope stability of the dam site was structurally controlled, after the mode of failures of the slope section are identified and the limit equilibrium method using the deterministic method was used to determine the stability of slope in terms of factor of safety by correlating the force leading the rock mass to fail along the failure surface (driving force) and the force resisting the rock mass to fail (resisting force) (Wyllie and Norrish, 1996; Aprilia and Indrawan, 2014). The modes of rock slope failures are usually identified as discussed earlier kinematic analysis (Wyllie and Norrish, 1996).

In case of determining the factor of safety for planar mode of failure, RocPlane 2.0 software (Rocscience, 2004c) was utilized by inputting the slope orientation, upper slope orientation, failure plane orientation, bench width, slope height, unit weight of rock, waviness, shear strength parameters of joints (friction angle and cohesion), and forces (water pressure and seismic coefficient). Similarly, for wedge mode of failure, Swedge 4.0 software (Rocscience, 2004d) was used by providing the input parameters like slope angle, potential failure plane orientation, slope height, bench width, unit weight of rock, and shear strength parameters (cohesion and friction angle) the factor of safety of slope section with wedge mode of failure was computed.

3.10. Materials Used

For purposes of this research work, the materials used and exploited are described as the following.

The Topographic map, inclinometer compass, GPS, geological hammer, sample bag, tape meter and notebook with pens, pencil, coloured pencils and markers were used for geological modelling and discontinuity surveying during the field work. In addition, mobile phone camera with 64M Quad camera was used to take field photographs and rock outcrops with an enhanced resolution. The type L Schmidt hammer and point load index (PLI) machine were used to determine the uniaxial compressive strength (UCS) of rock mass in the field and intact rock samples in the laboratory. Unit weight determination and water absorption apparatus were used in the laboratory analysis of rocks.

The water content determination, specific gravity, grain size analysis (sieve analysis and hydrometer analysis), Atterberg limits (consistency limits), standard compaction test, direct shear test and falling head permeability test apparatus were used in the analysis of the soil samples in the laboratory.

To produce location map and drainage map, and 3D physiographic map of the study area, the ArcGIS 10.8 software and Surfer 21 software were used respectively. The Strater 5 software was used to prepare the lithological log from the drilled borehole data at the dam site. The RocData 2.0 software was used to determine the shear strength parameters of rock mass and joints. For the slope stability analysis of the study area, Dip 6 software, RocPlane 2.0 software ,and Swedge 4.0 software were used.

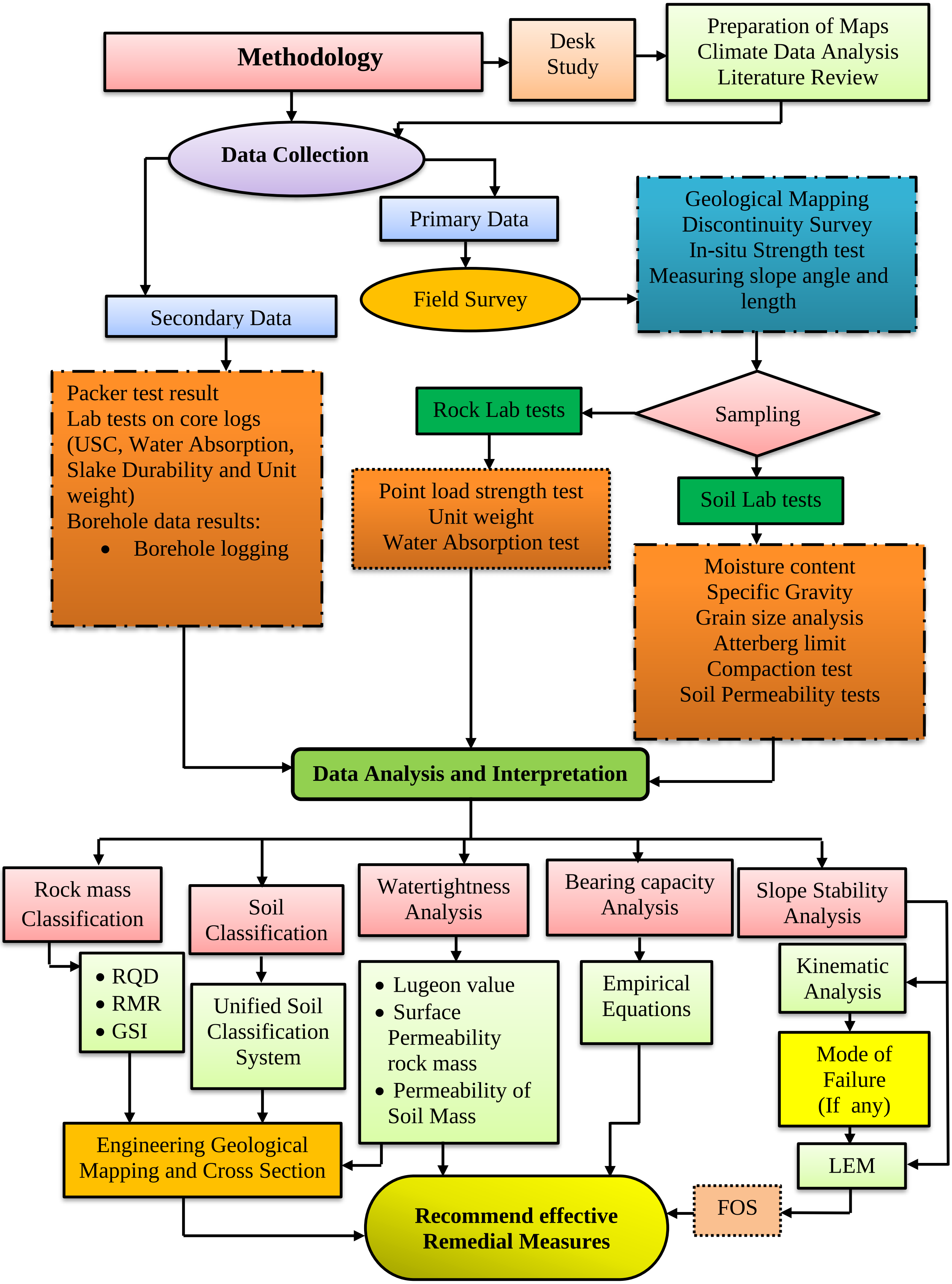

Figure 3. 5. Flowchart of the Research Methodology.

CHAPTER FOUR

4. GEOLOGY OF THE STUDY AREA

In this chapter, location and accessibility, physiography and drainage aspect, climate characteristics, hydrological aspect, seismicity, geological setting of the study area were discussed below.

4.1. Background

Precambrian basement rocks to recent volcanic rocks have been portrayed in Ethiopian geology (Allen & Tadesse, 2003). These lithological units are classified into the geological formations listed below: Precambrian, Paleozoic-Mesozoic, and Cenozoic volcanic rocks and related sediments (Allen and Tadesse, 2003). Precambrian metamorphic and related intrusive igneous rocks are exposed in the country's northern, western, southern, and eastern parts. The Precambrian rocks of southern and southwestern Ethiopia have historically been classified as Lower, Middle, and Upper Complex based on metamorphism grade variation (Kazmin, 1972; Kazmin et al., 1978). Kazmin (1978) developed the first geologic map of Ethiopia at a scale of 1:2,000,000, which was later amended by Tefera et al. (1996).

4.2. Location and Accessibility of the study area

The Bowa Dayole gravity dam project is in Oromia Regional State, North Shewa Zone, Abichugna Wereda, near Dayole Village. The dam site area's geographic location lies within the coordinates between 39º 17' to 39º 18 E Longitude and 9º 33' to 9º 34' N Latitude Adindan Zone 37. The project area is about 120 km from Addis Ababa and accessible through Addis Ababa to Sheno asphalt road, then turning to the left around Sheno and driving on a gravel road to the site.

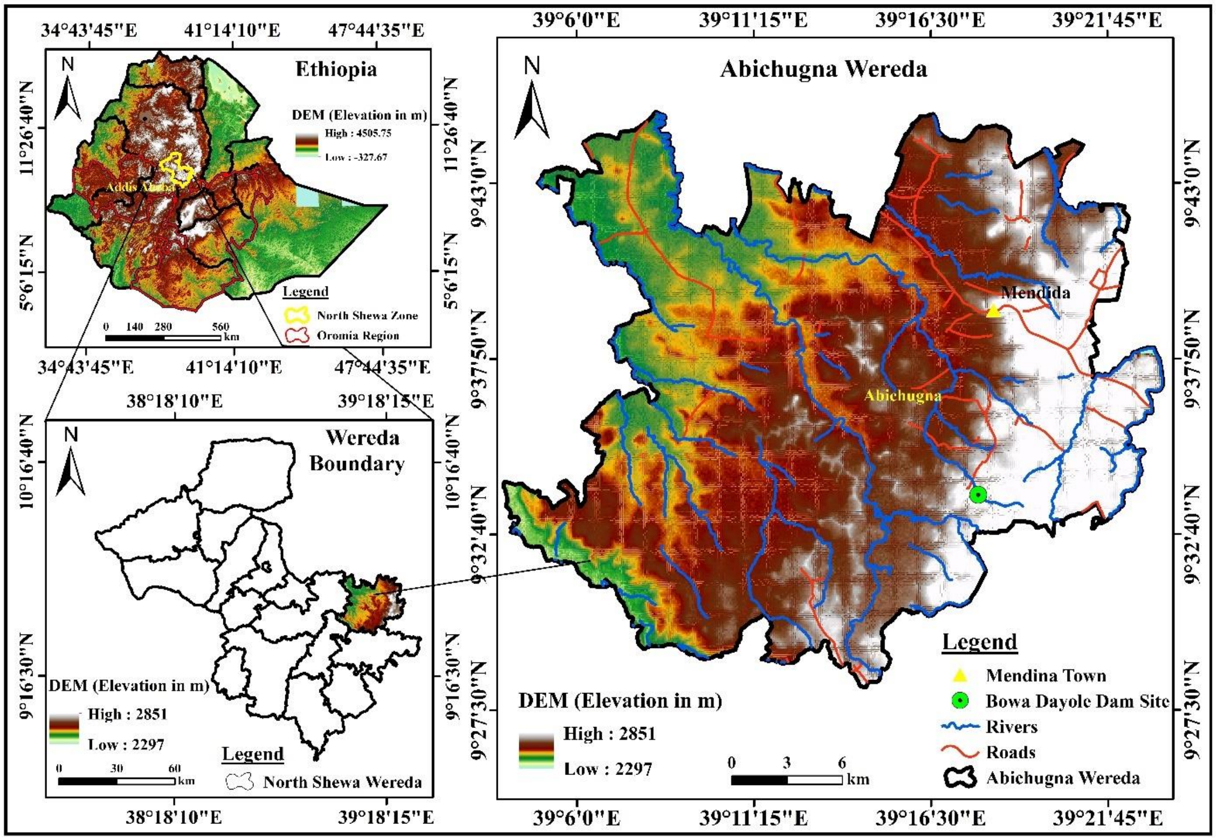

Figure 4. 1. Location and Accessibility map of the study area.

4.3. Physiography and Drainage Aspect of Study Area

The Shewa Plateau is the smallest of the Western highlands, accounting for approximately 11% of the total area of the physiographic region (Bekele, 1993). Almost three-quarters of its land area is above 2,000 meters above sea level. It has the most significant percentage of elevated ground. The elevation ranges from 2300m to 2850m above mean sea level, with an average elevation of 2575m. The research area is distinguished by flat to undulating terrains with flat-topped hills. The study area includes rivers such as the Bilet, Dayole, and Bowa Rivers. The Bowa River is where the dam is planned to be constructed. The dam will be built between two basaltic rock hills with steep slopes at the dam site and gently undulating topography with surrounding hills in the reservoir area. The study area has a dense drainage network featuring parallel, sub-parallel, and dendritic drainage patterns.

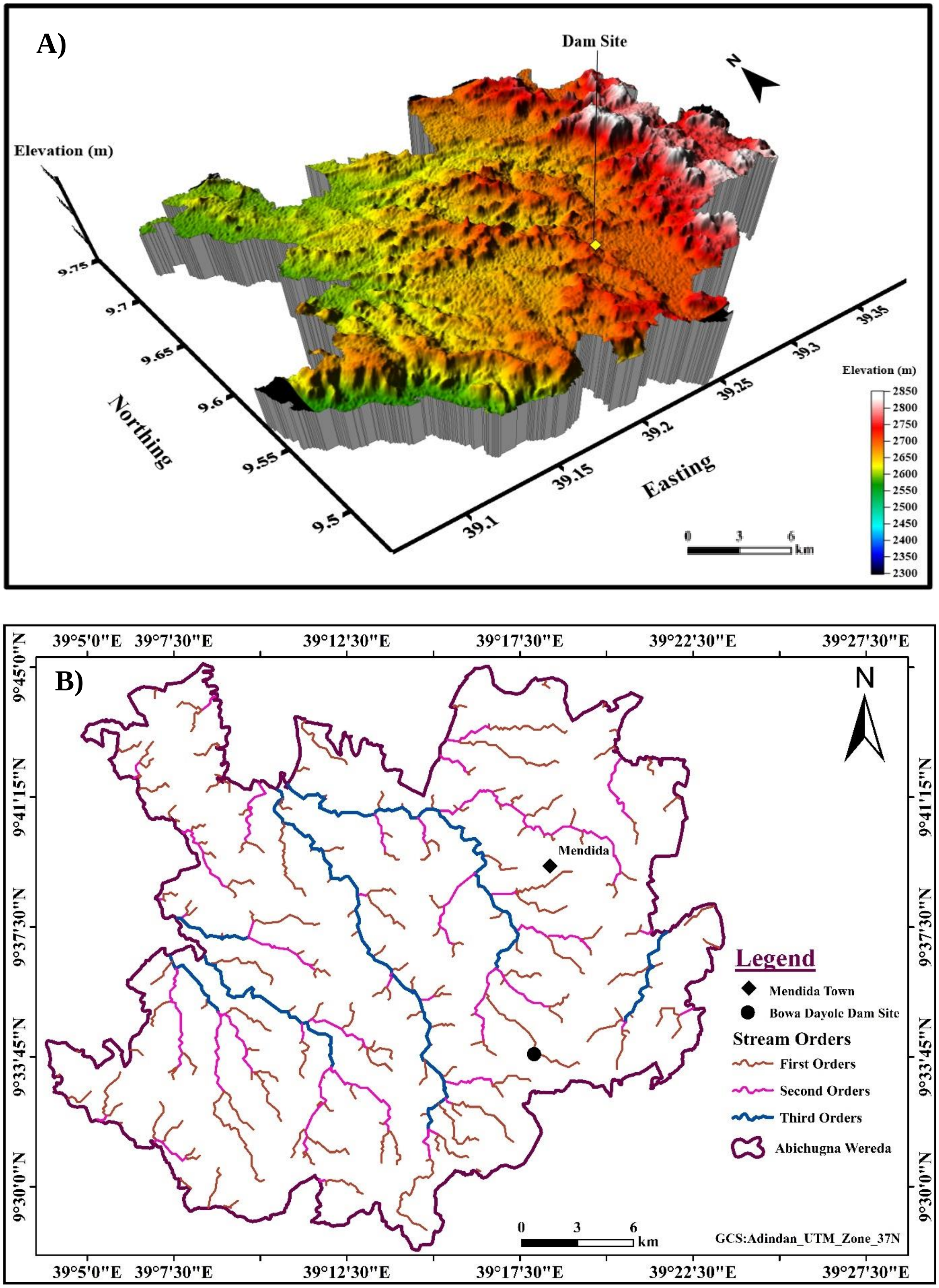

Figure 4. 2. A) Physiographic map of the study area and B) Drainage map of the study area.

4.4. Climate Characteristics of the Area

The Climate data such as rainfall and temperature were collected from the National Meteorological Agency of Ethiopia (NMAE) and analyzed in terms of annual total rainfall/temperature, average seasonal rainfall/temperature, and monthly average rainfall/temperature in 31 years (1990-2021) distribution for Mendida station. Rainfall is a significant dam construction factor (Dhandre et al., 2016). Rainfall amount and distribution in a specific location can considerably influence dam design and construction (Nohara et al., 2011; Naabil et al., 2020). Rainfall is essential because it controls how much water is stored in the reservoir behind the dam (Biswas and Tortajada, 2001). This, in turn, impacts the dam's size and capacity. Rainfall can also have an impact on the dam's stability and its surroundings.

The temperature of the surrounding environment can affect the materials used to construct the dam. For example, extreme temperatures can cause concrete to expand or contract, leading to cracks and other structural issues. Additionally, the temperature can affect the evaporation rate from the reservoir behind the dam, which can impact the water supply for nearby communities (Helfer et al., 2012). It is crucial to consider the temperature patterns in a particular area when designing and constructing a dam to ensure that the materials used are appropriate for the environment and that the dam can withstand temperature fluctuations over time.

Table 4. 1. Climate characteristics of the Study area (Rainfall and Temperature distribution).

Rainfall Distribution of Study Area						
	Annual Total Distribution	**Winter (Bega)**	**Autumn (Belg)**	**Summer (Kiremt)**	**Spring (Tseday)**	**Monthly Average in 31 Years**
Max. (mm)	1374	93.7	266.5	990.5	277.5	320.23
Min. (mm)	202.2	4.1	33.9	442.9	66.4	3.82
Ave. (mm)	974.6	33.41	114.9	677.18	149.12	81.80
Temperature Distribution of Study Area						
Max.(ºC)	293.8	24.88	23.72	24.68	25.96	25.05
Min. (ºC)	251.28	21.59	19.52	20.82	21.64	20.72
Ave. (ºC)	275.05	23.35	21.02	22.95	24.37	22.92

The mean annual rainfall and the monthly average of the study area's rainfall are **974.6 mm** (maximum value of 1374 mm and minimum value of 202.2 mm) and 81.80 mm (maximum value of 320.23 mm and minimum value of 3.82 mm), respectively. The average highest rainfall amount is encountered in the summer season, with the mean value of 677 mm (maximum value of 990.5mm and minimum value of 442.9mm) in June, July, and August. The average minimum rainfall distribution occurs in the winter season, with a value of 33.41mm.

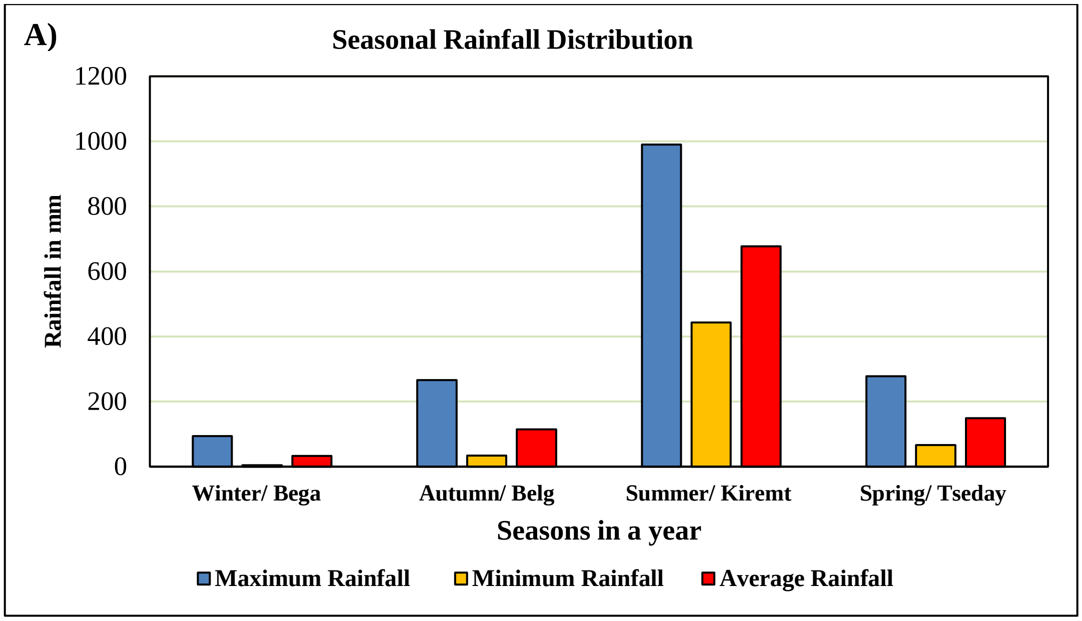

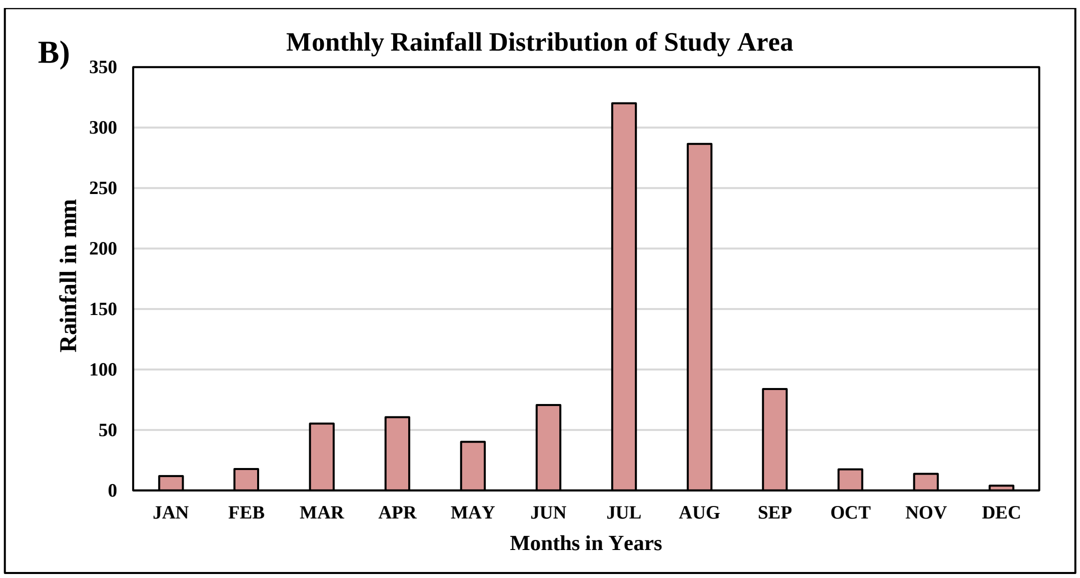

Figure 4. 3. Rainfall characteristics of the study area. A) Seasonal rainfall distribution, B) Monthly rainfall distribution.

The total annual temperature and a monthly average of the temperature of the study area are 275.05 ºC (maximum value of 293.8 ºC and minimum value of 251.28 ºC) and 22.92 ºC (maximum value of 25.05 ºC and minimum value of 20.72 ºC) respectively. The average highest rainfall amount is encountered in spring, which has an average value of 24.37 ºC (maximum value of 25.96 ºC and minimum value of 21.64 ºC).

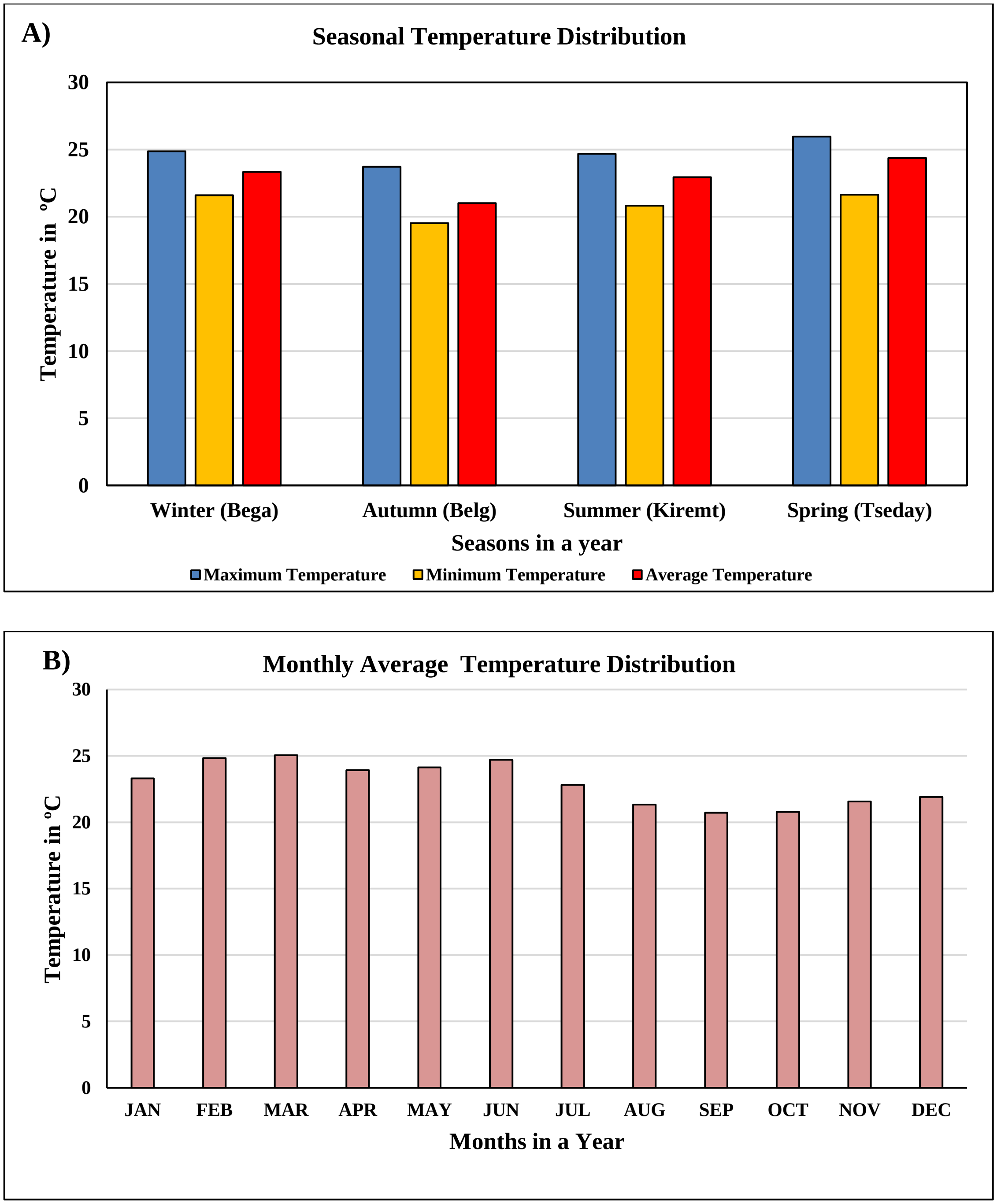

Figure 4. 4. The temperature of the study area. A) Seasonal temperature distribution, and B) Monthly temperature distribution.

4.5. Hydrological Aspects of the Study Area

4.5.1. River flow Estimation for Water Harvesting

According to ECO's Final Report of the Feasibility Study and Detail Design Engineering Report (2022), the streams in the study area have no dry season discharge. This means that there is only flow during the rainy season. The anticipated discharge from the stream has demonstrated the following flow pattern in connection to the area's catchment characteristics and rainfall pattern. The SWAT model analysis determined the mean monthly flow based on the average daily rainfall values obtained from 25 years of data and those local rainfall seasons.

Table 4. 2. Mean Monthly Discharge and Volume of the River (ECO, 2022).

Months	Mean Monthly Discharge (m^3/s)	Mean Monthly Volume (MMC)	Degree of Utilization (MMC)
January	0.01	0.02	**Not Utilized**
February	0.00	0.01	
March	0.01	0.04	
April	0.01	0.03	
May	0.01	0.02	**4.17**
June	0.01	0.03	
July	0.32	0.84	
August	0.47	1.26	
September	0.41	1.05	
October	0.25	0.66	
November	0.12	0.31	
December	0.04	0.11	**Not Utilized**
Average Annual Flow Volume		**4.38**	
Assuming 75% Utilizable Flow			**3.13**

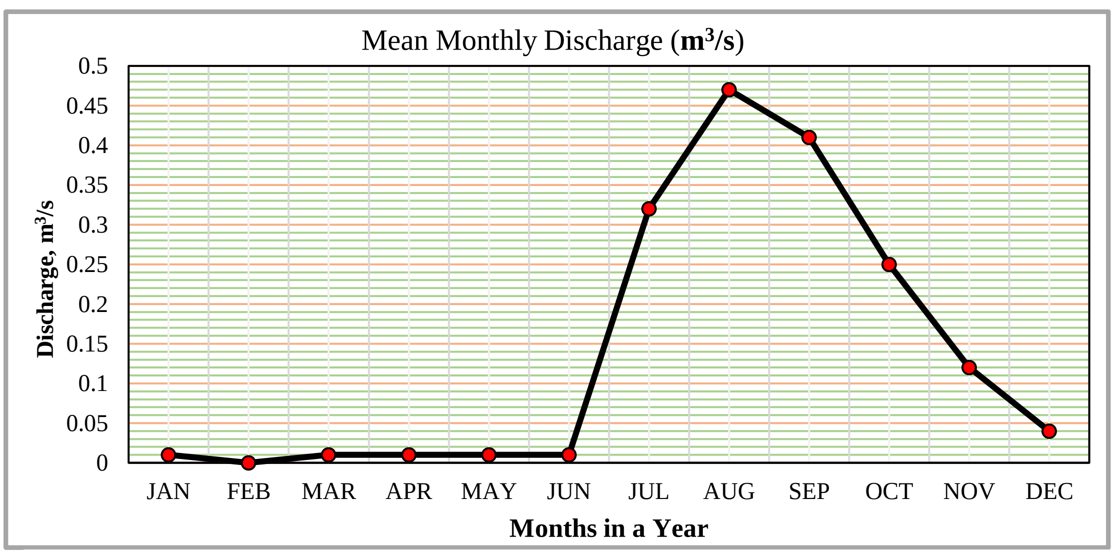

Figure 4. 5. Mean Monthly Discharge of the River (ECO,2022).

4.5.2. Peak Flow of the River

Gumbel's Extreme value distribution from the maximum daily precipitation of each year as input data has been used to forecast flows for 50, 100, 500, 1000, and 10,000 years return periods based on the annual peak flow with the existing soil, land use, cover, and overall characteristics of the catchment. Different return period outputs have been subtracted from the analysis, as shown in the table below.

Table 4. 3. Estimated peak flows for different Return periods (ECO,2022).

Return Period (Years)	Peak Flow (m^3/sec)
50	17.72
100	20.00
500	25.38
1000	27.77

4.5.3. Flow Over the Spillway

Based on the decision of the dam engineer to fix spill way crest level to be fixed at 2746 m elevation to see the head of water based on the peak inflow hydrograph computed for 50, 100, 500, and 1000 years return period on the assumptions tabulated below.

Table 4. 4. Reservoir routing input data (ECO,2022)

Dam Reservoir, Elevation(m.a.s.l)			Area & Volume at FSL	
Riverbed level	**Dead storage level**	**Full supply level**	**Area(ha)**	**Volume (MCM)**
2715	2723	2743	42	1.84

Richard H. Hawkins and Armando Barreto-Munoz of the Rocky Mountain Research Station developed the Excel software Wildcat 5 Rainfall- Runoff Hydrograph Model to resize and determine the extent of the necessary spillway for the rejecting the excess flood coming for various years return period.

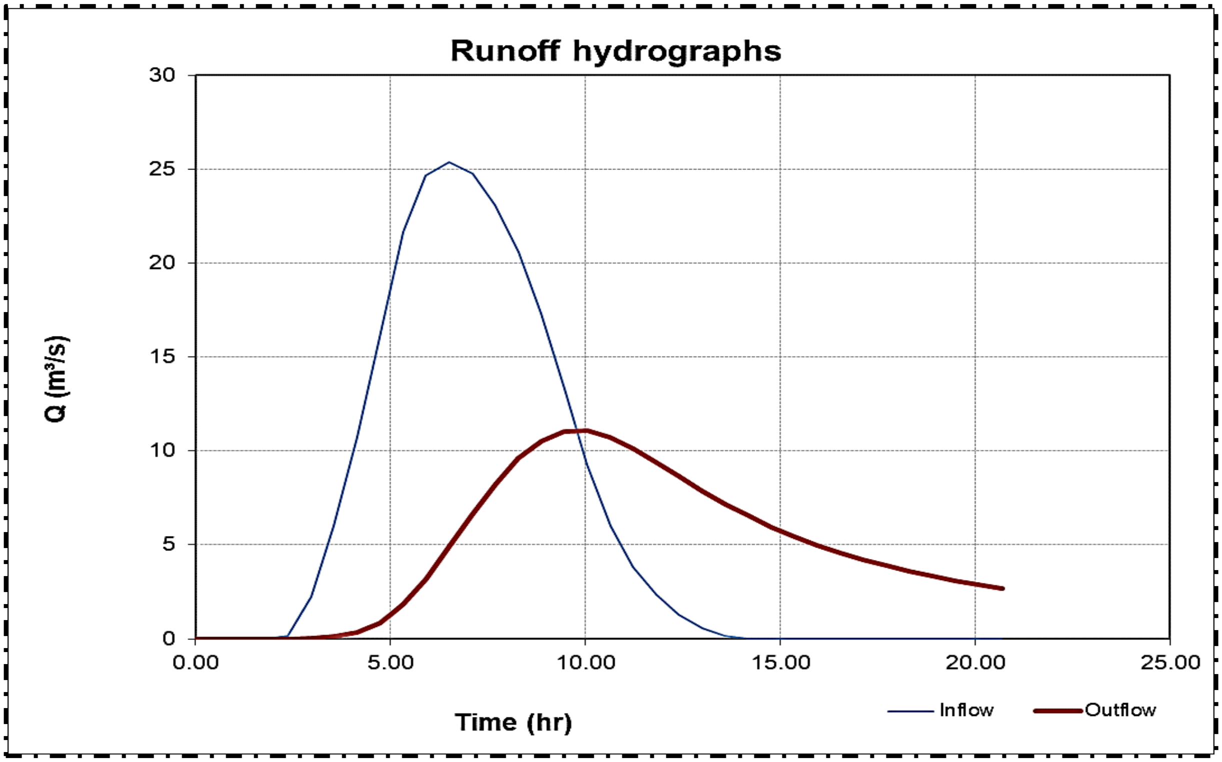

Figure 4. 6. Routed flow of the river (ECO,.2022).

The river's routed flow has been calculated as shown in the table below by using the output data from SWAT software analysis for catchment features calculation of curve numbers and river slope as well as computed peak discharge for various return times.

Table 4. 5. Description of Routed outflow and Depth (ECO, 2022).

Return Periods	Routed Outputs	Spillway Crest Lengths (m)			
		5	10	15	20
50	Outflow(m^3/sec)	4.39	1.74	2.47	3.12
	Maximum Flow Depth(m)	0.64	0.22	0.21	0.20
100	Outflow(m^3/sec)	5.17	8.19	10.25	11.72
	Maximum Flow Depth(m)	0.71	0.61	0.54	0.49
500	Outflow(m^3/sec)	7.12	11.08	13.76	15.56
	Maximum Flow Depth(m)	0.88	0.75	0.66	0.59
1000	Outflow(m^3/sec)	8.03	12.43	15.36	17.36
	Maximum Flow Depth(m)	0.96	0.81	0.71	0.64

High return periods of 500 and 1000 years have been chosen for resizing because to the urgency of the research period and the use of primarily secondary data for analysis. Accordingly, a spillway has been chosen for the specified project based on a 500-year return time with a crest length of 10 meters and a maximum depth of flow of 0.75 meters.

4.6. Seismicity of the Study Area

Dams are constructed to withstand a specific amount of seismic activity, and the seismicity zone determines the level of seismic activity the dam can endure (Wieland, 2008; Wieland, 2014). If the seismicity zone is underestimated, the dam may be unable to sustain the degree of seismic activity in the area, perhaps resulting in failure and disastrous consequences. In addition to ensuring the dam's safety, determining the seismicity zone impacts the dam's design and construction (Paulay and Priestley, 2009). Identifying the seismicity zone is to assess the site's seismic hazard. Seismic hazard refers to the possibility of an earthquake occurring in a specific place and the possible damage caused by this earthquake. Regional seismic hazard or risk map may provide a reliable determination of the seismicity zone (Asfaw, 1992).

The Ethiopian Building and Construction Standard (EBCS-8, 1995) give guidelines for defining the seismicity zone while building a dam. The guidelines consider seismic activity in the area, as well as the geological parameters of the site. The seismicity zone is divided into four categories ranging from low to high, which are seismic-free areas (zone 0) to fewer damaging zones to moderate damage (zone 1 and 2), considerable damage (zone 3), and high-risk areas (zone 4). As a result, in this research work, the seismic hazard map of the country generated by EBCS (1995) was used to determine the study region's seismic hazard rating. This map is based on the estimated amplitude of ground acceleration over 100 years and divides the country into various seismic risk zones based on the history of damaging earthquakes (Gouin, 1970; Asfaw and Woldeyes, 1986).

Table 4. 6. The horizontal seismic acceleration (α0) as per (EBCS-8, 1995) and moment magnitude scale (MMS) as per Johnson and DeGraff (1991) with respect to the seismicity zones.

Seismicity value	Seismicity Zone				
	4	3	2	1	0
α0	0.1	0.07	0.05	0.03	<0.03
MMS	8	7	6	5	<5

The location of Bowa Dayole Gravity Dam site is at the foot of the western margin of the Main Ethiopian Rift (MER). In addition, based on the seismic risk map of Ethiopia, the Bowa Dayole dam site lies in zone 3 in the considerable damage seismicity zone with an intensity moment magnitude scale of 7 and 0.10g of ground acceleration coefficient, or horizontal seismic acceleration (α0), which entails that the dam design must account for the possibility of significant seismic activity that results in cracking, deformation, and even dam failure. The design considerations involve selecting suitable materials, adequate foundation design, and ensuring the dam's components can endure anticipated seismic forces. The dam's foundation and abutment should be constructed to resist seismic forces and reinforced to avoid cracking or failure.

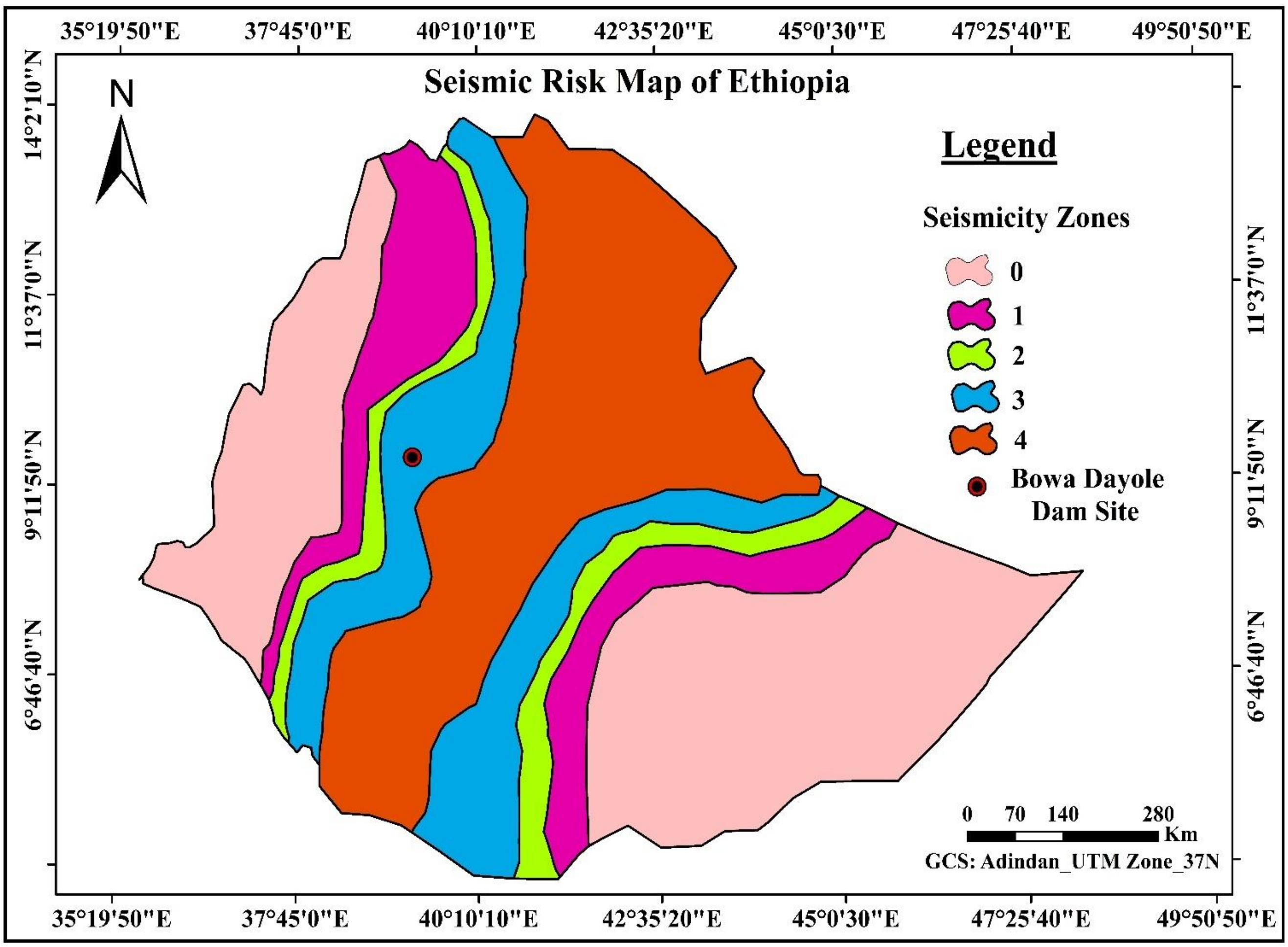

Figure 4. 7. Seismic Risk Map of Ethiopia for a 100-year return period and 0.99 Probabilities (EBCS-8,1995).

4.7. The Regional Geology of the Study area

Several surges of volcanic activity were detected that were associated with or preceded by large tectonic events (Justin-Visentin et al., 1974). The East African swell was caused by the epi-erogenic uplift of the AfroArabian plate during the Early Tertiary. The cause of this uplift corresponds to the decompression of the mantle plume, which resulted in temperature rise and melting. As a result, massive amounts of basaltic magma erupted, resulting in the first eruption of the Ethiopian Flood Basalt Province (Mengesha et al., 1996). However, the currently known geochemical database strongly implies that widespread volcanism, which generated the Trap Basalts of Ethiopia, did not commence until the Late Eocene or Early Oligocene. These early flood basalts have already covered large areas of the NW and SE plateaus. The research site is in the central Ethiopian plateau, which is part of the NW Ethiopian plateau and the western portion of the Main Ethiopia Rift.

Aiba basalt, Alagi rhyolites and basalts, Tarmaber basalt, and Balchi rhyolites make up the Tertiary volcanic rock of the central Ethiopia plateau (Justin-Visentin et al., 1974). The Alagi series consists of interbedded layers of rhyolites and basalts ranging in age from 32 to 16 Ma (Oligocene-Miocene) that overlie the Aiba basalts (34-28 Ma; Middle-Upper Oligocene). The Alagi rhyolites are the first silicic rocks released in the middle eastern Ethiopia plateau, forming a massive ignimbrite block sitting immediately on the Aiba basalts or inter-layered with the Alagi basalts in different quantities (Justin-Visentin et al., 1974). The Aiba basalt is a thick overlay of flood basalts that poured out into the Ashangi peneplain due to distensile crustal activity. Tarmaber Meghezez basalt (Late Miocene) is the name given to the Tarmaber basalt that covers the Oligocene Alagi. With the exception of Tarmaber basalts, the Alagi volcanics, and Aiba basalts were formed by fissural volcanism.

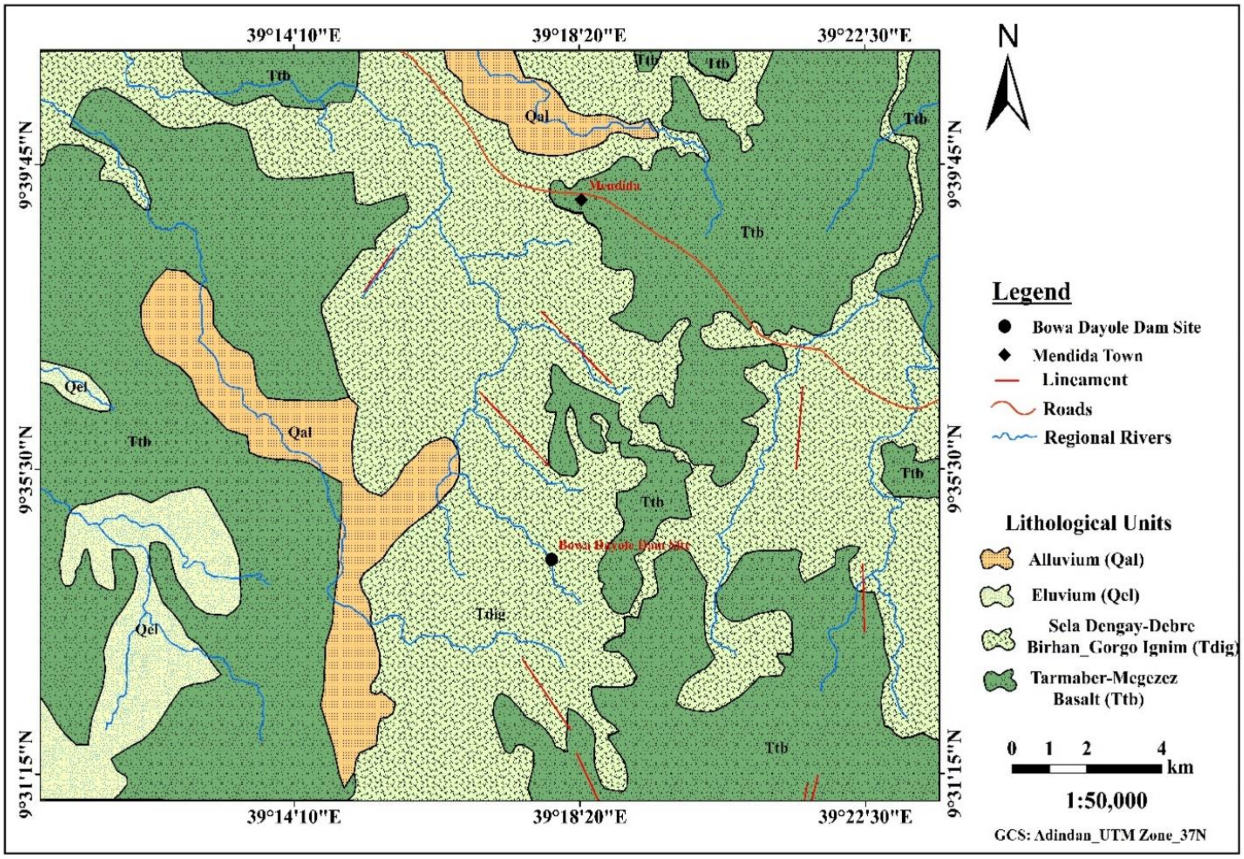

Figure 4.8. The Regional Geological and Structural Setting of the Study Area (After Solomon et al., 2010).

According to Mengesha et al. (1996), the geology of the central Ethiopia plateau consists predominantly of alkali basalts with interbedded pyroclasts, and rare rhyolites erupted from fissures. The upper part of these groups is more tuffaceous, containing lacustrine deposits, including lignite seams and acidic volcanics. The study area regional lithology comprises of alluvium (Qal), Eluvium (Qel), Tarmaber-Meghezez basalts (Ttb), and Sela Dengay-Debre Birhan Gorgo Ignimbrite (Tdig) and the regional structures of the study area are characterized by the lineaments having three distribution trends of SSW-NNE, NNW-SSE and N-S directions.

4.8. Local Geology of the study area

During the fieldwork investigation, four lithological units were identified and described in terms of their colour, texture and rock type in the study area. The identified lithological units are colluvial deposits, alluvial deposits, welded tuff, and aphanitic basaltic rock.

4.8.1. The Colluvial Deposits

Colluvial deposits are a loose accumulation of sediments, soil, and rock fragments that have been transported and deposited on heel slopes or at the base of slopes by gravity-driven processes such as slope failure, creep, or surface wash of slopes. They typically form in locations with steep and rocky terrain, and the material can range in size from fine-grained soil to massive boulders. Colluvial deposits cover the base of the dam abutments on both the upstream and downstream sides of the dam site in the study area as shown in Figure 4.9.

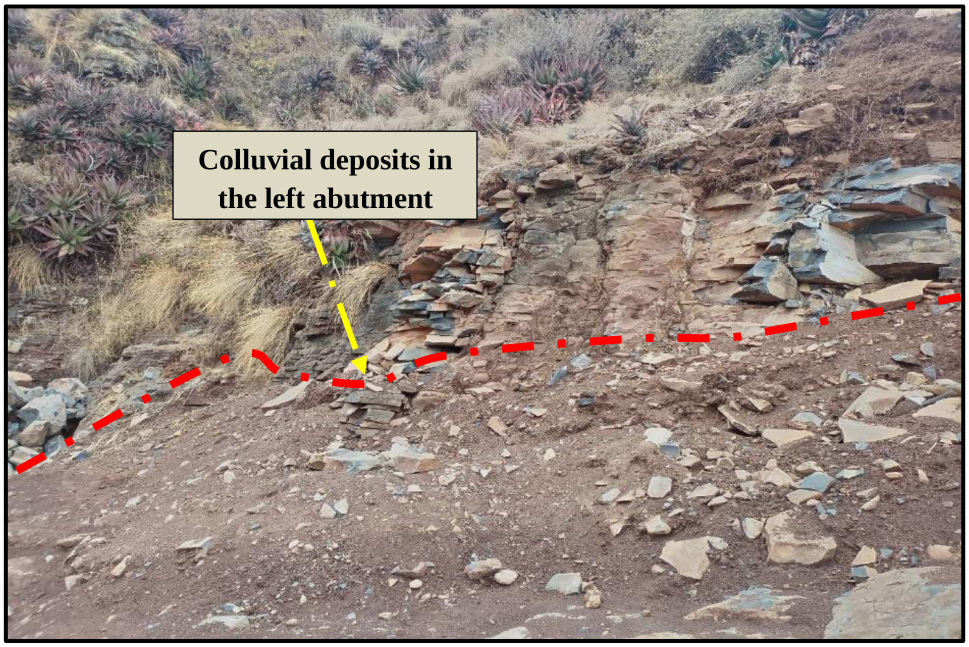

Figure 4.9. Colluvial deposits in the study area.

4.8.2. The Alluvial Deposits

Alluvial deposit refers to a type of sediment that accumulates on the surface of the Earth in the form of sand, gravel, silt, or clay. These deposits are formed by the action of water, such as rivers, streams, or coastal waves, which erodes and transports rock and other materials from one location to another. In the study area, the alluvial soils are deposited covering the Bowa river areas of the dam reservoir and downstream side of the dam as shown in Figure 4.10.

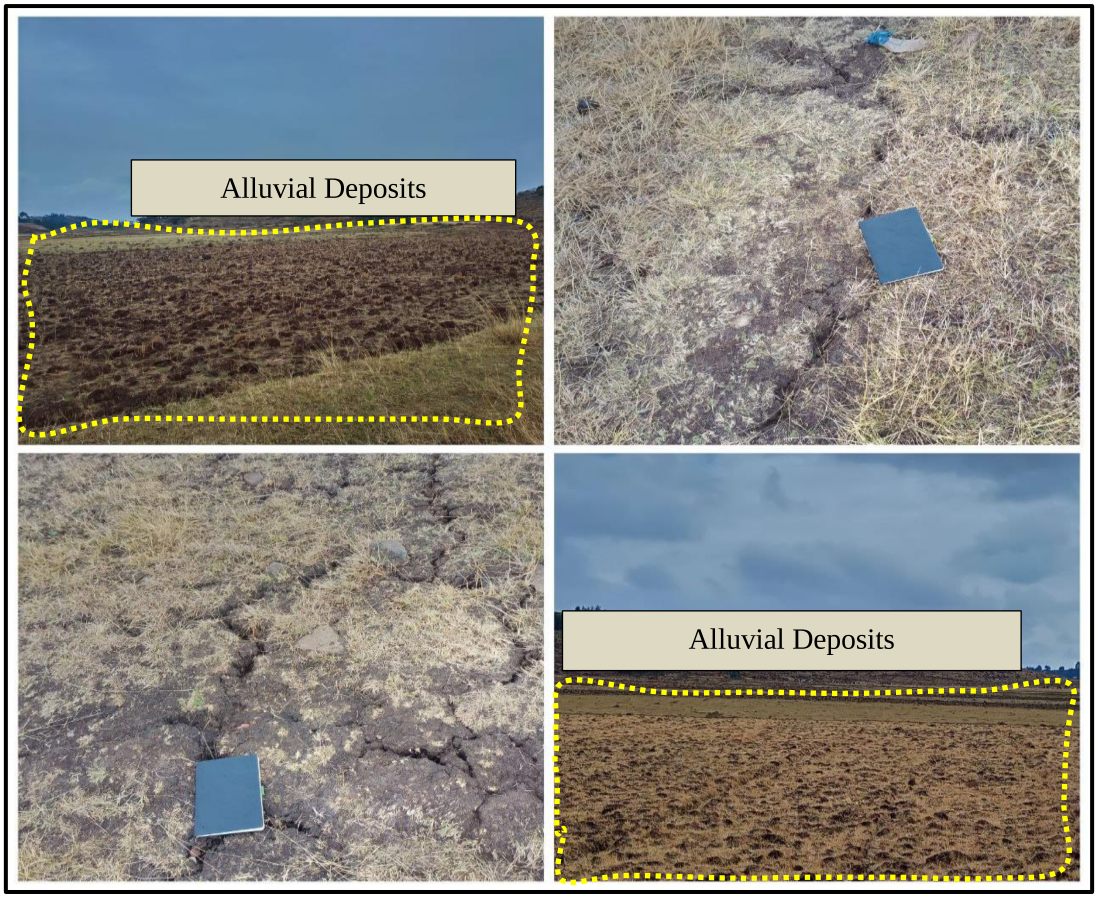

Figure 4.10. The Alluvial deposits of the study area.

4.8.3. Welded tuff

Welded tuff is a type of rock that forms when volcanic ash and other volcanic materials fall to the ground during a volcanic eruption and become compacted, heated, and partially fused together. This process is known as welding, and it causes the individual particles of ash and debris to become firmly cemented together, creating a strong and solid rock mass. Welded tuff is typically found in areas with past volcanic activity and can be recognized by its overall structure, color, and texture. The welded tuff in the study area is exposed by stream cut and covers most part of the reservoir area. It has a moderate weathering condition with colour of greyish white.

Figure 4. 11. Welded tuff exposure in the reservoir area.

4.8.4. Aphanitic Basalts

In the study area, the aphanitic basalts cover the dam site in both the abutment and left reservoir rim and are exposed by stream cut and excavation process. The aphanitic basalts in the right abutment have fine-grained texture, black in colour and the weathering and fracturing condition ranges from slightly weathered to moderately weathered and moderately fractured rock mass as shown in Figure 4.5a, and the aphanitic basalts in the left abutment differ from the right in terms of the fracturing and weathering. Its fracturing condition ranges from moderately to highly fractured and weathering condition entails the highly fractured and weathered rock mass as shown in Figure 4.12b. The aphanitic basalts in the left bank of the reservoir are slightly fractured and weathered rock mass exposed in gentle slope topography with a flattened top surface.

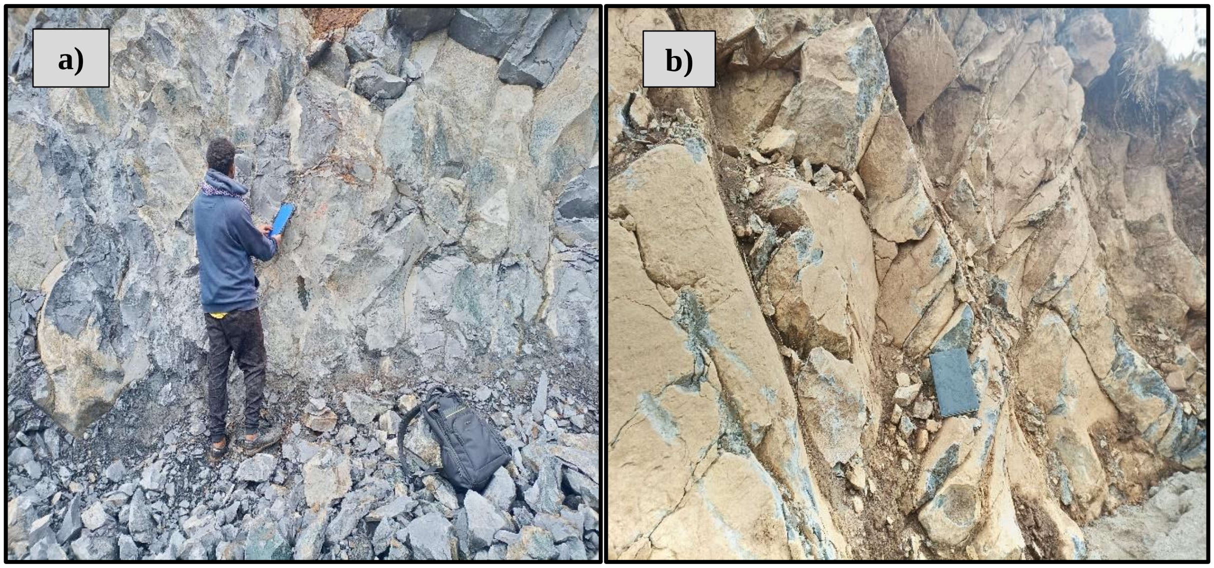

Figure 4.12. The aphanitic basalts: a) excavation exposure in the right abutment, b) stream-cut rock outcrops in the left abutment.

4.9. Geological Structures of the study area

4.9.1. Joints

As a result of numerous stresses, including variations in temperature, pressure, and rock composition, joints in rocks are natural fractures or fissures that appear in geological formations (Aguilera, 1998). According to Gabrielsen and Braathen (2014), joints differ from faults in that they often do not entail any considerable displacement or movement of the rock layers on either side of the fracture. Joints may provide passageways for liquids (like water) to move through rocks, affecting engineering projects like tunnels or foundations as well as the distribution of natural resources.

In the study area, the dominant geological structures are joints. The joints in the study area are characterized by different properties such as orientations, roughness, persistence, spacing, infilling, and weathering condition. The two joint sets in the right abutments of the dam site have a strike direction of E-W and ENE-WSW, moderately weathered and rough with an average spacing of 36cm, and no infilling in some but hard in filling in some. The two joint sets in left abutments have the strike direction of ENE-WSE and N-S, moderately weathered and rough with an average spacing of 27cm and no infilling in some but soft infilling like clay soils in some. Consequently, the geological structures of the study area are joints accompanied by some random fractures.

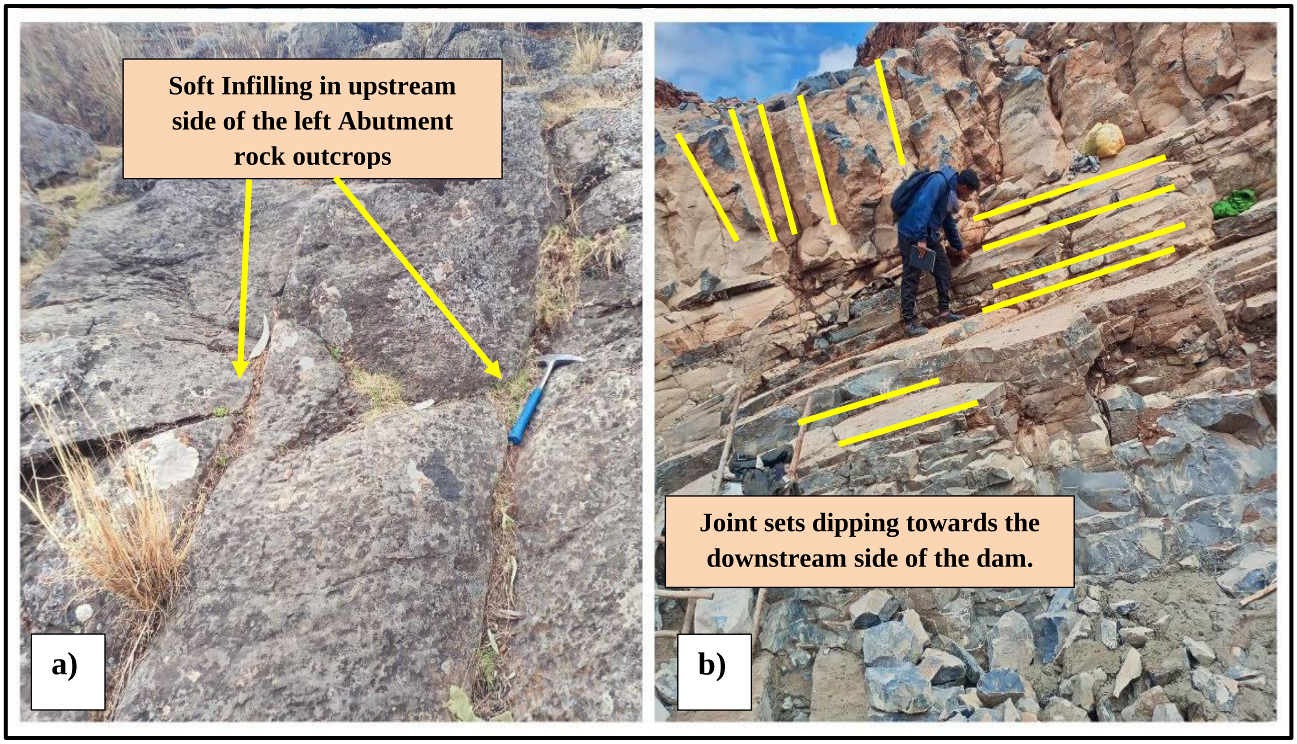

Figure 4.13. Joints and their representative description of the dam site. a) joint sets at the upstream side of left abutment and b) joint sets at the dam axis of left abutment dipping towards the downstream.

A)

B)

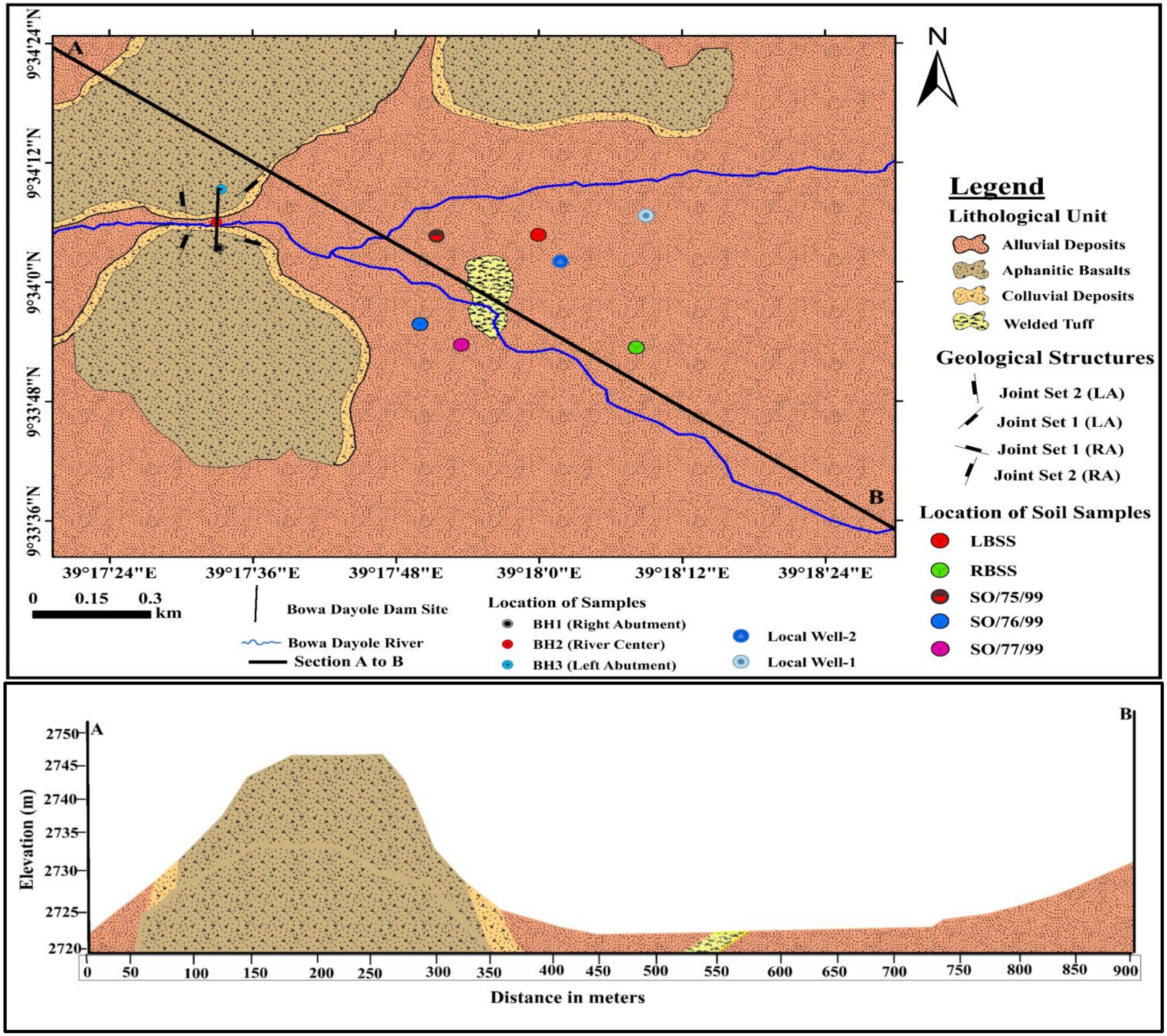

Figure 4. 14. Geological Setting of the study area. A) Geological map. B) Geological Cross Section

CHAPTER FIVE

5. RESULT AND DISCUSSION

5.1. Introduction

The fundamental aspect of dam site investigations is engineering geological characterization of soils and rocks in the study area, which involves systematically studying the geological materials, their physical and mechanical properties, and the nature of the terrain to assess the site's suitability for dam construction. This aids in predicting and mitigating geological and geotechnical problems that may affect the dam's safety, performance, and economy. In this study, the engineering geological evaluation of rocks and soils of the dam site and its reservoir is utilized with the integration of geological investigation of the study area during the fieldwork. Before assessing the engineering properties of soils and rocks, it was necessary to undertake fieldwork to determine the regional and local geology, joint and structural conditions, and groundwater conditions. Field mapping, drilling, sampling, and laboratory testing were employed to understand the dam site comprehensively. The collected data were analyzed to classify soils and rocks, comprehend their stratigraphy and structural features, and evaluate material durability, compatibility, and the potential for slope instability.

The stability of engineering structures is usually based on the engineering property of soils and rocks, such as strength, permeability, and deformability characteristics. The engineering properties of soils and rocks were characterized and classified by employing data from the fieldwork and laboratory testing like water content determination, specific gravity test, grain size analysis (sieve analysis and hydrometer analysis), and consistency limits. Here, the grain size analysis and hydrometer analysis were used to classify the soils in the study area in terms of plasticity and soil group. The permeability test of the soil samples was utilized to determine the watertightness of the reservoir area.

5.2. Engineering Classification and Characterization of Rock Mass

The engineering geological evaluation of rock masses at the dam site was characterized and classified in terms of surface and subsurface characterization and classification. The surface engineering geological characterization of rock masses was carried out through rock mass classification and further assessment of the engineering properties by the implication of rock mass classification systems and discontinuity survey analysis. The engineering properties of the rock masses were adopted from the field investigation and laboratory analysis of the representative rock samples. The subsurface characterization of the rock masses was carried out using secondary data such as geotechnical drillings and packer tests at the dam site.

5.2.1. Surface Classification and Characterization of the Rock Mass

5.2.1.1. Characterization and Orientations of the Discontinuity

During fieldwork, discontinuity data such as joint spacing, alignment, texture (openings, fill material, and roughness), and number of joints were collected and analyzed on the exposed rocks on the slope face of the two abutments. These discontinuity data are used for slope stability analysis, water tightness assessment, and rock mass classification as basic input parameters for calculating rock mass values and determining the engineering properties of the rocks.

The characteristics of the discontinuities at the dam site vary left to right in the discontinuity condition. Many of the discontinuities at the right abutment of the dam site are characterized by the average spacing ranging from closely to moderately spaced, orientation ranging from vertical to sub-vertical, rough surfaces, and tight to open with no infilling materials as the shown in Table 5.1. In left abutment, the majority of the discontinuities are characterized by average spacing ranging from closely to moderately spaced, vertical to sub-vertical orientation, rough surfaces and tight to open with soft infilling materials like clay soil as the shown in Table 5.1.

Table 5.1. Joints characteristics of the study area.

Joint Sets	Right Abutment		Left Abutment	
	JS1	**JS2**	**JS1**	**JS2**
Spacing of joints (cm)	5-65	5-15	40-50	5-15
Aperture(mm)	1.0-3.0	1.0-2.0	1.5-2.5	1.0-2.0
Persistence (m)	Greater than 10	Greater than 10	Greater than 10	Greater than 10
GW condition	Completely dry	Completely dry	Damp	Damp
Infilling	Open, No Infilling	Open, No Infilling	Open, No Infilling	Soft, fine material (Soil)
Degree of Weathering	Moderate	Moderate	Moderate	Moderate
Roughness	Rough	Rough	Rough	Rough

From the discontinuity survey during the fieldwork, in the right abutment there are two dominant joint sets with joint orientation of NE-SW (JS1) and NNW-SSE (JS2) strike directions. Similarly, in the left abutment there are also two major dominant joint sets with the joint orientation of WWN-SSE (JS2) and W-E (JS2) strike directions.

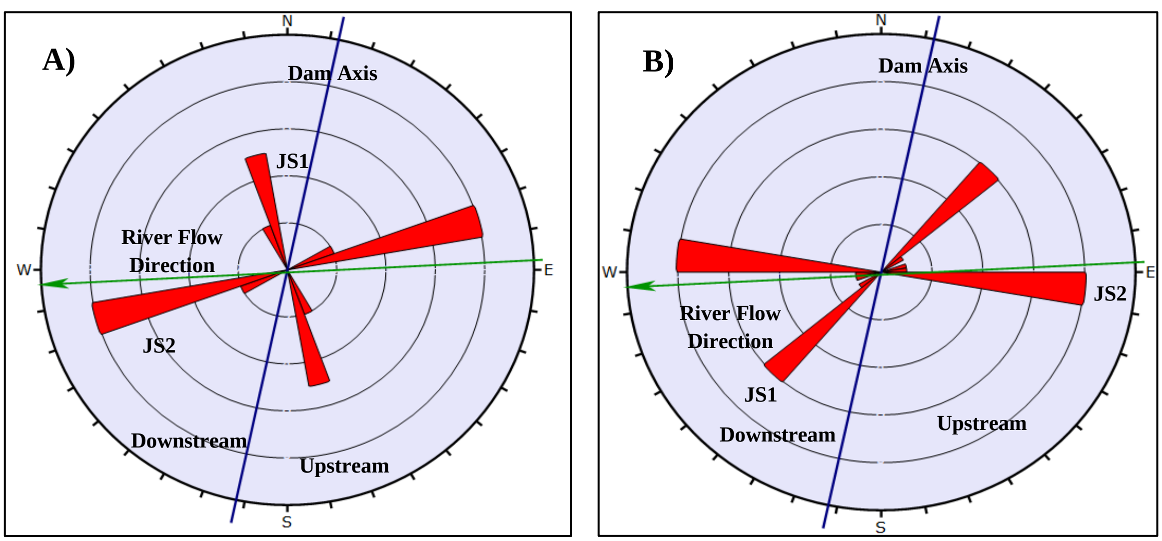

Figure 5.1. The Rosette Diagram of the discontinuities with respect to the Dam Axis and River Flow Direction. A) Right Abutment, B) Left Abutment.

From the Rosette diagram of the right abutment, Joint set 2(JS2) and left abutment, joint set 2 (JS2) are very favorable orientation for leakage of water through the discontinuities since their strike direction is near parallel to the direction of the river flow and the joints are dipping towards the downstream as shown in Figure 5.1. As shown in Table 5.1, Joint Set 2 at the right abutment have no infilling and Joint set 2 at left abutment have soft infilling mostly soil which could result in leakage of water by integrating with the joint orientation. Such joint sets can also affect the overall structure of the dam and operational life of the dam. Therefore, both dam abutments may require special treatment during the construction stage to prevent potential leakage.

5.2.1.2. Laboratory Analysis of Rock Samples

Three laboratory tests, such as point load index, unit weight, and water absorption tests, were conducted on three rock samples to characterize surface rock masses.

The unit weight test was conducted on the rock samples from the left and right abutment and reservoir areas. The test was carried out per the standard ISRM (1978) suggested using buoyancy techniques. The unit weight value of the rock samples can be used as an input parameter in rock slope stability analysis and as an input parameter in determining the UCS value from the Schmidt rebound value. The test results show that the welded tuff rock samples from the reservoir area (RSS) have a dry unit weight and saturated unit weight of 15.02KN/m^3 and 15.58KN/$m^{3,}$ respectively. The test conducted on aphanitic basaltic rock samples of both the right and left abutments of the dam site (RARS) and (LARS) revealed the dry and saturated unit weight values of 28.15 KN/m^3, 28.16 KN/$m^{3,}$ and 28.01KN/m^3, 28.05 KN/m^3 respectively (as given in Table 5.2. and Appendix 7).

ISRM (1978) defines strong rock as having a water absorption between 1% and 2%, medium strength rock as having a water absorption between 2% and 3%, and weak rock as having a water absorption greater than 3%. The water absorption test on rock samples was conducted to determine the water absorption amount of the rock samples. The test findings reveal that the welded tuff rock sample has a water absorption value of 26.27% which indicates weak rock mass, whereas the aphanitic basaltic rock samples from right abutment and left abutment has water absorption values of 0.58% and 0.76%, respectively which shows that rocks are strong. The specific gravity of each rock sample was calculated in addition to the water absorption of the rock samples. The specific gravity of oven-dried rocks is 1.19, 2.94, and 2.96 for reservoir area, left abutment, and right abutment samples, respectively. RSS, LARS, and RARS have saturated surface dry specific gravity values of 1.50, 2.96, and 2.98, respectively. The apparent specific gravity of the rock samples is 1.73, 3.01, and 3.01 for the rock samples from the reservoir area, right and left abutment, respectively. The point load index test results of the rock samples indicated that the RSS rock samples from the reservoir area have a uniaxial compressive strength (UCS) value of 55.68MPa, the RARS sample from the right abutment has the UCS values of 146.88MPa, and the LARS sample from the left abutment has the UCS values of 146.44MPa. These UCS values of rock samples show medium strength for RSS and high strength for LARS and RARS, as given in the table below (Table 5.3.) and Appendix 11.

Table 5. 2. Summarized table of the Specific Gravity, water absorption, and unit weight test.

Sample Code	Specific Gravity			Water Absorption (%)	Rock Description (ISRM,1978)	Unit Weight	
	Oven Dried	Saturated Surface Dry	Apparent Specific Gravity			Dry (KN/m^3)	Saturated (KN/m^3)
RSS	1.19	1.50	1.73	26.27	Weak	15.02	15.58
RARS	2.96	2.98	3.01	0.58	Strong	28.15	28.16
LARS	2.94	2.96	3.01	0.76	Strong	28.01	28.05
RSS = Welded Tuff rock, RARS = Aphanitic Basaltic rock from Right Abutment, LARS = Aphanitic Basaltic rock from Left Abutment.							

Table 5. 3. Summarized table of point load index test for rock samples.

S. No.	Sample Code	$Is_{(50)}$, MPa	Uniaxial Compressive Strength(UCS), MPa	Strength Classification (Deere and Miller, 1966)	Rock Unit Description
			24 x $Is_{(50)}$		
1.	RSS	2.32	55.68	Medium Strength	Welded Tuff
2.	LARS	6.06	145.44	High Strength	Aphanitic Basaltic Rock
3.	RARS	6.12	146.88	High Strength	Aphanitic Basaltic Rock
RSS = Welded Tuff rock, RARS = Aphanitic Basaltic rock from Right Abutment, LARS = Aphanitic Basaltic rock from Left Abutment.					

5.2.1.3. In-situ Strength Test Analysis of the Rock Mass

The uniaxial compressive strength of the study area was also estimated using the Schmidt hammer rebound values and dry unit weight of the rock samples determined in the laboratory.

The Schmidt rebound values were collected from two stations at the reservoir area, right abutment, and left abutment, as given in Table 5.4. The UCS value for the outcrop at the reservoir area is estimated to be ranging from 22.13MPa to 25.11MPa. According to Deere and Miller (1966), These estimated uniaxial compressive strength values of the outcrop show very low rock mass strength. The right and left abutment rock outcrop have the UCS value ranging from 188MPa to 194MPa, and 173.78MPa to 139.31MPa. The UCS values of both abutments indicate high-strength rock mass.

Table 5. 4. The uniaxial compressive strength of the rocks was estimated from the Schmidt hammer rebound values.

Test Stations	Average Schmidt Rebound Value	Dry Unit Weight (KN/m^3)	UCS value (MPa)	Strength Classification (Deere and Miller, 1966)	Rock Unit Description
Reservoir Area					
Station 1	25.4	15.02	22.13	Very Low Strength	Slightly weathered Welded tuff
Station 2	25.7	15.02	25.11	Very Low Strength	Slightly weathered Welded tuff
Left Abutment					
Station 1	49.9	28.01	173.78	High Strength	Moderately weathered aphanitic basaltic rocks
Station 2	46	28.01	139.31	High Strength	Slightly to Moderately weathered aphanitic basaltic rocks
Right Abutment					
Station 1	51.3	28.15	188	High Strength	Slightly weathered aphanitic basaltic rocks
Station 2	51.6	28.15	194	High Strength	Slightly weathered aphanitic basaltic rocks

5.2.1.4. Rock Quality Designation

The result of the analysis showed that Jv of aphanitic basaltic rock at the right and left abutment of the dam site ranges from 14-17 and 17-21. The Jv values was interpreted according to Palmstrom (2005). According to Palmstrom (2005), the statistical distribution of determined Jv value of rocks at the dam site showed that 100% of Jv of aphanitic basaltic rock at both abutments fall into high degree of jointing as shown in Table 5.5 and Figure 5.2a. Rock Quality Designation of the exposed rock masses at the dam site was calculated using joint volumetric count (JV) using Palmstrom's (1982) equations and determined RQD value is given in the table below (Table 5.5). Therefore, the RQD of the right abutment rock outcrop ranges from 59% to 69%, indicating that the rock masses in the right abutment have a high degree of jointing (Palmstrom, 2005) and fair rock mass quality (Deere and Deere 1988). The outcrop in the left abutment has an estimated RQD value ranging from 46% to 59%. The RQD values of the left abutment show that the rock masses have a high degree of jointing and rock mass quality ranging from poor to fair (Deere and Deere, 1988). According to the estimated RQD values, the rock mass outcrops at both abutments are heavily jointed and subjected to joints and fractures.

Table 5. 5. Estimated RQD values from the volumetric joint count.

	Survey Stations			
	RADS-1	**RADS-2**	**LADS-1**	**LADS-2**
Volumetric Joint Count Values(Jv)	14	17	17	21
Rock Quality Designation (RQD)	69	59	59	46
Degree of Jointing According to Palmstrom (2005)	High	High	High	High
Rock Quality According to Deere (1968)	Fair	Fair	Fair	Poor

According to Deere and Deere (1988), the relationship between RQD values and rock mass quality was determined. Depending on this, 100% of RQD values of aphanitic basaltic rock at the right abutment falls in to fair RQD class. This infers that the aphanitic basaltic rock is characterized by high degree of jointing and weathering. Similarly, 25% and 75% of RQD values of aphanitic basaltic rock at left abutment of the dam site fall into poor to fair RQD class which indicates that the rock is characterized by high degree of jointing and weathering as shown in Table 5.5 and Figure 5.2b.

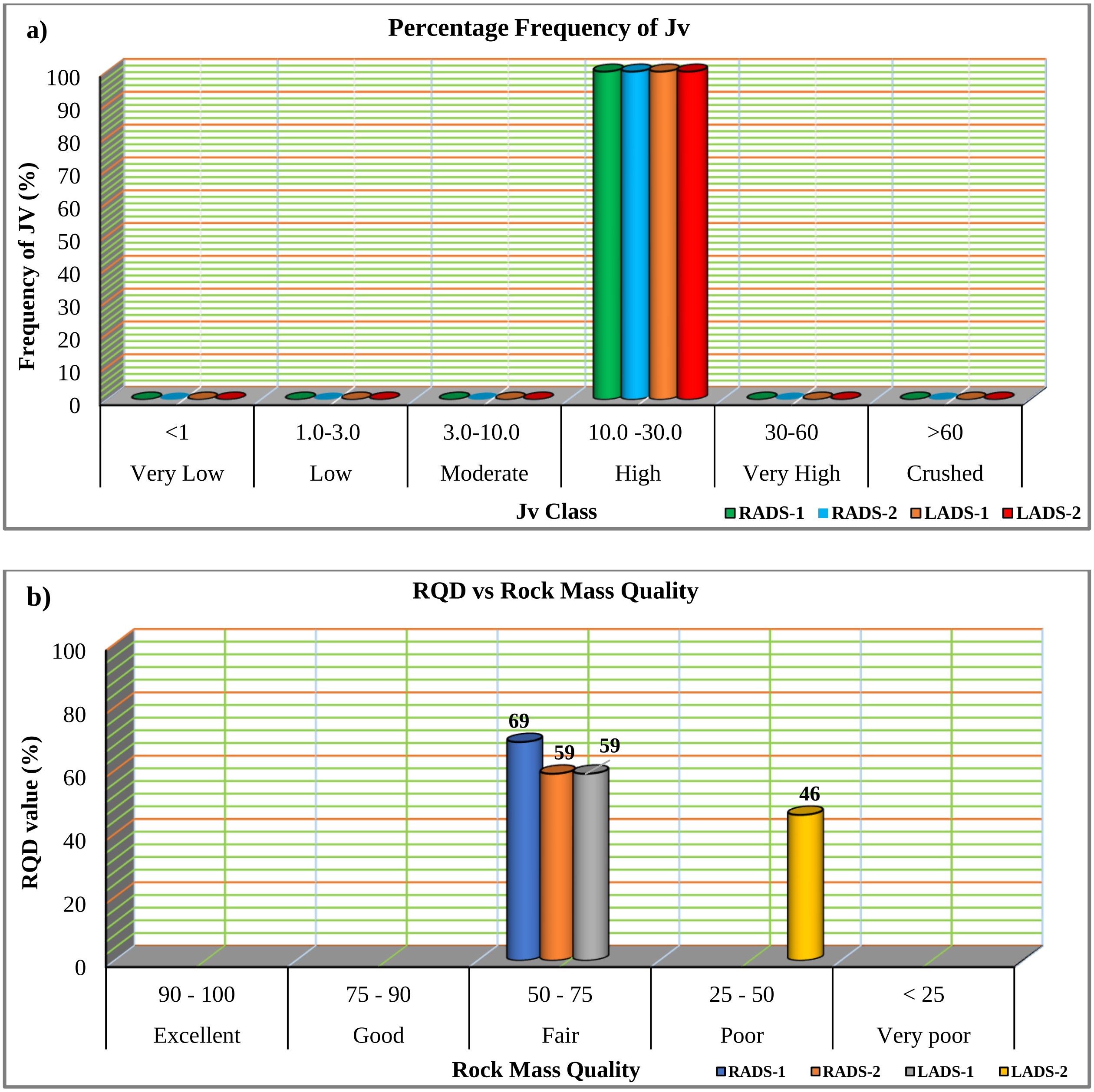

Figure 5. 2. a) Percentage frequency of Jv variation of Aphanitic Basaltic Rock at the dam site in each Jv class according to Palmstrom (2005) and b) Percentage frequency of RQD variation of Aphanitic Basaltic Rock at the dam site in each RQD as per Deere and Deere (1988).

5.2.1.5. Engineering Classification of the Rock Mass

The two most extensively used rock mass classification methods, RMR (rock mass rating) (Bieniawski, 1989) and GSI (geological strength index) (Marinos and Hoek, 2000), were utilized in the current study for rock mass characterization and estimation of rock mass quality at the dam abutments. The RMR system comprises five fundamental factors that describe various rock mass and discontinuity conditions, such as UCS of intact rock, RQD, spacing of discontinuities, discontinuity condition, and groundwater condition. The UCS values from the point load test and the RQD data from the volumetric joint count were employed in rock mass classification. The fieldwork was utilized to estimate the joint spacing, discontinuity state, and groundwater condition employed in the rock mass classification. Accordingly, the rock mass rating outcome for the right abutment ranges from 64 to 68, indicating that the rock mass quality of the right abutment is good, as given in Table 5.6. Furthermore, the rock mass rating values on the left abutment range from 61 to 48, indicating good to fair rock mass quality. Table 5.7 shows the complete discontinuity characteristics, including rating values and computed RMR with rock mass quality.

The GSI values were obtained from RMR using an empirical equation (2.17) (Hoek and Brown, 1997) and compared to GSI values determined in the field by visual observation using the quantitative GSI chart Marinos and Hoek (2000) presented. The condition of the discontinuity surfaces and structures in the rock masses were used to estimate the GSI of the rock mass at surface outcrops on the abutments.

According to the GSI values that were estimated during the fieldwork, the rock mass on the right abutment can be classified as very blocky to blocky rock mass at the RADS-1 survey station, with GSI values ranging from 55-57, and blocky to very blocky rock mass at the RADS-2 survey station, with GSI values ranging from 50-54 (Table 5.6). Additionally, the GSI results showed that the rock mass on the right abutment can be categorized as very block-to-block rock mass at the LADS-1 survey station, with GSI values ranging from 40 to 43. In contrast, it is blocky to very blocky rock mass at the LADS-2 survey station, with GSI values ranging from 33 to 38 (Table 5.6).

The rock mass rating values were also used to calculate the rock masses' geological strength index (GSI). The right abutment has a GSI value of 58 for RADS-1 survey station and 54 for RADS-2 survey station. LADS-1 and LADS-2 survey station had GSI values of 51 and 38 for the left abutment, respectively as shown in Table 5.6.

Table 5. 6. GSI values from field observation (Marinos and Hoek, 2000) and RMR_{89}.

	Survey Stations			
	RADS-1	**RADS-2**	**LADS-1**	**LADS-2**
RMR_{89}	**68**	**64**	**61**	**48**
Geological Strength Index (RMR_{89} -5)	63	59	55	43
Geological Strength Index (Field Observation) Marinos and Hoek (2000)	55-57	50-54	40-43	33-38
	Ave. **56**	Ave. **52**	Ave. **42**	Ave. **36**
Outcrop Description	Slightly weathered Aphanitic Basaltic rock	Moderately weathered Aphanitic Basaltic rock	Slightly to Moderately weathered Aphanitic Basaltic rock	Moderately weathered Aphanitic Basaltic rock

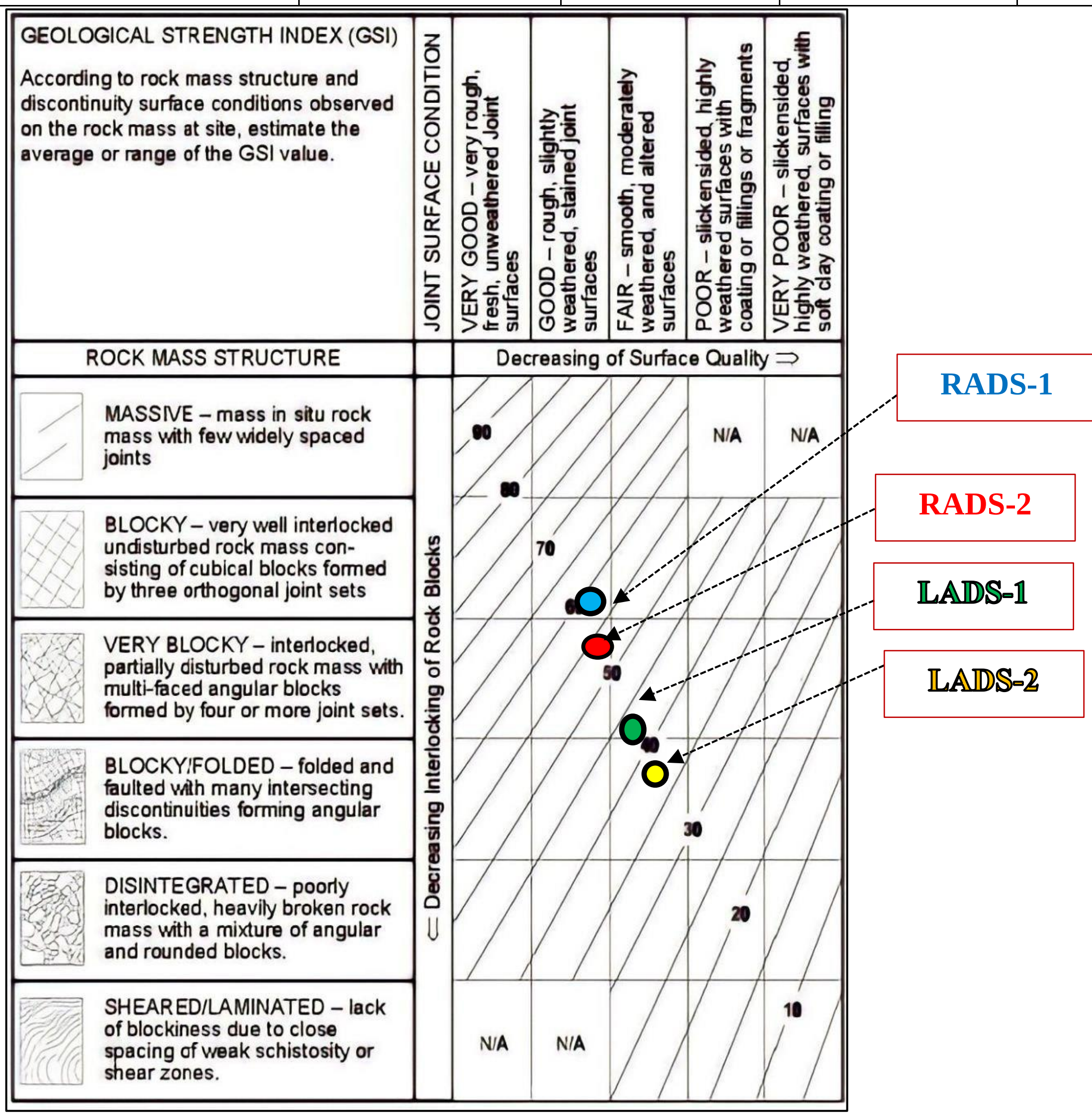

Figure 5. 3. Rock mass classification based on GSI system (after Marinos and Hoek, 2000).

Table 5. 7. RMR input parameters, their rating, and RMR values.

Rock Mass Rating Parameters										
No	**Parameters**		**RADS-1**		**RADS-2**		**LADS-1**		**LADS-2**	
			Status	**Rating values**	**Status**	**Rating values**	**Status**	**Rating values**	**Status**	**Rating values**
1.	Strength of Intact Rock	UCS, (MPa)	146.88	12	146.88	12	140.76	12	140.44	12
2.	RQD, (%)		69	13	59	13	59	13	46	8
3.	Spacing of Discontinuities (cm)		5-65 (a=35)	10	5-15 (a=10)	8	40-50 (a= 40)	10	5-15 (a=10)	8
4.	Condition of Discontinuities	Length, Persistence(m)	>10	1	>10	1	>10	1	>10	1
		Separation(mm)	1-3 (a=2.5)	1	1-2 (a=1)	1	1.5-2.5 (a=1.8)	1	1.0-2.0 (a=1.5)	1
		Roughness	Rough	5	Rough	5	Rough	5	Rough	5
		Infilling	No Infilling	6	No Infilling	6	No Filling	6	Soft Infilling,>5 mm (Clay)	0
		Weathering	Slightly Weathered	5	Moderately Weathered	3	Slightly Moderately Weathered	3	Moderately Weathered	3
	Sum Rating		18		16		16		10	
5.	Groundwater Conditions		Completely Dry	15	Completely Dry	15	Damp	10	Damp	10
RMR Values			**68**		**64**		**61**		**48**	
Rock Class			**II**		**II**		**II**		**III**	
Classification			**Good**		**Good**		**Good**		**Fair**	

RADS-1 and RADS-2 is the right abutment discontinuity survey station at upper face towards the upstream side and along the dam axis, LADS-1 and LADS-2 is the left abutment discontinuity survey station at the upper face towards the upstream side and along dam axis.

5.2.1.6. Determination of Shear Strength and Deformation Modulus Parameters

The geomechanical characteristics of rock mass were determined using RocData software for structurally controlled slope sections in the present study. For determining the shear strength parameters, deformation modulus of the rock mass, and Hoek-brown criterion constants, the RocData software utilizes the input parameters of Geological Strength Index (GSI), Uniaxial Compressive Strength of intact rocks (σ_i), material constant of intact rock (mi), and Disturbance factor (D). In this case, The GSI values were determined from the field observation. The UCS of intact rocks was determined in the laboratory. For this research, the dam abutment slope was mechanically excavated. As a result, the value of D was assumed to be 0.7, which is already included in the RocData program. The Hoek-Brown criterion constants such as mb, S, and *a* were determined and can be used as input parameters in computing the rock masses' bearing capacity. The input parameters for determining the shear strength parameters of rock mass and output parameters are given in Table 5.8 and Table 5.9, Appendix 14 respectively.

Table 5. 8. Input parameters of RocData software.

RocData Input Parameters	Rock Type			
	SW*	MW*	SW**	SW**
UCS (MPa)	146.88	146.88	145.44	145.44
GSI (Field Observation)	56	52	42	36
mi	25	25	25	25
D	0.7	0.7	0.7	0.7
UCS = Uniaxial Compressive Strength of intact rocks, GSI = Geological Strength Index, mi= constant value for rocks, D = Disturbance factor.				

Table 5. 9. Output parameters of RocData software.

RocData Output Parameters	SW*	MW*	SW**	SW**
mb	2.228	1.789	1.033	0.596
S	0.0017	0.001	0.0002	0.0001
a	0.504	0.505	0.510	0.520
C (MPa)	7.917	7.305	5.845	4.572
Φ (Deg)	33	31	26	22
UCSrm(MPa)	5.913	4.378	2.0	0.869
Erm (MPa)	9182	7293	4101	2306.29
mb, S, and *a* are Hoek-Brown Criterion constants.				

The values show that the moderately weathered aphanitic basalt (MW*) in the right abutment, with a value of 4.378 MPa, has a lower strength than the slightly weathered aphanitic basalt (SW*). In addition, cohesion and friction angle are lower than moderately weathered aphanitic basalt. In the left abutment, the moderately weathered basaltic rock (MW**) has lower strength than the slightly weathered basaltic rock (SW**), as shown in Table 5.9. and Appendix 14. The slightly weathered aphanitic basalts (SW*) have a higher value of deformation modulus than the moderately weathered aphanitic basalts (MW*), resulting in a higher deformability of the rock mass. The slightly weathered basaltic rock (SW**) has a higher value of deformation modulus than the moderately weathered basaltic rock (MW**), as shown in Table 5.9. and Appendix 14.

RocData software (Rocscience, 2004) was also used to calculate the rock joints' shear strength parameters (cohesion and friction angle) along the discontinuity failure plane for structurally controlled slope sections, based upon the empirically derived correlation described by (Barton, 1973) which has already been integrated into RocData software. The input parameters for determining the shear strength parameters of joint sets (RASS and LASS) are given in Table 5.10. and Appendix 15. The uniaxial compressive strength used in the analysis was estimated from the Schmidt Rebound values (Table 5.4). Hence, the joint roughness coefficient was determined in the field and the joint wall compressive strength corresponds to 50% of uniaxial compressive strength of intact rock determined from Schmidt hammer was used in the analysis. The unit weight of rocks is determined in the laboratory using buoyancy techniques (Table 5.2).

Table 5. 10. Barton and Bandis Failure Criteria input and output parameters of RocData software.

Critical Slope Section	**Potential Failure Joint sets**	**UCS (MPa)**	**Input Parameters for BBFC**					**Output Shear Strength Parameters**	
			JCS, MPa	**JRC**	**ϕr (°)**	**γ(MN/m^3)**	**H(m)**	**ϕ (°)**	**C(MPa)**
RASS	JS1	191	95.5	7	36.5	0.02815	21	49	0.048
	JS2	187	93.5	9	36.5	0.02815	21	53	0.087
LASS	JS1	139	69.5	7	36.5	0.02805	21	49	0.046
	JS2	156.5	78.25	5	36.5	0.02805	21	46	0.026
H is sloping height, γ is unit weight of the rock samples, BBFC is Barton and Bandis Failure Criteria									

5.2.1.7. Permeability of Rock Mass from Discontinuity features

In addition to the rock material itself, discontinuities orientation, spacing, and surface quality, as well as presence of infilling and type, all play important roles in the permeability of the rock mass. The permeability of the earth is significant for surface constructions such as dams and foundations (Foyo et al., 2005). The existence and frequency of discontinuities influence the permeability of the complete rock and the rock mass. The persistence, tightness, aperture, roughness, infill type, and filling thickness of discontinuities determine the water flow rate through a rock mass as well as the rock mass strength (Öge, 2017). The relation between hydraulic conductivity (k) and fracture parameters (spacing, S, and aperture, e) is provided by equation (2.22), which is used to estimate the hydraulic conductivity of the rock mass exposed on the dam abutments by (Snow, 1968) and (Louis, 1974).

To estimate the permeability of rock masses at the dam site, the spacing and aperture of discontinuities were collected at total 40 survey stations of the dam abutments (10 points at each RADS-1, RADS-2 of the right abutment and LADS-1, LADS-2 of the left abutment). The estimated results of the surface permeability of the rock outcrops are given in the table below and Appendix 2 and 3. The classifications of the permeability values were given according to Terzaghi et al. (1967) and ISRM (1981) as given in Appendix 17.

The estimated values indicated that the slightly weathered basaltic rock at right abutment outcrop (RADS-1) have a coefficient of permeability values ranging from 2.75 $x10^{-6}$ m/s^2 to 8.83 $x10^{-4}$ m/s^2 with permeability classification ranging from slightly permeable to moderately permeable. The RASD-1 survey station has an average coefficient of permeability values of 1.79 $x10^{-4}$ m/s^2 with moderate permeability of rock mass. Furthermore, the surface permeability of the moderately weathered basaltic rock at right abutment outcrop (RADS-2) ranges from 1.18$x10^{-6}$ m/s^2 to 1.77$x10^{-5}$ m/s^2 with slightly permeable permeability characteristics. The RASD-2 survey station has an average coefficient of permeability values of 1.18 $x10^{-5}$ m/s^2 with slightly permeable permeability features of the rock mass as shown in Table 5.11 and Appendix 2.

The surface permeability of rock outcrop was also estimated for the left abutment rock mass. The slightly-moderately weathered aphanitic basaltic rock (LADS-1) have coefficient of permeability values ranging from 1.02 $x10^{-6}$ m/s^2 to 5.65 $x10^{-5}$ m/s^2 with slightly permeable permeability characteristics. The LADS-1 survey station has an average coefficient of permeability values of 2.01 x10^{-5} m/s^2 with slight permeability of rock mass. The moderately weathered aphanitic basaltic rock has coefficient of permeability values ranging from 18.28 x10^{-5} m/s^2 to 2.21 x10^{-6} m/s^2 with an average coefficient of permeability values of 3.84 x10^{-5} with a slightly permeable permeability characteristic as shown in Table 5.12 and Appendix 3.

Generally, the estimated surface permeability of the rock outcrops at the dam abutments show that the rock masses exposed at the abutments have slightly permeable permeability characteristics due to the widely to very widely spaced discontinuities, variation in degree of weathering and jointing, and minimum values of aperture discontinuities.

Table 5. 11. The summarized table of estimated surface permeability of the right abutment rock outcrops (RADS-1 and RADS-2).

S.No.	**RADS-1**		**RADS-2**	
	Coefficient of Permeability, K(m/s^2)	**Permeability Class**	**Coefficient of Permeability, K(m/s^2)**	**Permeability Class**
1.	9.35x10^{-6}	Slightly Permeable	1.67 x10^{-5}	Slightly Permeable
2.	3.67x10^{-6}	Slightly Permeable	1.25 x10^{-5}	Slightly Permeable
3.	2.75x10^{-6}	Slightly Permeable	1.47 x10^{-5}	Slightly Permeable
4.	4.42x10^{-6}	Slightly Permeable	1.15 x10^{-5}	Slightly Permeable
5.	5.23 x10^{-6}	Slightly Permeable	1.18 x10^{-6}	Slightly Permeable
6.	2.30 x10^{-5}	Slightly Permeable	1.11 x10^{-5}	Slightly Permeable
7.	1.7 x10^{-5}	Slightly Permeable	1.60 x10^{-5}	Slightly Permeable
8.	5.05 x10^{-5}	Slightly Permeable	1.77 x10^{-5}	Slightly Permeable
9.	8.83 x10^{-4}	Moderately Permeable	3.90 x10^{-6}	Slightly Permeable
10.	7.95 x10^{-4}	Moderately Permeable	1.28 x10^{-5}	Slightly Permeable
Max	**8.83 x10^{-4}**	**Moderately Permeable**	**1.77 x10^{-5}**	**Slightly Permeable**
Min	**2.75 x10^{-6}**	**Slightly Permeable**	**1.18 x10^{-6}**	**Slightly Permeable**
Ave	**1.79 x10^{-4}**	**Moderately Permeable**	**1.18 x10^{-5}**	**Slightly Permeable**

Table 5. 12. The summarized table of estimated surface permeability of the left abutment rock outcrops (LADS-1 and LADS-2).

S.No.	LADS-1		LADS-2	
	Coefficient of Permeability, K(m/s^2)	**Permeability Class**	**Coefficient of Permeability, K(m/s^2)**	**Permeability Class**
1.	4.56 x10^{-5}	Slightly Permeable	5.14 x10^{-5}	Slightly Permeable
2.	5.60 x10^{-5}	Slightly Permeable	3.5 x10^{-5}	Slightly Permeable
3.	7.24 x10^{-6}	Slightly Permeable	4.24 x10^{-5}	Slightly Permeable
4.	1.02 x10^{-6}	Slightly Permeable	2.21 x10^{-6}	Slightly Permeable
5.	2.35 x10^{-6}	Slightly Permeable	3.18 x10^{-5}	Slightly Permeable
6.	2.83 x10^{-5}	Slightly Permeable	3.85 x10^{-5}	Slightly Permeable
7.	5.65 x10^{-5}	Slightly Permeable	3.03 x10^{-6}	Slightly Permeable
8.	9.18 x10^{-6}	Slightly Permeable	4.24 x10^{-5}	Slightly Permeable
9.	6.18 x10^{-6}	Slightly Permeable	8.28 x10^{-5}	Slightly Permeable
10.	4.06 x10^{-5}	Slightly Permeable	9.42 x10^{-5}	Slightly Permeable
Max	**5.65 x10^{-5}**	**Slightly Permeable**	**8.28 x10^{-5}**	**Slightly Permeable**
Min	**1.02 x10^{-6}**	**Slightly Permeable**	**2.21 x10^{-6}**	**Slightly Permeable**
Ave	**2.01 x10^{-5}**	**Slightly Permeable**	**3.84 x10^{-5}**	**Slightly Permeable**

5.2.2. Engineering Characterization of Subsurface Rock Mass

Geotechnical drilling of boreholes was utilized to characterize and determine the condition of subsurface geological material (ECDSWC, 2022). The direct geotechnical investigation of the Bowa Dayole gravity Dam Site was carried out by using the geotechnical core drilling and extraction of core samples, which were conducted following ASTM D12 113-99: standard practice for Rock drilling and sampling of rock for site investigation by using wireline rotary core drilling method. The in-situ permeability test was also conducted during the geotechnical investigation.

The geotechnical boreholes drilled at the dam site were three(3) boreholes. The three boreholes drilled at the dam site are two (2) boreholes at both dam abutments (BH1 and BH3) and one (1) at the river center of the dam (BH2). These boreholes were used to evaluate the subsurface geological materials (in terms of rock mass quality, and permeability), determine the groundwater level, and conduct in-situ tests such as falling head permeability tests and packer tests in order to determine the permeability of subsurface geological materials. Furthermore, the drilled boreholes were also used to determine the rock quality designation (RQD) in each borehole at various depths (ECDSWC, 2022). After in-situ tests were conducted at the dam site, core samples of each borehole were taken to the laboratory for further analysis.

5.2.2.1. Lithological Logging and Intact Rock Properties of Dam Site

According to ECDSWC (2022) at the right abutment of the dam site, one borehole (BH-1) was drilled to a depth of 25m. In this borehole, the geotechnical investigation of subsurface geological materials shows that throughout the borehole depth from 0.0m to 25.10m, one rock unit was recovered with rock characteristics of grey, a strong, fresh unweathered, massive basaltic rock with higher total core recovery ranging from 85% to 100% shown in Figure 5.4. The laboratory tests were conducted on the samples from the right abutment borehole as shown in Table 5.13. The UCS of the samples at the depth range of 5.50 to 6m, 13.00 to 13.30m, and 20.60 to 20.90m indicate the values of 95.90MPa, 78.64MPa, and 20.30MPa, respectively. The UCS values of the massive basaltic rock at the depth 5.50 to 6.0m and 13.00 to 13.30m shows medium strength rock according to Deere and Miller (1966). The UCS value of the massive basaltic rock at the depth range of 20.60 to 20.90m indicates weak strength rock. These UCS values of the rocks show decreasing trend of strength with depth as shown in Table 5.13.

Besides determining the UCS values of the core samples, other laboratory tests such as specific Gravity (specific gravity oven dried, saturated surface dry specific gravity, apparent specific Gravity), water absorption test, unit weight, and slake durability were conducted on cores samples at various depths. The specific gravity of the rocks shows values ranging from 2.42 to 2.91, 2.43 to 2.97, and 2.44 to 2.97 for a specific gravity of oven-dried, saturated surface dry specific gravity, and apparent specific gravity respectively (Appendix 10). The water absorption test revealed that the core samples have values to be ranging from 0.18% to 4.71% as given Table 5.13. The core rock samples from the depth range of 5.50m to 6.0m and 13.00m to 13.30m have the water absorption value of 0.26% and 0.26% respectively indicating that the rock samples are strong rock according to the ISRM (1978). The unit weight of the core samples has a value ranging from 2.43g/cm^3 to 2.94g/cm^3 at various depths in the borehole. According to Ankara et al.(2016), the slake durability index of the core samples indicates how resistant rock is to degradation or weathering when put through two wetting and drying cycles. The core samples have a slake durability index ranging from 97.8% to 100% at depths of 6m, 13.30m, and 20.90m as given in Table 5.13. According to Bryson et al. (2011), These values of the index show the high quality of rock mass inferring less than 15% of material loss.

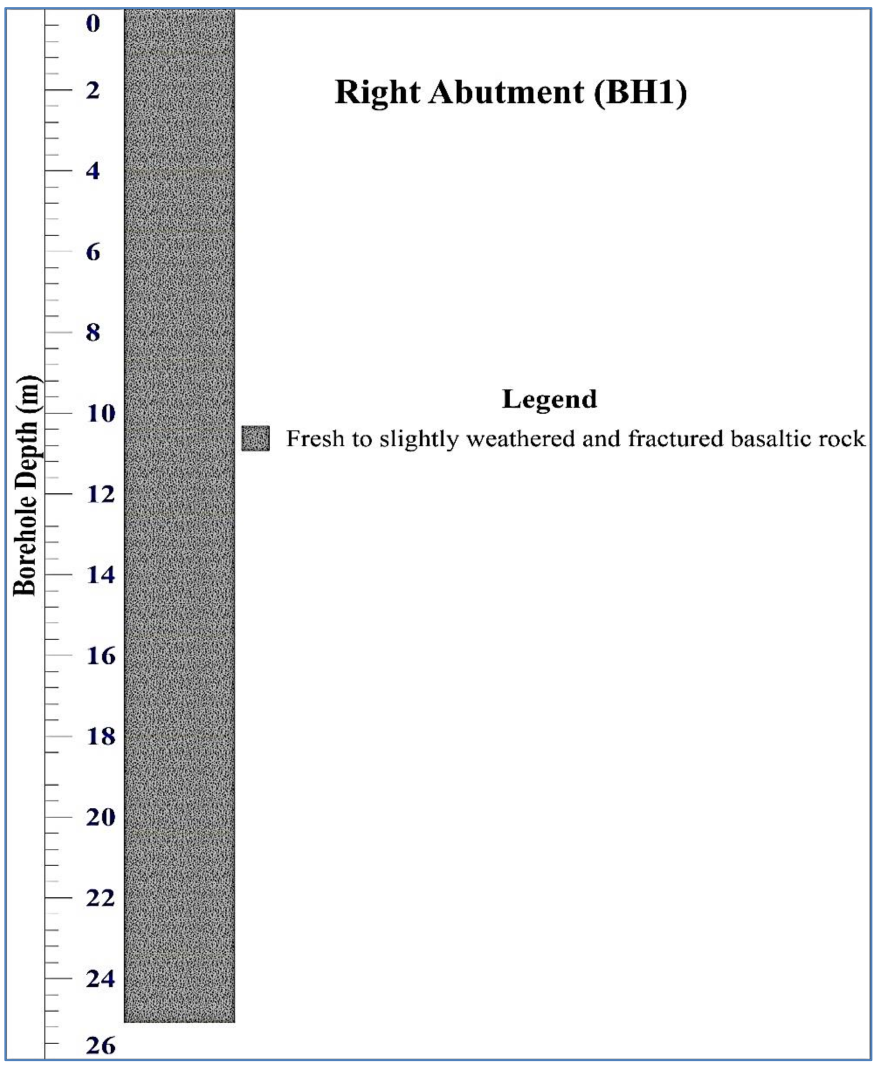

Figure 5. 4. Lithological log of the borehole at the right abutment (BH1) of the dam site.

At the left abutment of the dam site, a borehole (BH-3) was drilled up to a depth of 25m. The drilling results showed that the upper part of the borehole up to a depth of 0.30m is covered with reddish brown, dry, medium stiff, sandy silt with some clays with an average total core recovery of 55%. After the sandy silt unit, the underlying rock unit recovered is a basaltic rock with distinctive features such as grey in color and medium strength with an average total core recovery of 75% shown in Figure 5.5 . This rock unit has a characteristic of a fresh to slightly weathered and highly fractured degree of weathering and fracturing respectively. The fresh to slightly weathered and highly fractured rock unit only extends to a depth of 7m. After a depth of 7m, the degree of weathering and fracturing decreases and the rock unit becomes fresh, strong, and massive which further extends to a depth of 25.10m. The laboratory tests on the core samples from the left abutment borehole were also conducted. The UCS value of rock samples taken at the depth of 7.30m is 51.33MPa, and at the depth of 16.65m is 67.24MPa, and at the depth of 23.40m is 28.76MPa as given in Table 5.13. According to Deere and Miller (1966), These UCS values have different strength classifications at each depth of the samples. At depths of 7.30m and 16.65m, the UCS values of rock samples can be classified as medium strength, and at depths of 23.40m, the UCS values of the cores show low strength of rock mass. Like BH-1, UCS values of the rocks show-decreasing trend of strength with respect to depth. Other laboratory tests were conducted on the core samples from the depth range of 7m to 16.65m. The specific gravity of the rocks shows values ranging from 2.61 to 2.82, 2.62 to 2.83, and 2.63 to 2.86 for a specific gravity of oven-dried, saturated surface dry specific gravity, and apparent specific gravity respectively as given in Appendix 10. The water absorption and slake durability index of the core samples at this specific range of depth show values varying from 0.10% to 0.42% and 99.04% to 100% respectively. The core rock samples from the depth range of 7.00m to 7.30m, and 16.40m to 16.65m have the water absorption values of 0.42% and 0.10% showing strong rock according to the ISRM (1978). These higher values of slake durability index of the rock samples show high weathering-resistant rock mass with very lower material loss.

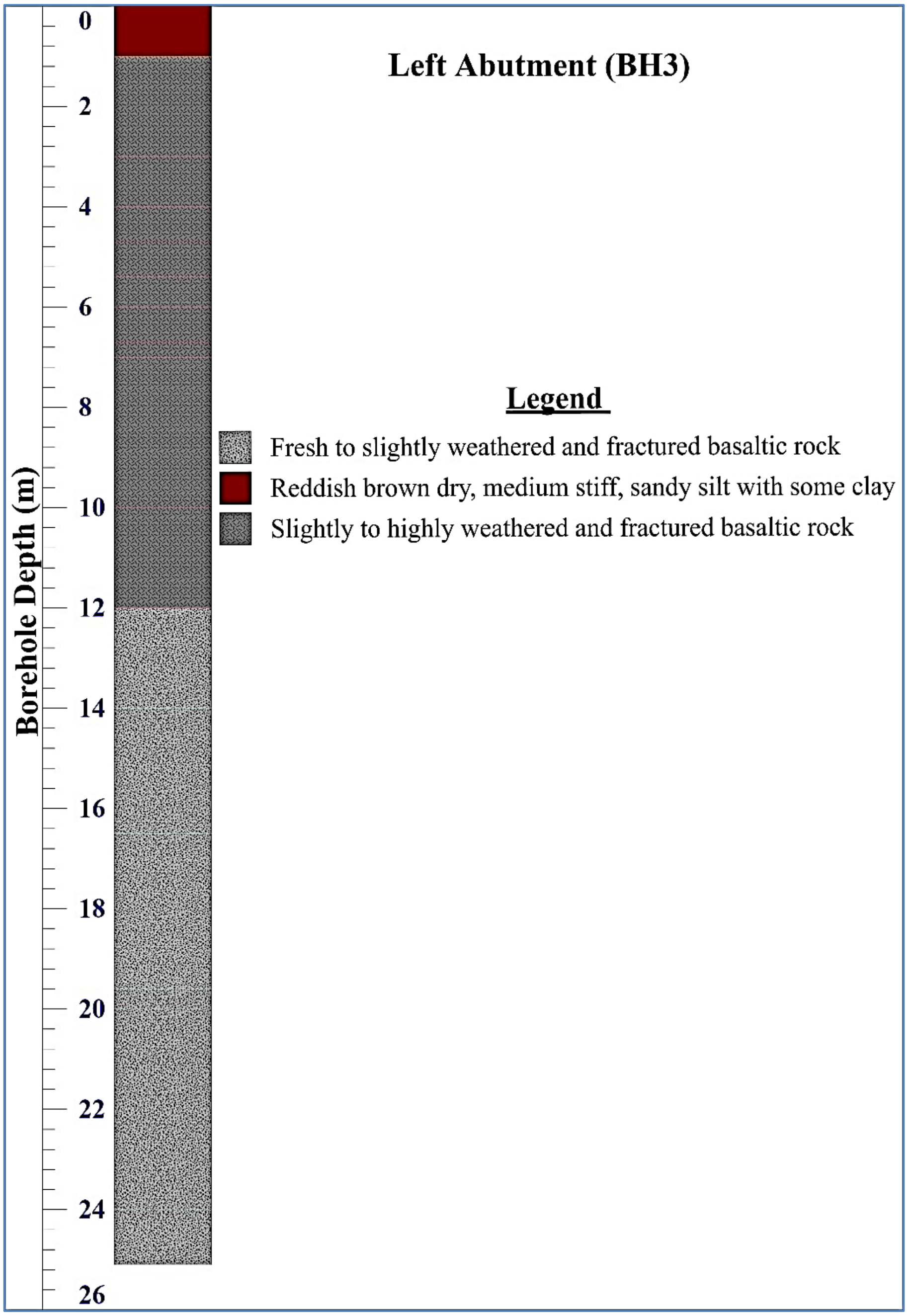

Figure 5. 5. Lithological log of the borehole at the left abutment (BH3) of the dam site.

Like both dam abutments, a geotechnical investigation of the river center (BH-2) was carried out by geotechnical core drilling up to the depth of 23m. The drilling results revealed that the subsurface geological material of the river center is comprised of basaltic rock and welded tuff at various depths throughout the borehole. The upper part of the river center borehole is covered by the basaltic rock up to the depth of 4.20m with characteristics such as grey in color, fresh to moderately weathered, and moderately to highly fractured rock with the total core recovery ranging from 75% to 100% shown in Figure 5.6. After the depth of 4.20m, the rock unit of welded tuff underlines the basaltic rock where the degree of weathering and fracturing increases with increasing depth with the total core recovery of 100%. This rock unit extends to the depth of 16.55m until the light grey; moist, weak to medium strength of altered basaltic rock with thickness of 1.45m underlines it where the total core recovery value is 100%. Then the slightly welded to unwelded tuff is recovered back again extending all the way up to the depth of 23m with the total core recovery value ranging from 60% to 100%.

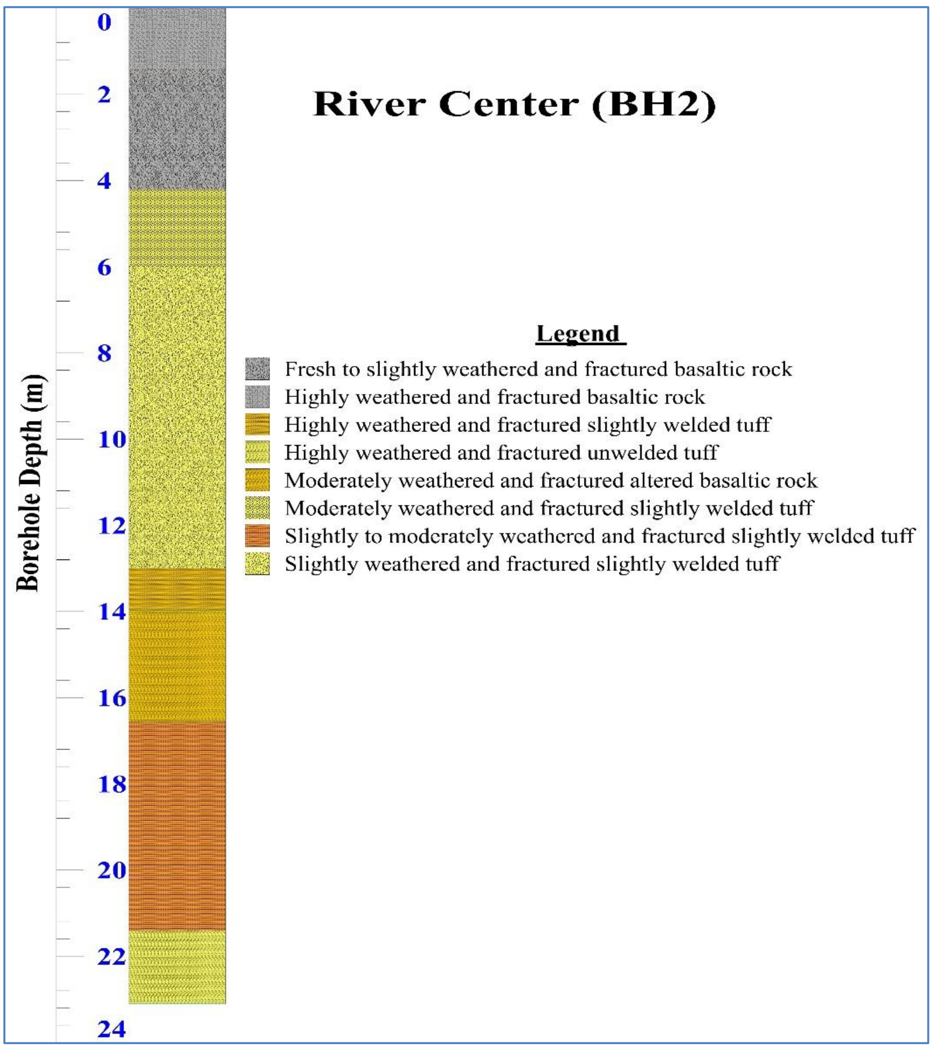

Figure 5.6. Lithological log of the borehole at the river center (BH-2) of the dam site of the study area.

The laboratory tests were conducted on samples taken at various depths in the BH-2 where the samples taken from basaltic rock and welded tuff. The laboratory test on basaltic rock recovered at the depth of 3.30m-3.55m showed the UCS value of 81.91MPa indicating medium strength of the rock mass as given Table 5.13. The unit weight and water absorption values are 2.83g/cm^3 and 0.71% respectively as given in Appendix 10. The obtained values of the water absorption shows that rock was strong according to the ISRM (1978). The specific Gravity of the rocks shows values of 2.83, 2.83, and 2.84 for a specific gravity of oven-dried, saturated surface dry specific gravity, and apparent specific gravity respectively as given in Appendix 10.

The laboratory tests on the tuff rock unit revealed a lower value of UCS which are 0.20MPa , 0.17MPa, and 0.16MPa of rock samples at the depth of 6m, 8.80m and 20.36m respectively as given Table 5.13. These values show the extremely low strength of the rock unit due to the higher degree of weathering and the UCS values of the rock samples show a decreasing trend with respect to depth. The specific gravity of the core samples indicated the saturated surface dry specific gravity values of 2.54 at the depth of 6m, 2.38 at the depth of 8.80m and 2.44 at the depth of 20.36m as given in Appendix 10.

Table 5. 13. Summarized laboratory analysis of the core samples (ECDSWC, 2022).

BHID	Sample Depth (m)	Unit Weight (KN/m^3)	UCS (Mpa)	Strength Classification According to Miller and Deere(1966)	Slake Durability (%)	SDI According to Bryson et al. (2011)
BH-1	5.50-6.00	24.3	95.9	Medium Strength	97.8	High
	13-13.30	29.2	78.6	Medium strength	100	High
	20.60-20.90	29.4	20.5	Very low strength	100	High
BH-2	3.30-3.55	28.3	81.9	Medium Strength	99.04	High
	5.60-6.00	15.1	0.20	Very low strength	-	-
	8.35-8.80	19.2	0.17	Very low strength	-	-
	20.00-20.36	17.8	0.16	Very low strength	-	-
BH-3	7.00-7.30	28.0	51.3	Low Strength	100	High
	16.40-16.65	26.0	67.4	Medium Strength	99.04	High
	23.10-23.40	26.1	28.8	Low Strength	-	-

Laboratory analysis of the rock samples from each borehole at different depth shows differences in the values of UCS with increasing depth as shown in Figure 5.4b.

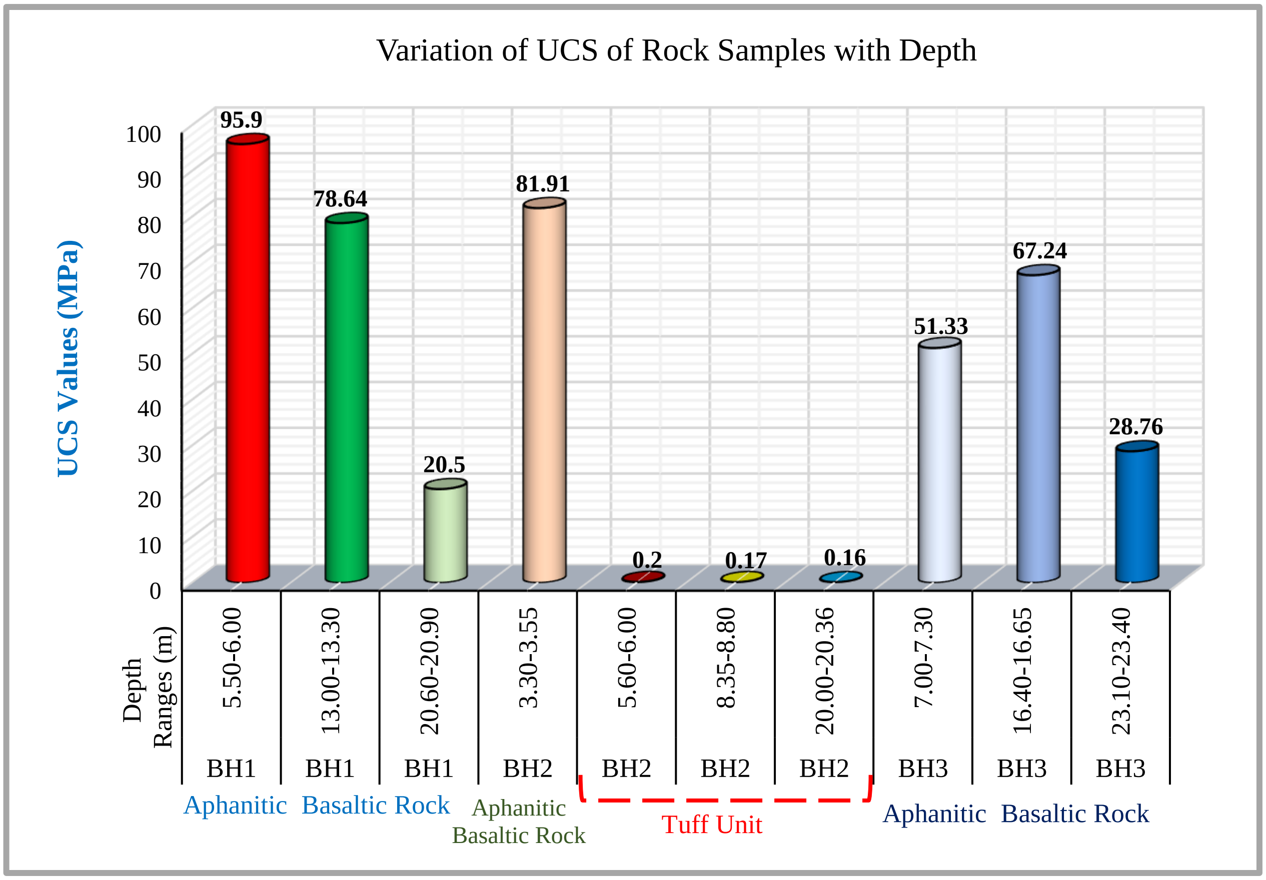

Figure 5. 7. Variation of Uniaxial Compressive Strength of Rock Samples with Depth in each borehole of the dam site.

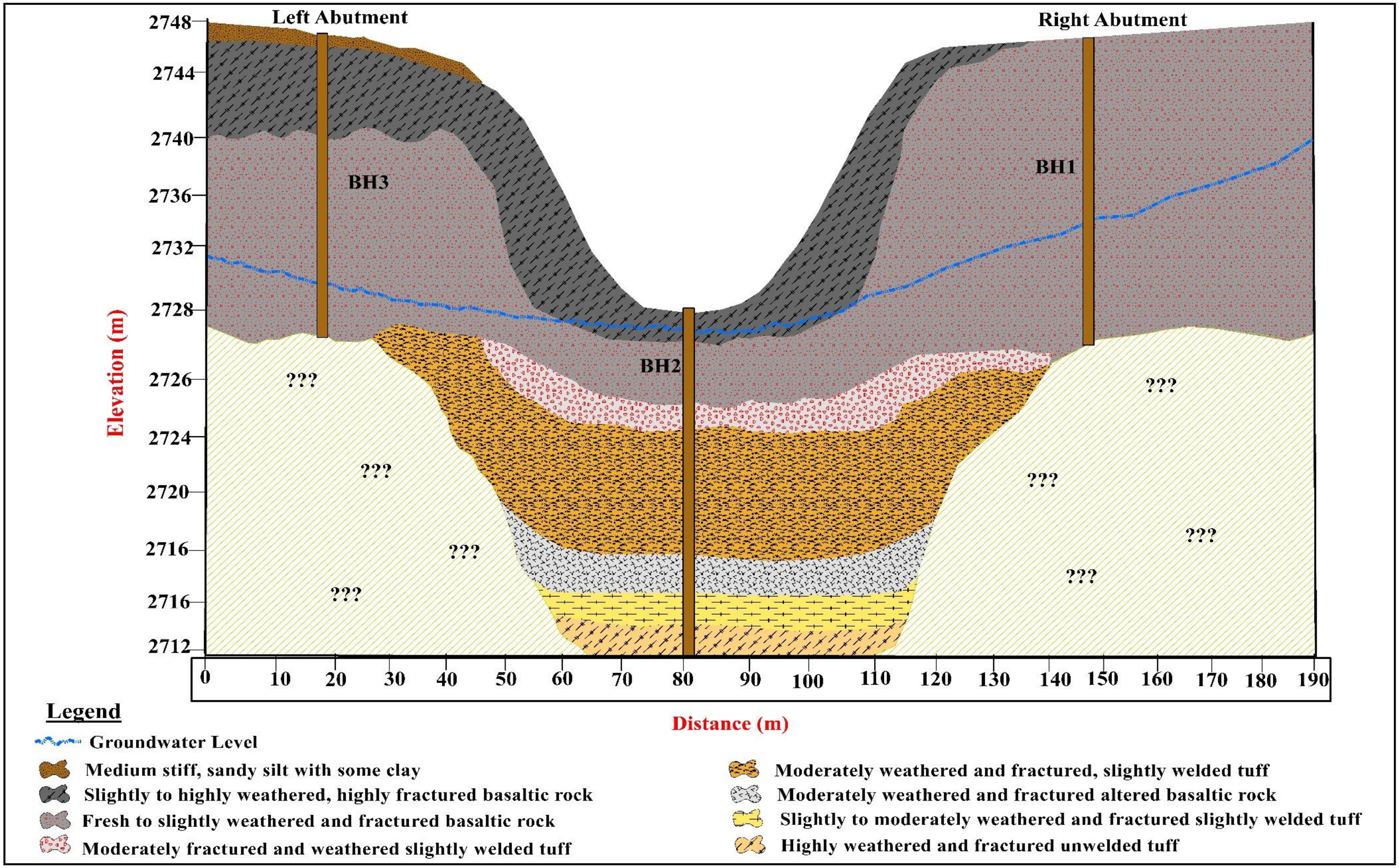

Figure 5. 8. Dam Site Cross section from Lithological Logging in each borehole (Modified after ECDSWC, 2022).

5.2.2.2. RQD Variation with Depth

The rock quality (as measured by RQD) can vary greatly with depth due to changes in rock types, the presence of fractures, bedding planes, or other geological structures. However, there may be some general trends or patterns in the correlation between RQD and drilled depth. For example, RQD might decrease with depth if deeper rocks are more fractured or have more significant weathering than shallower rocks. Alternatively, RQD might increase with depth if deeper rocks are more competent and less fractured than shallower rocks.

In the borehole at the right abutment (BH-1), The overall rock quality designation (RQD) of the right abutment borehole from core recovery shows a range from 85% to 100%. According to Deere and Deere (1988), the rock mass quality classification were plotted to be in good to excellent, indicating a low degree of fracturing of the aphanitic basaltic rock.

At the depth range from 0.0 to 1.10m, 8.70 to 10.40m, 23.40 to 25.10m, the RQD values of the aphanitic basaltic rock were platted to be in the good rock mass quality with an average RQD value of 87% according to Deere and Deere (1988) as shown in Figure 5.10a. At the depth range of 1.10 to 8.70m, 10.40 to 18.0m, and 20.40 to 23.40m, the RQD values were platted to be in the excellent rock mass quality with an average RQD value of 96% according to (Deere and Deere, 1988). The degree of jointing within the rock mass according to Deere and Deere (1988) was relatively sound rock mass since the RQD values were greater than 75%. The analysis of RQD variation with depth revealed that the geological formation in the right abutment borehole at the dam site is characterized by higher RQD with overall average of RQD of 85% indicating good rock mass quality according to Deere and Deere (1988). This higher RQD values were due to the low degree of jointing and weathering of aphanitic basaltic rock in the borehole depth interval. Therefore, the geological formations in the right abutment borehole are not problematic due to the higher RQD values indicating good rock mass quality for engineering applications.

Similarly, the RQD values of rock unit at the river center borehole (BH-2) shows various values with respect to depth as shown in Figure 5.10b. At the depth range from 17.10 to 19.0m, and 21.40 to 23.10m, the RQD values of the tuff rock unit were 10%, and 14% respectively and platted to be in the very poor rock mass quality according to Deere and Deere (1988). According to Deere and Deere (1988), the degree of jointing and weathering of the rock mass with RQD values can be determined as weathered and highly jointed rock mass since the RQD values were between 10%-50%. At the depth range of 10.10 to 13.0m, the RQD value of the slightly welded weak tuff was 34% and platted to be in the poor rock mass quality according to Deere and Deere (1988). The degree of jointing and weathering of the rock unit with RQD value can be given as weathered and highly jointed rock mass. The slightly welded tuff unit at the depth range of 9.0 to 10.10m and 13.0m and 14.0m have the RQD values of 52% and 73% where the rock mass quality was considered to be fair. From this RQD values, the degree of jointing was moderately jointed rock mass according to Deere and Deere (1988). The tuff unit at the depth range of 4.20 to 6.0m and 19.0 to 21.40m have the RQD values of 75% and 85% and the RQD values were platted to be in the good rock mass quality and indicating moderately jointed rock mass according to Deere and Deere (1988). At the depth range of 7.80 to 9.0m, the RQD value was 95% which indicates excellent rock mass quality according to Deere and Deere (1988). This higher RQD value shows that the rock mass was relatively sound to sound since the RQD value was greater than 75% according to Deere and Deere (1988). At the depth range of 0.0 to 1.40m, 1.40 to 3.0m, 3.0 to 4.20m, and 14.0 to 17.10m, the RQD value of the slightly to highly fractured aphanitic basaltic rock was 0%, 72%, 66% and 61% respectively and platted to be in the very poor, and fair respectively according to Deere and Deere (1988). This lower values of RQD were due to the high degree fracturing of the rock unit at these depths since the RQD values were lesser than 75% which indicated that highly weathered and jointed rock mass for RQD values at the depth of 0.0 to 1.40m and moderately jointed rock mass at the depth of 1.40 to 3.0m, and 3.0 to 4.20m.

At the river center, the RQD values showed a very changeable characteristic as the drilled borehole depth increases. According to the RQD variation with depth analysis at the river center (BH2), the plotted RQD values indicated no clear trend with increasing depth as shown in Figure 5.10b. This is due to the variation in rock types and degree of jointing encountered with depth. In this situation, it is very challenging to rely on the RQD values for determining the subsurface geological material conditions, and groutability of the section and depths according to (Berhane and Walraevens, 2013). The depths of the low RQD values provide the preliminary information on the subsurface conditions of the geological materials and the extent of the need for the ground treatment to reduce potential engineering geological issues. Hence, to determine the depth and groutability of the sections, lugeon tests must be employed with an integration of RQD values.

The rock quality designation (RQD) of the aphanitic basaltic rock unit at the left abutment borehole (BH-3) was determined from core recovery shows a clear increasing trend as the drilled depth of the borehole increases as shown in Figure 5.10c. The RQD value at the depth range of 0.0 to 1.0m, 4.0 to 4.70m, and 5.40 to 6.0m was 0%. At the depth range of 1.0 to 3.0m, the RQD value was 12%. This lower values of RQD show that the rock unit at these depths have very poor rock mass quality which indicated the rock unit was highly weathered and jointed rock mass according to Deere and Deere (1988). The RQD values at the depth range of 3.0 to 4.0m, 4.70 to 4.50m, 6.0 to 6.7m, and 6.70 to 7.0m were 26%, 43%, 33% and 27.5% respectively. At these depths, the average RQD values was 32.4% which indicates poor rock mass quality due to the higher degree of weathering and jointing according to Deere and Deere (1988). At the depth range of 7.0 to 10.0m, 10.0 to 12.0m, 20.0 to 23.10m, and 23.10 to 25.10m, the RQD values were 85%, 76%, 89%, and 87% respectively. At these depths, the average RQD value was 84.25% which indicates good rock mass quality according to Deere and Deere (1988). Since the RQD values were higher due to the lower degree of jointing and weathering, the rock mass at these depths can be considered to relatively sound to sound according to Deere and Deere (1988). Similarly, the RQD values at the depth range of 12.0 to 14.0m, 14.0 to 16.5m, 16.5 to 19.6m, and 19.6 to 20.0m were given as 97.5%, 92%, 92%, and 100%. The RQD values at these depths show that rock unit have an excellent rock mass quality with an average value of 95.4%. The higher RQD values show that the lower degree of weathering and jointing and determine the rock mass is sound rock since the values were greater than 75%. In this borehole, the RQD value increases with increasing drilled borehole depth due to the lowering of the degree of weathering and jointing. Since there is a clear trend of increasing in values of RQD with depth, the depth of lower RQD values provides initial information on the extent of the section treatment to reduce the potential expected issues. Generally, the rock unit in the left abutment has got suitable quality of rock mass for an engineering application.

5.2.2.3. Distribution of RQD with Lithological Units

The RQD statistical distribution for the rock units identified from the three boreholes at the dam site was determined in to RQD class according to Deere and Deere (1988) as shown in Table 5.14. In the borehole of the dam abutments (BH1 and BH3), aphanitic basaltic rock was identified with variable RQD values with depth. In the river center borehole, both aphanitic basaltic and tuff rock units were identified having different RQD values with depth. Based on the analysis, the RQD values of aphanitic basaltic rock at the right abutment showed that percentage distribution of RQD value of 27.3% and 72.7% of the values which are distributed to be in the good and excellent of RQD class respectively as shown in Table 5.14.

Table 5. 14. RQD values distribution of rocks into Deere and Deere (1988) RQD classes.

Borehole Location	Rock type	Distribution of RQD of each rock types in to RQD class according to Deere and Deere (1988)						Average RQD (%)	RQD Class
		Percentage Distribution of RQD (%) in each RQD class	RQD Class						
			V. Poor	Poor	Fair	Good	Exc.		
Right Abutment (BH1)	Aphanitic Basaltic rock		--	--	--	36.4	63.6	93.1	Excellent
Left Abutment (BH3)	Aphanitic Basaltic rock		23	7.7	38.5	15.4	7.7	53.75	Fair
River Center (BH2)	Aphanitic Basaltic rock		25	--	75	--	--	49.75	Poor
	Tuff unit		25	12.5	25	25	12.5	54.75	Fair

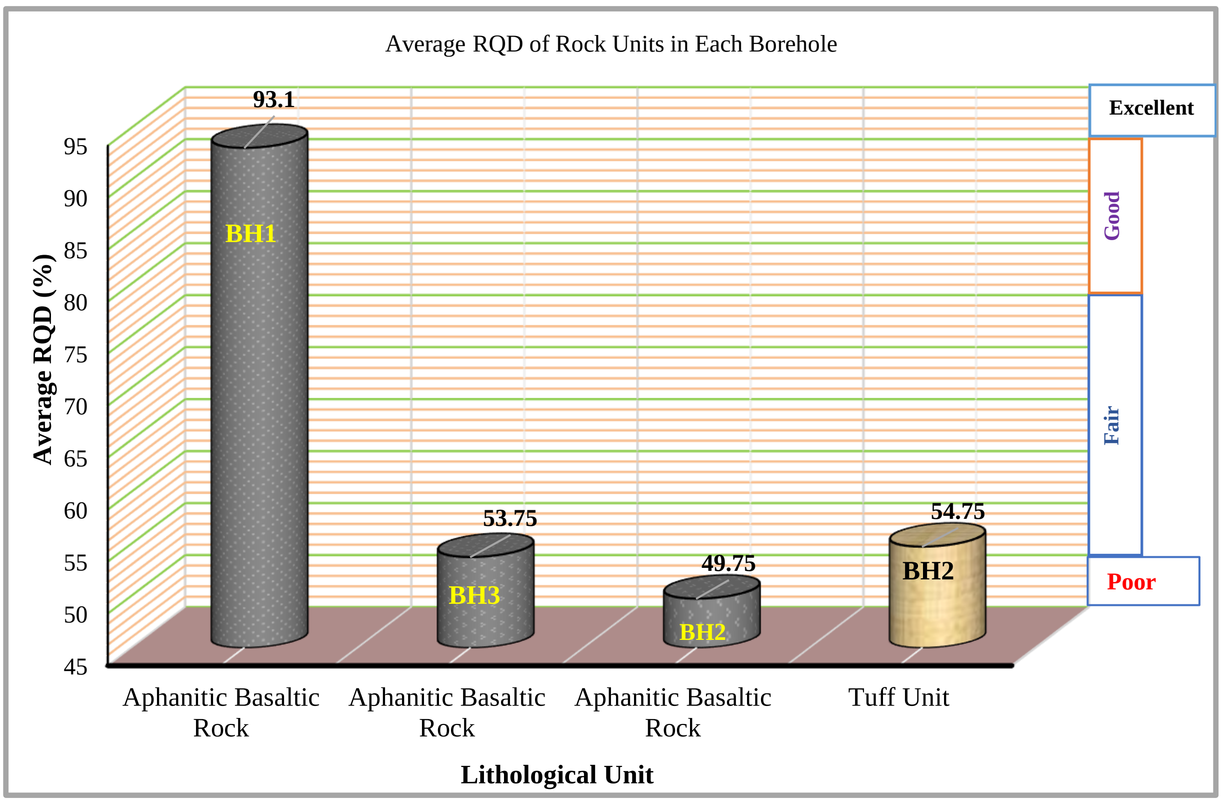

Figure 5. 9. Average RQD values of rocks into Deere and Deere (1988) RQD classes.

Similarly, the aphanitic basaltic rock in the right abutment borehole (BH-1) has an average RQD value of 93.1% indicating an excellent rock mass quality according to Deere and Deere (1988). This value shows that aphanitic basaltic rock in the right abutment borehole (BH-1) have lower degree of jointing. In the left abutment borehole (BH-3), the aphanitic basaltic rock unit have the percentage of RQD value distribution of 23%, 7.7%, 38.55%, 15.4% and 7.7% that were distributed to the rock mass quality of very poor, poor, fair, good, and excellent respectively as shown in Table 5.14. The aphanitic basaltic rock has an average RQD value throughout the borehole depth was 53.75% with fair rock mass quality indicating that the rock unit was moderately jointed rock mass. In the river center borehole (BH-2), the aphanitic basaltic rock has the percentage of RQD value distribution of 25%, and 75% that are with a RQD class to be in the very poor and fair respectively as shown in Table 5.14. The average RQD of the rock unit was 49.75% with RQD class of poor rock mass quality according to Deere and Deere (1988). The tuff rock unit has a percentage of RQD value distribution of 25%, 12.5%, 25%, 25%, and 12.5% that were distributed to be in very poor, poor, fair, good, and excellent respectively as shown in Table 5.14. The average RQD of the rock unit was 54.75% with RQD class of fair rock mass quality according to Deere and Deere (1988).

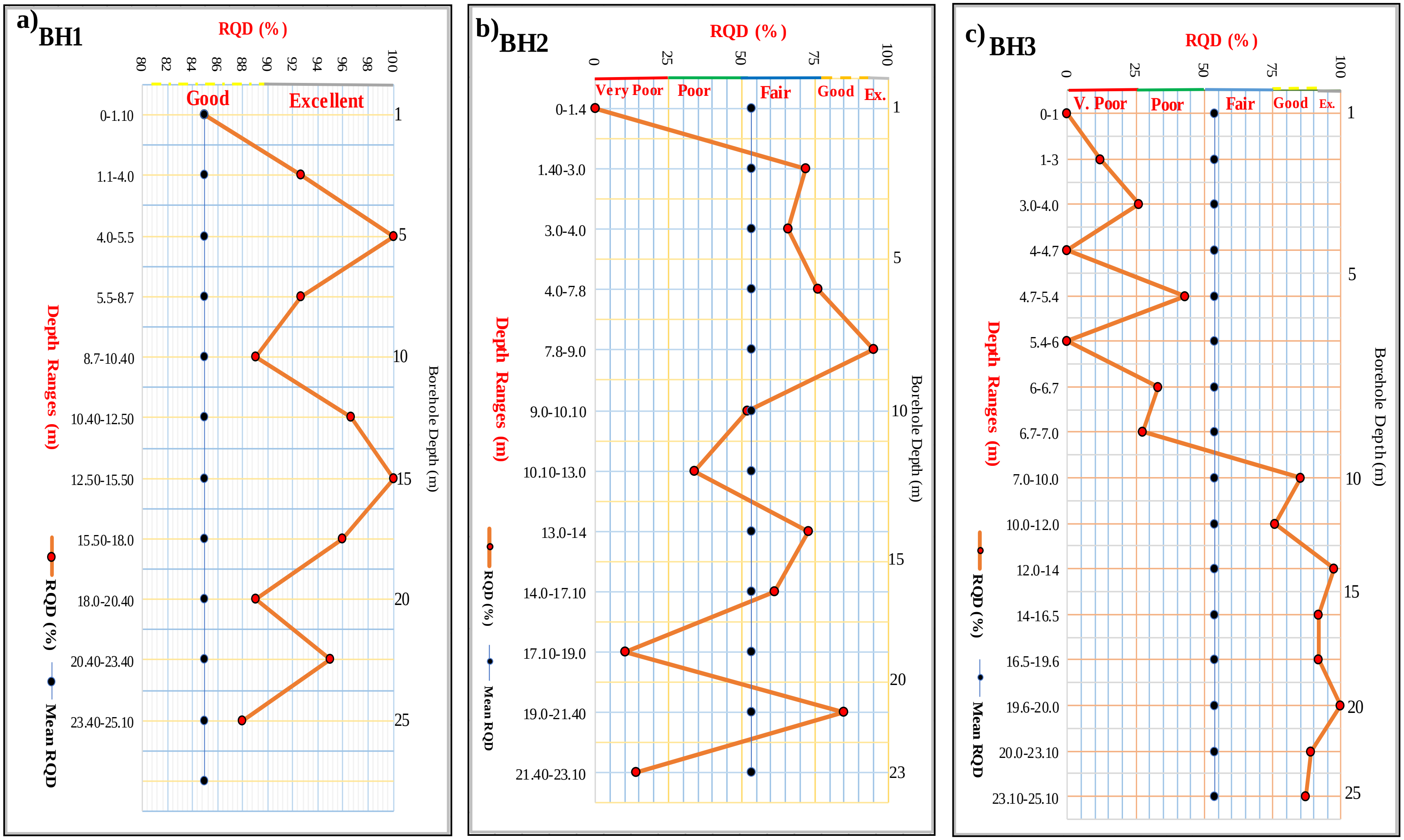

Figure 5. 10.Variation of RQD with depth at the dam site of the study area. a) right abutment (BH-1), b) left abutment (BH-2), and c) river center (BH-3).

5.2.2.4. Subsurface Rock Mass Permeability and Packer Test Interpretation

The lugeon or packer test and falling head tests were performed at the dam site to measure the hydraulic conductivity of subsurface rock mass. Ethiopian Construction Design and Supervision Works Corporation (ECDSWC, 2022) conducted these tests. During the investigation phase, water pressure (Lugeon) tests were conducted in three boreholes at abutments and along the dam axis. The packer test was conducted on the right abutment (BH-1) and left abutment (BH-3), and river center (BH-2).

The packer test on the right abutment (BH-1) indicated the Lu values of 0.32 at 5.50m and 0.04 at 15.0m. The Lu values at 10m and 25m depths were zero. The test on the river center borehole showed the Lu values of 0.092, 0.022, 0.043, and 0.28 at 5m, 14m, 20m, and 23m respectively. The Lu value at the depth of 9m was zero. As shown in Figure 5.12, the permeability values of the borehole decrease as the depth of the borehole increases. The packer test on the left abutment revealed the Lu values of 0.076, 0.0784, and 0.37 at 5m, 10m, and 15m depth and became zero at depth of 20m and 25m. Since the Lu values of each borehole is less than 1, the permeability class can be classified as low (Fell et al.(2005). These low Lu values show that the present joints with the rock masses are very tight and impermeable. The types of flow were also determined based on the packer test results. The flow type can be utilized to identify discontinuity and grouting-type features. At both dam abutments, the dominant flow type is laminar with distribution percentages of 100%. The dominant flow pattern at the river center is laminar which constitutes 75% of the packer test on the three boreholes and the 25% of the flow pattern is washout flow types as shown in Figure 5.11.

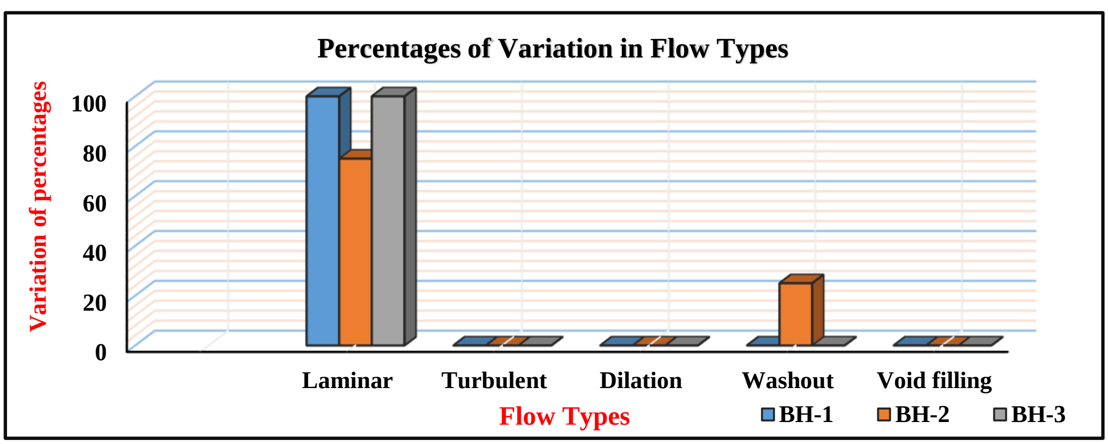

Figure 5. 11. Flow Pattern Distributions of the three boreholes.

Table 5. 15. Summarized Permeability test results and Lu values with respect to the depth (ECDSWC, 2022).

BH ID	**Test Section(m)**	**Falling Head test HydraulicConductivity (cm/sec)**	**Packer test Lugeon values**	**Representative Lugeon**	**Flow Pattern**	**Permeability Class (Fell et al.(2005)**
BH-01	1.50-5.50	-	0.32	<1	Laminar	Low
	5.00-10.00	-	0	<1	,,	Low
	10.00-15.00	-	0.04	<1	,,	Low
	15.00-20.00	-	0	<1	,,	Low
	20.00–25.00		0	<1	,,	Low
BH-02	0.00-5.00	1.20E-06	0.092	<1	-	Low
	4.00-9.00	-	0	<1	Laminar	Low
	9.00-14.00	-	0.022	<1	Laminar	Low
	14.00-20.00	-	0.043	<1	,,	Low
	20.00-23.00	-	0.28	<1	Wash out	Low
BH-03	0.0-5.0	9.89E-07	0.076	<1	-	Low
	5.0-10.0	1.02E-06	0.0784	<1	-	Low
	10.0-15.0	-	0.37	<1	Laminar	Low
	15.0-20.0	-	0	<1	Laminar	Low
	20.0-25.0	-	0	<1	Laminar	Low

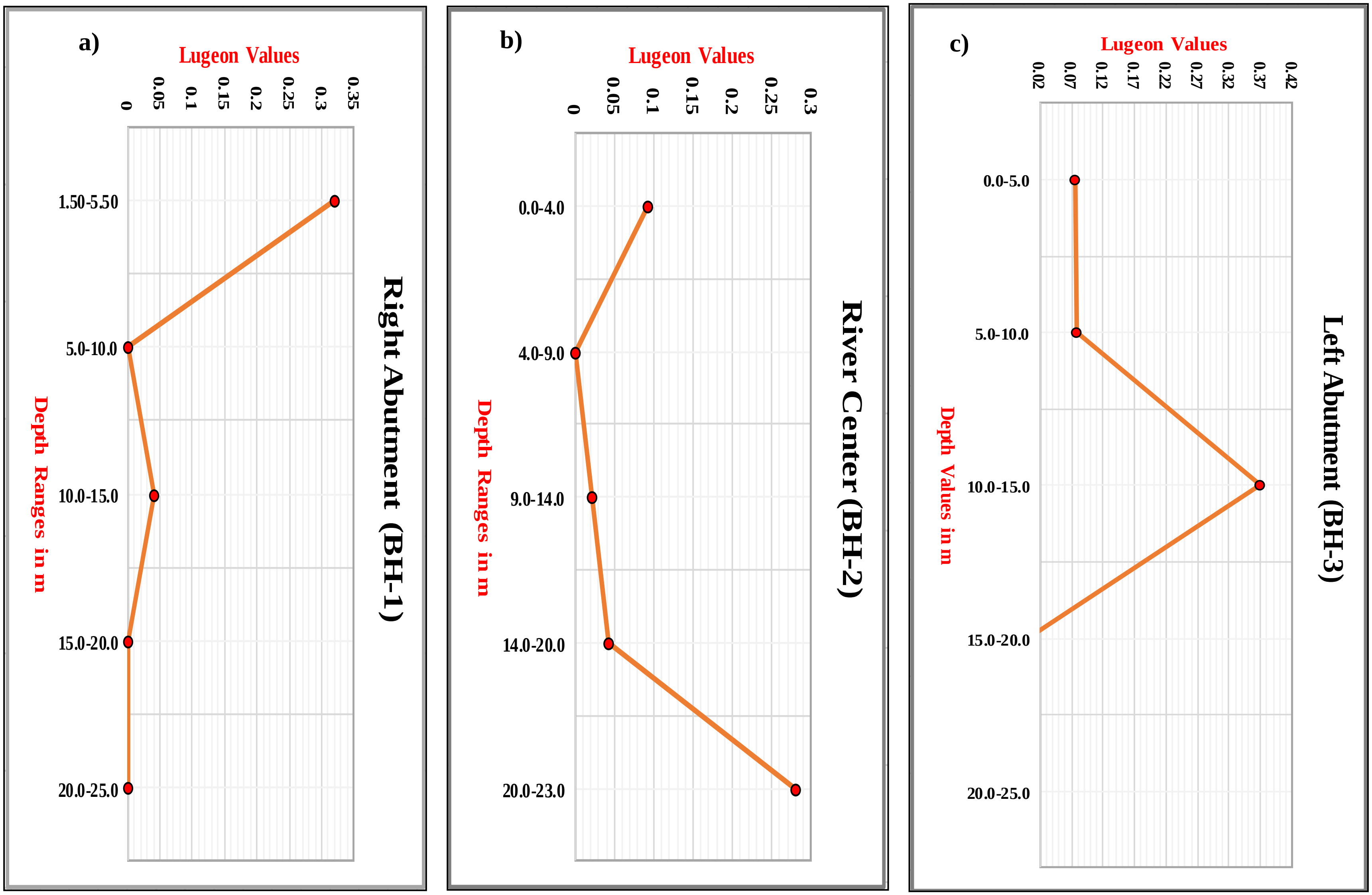

Figure 5. 12. Lu values with respect to depth. a) Right Abutment (BH-1), b) River Center (BH-2), and c) Left Abutment (BH-3).

5.2.2.5. Statistical Relation Between the Lugeon Value with RQD and Depth

The statistical relationship between the lugeon values and the drilled borehole depth was done for the river center and dam abutments. According to the analysis, even if the Lu values are less than 1 it tends to decrease with increasing depth and reaches zero after a particular depth at both dam abutments as shown in Figure 5.13a and 5.13b. The decrease in Lu values with drilled depth can be related to the decrease in the degree of jointing and weathering. Despite the Lu values are less than 1, at the test section depth range from 0.0-5.0m the Lu value was 0.092 and becomes zero at the test section depth range of 4.0-9.0m. Eventually the Lu value increases from zero to 0.28 at the test section depth range of 20.0-23.0m. At the test section depth range of 9.0-14.0m, and 14.0-20m, the Lu value was 0.022 and 0.043 respectively. Generally, the Lu values show a clear trend of increasing with depth at the river center as shown in Figure 5.13c.

Lu values and RQD can provide insight information about the rock mass quality and permeability. In some cases, a lower RQD value may be associated with the higher Lu value as more fractured rock mass can have greater permeability (higher Lu values) according to Hedayati et al. (2012) and Garo and Meten, (2021). The correlation of Lu values with RQD was also done for the dam abutments and river center at the dam site. The Lu values of aphanitic basaltic rock at the right abutment of the dam site show a correlation with RQD where the Lu values are lower with a higher average RQD value of 85%. At this section of the dam, the increase in the RQD values and decrease in the Lu values show that lower degree of jointing and weathering.

Considering the above correlation case, there is a vague correlation between the Lu and the RQD values throughout the test section at the river center and left abutment. In the river center at the depth range of 20.0-23.0m, the Lu value of slightly welded tuff was 0.28 with an average RQD value of 49.5% showing highly jointed rock mass. At the depth range of 0.0-5.0m, 9.0-14.0m, and 14.0-20.0m, the Lu value of basaltic rock and welded tuff was 0.092, 0.022, 0.043 respectively with average RQD values of 53.25%, 54.7%, and 58.5% indicating that moderately jointed rock mass. In the left abutment at the depth interval of 0.0-5.0m and 5.0-10m, the Lugeon value of the aphanitic basaltic rock was 0.076 and 0.0784 with an average RQD values of 16.2% and 29.1% respectively. With this lower value of RQD value, the Lu values are not considered to be reasonable. However, at depth interval of 10.0-15.0m, 15.0-20.0m, and 20.0-25.0m the Lu value of the aphanitic basaltic rock was 0.37 which decreased to zero with an average RQD values of 88.5%, 94.7% and 88%. At this section, the determined Lu values was reasonable based on the RQD value the rock mass was relatively sound to sound according to Deere and Deere (1988). The reason of the vague correlation was justified by numerous studies that have shown higher RQD values does not always show lower Lu values indicating that there are some conditions where lower RQD values result in the lower Lu values (Foyo et al., 2005; Ghafoori et al., 2011; Berhane and Walraevens, 2013). This shows that the inconsistency of the correlation which reveals permeability of rock mass can also depend on the aperture and continuity of fractures, the presence of clay minerals (presence of infilling material and type) and other factors that can affect the pathways and flow rate of water within the rock mass and failure of RQD to not consider the joint continuity and presence of infilling material.

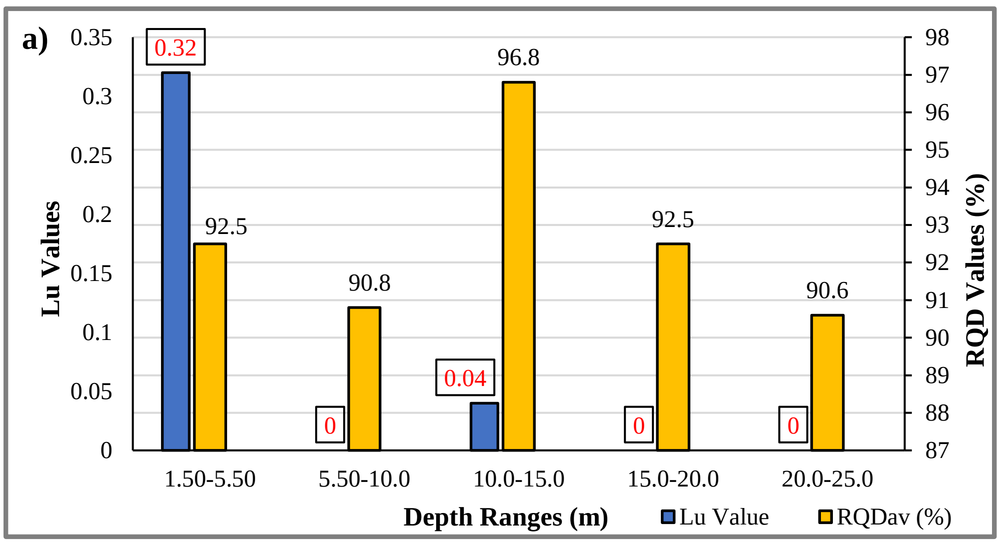

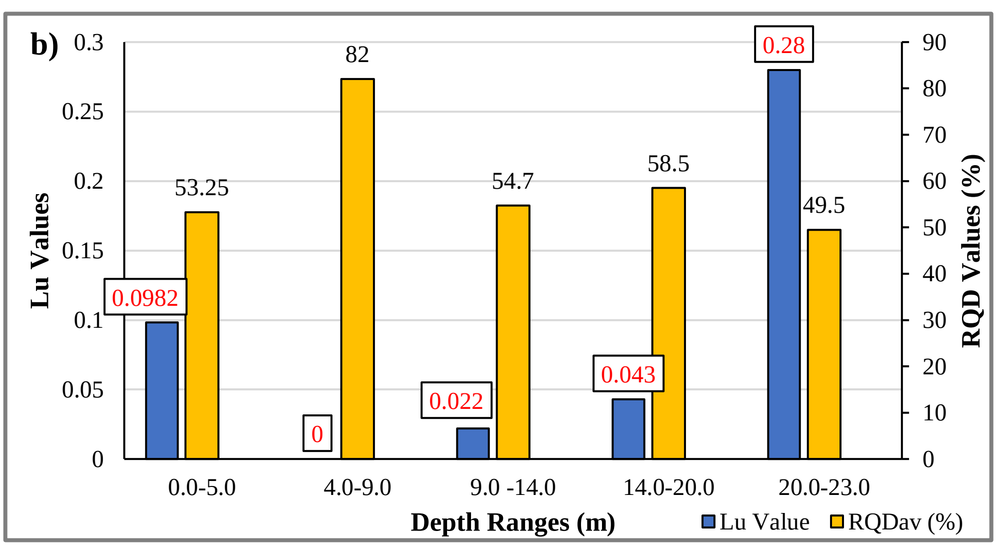

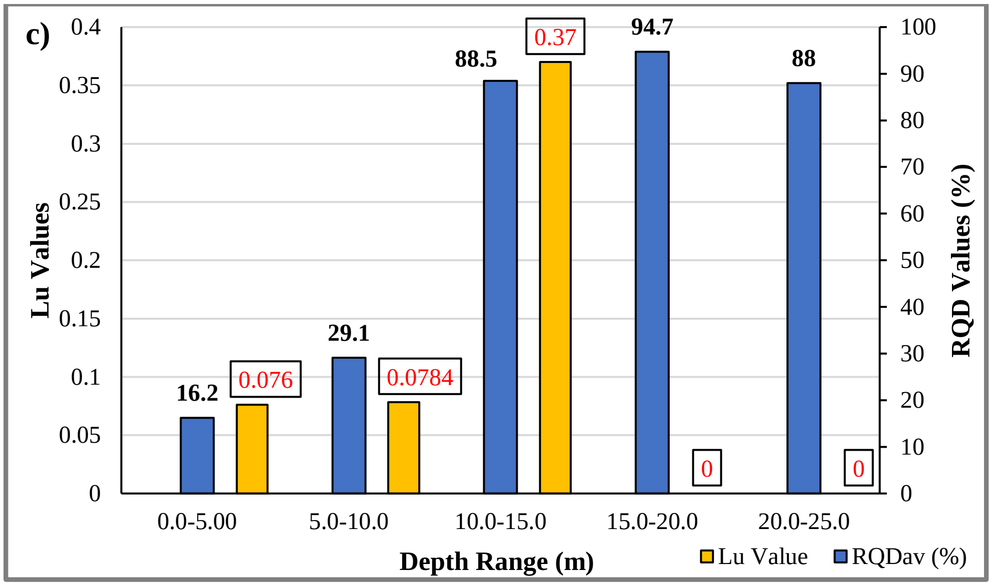

Figure 5. 13. Statistical relation between Lu values and RQD and depth. a) right abutment (BH-1), b) river center (BH-2), and c) left abutment (BH-3).

5.2.3. Groundwater Condition

The available groundwater data in the study area are from the drilled boreholes, and local well for domestic purposes. Groundwater level was recorded in these three boreholes during the geotechnical drilling and in-situ investigation by ECDSWC(2022). The groundwater level at the dam axis was determined from the borehole drilling and the groundwater level at the reservoir area was determined from the questionnaires to the local people at the dam site. At the right and left abutment, the groundwater table was located at the depth of 11.30m and 14.70m respectively. The river center, the groundwater table was located at the shallow depth of 0.60m. This groundwater table data utilized in the preparation of engineering geological cross section. At the reservoir area, the groundwater table at local well 1 and 2 was found at the depth of 6.0m and 5.0m respectively.

Table 5. 16. Groundwater levels in this study area at various boreholes.

<table>
<tr><th>S.No.</th><th colspan="2">Groundwater Location</th><th>Groundwater Level (m)</th></tr>
<tr><td>1.</td><td colspan="2">Right Abutment (BH-1)</td><td>11.30</td></tr>
<tr><td>2.</td><td colspan="2">River Center (BH-2)</td><td>0.60</td></tr>
<tr><td>3.</td><td colspan="2">Left Abutment (BH-3)</td><td>14.70</td></tr>
<tr><td rowspan="2">4.</td><td rowspan="2">Local Well-1</td><td>E = 39º 18’ 13.126”E</td><td rowspan="2">6.0</td></tr>
<tr><td>N = 9º 34' 02.737" N</td></tr>
<tr><td rowspan="2">5.</td><td rowspan="2">Local Well-2</td><td>E = 39º 17’ 57.316”E</td><td rowspan="2">5.0</td></tr>
<tr><td>N = 9º 34' 02.191" N</td></tr>
</table>

5.2.4. The Bearing Capacity of Dam Site Rock Mass

The load-bearing capacity of the rock masses in the dam site were determined with respect to the degree of weathering and fracturing surface for surface rock mass exposures using the empirical equation suggested by Carter and Kulwahy (1992) using equation (2.26), Wyllie(1992) using equation (2.27), Bell (2007) for rock on foundation sloped surface using equation (2.28) and (2.29), Bowles (1996) using equation (2.30) and (2.31).

The load-bearing capacity of rock mass calculated using Carter and Kulhawy (1992) was done to demonstrate the influence of weathering condition on the bearing capacity of rock mass. According to the study by Chala and Rao (2021) and Lamplmair et al.(2021), Weathering of rocks is one of the most important elements in reducing the mechanical attributes of rocks. Weathering generally results in adverse effects on the mechanical properties of the rock mass such as a reduction in strength and modulus of deformation. Many studies (Singh and Goel, 2011; Ramamurthy, 2004; Fookes et al., 1988; Ogunsola et al., 2017) have shown that weathering condition of the rocks considerably lower the UCS and tensile strength compared to their unweathered counterparts. The decrease in these mechanical properties directly affects the ultimate load bearing capacity of the rock mass. According to Lamplmair et al.(2021), there is a parallel correlation between the bearing capacity and mechanical properties of rocks. The bearing capacity of the rock mass was determined using the rock mass strength parameters such as S, mb, and *a* produced by RocData software. Using these parameters in the empirical equations suggested by Carter and Kulhawy (1992), the ultimate bearing capacity of the basaltic rock in the dam site was determined. The results shows that the rock mass on right abutment such as the slightly weathered aphanitic basaltic rock (SW*) have an ultimate bearing capacity of 49.85MPa and allowable bearing capacity of 16.62MPa and the moderately weathered aphanitic basaltic rock (MW*) have an ultimate bearing capacity of 38.64MPa and allowable bearing capacity of 12.88MPa. Similarly, In the left abutment the slightly weathered aphanitic basaltic rock (SW**) has an ultimate bearing capacity of 18.15MPa and allowable bearing capacity of 6.05MPa. The moderately weathered aphanitic basaltic rock (MW**) has an ultimate bearing capacity of 10.52Mpa and allowable bearing capacity of 3.51Mpa. The results show that the bearing capacity of basaltic rocks in the right abutment are higher than the bearing capacity of the basaltic rock in the left abutment. The results are given in the Table 5.17 and Figure 5.14.

Table 5. 17. Summarized and computed the bearing capacity of basalts at the dam site(Carter and Kulhawy, 1992).

Rock Unit Code	Input Parameters				Computed Outcome		
	UCS(MPa)	mb	S	*a*	qu,(Mpa)	FOS	qa,(Mpa)
SW*	146.88	2.228	0.0017	0.504	49.85	3	16.62
MW*	146.88	1.789	0.001	0.505	38.64	3	12.88
SW**	145.44	1.033	0.0002	0.510	18.15	3	6.05
MW**	145.44	0.596	0.0001	0.520	10.52	3	3.51
SW*= Slightly weathered Aphanitic Basaltic rock, and MW*= Moderately weathered Aphanitic Basaltic rock at right abutment, SW**=Slightly weathered Aphanitic Basaltic rock, and MW**= Moderately weathered Aphanitic Basaltic rock at left abutment.							

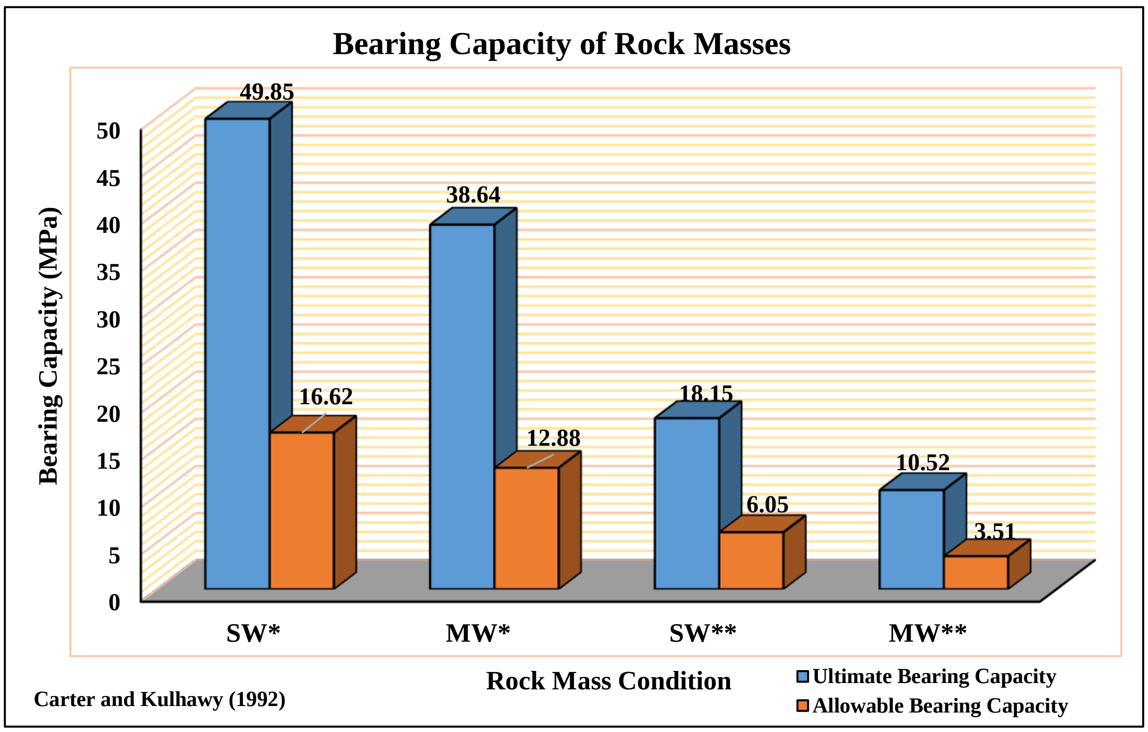

Figure 5. 14. The ultimate and allowable load-bearing capacity of basalts at the dam site (Carter and Kulhawy, 1992).

The bearing capacity of basalts at the dam site considering the fractured rock surface were also determined by using the Wyllie (1992) empirical equation. The basaltic rock masses in the right abutment have an ultimate bearing capacity of 50.45Mpa and allowable bearing capacity of 19.75Mpa. These results show that the right abutment basaltic rock have higher bearing capacity values. Table 5.18 and Figure 5.15 summarize the input parameters and computed outcome of the bearing capacity according to Wyllie (1992).

Table 5. 18. Summarized and computed the bearing capacity of basalts at the dam site according to Wyllie (1992).

Rock Unit	Input Parameters				Computed Outcome		
	GSI	UCS(MPa)	mb	S	qu,(Mpa)	FOS	qa,(Mpa)
Aphanitic Basaltic Rock*	56	146.88	2.228	0.0017	50.45	3	16.81
Aphanitic Basaltic Rock**	42	145.44	1.033	0.0002	19.75	3	6.58
Aphanitic Basaltic Rock* and Aphanitic Basaltic Rock**shows rock mass at the right and left abutment respectively.							

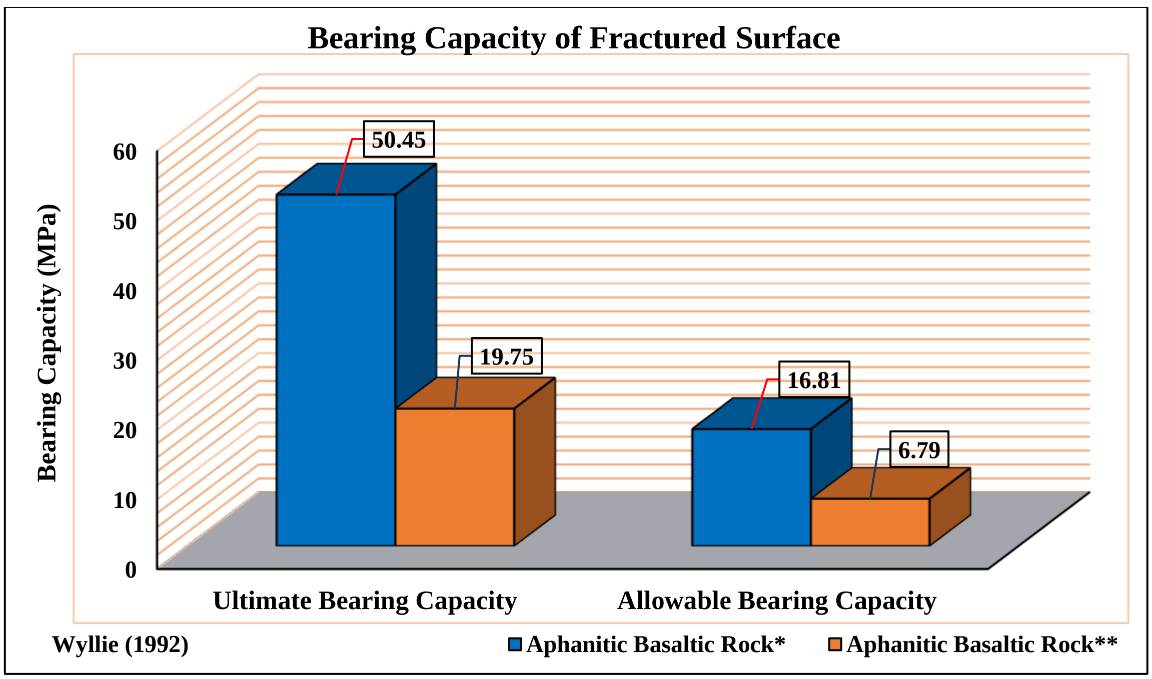

Figure 5. 15. The ultimate and allowable bearing capacity of basalts at the dam site according to Wyllie (1992).

The Bearing capacity of basaltic rocks on sloped ground surface are intensively controlled by the inclination of the slope due to reduced resistance provided by smaller mass of the rock on the downstream side of the footing (Wyllie ,1992). The bearing capacity of the aphanitic basaltic rocks were determined by using the equation suggested by Bell (2007). The results show that the right abutment aphanitic basaltic rock have an ultimate bearing capacity and allowable bearing capacity of 39.5Mpa and 13.17MPa respectively. Similarly, the aphanitic basaltic rock in the left abutment has an ultimate bearing capacity of 23.31MPa and allowable bearing capacity of 7.77MPa. The computed outcome indicates that the right abutment rock mass has higher bearing capacity than the left abutment rock mass as shown in the Table 5.19 and Figure 5.16.

Table 5. 19. Summarized and computed the bearing capacity of basalts at the dam site according to Bell (2007).

Rock Unit	Input Parameters									Computed Outcome	
	C (MPa)	Φ (º)	Bearing Capacity Factor			β(º)	H (m)	B (m)	γ (MN/m^3)	qu (MPa)	qa (MPa)
			No	N_{cq}	$N_{\gamma q}$						
ABR*	7.305	31	0.081	5.15	22.5	79	21	6	0.02816	**39.5**	**13.17**
ABR**	4.572	22	0.129	4.96	7.5	84	21	6	0.02805	**23.31**	**7.77**
ABR* and ABR** shows Aphanitic basaltic rock at the right and left abutment respectively.											

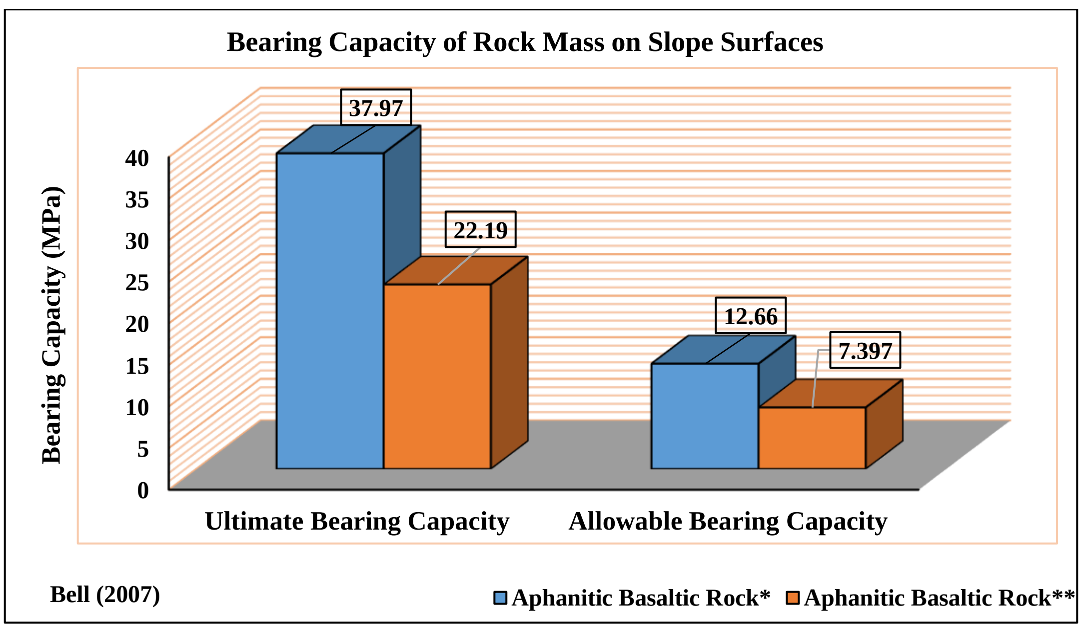

Figure 5. 16.The ultimate and allowable bearing capacity of basalts at the dam site according to Bell (2007).

The Bearing capacity of the rock mass in the river center and both abutments borehole units was determined using the Bowles (1996) equation using the RDQ and Uniaxial compressive strength of the rocks with respect to the depth and lithological unit. In the right abutment of the dam site, one lithological unit (ABR*) was identified with same degree of weathering and fracturing throughout the boreholes as shown in Appendix 5. In river center, five lithological unit (ABR1, TU1, TU2, ABR2,TU3) were identified based on depth and variation in RQD and UCS values (Appendix 5). In the left abutment, two distinctive lithological units were identified (ABR**1 and ABR**2) as given in Appendix 4. Accordingly, the rock mass's ultimate and allowable bearing capacity in the boreholes were determined.

The bearing capacity of the rock masses at the right abutment indicates the ultimate bearing capacity values of 56.59MPa and allowable bearing capacity of 18.86MPa. In the left abutment, the rock unit ABR**1 has an ultimate bearing capacity and allowable bearing capacity of 1.61MPa and 0.54MPa, respectively and the rock unit ABR**2 have the ultimate bearing capacity and allowable bearing capacity of 38.7MPa and 12.91MPa respectively. The river center rock mass indicates lower bearing capacity than both abutments rock units. The river center rock unit has ultimate bearing capacity and allowable bearing capacity ranging from 3.18×10^{-1}MPa to 20.31MPa and 1.06×10^{-2} MPa to 6.77MPa. The river center borehole's ultimate and allowable bearing capacity (BH-2) decreases with increasing depth. Similarly, the aphanitic basaltic rock at the river center borehole has the ultimate and allowable bearing capacity values ranging from 0.30MPa to 20.31MPa and 0.10MPa to 6.77MPa, respectively. The tuff unit have the ultimate and allowable bearing capacity values ranging from 0.11MPa to 0.34MPa and 0.037MPa to 0.11MPa.

From the analysis, the bearing capacity of aphanitic basaltic rock at both dam abutments is greater than the same rock unit at the river center. The tuff rock unit in the river center have lower bearing capacity compared to the aphanitic basaltic rock at the river center and both dam abutments.

Table 5. 20. Summarized ultimate and allowable bearing capacity of rock units in the borehole at the dam site with respect to the depth.

S.No.	Depth Range (m)	Rock Unit ID	Rock Unit Description	RQD_{av}		Average RQD Rock Mass Quality	UCS_{av} (MPa)	Qult (MPa)	Qall (MPa)
				%	In Decimal				
1.	0-25.10	ABR*	Gray, strong, fresh, massive basaltic rock	93.073	0.93073	Excellent	65.05	56.59	18.86
2.	0.0-4.20	ABR1	Slightly to highly fractured, fresh to moderately, medium to very strong basaltic rock.	49.8	0.498	Poor	81.91	20.31	6.77
3.	4.20-6.0	TU1	Reddish to light gray, slightly welded , weak tuff	74.3	0.743	Fair	0.2	0.11	0.037
4.	6.0-16.55	TU2	Light gray, slightly welded, weak tuff	65	0.65	Fair	0.7525	0.318	0.106
5.	16.55-18.0	ABR2	Dull to light gray, weak to medium strength, altered basaltic rock	35.5	0.355	Poor	0.70	0.30	0.1
6.	18.0-23.10	TU3	Dull to light gray, unwelded to slightly tuff	36.3	0.363	Poor	2.59	0.34	0.11
7.	0.0-7.0	ABR1**	Gray, medium strength, fresh to slightly weathered, highly fractured basaltic rock.	17.69	0.1769	Very Poor	51.33	1.61	0.54
8.	7.0-25.10	ABR2**	Gray, strong, fresh, massive basaltic rock.	89.81	0.8981	Good	48	38.7	12.91
	Note that: Factor of Safety (FOS) of 3 was used to determine the allowable bearing capacity.								

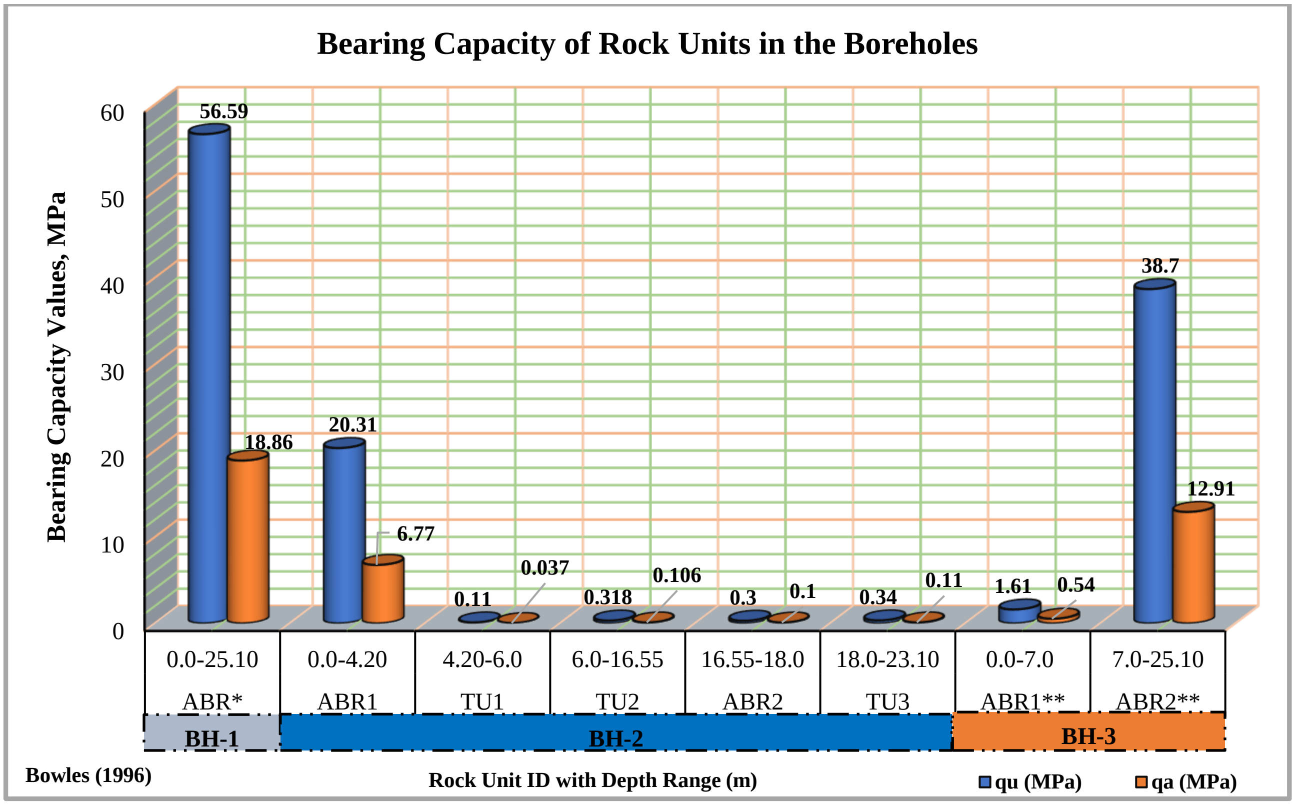

Figure 5. 17. The ultimate and allowable bearing capacity of basalts at the dam site according to Bowles (1996).

According to the design report by ECO (2022), the total load pressure of the dam is determined to be 7.7 MPa. Considering the low allowable bearing capacity of the underlying welded tuff unit, it is possible that the dam could experience settlement or even failure due to total settlement if the loads are not distributed appropriately. This could result in damage to the dam structure, leaks, or even catastrophic failure. On the other hand, the 4.20-meter-thick layer of aphanitic basaltic rock with its high allowable bearing capacity of 6.77 MPa provides a strong and stable foundation for the dam. This layer can help distribute the load more evenly and reduce the risk of total settlement.

5.3. Soil Engineering Characterization and Classification

5.3.1. Water Content of Soils

The water content of soil samples is important since it affects various soil properties, such as compaction, permeability, compressibility, and shear strength. Water content was determined using a laboratory test known as the oven-dry method, where a sample is weighed before and after drying in an oven at a specified temperature.

The obtained result indicates the natural moisture content of the soils with values ranging from 12.4% to 14.1% for the left bank and 15.2% for the right bank of the reservoir area. Additionally, ECO (2022) also investigated and analyzed the water content of the soil samples from the reservoir area where the values of the water content of the soils are 8.7%, 17.6%, and 7.3% for the right upper bank, right bank, and left bank of the reservoir area respectively as given in Appendix 9.

5.3.2. Specific Gravity of the Soils

The specific gravity of the solid soil was conducted using a pycnometer according to ASTM D 854(1998) standard, where the results of the test show that the specific gravity of the soil samples from the reservoir area of the study area ranges from 2.60 to 2.7 as shown in below tables.

Table 5. 21. The laboratory results of the specific gravity of the soil samples.

S. No.	Soil Sample Code	Gs Values
1.	LBSS-1	2.7
2.	LBSS-2	2.60
3.	RBSS-1	2.7
LBSS-1= Left Bank Soil Sample-1, LBSS-2= Left Bank Soil Sample-2, RBSS-1= Right Bank Soil Sample-1		

5.3.3. Consistency of the Soils

The moisture content of soil greatly influences its consistency; at very high moisture content, soil behaves more like a liquid form, and as moisture content steadily declines in the soil, soil behavior changes from one state to the other. The plasticity index was qualitatively characterized by Burmeister (1949) as follows:

Table 5. 22. Plasticity State Classification of Soils (Burmeister, 1949).

Plasticity Index(PI), %	Plasticity State
0	Non-Plastic
1-5	Slightly plastic
5-10	Low
10-20	Medium
20-40	High
>40	Very high

To ascertain the liquid limit, plastic limit, and plasticity index and classify soil samples via the Unified Soil Classification system, the Atterberg limit test was conducted for three representative soil samples from the reservoir area of the study area as shown in the Appendix 13. The result of the test shows liquid limit values of 62.48%, 48.13%, and 61.39% for the left bank soil sample at a depth of 1m, the left bank of the reservoir area at a depth of 1.7m, and the right bank of soil sample at a depth of 1m. Then, the plastic limit of the soil samples obtained from the test indicates values of 36.38% and 32.34% for left bank soil samples at a depth of 1m and 1.70m, respectively, and 37.14% for the right bank of the reservoir area. Finally, after determining the liquid limit and plastic limit of the soil sample, the plasticity index of the representative soil sample is determined from the difference between the liquid limit and plastic limit. In this case, the plasticity index of the samples indicates values of 26.1% and 15.79% for left bank soil samples at a depth of 1m and 1.70m, respectively, and 24.25% for the right bank of the reservoir area. Generally, the plasticity index values show the plasticity state of the soil that ranges from medium to high plasticity state, as shown in Table 5.23.

Similarly, ECO (2022) also conducted an Atterberg test of the soil samples' consistency from the study area's right and left riverbanks as given in Appendix 13. Consequently, the liquid limit results indicate 65.51%, 50.20%, and 50.50% for the right upper bank, right bank, and left bank of the reservoir area, respectively. Furthermore, the plastic limit of the soil samples has values of 39.75%, 33.39%, and 36.66% for the right upper bank, right bank, and left bank of the reservoir area, respectively. Finally, the soil samples have a plasticity index of 13.84%, 16.81%, and 25% for the right upper bank, right bank, and left bank of the reservoir area, respectively. According to Burmeister (1949), the Plasticity index of soil samples shows a plasticity state that ranges from medium plasticity to high plasticity. The summarized results of the Atterberg limit test and Casagrande Chart of the soil sample are in the table below (Table 5.23) and the figure below (Figure 5.18).

Table 5. 23. The Atterberg test result of the soil samples.

S.No.	Atterberg Limits (%)	Soil Sample Codes			Soil Sample Codes (Data sources: ECO, 2022)		
		LBSS-1	LBSS-2	RBSS-1	SO/75/99	SO/76/99	SO/77/99
1.	LL	62.48	48.13	61.39	65.51	50.20	50.50

2.	PL	36.38	32.34	37.14	39.75	33.39	36.66
3.	PI	26.1	15.79	24.25	25	16.81	13.84
USCS		MH	ML	MH	MH	ML	ML
Plasticity State (Burmeister,1949)		**High Plasticity**	**Medium Plasticity**	**High Plasticity**	**High Plasticity**	**Medium Plasticity**	**Medium Plasticity**
LL= Liquid Limit, PL= Plastic Limit, PI= Plasticity Index, LBSS-1= Left Bank Soil Sample-1, LBSS-2= Left Bank Soil Sample-2, RBSS-1= Right Bank Soil Sample-1, SO/75/99= Pit 1 Right Upper Bank, SO/76/99= Pit 1 Right Bank, SO/77/99 = Pit 1 Left Bank.							

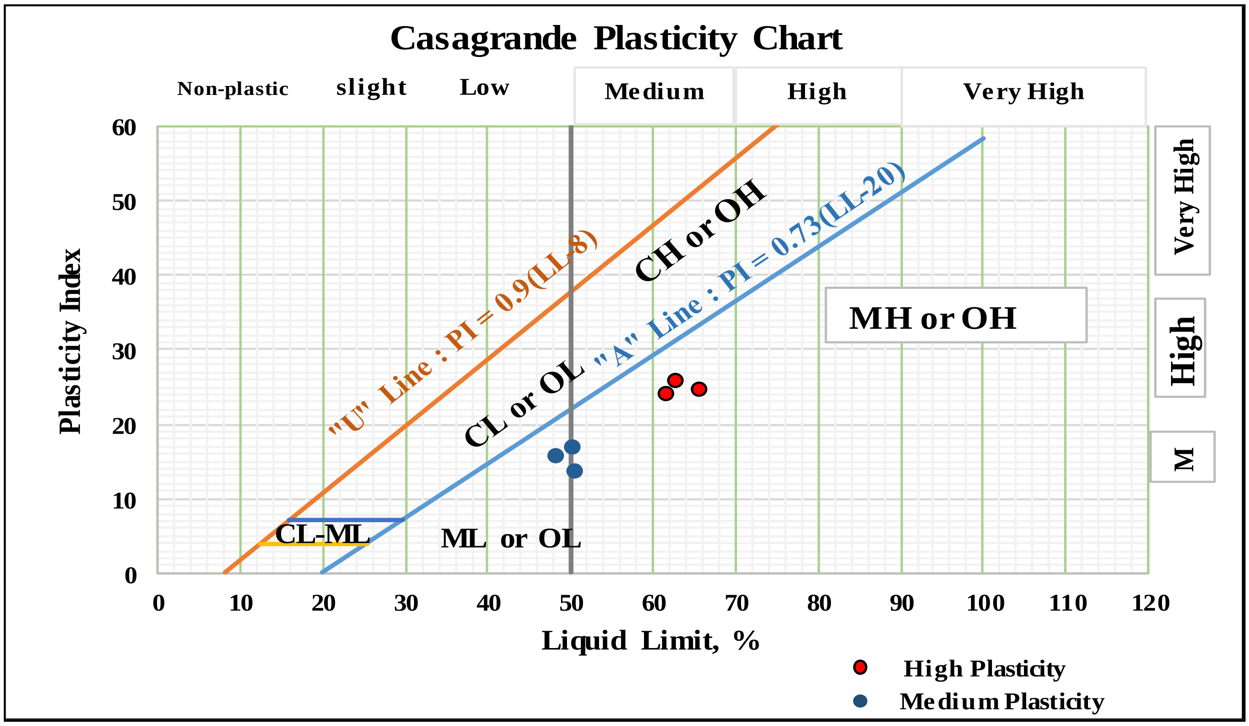

Figure 5. 18. Plasticity chart showing the distribution of soil in the study area (after Burmeister,1949).

5.3.4. Activity of Soils

According to Skempton (1953), the soil's activity indicates how flexible the soil is with the amount of clay. The importance of the clay's influence on the qualities of the soil increases with activity. The results of the activity of soils in (Table 5.3.) show that the LBSS-1 and RBSS-1 have activity values of 0.43 and 0.37, indicating the inactive type of soils and the soil samples from LBSS-2 test pit taken at a depth of 1.70m have an activity value of 1.05 showing the normal activity classification.

Table 5. 24. The activity of soils of the study area.

Soil Sample Code	Soil Activity Input Parameters		$Activity\ of\ Soil = \frac{PI}{\% <\ 2\mu m}$	Activity Classification
	Plasticity Index (%)	% Finer (%< 2μm)		
LBSS-1	26.1	60	0.43	Inactive
LBSS-2	15.79	15	1.05	Normal
RBSS-1	24.25	66	0.37	Inactive
LBSS-1= Left Bank Soil Sample-1, LBSS-2= Left Bank Soil Sample-2, RBSS-1= Right Bank Soil Sample-1				

5.3.5. Particle Size Distribution of the Soils

Particle size distribution of the soil samples from the reservoir area's left and right banks was done using sieve analysis and hydrometer analysis to determine the grain size percentage of the study area soils. The particle size distribution for soil particles greater than 75µm in diameter was conducted using the sieve analysis whereas for soil particles less than 75µm in diameter hydrometer analysis was carried out. The particle size distribution curve was plotted using the percent finer and particle diameter for the soil samples from both analysis outcomes. The result from both tests indicates the different percent of grain size ranging from sand to clay size with 0% of gravel particle size of soils as shown in Table 5.4. The soil samples left bank at a depth of 1m show a particle size percentage of 14% of sand, 26% of silt, and 60% of clay, and at a depth of 1.70m, the soil samples have a particle size of 48% of sand, 23% of silt and 15% of clay. The soil samples from the right bank of the reservoir area show the particle size of 12% of sand, 22% of silt, and 66% of clay size particles of soil. Therefore, the predominant size of soil particles in the research area is fine-grained soil. The grain size distribution of the soil samples from the reservoir area is given in the Figure 5.19.

Table 5. 25. The Particle size distribution of soil samples of the study area.

Soil Sample Codes	**Depth (m)**	**Particle Size Distribution (%)**			
		Gravel	**Sand**	**Silt**	**Clay**
LBSS-1	0.0-1.0	0	14	26	60
LBSS-2	1.0-1.70	0	47	23	15
RBSS-1	0.0-1.0	0	12	22	66

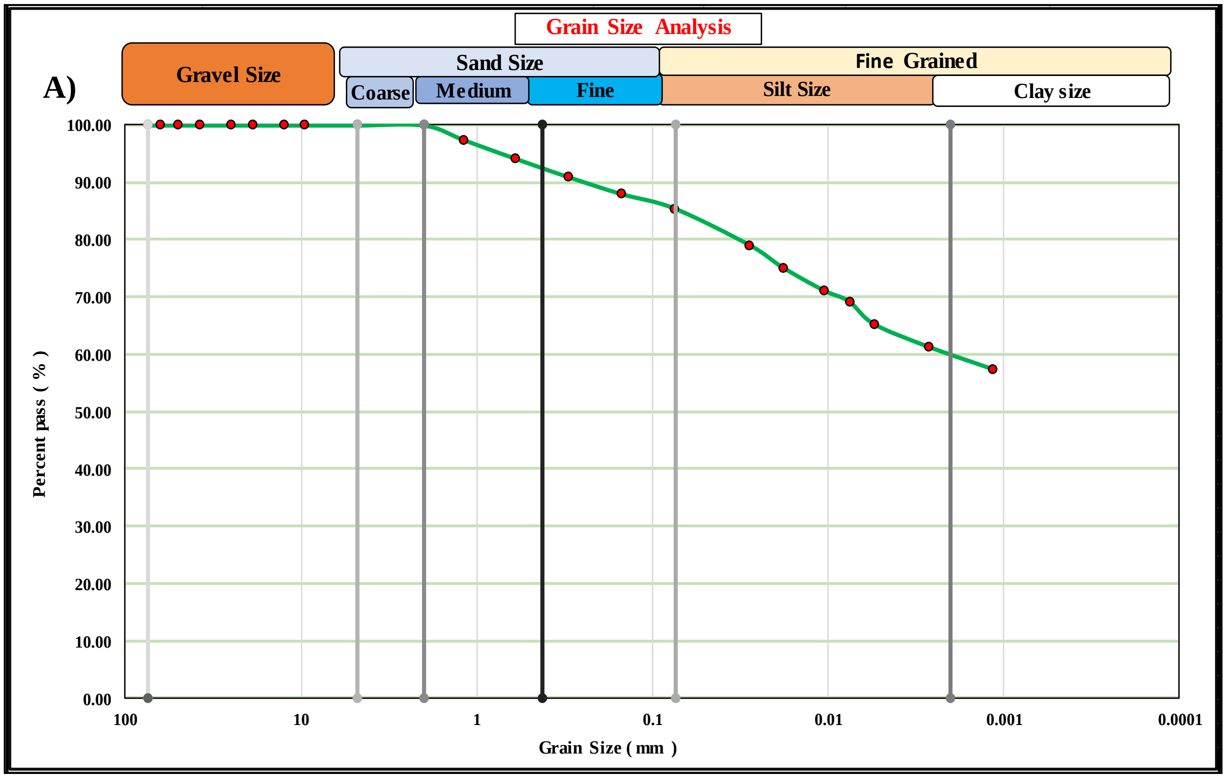
Grain Size Analysis
A)
Gravel Size
Sand Size
Coarse
Medium
Fine
Fine Grained
Silt Size
Clay size
Percent pass (%)
100.00
90.00
80.00
70.00
60.00
50.00
40.00
30.00
20.00
10.00
0.00
100
10
1
0.1
0.01
0.001
0.0001
Grain Size (mm)

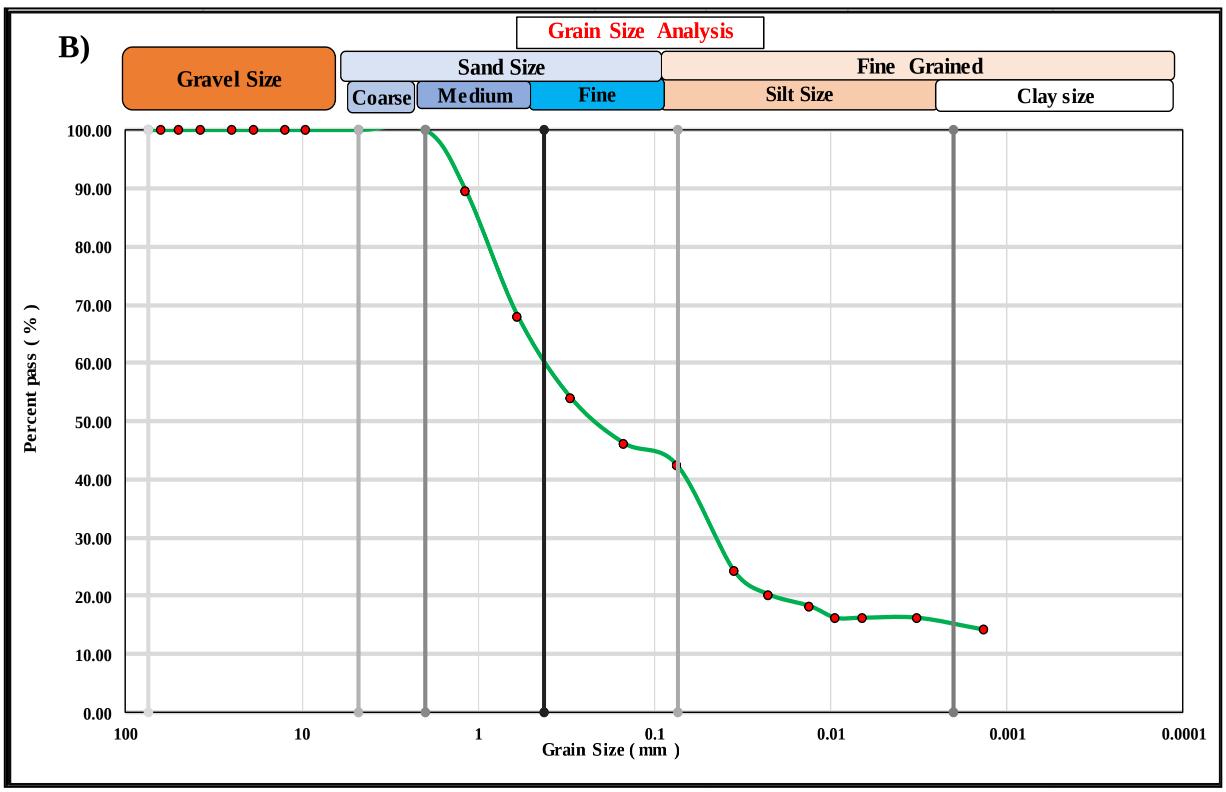
Grain Size Analysis
B)
Gravel Size
Sand Size
Coarse
Medium
Fine
Fine Grained
Silt Size
Clay size
Percent pass (%)
100.00
90.00
80.00
70.00
60.00
50.00
40.00
30.00
20.00
10.00
0.00
100
10
1
0.1
0.01
0.001
0.0001
Grain Size (mm)

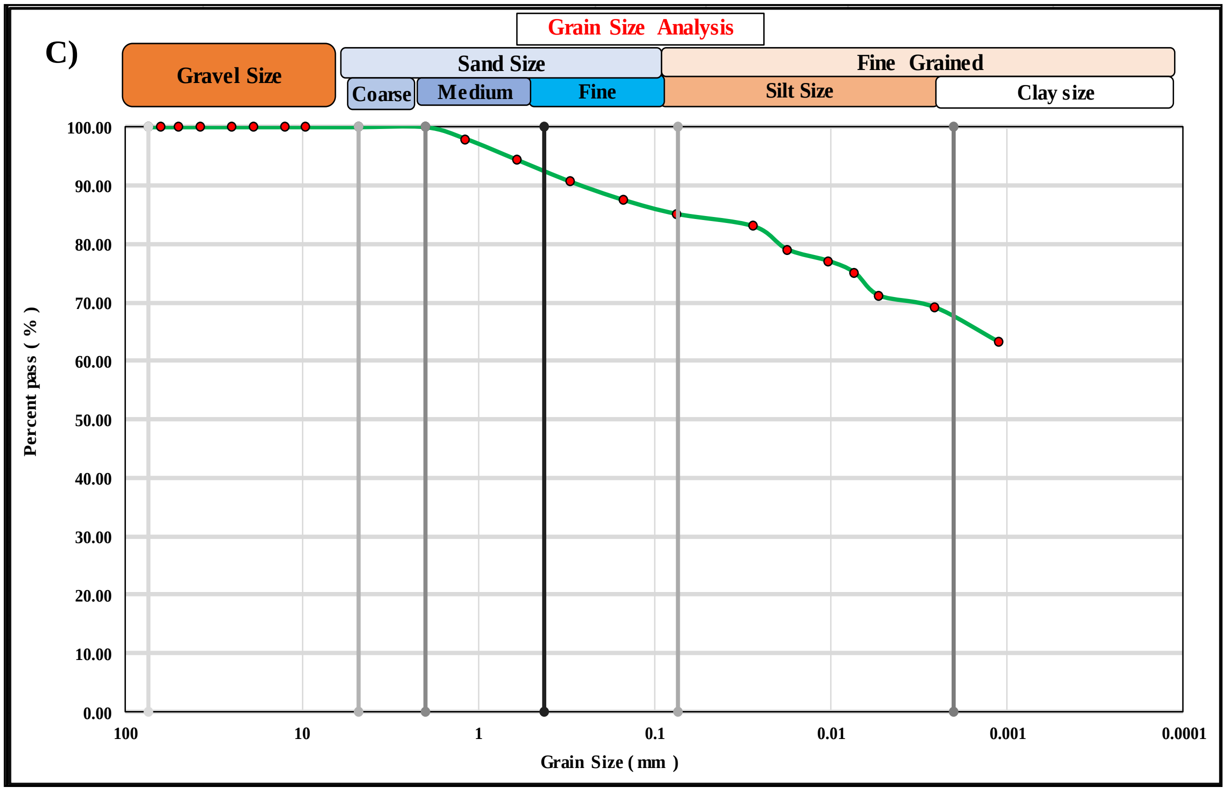

Figure 5. 19. Grain Size Distribution curve for the soil samples. A) LBSS-1, Left Bank Soil Sample-1, B) LBSS-2, Left Bank Soil Sample-2, C) RBSS-1, Right Bank Soil Sample-1.

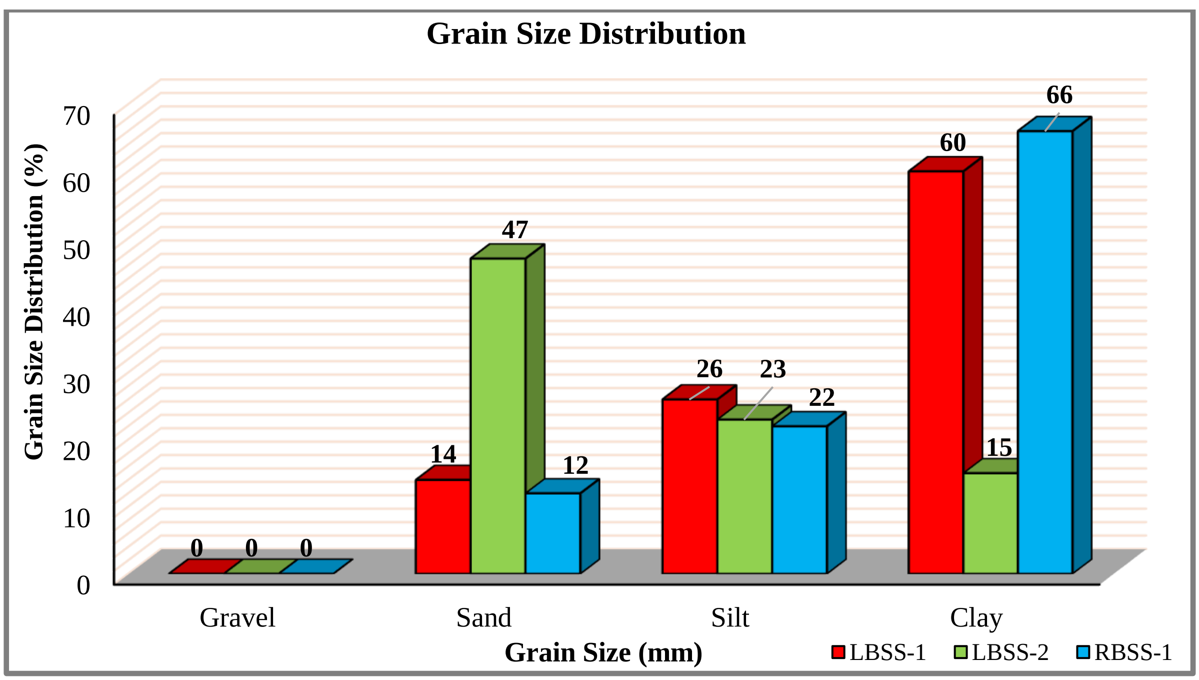

Figure 5. 20. Grain size distribution for the soil samples.

5.3.6. Engineering Classification of Soils

The results of particle size analysis showed that most of the soil samples from reservoir area consists of finer soil particles mainly silty soil and clayey soil with minimum percentage of sandy soil and no gravel in their particle size distribution. The soil sample from LBSS-2 at the depth of 1.0-1.70m mainly have greater percentage of sandy soil with silty soil and smaller amounts of clayey soils.

Table 5. 26. Summarized results of grain size distribution and the Atterberg limits (LL, PL, and PI) of soil Samples.

Soil Sample Codes	Atterberg limits			Grain Size Distribution (%)				(USCS)	Group Name
	LL	PL	PI	Gravel	Sand	Silt	Clay		
LBSS-1	62.48	36.38	26.1	0	14	26	60	MH	Clayey silt
LBSS-2	48.13	32.34	15.79	0	47	23	15	ML	Sandy silt
RBSS-1	61.39	37.14	24.25	0	12	22	66	MH	Clayey silt

5.3.7. Compaction of Soils

According to Craig (2004) and Kasim and Lah (2008), A proper understanding of the relationship between compaction, MDD, and OMC is crucial for many geotechnical engineering applications, such as the construction of embankments, dams, and foundations, where the stability and durability of the structure depend on the compacted soil's strength and compressibility characteristics. The compaction of soils can be described in terms of maximum dry density (MDD) and optimum moisture content. Maximum dry density (MDD) is the maximum weight of dry soil per unit volume when compacted under a specific compaction effort. In contrast, optimum moisture content (OMC) refers to the water content at which the soil can attain the maximum dry density when compacted to a certain degree (Craig, 2004).

The maximum dry density of the soil samples shows values ranging from 1.418 g/cm^3 to 1.57 g/cm^3 and 1.181 g/cm^3 to 1.534 g/cm^3 on the right bank and the left bank of the reservoir area, respectively. Furthermore, the optimum moisture content of the soils indicates values that range from 26.0% to 26.7% and 21.27% to 27.2% on the right bank and left bank of the reservoir area of the study area. The results of the Standard proctor test are summarized in Table 5.27.

Table 5. 27. Summarized table of the compaction test results in terms of maximum dry density and optimum moisture content.

S.No.	Soil Sample code	Compaction Parameters	
		MDD (g/cm^3)	OMC (%)
1.	LBSS-1	1.5	27.2
2.	LBSS-2	1.534	24.3
3.	RBSS-1	1.485	26
4.	SO/75/99	1.418	26.2
5.	SO/76/99	1.57	25.7
6.	SO/77/99	1.181	21.27

MDD = Maximum Dry Density, OMC= Optimum Moisture Content, LBSS-1= Left Bank Soil Sample-1, LBSS-2= Left Bank Soil Sample-2, RBSS-1= Right Bank Soil Sample-1, SO/75/99= Pit 1 Right Upper Bank, SO/76/99= Pit 1 Right Bank, SO/77/99 = Pit 1 Left Bank.

5.3.8. The Permeability of Soil Mass

The permeability of the soil at the dam reservoir area accounts for the stability of the dam and the operational life of the dam itself. The soil samples from the dam reservoir area at various locations and depths were collected and taken to the laboratory during the fieldwork. The soil laboratory analysis of its permeability was also conducted by ECO (2022) to determine the permeability of the soil masses in the reservoir area. The laboratory results of the test are summarized in the table below.

The results of the test show that most of the soil samples from the reservoir area show impermeable characteristics of the soil mass, which as a result, is suitable for the water to be stored in the reservoir area. The soil samples collected from 1.0m depth shows the permeability value ranging from 2.0686×10^{-6} cm/s to 9.0343×10^{-6} cm/s indicating impermeable class according to USBR (1987). The LBSS-2 soil samples have a permeability value of 1.08x10-4 cm/sec, showing semi-pervious features of the permeability, and this soil sample is located at a depth of 1.70m underlining the LBSS-1. This semi-pervious soil sample could not be an issue of seepage since it is overlined by the impermeable soil mass. This makes it an ideal choice for dam reservoir, as the impermeable soil will prevent significant water seepage, ensuring the dam's efficiency and stability. The impermeable soil also reduces the risk of potential leaks. The impermeable soils are ideal for dam reservoir construction due to their ability to prevent water leakage, while semi-permeable soils may still be suitable, but might require additional engineering techniques to enhance their performance in the reservoir's base to reduce seepage losses. Soil permeability analysis is critical in determining the suitability of a site for dam reservoir construction and plays a significant role in the overall efficiency and longevity of the dam project.

Table 5. 28. Summarized table of the Falling head permeability test results in terms of hydraulic conductivity soils and soil permeability classification according to Bell, (2007) and USBR, (1987).

Soil Sample Code	Depth of test pit (m)	Hydraulic Conductivity, K(cm/sec)	Soil Permeability Classification	
			Bell (2007)	(USBR, 1987)
LBSS-1	0.0-1.0	9.0343×10^{-6}	Low	Impermeable
LBSS-2	1.0-1.70	1.08×10^{-4}	Medium	Semipervious
RBSS-1	0.0-1.0	8.010×10^{-6}	Low	Impermeable
SO/75/99	0.0-1.0	2.0686×10^{-6}	Low	Impermeable
SO/76/99	0.0-1.0	1.055×10^{-3}	Medium	Semipervious
SO/77/99	0.0-1.0	6.081×10^{-6}	Low	Impermeable

LBSS-1= Left Bank Soil Sample-1, LBSS-2= Left Bank Soil Sample-2, RBSS-1= Right Bank Soil Sample-1, SO/75/99= Pit 1 Right Upper Bank, SO/76/99= Pit 1 Right Bank, SO/77/99 = Pit 1 Left Bank.

In general, the permeability of the soils at the reservoir site is relatively low and watertight allowing water to be retained in the reservoir area following impoundment. As a result, the reservoir site is nearly watertight ensuring long-term durability and reliability of the reservoir.

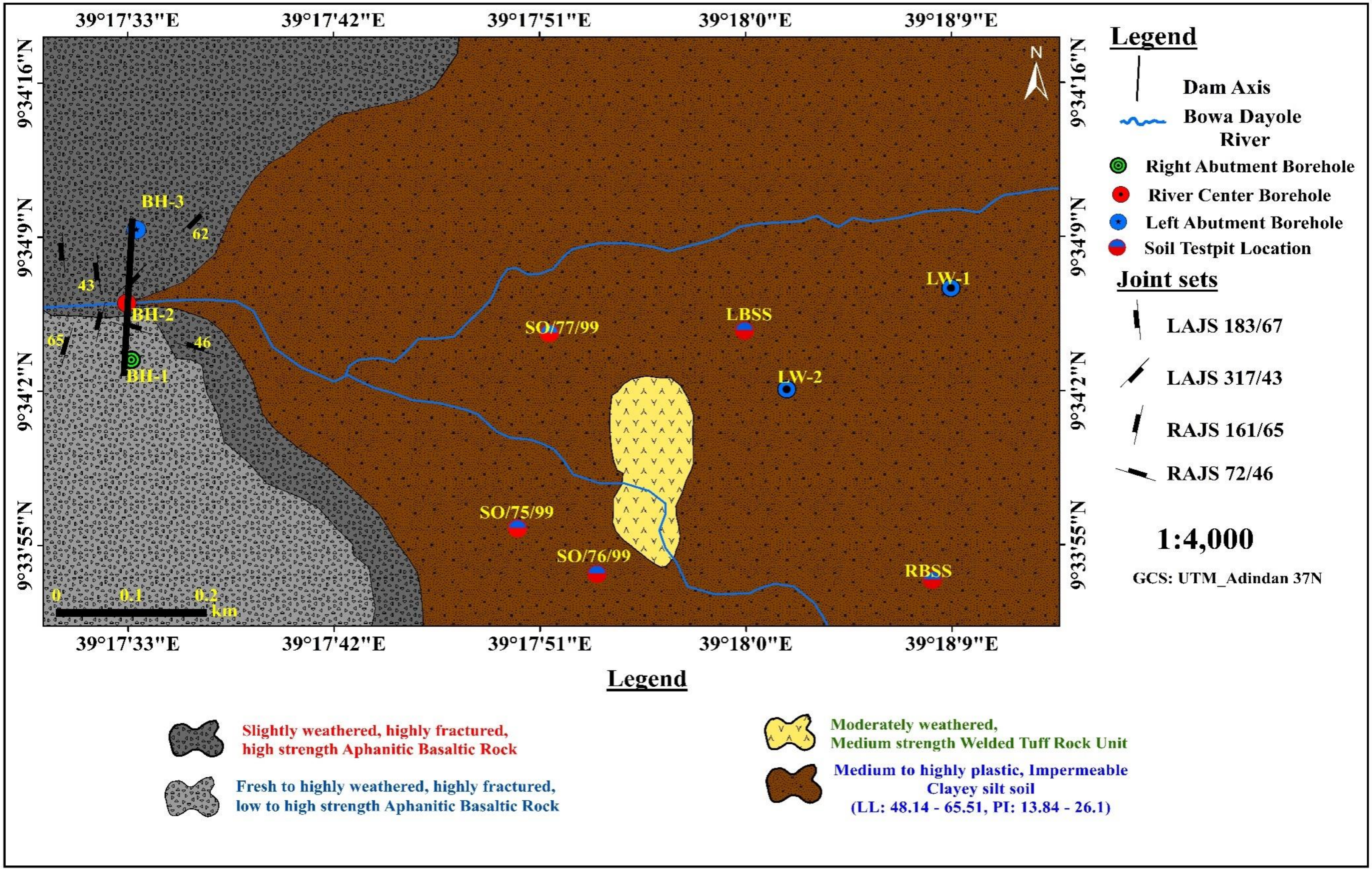

Figure 5. 21. Engineering geological map of the dam site and its surroundings at a scale of 1: 4,000.

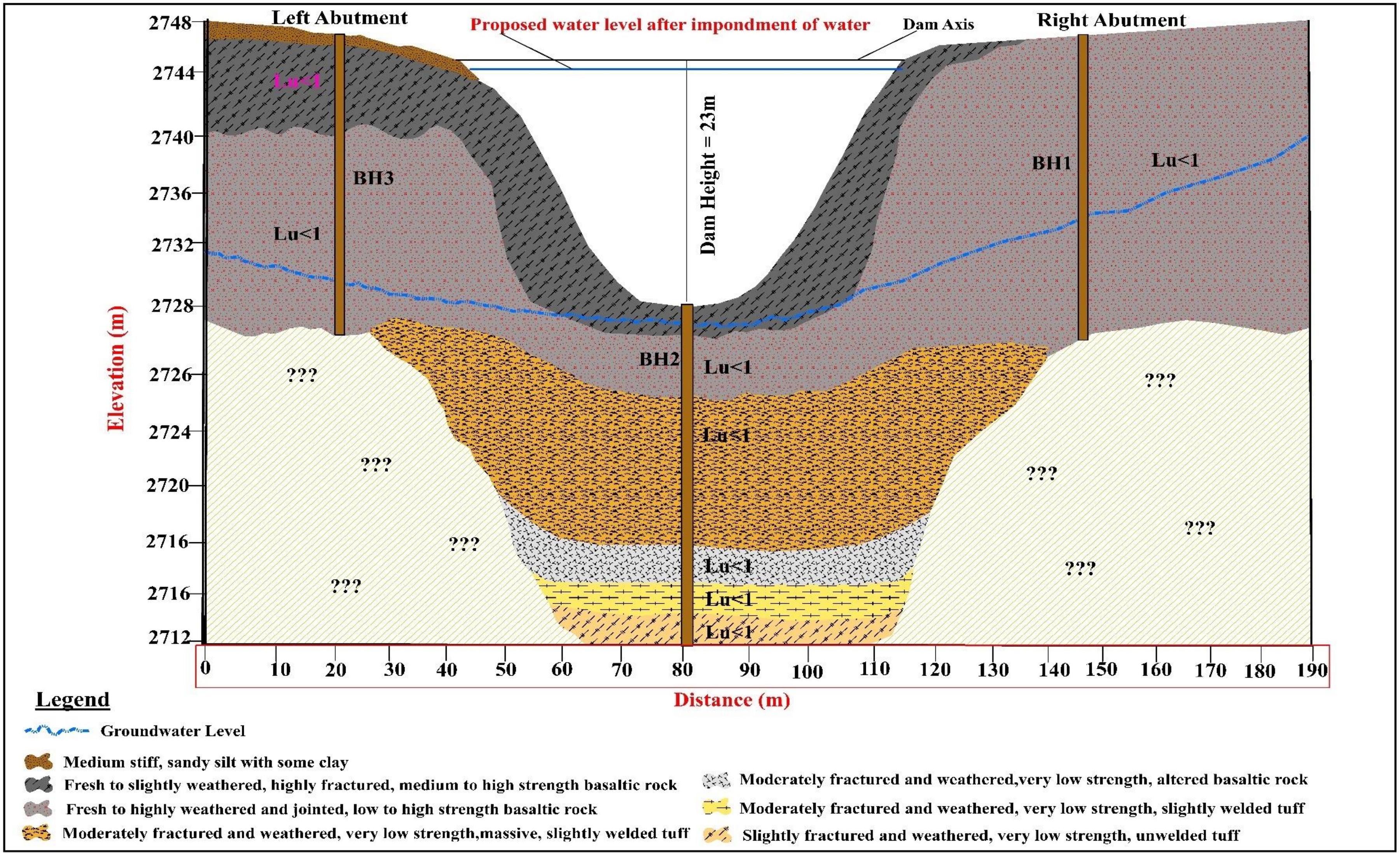

Figure 5. 22. Engineering geological cross-section along the dam axis (location of borehole, inferred geological structures and proposed mean water level after impoundment of the dam were shown).

5.4. Slope Stability Analysis of the Dam Abutments

The critical slope sections at the dam abutments and reservoir rim may pose problems for the dam's safe operation. Identifying such potentially unstable slopes at the reservoir rim and abutments during the initial phase of the investigation may help to determine appropriate remedial actions. During the field investigation, potential slope critical sections were identified based on the factors controlling the failure mechanism, i.e., either structurally controlled failures or non-structurally controlled failures (rock mass-controlled failures). In this study, the critical slope sections at the dam abutments are structurally controlled failures. The reservoir rims at the study area are safe since their slope angle tends to be relatively horizontal.

5.4.1. Kinematic Analysis

Kinematic analyzes were performed for the structurally controlled slope failure on the right abutment slope sections (RASS) and the left abutment slope sections (LASS), as shown in Figure 5.24, and analyzed using Dips 6 software (Rocscience, 2004). Input parameters used in the Dips software include slope and dip direction of joints and slope, and friction angle as shown in Table 5.29. The dip and dip direction of joints and slope were determined in the field, while the friction angle along the failure plane and cohesion were determined according to the Barton-Bandis failure criterion since it is used to determine the shear strength parameters of the discontinuities using the RocData software (Table 5.10).

In the right abutment slope section (RASS), there is no expected failure modes like planar failure modes since there is no any joint sets plotted in the critical zone of the planar mode of failure as shown in the Figure 5.23a and wedge failure modes are not expected to occur, as there are no preconditions for such an occurrence as shown in Figure 5.23c. Similarly, In the left abutment slope section (LASS) the expected mode failure according to the kinematic analysis is planar mode of failure due to JS2, wedge mode of failure due to the intersection of JS1 and JS2 in the critical zone of the wedge failure, since the intersection between the joint sets dips at a greater angle than the slope face as shown in Figure 5.23b, 5.23d and toppling mode of failure is not imminent since there are no preconditions for such an occurrences where the stereographic projection was not given.

Table 5. 29. Input parameters of the geometry of joints and slope face for the Dips 6.0 Software.

Right Abutment Slope Sections (RASS)				**Left Abutment Slope Sections(LASS)**		
Slope and Discontinuity Orientation	**JS1**	**JS2**	**Slope Face**	**JS1**	**JS2**	**Slope Face**
Strike Direction	280º WWN	94ºE	308ºNW	41ºNE	136 ºSE	284 ºWNW
Dip Direction	72º NE	166ºSE	81ºNE	317ºNW	183 ºS	175 ºSSE
Dip Amount	46 º	65 º	75 º	43 º	62 º	83 º
Friction Angle (ϕ)	**51 º**			**47 º**		

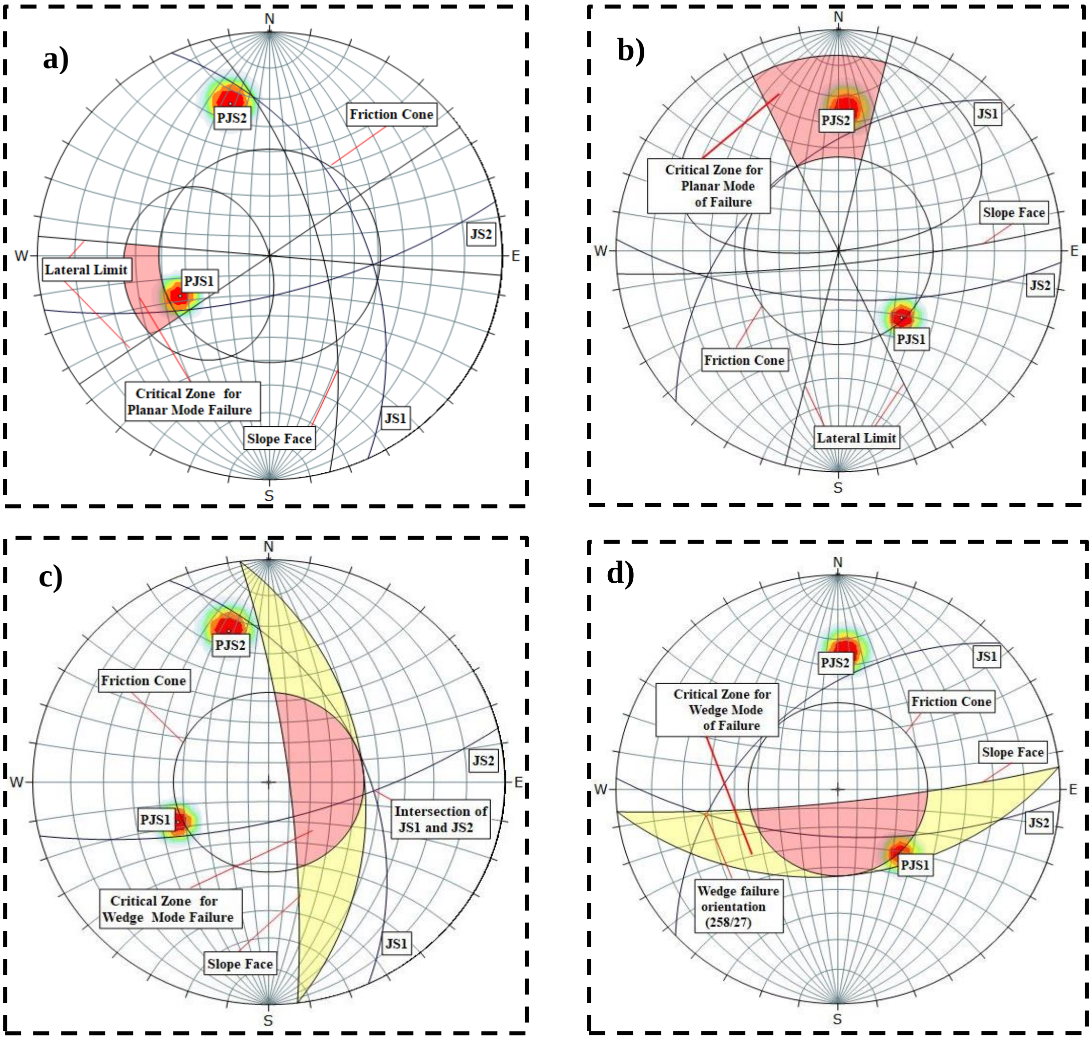

Figure 5. 23. Kinematic analysis for Right Abutment Slope Section (RASS) and Left Abutment Slope Section using Dips 6.0 software; (A) Checking for Planar mode of failure for RASS (B) Checking for Planar mode of failure for LASS (C) Checking for Wedge mode of failure for RASS (D) Checking for Wedge mode of failure for LASS.

5.4.2. The Stability Analysis using the Limit Equilibrium Method

The results of the kinematic analysis indicate that a planar failure mode is expected in the left abutment slope section (LASS) due to the discontinuity set JS2. Therefore, the deterministic method was further utilized for stability analysis with respect to FOS, in which the possibility of kinematic failure modes was determined (Park and West, 2001). Accordingly, the factor of safety (FOS) was determined for each planar failure mode and analyzed using RocPlane software (Rocscience, 2004). The input parameters used in the RocPlane software were given in Table 2.30. The shear strength parameters were determined according to the Barton-Bandis failure criterion since this is used to determine the shear strength parameters of the discontinuities with the RocData software (Table 5.10).

During the field investigation, the slope's geometry and discontinuity orientation were determined. For this analysis waviness was determined in the field. Waviness is a factor that may be considered when estimating the failure plane's shear strength. It explains the failure plane surface's undulations, which may be seen at distances between 1 and 10 meters (Rocscience, 2004). The minimal dip of the failure plane is subtracted from the average dip of the failure plane to determine the amount of waviness. The effective shear strength of the failure plane will always grow as the waviness angle rises above zero.

Table 5. 30. Input parameters of the geometry of joints and slope face, shear strength parameters, forces (water forces and dynamic forces) for the RocPlane Software.

Critical Slope Section	Potential Failure Joint sets	Slope Geometry							Shear Strength Parameters		Forces	
		SO (º)	USO (º)	FPO (º)	B_W (m)	Slope Height (m)	γ (t/m³)	w (º)	ϕ (⁰)	C (MPa)	u_w (t/m³)	α(g)
LASS	JS2	81	20	60	65	21	2.86	7	46	0.026	1	0.1
Where SO, USO, and FPO stand for slope orientation, upper slope orientation, and failure plane orientation, respectively; B_w is bench width, γ is unit weight of rock, ϕ is frictional angle, w represents waviness; C is cohesion; u_w is water pressure; and α is the seismic coefficient.												

The stability of the rock slope of the abutments is evaluated by the safety factor. The safety factor considers the balance between the forces that promote instability (driving forces) and the forces that oppose instability (resisting forces) on the potential failure surface. FOS at the left abutment was estimated through modifying the percent water pressure in the slope section, with dry conditions at 0% fill, 15% fill, 30% fill, 45% fill, 60% fill, 75% fill and 100% for static condition (without seismic loading), and dry conditions at 0% fill, 15% fill, 30% fill, 45% fill, 65% fill, 68% fill and 100% for dynamic conditions (with seismic loading) as shown in Table 5.31.

In this study, the FOS was interpreted in accordance with Norrish and Wyllie (1996). They claimed that the driving and resisting forces are in balance when FOS = 1, and that FOS > 1 indicates a stable slope and FOS = 1 corresponds to in a critical state of equilibrium. After providing the input parameters in to the RocPlane software, the factor of safety was determined for planar mode of failure.

In the left abutment slope section LASS, the 2D and 3D view of the joint set JS1 failure plane was provided using RocPlane software as given in Figure 5.24. When the slope was assumed to be 100% fully saturated with water and considering the dynamic conditions, the seismic forces were expected to occur with the value of 22.04t which was applied to the failure plane. The factor of safety becomes 0 with resisting and driving forces of 0t/m and 209.06t/m respectively. In dry static condition, the factor of safety was 0.89 inferring that the slope section was unstable whereas during the fully saturated static condition was considered the factor of safety decreases to 0. This indicates that pore water pressure plays a significant role in the instability of the slope section. This was justified by increasing the pore water pressure level from 0% to 100% where the pore water pressure acts on the resisting force, consequently decreasing the factor of safety.

Therefore, by assuming dry dynamic condition, the factor of safety was 0.79 with a resisting force of 154.4t/m and driving force of 209.06t/m and the slope section was unstable. With water pressure levels of 15% and 30%, the factor of safety decreased to the value of 0.71 and 0.66 with resisting force of 150.36t/m and 138.11t/m respectively, and driving force was 209.06t/m and the slope section was unstable again. Similarly considering 45% of water pressure level, the factor of safety decreased to the value of 0.56 with decreased resisting force of 117.69t/m. The slope section was also unstable with a factor of safety of 0.34 when the water pressure level was 68% filled with a resisting force of 77.0t/m. As the water pressure level exceeds 68% percent filled, the safety factor becomes zero. During the dry static condition, the slope factor of safety is 0.89 with a resisting force of 177.58t/m, and a driving force of 199.75t/m. When the slope section was considered to be in static condition and the water pressure level was 15% and 30%, the factor safety was 0.87 and 0.80 respectively and eventually decreased to the value of 0.70 when the water pressure level increased by 45% filled showing an unstable slope section. Furthermore, when the water pressure level was 75% and the factor of safety was 0.38 with a resisting force of 75.48t/m and a driving force of 199.75t/m. As the water pressure level exceeds 75% percent filled, the safety factor becomes zero. This decreasing trend of a factor of safety with an increasing percentage of water pressure level indicates that a minimum amount of the water pressure level was required to displace the slope's wedge weight of 220.4t/m which is greater than the driving force and resisting force to result in the instability of the slope section. From the sensitivity analysis, the factors that resulted in the failure of the slope section are water pressure level, failure plane angle, and seismic coefficient. Since the difference between the slope and failure plane angle is minimum and the wedge weight created due to the difference between them, the water pressure level required to displace the wedge will be minimum. The seismic coefficient combined with the water pressure level also results in a factor of safety of less than 1. Besides the water pressure level, other factors that contribute to the instability of the slope section are failure plane angle and seismic coefficient.

Table 5. 31. The factor of safety determined at the critical slope sections having a planar mode of failure for LASS.

Static Condition				Dynamic Condition			
Water Pressure Level (%)	Resisting Force (t/m)	Driving Force (t/m)	FOS	Water Pressure Level (%)	Resisting Force (t/m)	Driving Force (t/m)	FOS
0 (Dry)	177.58	199.75	0.89	0 (Dry)	154.40	209.06	0.74
15	173.50	199.75	0.87	15	150.36	209.06	0.72
30	161.25	199.75	0.80	30	138.11	209.06	0.66
45	140.83	199.75	0.70	45	117.69	209.06	0.56
60	112.24	199.75	0.56	65	77.75	209.06	0.37
75	75.48	199.75	0.38	68	70.51	209.06	0.34
100	0	199.75	0	100	0	209.06	0

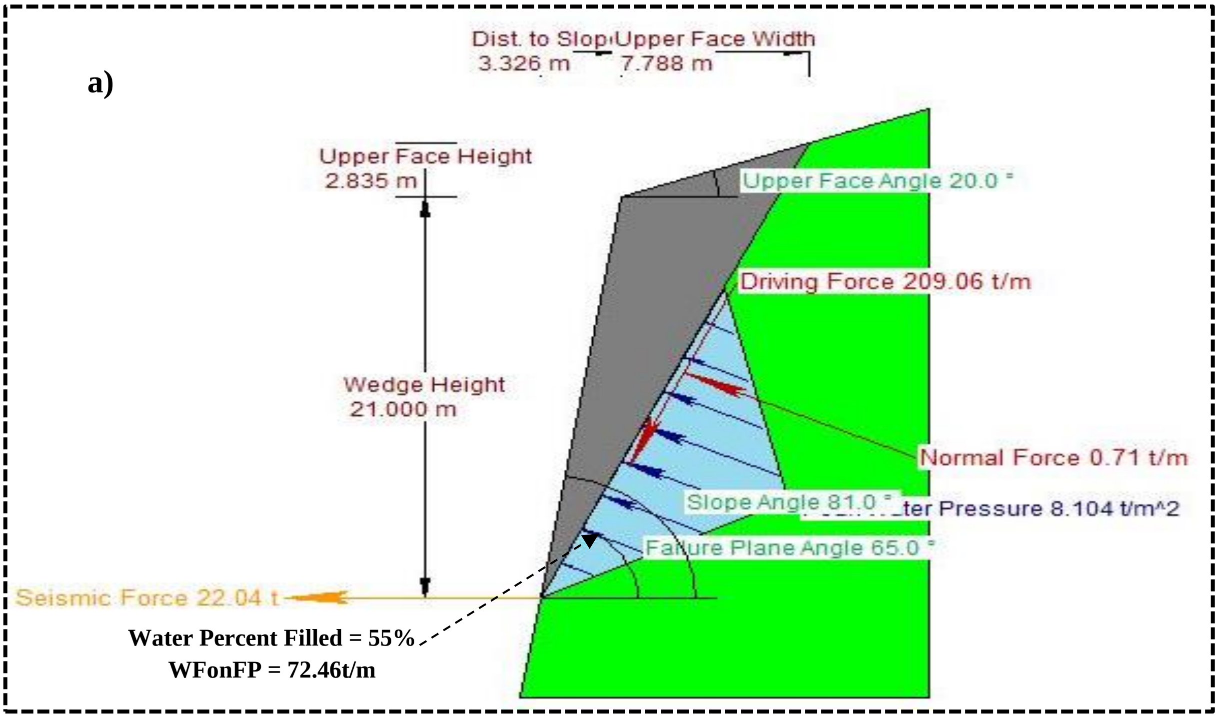

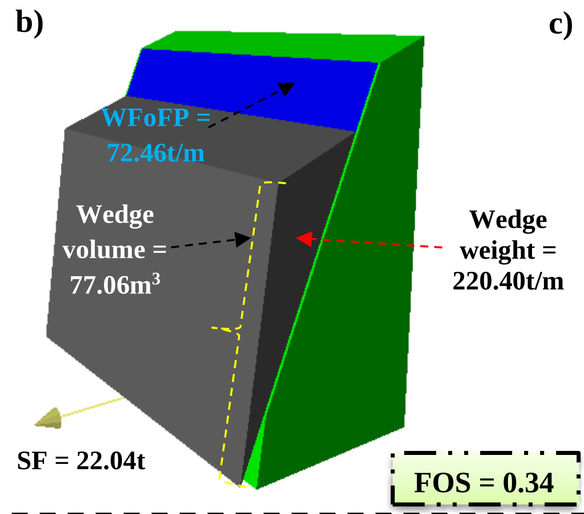

c)

Factor of Safety	0.34
Driving Force	209.06t/m
Resisting Force	70.51t/m
Wedge Weight	220.40t/m
Wedge Volume	77.06m^3/m
Shear Strength	70.43t/m^2
Normal Force	0.71t/m
Seismic Force	22.04t
Plane Waviness	7.0°
Water Force on Failure Plane	72.46t/m

Figure 5. 24. The Deterministic method of slope stability analysis by RocPlane software under 68% water pressure level and dynamic condition at both LASS slope section. a) 2D side view with forces acting on the plane of failure of JS1 for LASS. b) 3D view of failure plane of JS1 for LASS. c) The factor of safety at 68% of water pressure level under dynamic condition.

In conclusion, the deterministic method slope stability analysis for planar mode of failure in the left abutment slope section showed that the slope section was unstable during both the saturated static and saturated dynamic condition for left abutment slope section (LASS). In this case the pore water pressure plays a crucial role in the destabilization of the slope section compared to the seismic coefficient and others (Pan et al., 2020). This indicates that water pressure level combined with slope geometry and discontinuity orientation, seismic loading contributes a significant role in destabilizing the slope sections. As a result, adequate remedial measures were required for these specific slope portions in order to avoid the dam abutments from failing.

In the left abutment, beside planar mode of failure wedge mode of failure is anticipated due to the intersection of JS1 and JS2. Therefore, the deterministic method of slope stability analysis for the wedge mode of failure was assessed by Swedge 4.0 software. The input parameters for the wedge software are the discontinuity orientation, slope geometry, unit weight and shear strength parameters determined using RocData software in Table 5.10. The input parameters for the swedge software are given in Table 5.32.

Table 5. 32. The input parameters for determining the factor of safety at the left abutment critical slope sections having a wedge mode of failure.

Critical Slope Section	Potential Failure Plane	Discontinuity Orientation		Slope Geometry				γ (MN/m^3)	Shear strength parameters	
				Slope Angle		SH (m)	Bw (m)		C (MPa)	Φ(deg)
		DD	D	DD	D					
LASS	JS1	317°NW	43°	175°	81°	21	65	0.02805	4.7	49
	JS2	183°S	62°						2.1	46

D is the dip angle of the joints and slope face, DD is the dip direction of the joints and slope face, SH is slope height, Bw is the bench width, γ is the unit weight of the rock, C is cohesion and Φ is frictional angle.

After inserting the input parameters into the swedge software, the factor safety of the slope section was determined. The FOS was determined through modifying the percent water pressure in the slope section, with dry conditions at 0% fill, 25% fill, 50% fill, 70% fill and 100% for both static condition (without seismic loading) and dynamic conditions (with seismic loading). The results of the analysis showed that the slope section was stable with having the factor of safety of greater than 1 during the dry static and dry dynamic condition as given in Table 5.33. During the static condition without considering the water pressure, the factor of safety was 1.49 with the resisting force and driving force of 877.7t and 589.2t respectively. Therefore, the slope section was stable according to Norrish and Wyllie (1996). However, the slope section with wedge mode failure gradually becomes unstable as the water pressure level increases. The water pressure decreases the factor of safety by diminishing the resisting forces and increasing the driving force as shown in Table 5.33. At the water pressure level of 25%, The factor of safety shows slight decreasing change to 1.45 with resisting force of 861.98t and driving force of 592.8t. The factor of safety decreases 1.21 at moderate water percent fill of 50% with the resisting force and driving force of 752.21t and 618.04t respectively. Even if the slope section was stable with this factor of safeties, as the water pressure level increases to 70% the slope section becomes unstable with the factor of safety was 0.80 with the resisting force of 533.43t and driving force of 669.36t. As the water pressure level increases to become fully saturated (100% of water percent filled), the factor of safety becomes zero causing immediate collapsing of the slope section.

Similarly, the slope section with wedge mode of failure was also analyzed considering the dynamic condition. The seismic loading affects the resisting forces and increases the driving force down the slope section. The seismic force was expected to occur with the value of 66.73t which was employed on the failure planes. During the dry dynamic condition, the factor of safety was greater than 1 with the value of 1.41 having the resisting force and driving force of 877.7t and 624.71t respectively. This value of FOS indicates that slope section was stable according to Norrish and Wyllie (1996). As the degree of saturation increases to 25%, the factor of safety slightly decreases to 1.37 with decreased resisting force of 861.98t and increased driving force of 628.09t. As the water pressure level reaches moderate water percent filled with 50%, the factor of safety was 1.16 indicating the stable slope section with resisting force and driving force of 752.21t and 652t respectively. However, this stable slope section becomes unstable as the water pressure level increases to 70% resulting in the drastic decrease of resisting force to 533.4t and increase of driving force to 700.85t which decreases the factor of safety to 0.76. As the water pressure level becomes fully saturated (100% water percent filled), the factor of safety becomes zero indicating that the water pressure level required to displace the wedge created by the intersection of the JS1 and JS2 with the wedge weight of 667.28t as shown in Figure 5.25a.

According to study by Pan et al.(2020), pore water pressure plays a critical role in the stability of rock slopes because it influences the shear strength of rocks. When rainfall infiltrates into the rock mass, it increases the pore water pressure and reduces the effective stress acting on the rock mass. As a result, the shear strength of the rock slope decreases, significantly affecting the overall stability of the slope. During rainfall, water infiltrates into rock mass and raises the pore water pressure. This increases the likelihood of slope failure as rock strength decreases due to the increased water pressure. The increase in pore water pressure decreases the effective stress acting on the rock mass. Effective stress is the difference between total stress and pore water pressure. As effective stress decreases, the ability of the rock mass to support its load reduces. This results in reduced rock slope stability, increasing the potential for slope failure. At this slope section with wedge mode of failure, the analysis using swedge software shows that the most influencing factor governing the slope section failure was the water pressure level. The effect of the pore water pressure was higher when combined with seismic coefficient.

Generally, the deterministic method slope stability analysis for wedge mode of failure in the left abutment slope section showed that the slope section was stable during both dry static and dynamic condition. However, the slope section becomes unstable as the water pressure level exceeds the partially filled condition. This suggests that pore water pressure and seismic stress are important in destabilizing slope sections when paired with slope geometry and discontinuity direction. As a result, suitable remedial measures for these specific slope parts were necessary to prevent the dam abutments from failing.

Table 5. 33. The factor of safety determined at the left abutment critical slope sections (LASS) having a wedge mode of failure.

Static Condition				Dynamic condition			
Water pressure level (%)	Resisting Force (tons)	Driving Force (tons)	Factor of Safety (FOS)	Water pressure level (%)	Resisting Force (tons)	Driving Force (tons)	Factor of Safety (FOS)
0	877.70	589.20	1.49	0	877.70	624.71	1.41
25	861.98	592.80	1.45	25	861.98	628.09	1.37
50	752.21	618.04	1.21	50	752.21	652.00	1.16
70	533.43	669.36	0.80	70	533.40	700.84	0.76

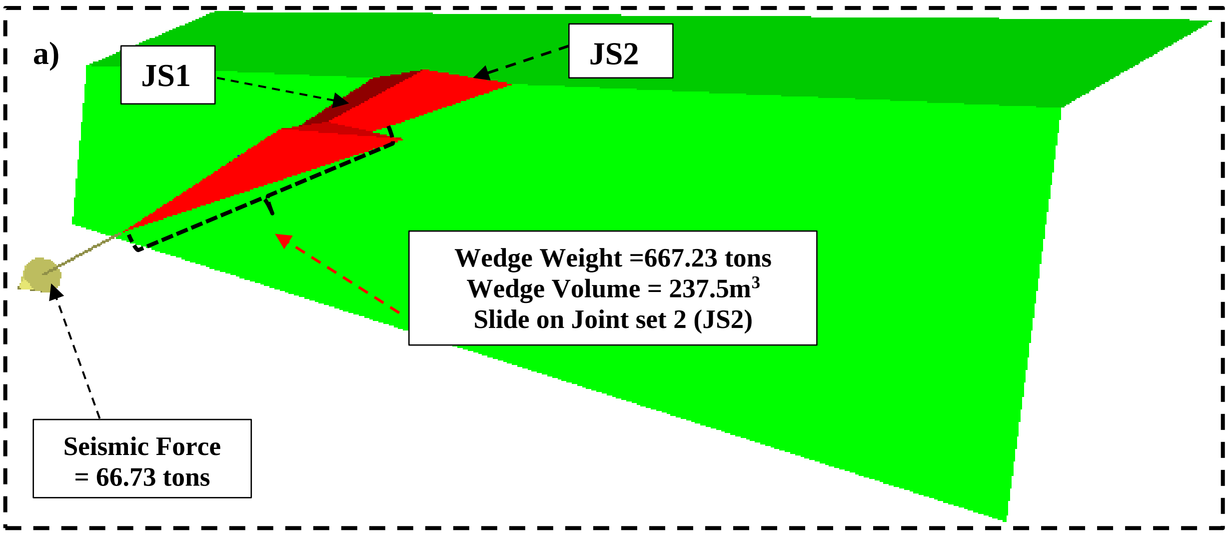

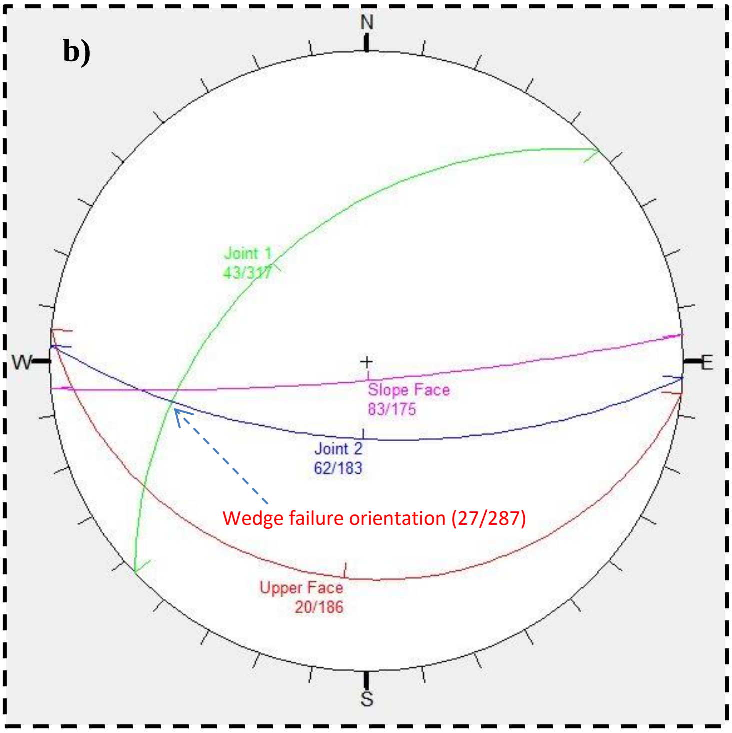

Figure 5. 25. The Deterministic method of slope stability analysis by Swedge software under fully saturated and dynamic condition at left abutment slope section LASS. a) 3D view of the joint sets with forces acting on the plane of failure for wedge mode of failure. b) The stereographic projection of the joint sets with slope face.

5.4.3. Possible Remedial Measures

Since the slope sections are found to be unstable considering the worst condition (saturated dynamic condition), the rock slope sections must be stabilized. The failure to do so could potentially compromise the structural integrity. Therefore, rock bolts are required for planar mode of failure and both the combination of shotcrete and rock bolts are implemented to stabilize the wedge mode of failures. The correct implementation of rock bolts and shotcrete could result in the increase of resisting force and shear strength which arise from the cohesion and frictional strength of sliding planes and decrease in the driving force (which includes the mass of accelerated through gravity, seismic force, and water pressure). The change in the resisting and driving forces increases the factor of safety consequently.

In this research work, the stabilization of planar mode of failure was done by employing RocPlane 2.0 software (RocPlane 2.0 Rocscience 2004 a, b, c. d) through the implementation of rock bolts that were installed across the failure plane to the relatively sound rock. Similarly, the stabilization of wedge mode of failure at the left abutment was done using the Swedge 4.0 software (Swedge 4.0 Rocscience 2004a, b, c, d) via the application of rock bolts exceeding the failure plane and shotcrete to slope face. All the stabilization design was carried out by considering the worst condition of the slope sections (i.e. dynamic saturated condition).

Similarly, about 2 rock bolts with length of 7m each were applied to the unstable slope section at the left abutment with planar mode failure due to JS2 at angle of 30º each , bolt capacity of 140t/m each and resultant active bolt force of 280t/m. After the rock bolts with these properties are applied to the slope section, the factor of safety has increased from 0.00 to 1.27 with the resisting force of 296.02t/m and driving force of 233.06t/m as shown in Figure 5.26 and Table 5.34. The increasing of the factor of safety with the implementation of rock bolts indicates that the importance of the rock bolts in the stabilization of rock slope sections.

Table 5. 34. Remedial measures for Planar Mode Failure and the Increased FOS.

Slope Section	FOS without support	Bolt No.	Angle (Deg)	Bolt Length (m)	Anchor Length (m)	Bolt Capacity (t/m)	Resisting Force (t/m)	Driving Force (t/m)	FOS
LASS	0.00	1.	30	7	2.07	140	296.02	233.47	1.27
		2.	30	7	3.50	140			

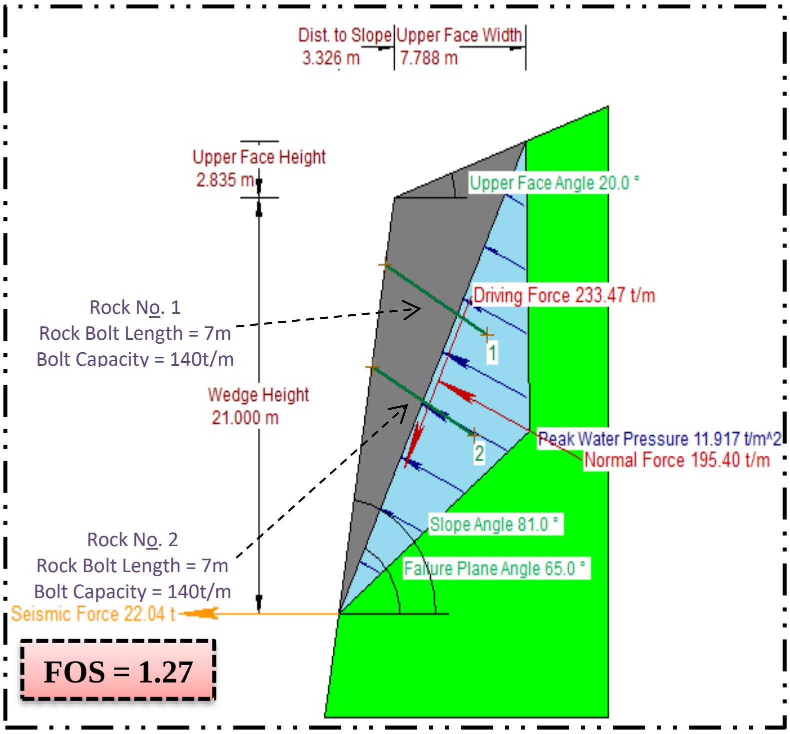

Factor of Safety	1.27
Driving Force	233.47t/m
Resisting Force	296.02t/m
Wedge Weight	220.40t/m
Wedge Volume	77.06m^3/m
Shear Strength	272.03t/m^2
Normal Force	195.40t/m
Seismic Force	22.04t
Plane Waviness	7.0°
Active Bolt Force	280.00t
Active Bolt Angle	330.0°
Passive Bolt Force	0.00t
Passive Bolt Angle	0.0°
Water Force on Failure Plane	156.71t/m

Figure 5. 26. Remedial measures for Planar Mode Failure and FOS at Left Abutment Slope Section (LASS).

To stabilize the wedge mode of failure due to the intersection JS1 and JS2 at the left abutment slope section (LASS), about 2 (two) rock bolts were applied to the slope section where each one of them have trend of 355° and plunge of 35°, bolt length of 7m, bolt capacity of 340t. Additional to the rock bolts, the shotcrete was also implemented stabilize the slope section with thickness of 0.1m and shear strength of 40t/m^2 which is expected to apply the shotcrete force of 467.51tons. These remedial measures increased the factor of safety from 0.00 to 1.28 with the resisting force and driving force of 1198.97t and 937.35t respectively as shown in Table 5.35 and Figure 5.27.

Table 5. 35. Remedial measures of wedge mode failure at left abutment slope section (LASS) and Increased factor of safety.

Slope Section	FOS without support	Bolt No.	Orientation		Bolt Properties		
			Trend (°)	Plunge (°)	Bolt Length (m)	Anchored Length (m)	Capacity (tons)
LASS	**0.00**	1.	355	35	5	4.26	340
		2.	355	35	5	3.94	340
		Shotcrete Properties					
		Thickness(m)	Shear strength(t/m^2)			Shotcrete Force (t)	
		0.1	40			467.51	
FOS with support			Resisting Force (t)			Driving Force(t)	
1.28			1198.97			937.35	
LASS- left abutment slope section, FOS- Factor of Safety.							

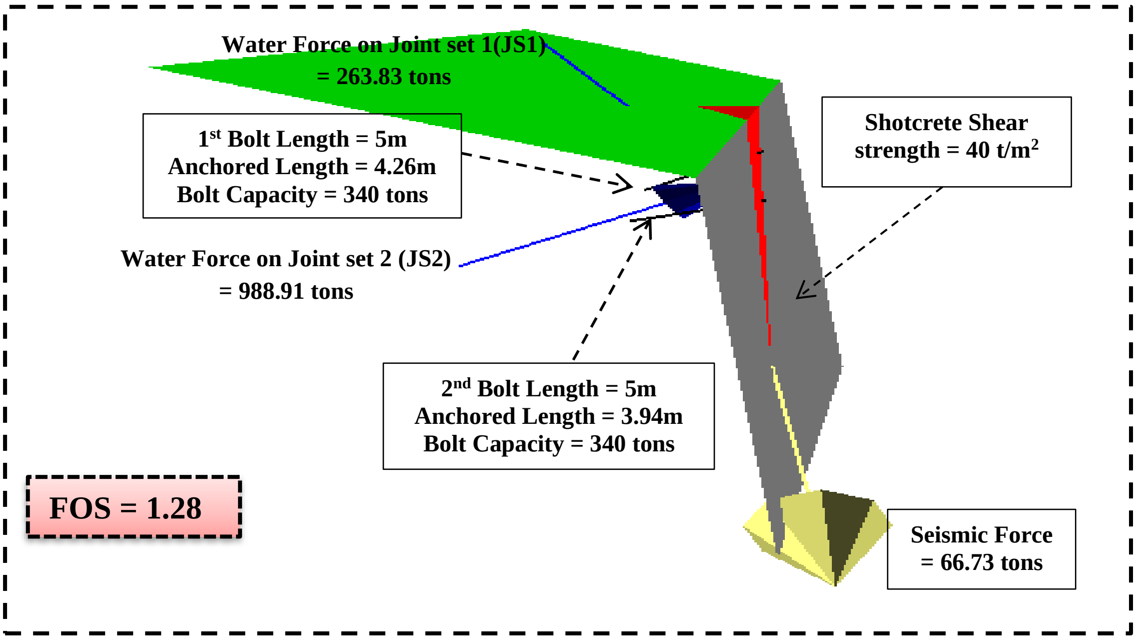

Figure 5. 27. Remedial measures for Wedge Mode Failure in 3D view and Increased FOS at the left abutment slope section (LASS).

CHAPTER SIX

CONCLUSIONS AND RECOMMENDATIONS

6.1. Conclusions

Depending on the finding of this study work, the following conclusion were drawn:

- The geological mapping of the study area entails that area constitutes colluvial and alluvial soils, aphanitic basaltic rock, and welded tuff.
- From the discontinuity surveying, two major joint sets with orientation favourable for leakage of water due to the joints are in parallel with the direction of river flow.
- The Alluvial deposits with a thickness of 1.70m at the reservoir area are mostly covered with clayey silt soils with medium to high plasticity and semi-pervious to impermeable permeability class. These permeability values show the soil deposits area suitable for the impoundment of water in the reservoir area.
- The surface and subsurface engineering geological mapping indicated that the dam site constituting rocks are aphanitic basaltic rock and unwelded to welded tuff.
- The RQD estimated using volumetric joint count shows the rock mass at the right and left abutment have values ranging from 59-69 with fair rock mass quality and 46-59 with poor to fair rock mass quality, respectively.
- The rock mass quality at the right and left abutment of the dam site was good with RMR value ranging from 68-64 and fair with RMR value of 48-61. The GSI values revealed that the rock outcrop at the dam is blocky rock masses.
- At the dam site, intact rock strength test indicated that the uniaxial compressive strength value ranges from 145.44MPa to 146.88MPa and the UCS estimated from the in-situ strength test shows a range of 139.31MPa to 194MPa showing the rock mass constituting dam site have high strength.
- At the reservoir area, intact rock strength test revealed that the uniaxial compressive strength value of 55.68MPa showing medium strength and the UCS estimated from the in-situ strength test shows a range of 22.13MPa to 25.11MPa showing the rock mass have low strength.
- The evaluation core drilling revealed that RQD shows a clear trend of increasing with drilled depth at both right and left abutment boreholes. However, RQD values at the river center borehole shows no clear trend with depth.

- The RQD values of basaltic rock at the right and left abutment borehole showed that the determined average RQD values are plotted to be in the excellent to fair rock mass quality due to the low to moderate degree of fracturing and weathering. Similarly, The RQD value at the river center borehole showed that the given average RQD values fall in the poor and fair for the basaltic rock and tuff rock units, respectively.
- Even if the Lu values are less than 1 it tends to decrease with increasing depth and reaches zero after a particular depth at both dam abutments. However, the Lu values increases with depth at the river center. At the right abutment, the Lu values and RQD shows a clear correlation. But there is a vague correlation between the Lu values and RQD at the river center and left abutment.
- The Water pressure test revealed that that there is no potential for the occurrence of leakage of water at the dam site in three boreholes with Lu value of less than 1 and further shows a positive indicator of the dam’s safety and stability.
- The Allowable bearing capacity of aphanitic basaltic rock at the left and right abutment ranges from 3.51MPa to 22.19MPa. The allowable bearing capacity of basaltic rock at the river center ranges from 0.1MPa to 6.77MPa. The tuff unit at the river center have the allowable bearing capacity values ranging from 0.037MPa to 0.11MPa.
- The surface permeability analysis showed that rock mass at the left and right abutment have slight to moderate permeability values. Therefore, there is slight leakage expected after the impoundment of the reservoir water through these rock masses at the dam abutments.
- The kinematic Analysis outcomes showed that the slope sections of the dam site were potentially unstable via planar mode of failure and wedge mode of failure for left abutment slope section.
- The limit equilibrium method using deterministic slope stability analysis method result showed that at the left abutment slope section, the slope was unstable in all conditions. Therefore, water pressure, failure plane angle, and slope angle significantly influenced in the destabilizing of these slope sections in contrast to the seismic coefficient.
- The possible remedial measures to stabilize the planar and wedge mode failure resulted in the increased the factor of safety to be greater than 1.20.

6.2. Recommendations

- Since the geotechnical drilling revealed the soil deposit with the thickness of 0.30m at the left abutment and it will not be necessary leave it be and should be removed before the dam construction commences.
- At river center, RQD should not be used as criteria for deciding test sections for packer test during detailed design stages and construction phase of the dam as it showed no clear trend with Lugeon value.
- The soil permeability from laboratory tests showed that the permeability falls in low permeability class. So that it can be generally stated that the permeability of the soils at the dam site is impermeable enough to retain water in the reservoir after impoundment. However, further detail study is recommended.
- Due to time and financial constraints, this investigation concentrated solely on surface soil investigation, with soil samples collected from 1m to 2m.The soils of the reservoir area should be further studied in detail if they are planned for construction purposes.
- Considering the reservoir area is covered by clayey silt soil which could cause siltation of the reservoir. Hence this research work recommended further assessment of reservoir issues in order to enhance the operational life of the dam and reservoir.
- For the unstable slope sections, stabilization of the slope section resulted in the increase of factor of safety. This study recommended additional evaluation for the design and implementation of remedial measures such as rock bolts.
- The study further recommends the assessment of the effect of surface and subsurface water on the dam abutment slope stability conditions.
- Since the packer tests determined the Lu values less than 1, the curtain grouting should not be necessary indicating that the dam site is safe with adequate dam design.
- Overall, the advantages of the 4.20m thickness aphanitic basaltic have higher bearing capacity and stable foundation. Therefore, foundation design will still be necessary to ensure the dam's stability and safety over the long-term.
- Due to time and financial constraints, this study was unable to conduct the geophysical investigation to gain the ideal information about the subsurface information of the geological materials, the presence of the geological structures and buried channels at the dam site and reservoir area. The seismic refraction method of geophysical investigations was further recommended.

REFERENCES

Abay, A., & Meisina, C. (2015). Engineering-geological properties of carbonates and shale: their implications for dam construction in Mekelle, Northern Ethiopia. *Momona Ethiopian Journal of Science*, *7*(1), 64. https://doi.org/10.4314/mejs.v7i1.117238

Abramson, L. W., Lee, T. S., Sharma, S., & Boyce, G. M. (2001). *Slope stability and stabilization methods*. John Wiley & Sons.

Aguilera, R. (1998). Geologic aspects of naturally fractured reservoirs. *The Leading Edge*, *17*(12), 1667–1670.

Aksoy, C. O. (2008). Chemical injection application at tunnel service shaft to prevent ground settlement induced by groundwater drainage: A case study. *International Journal of Rock Mechanics and Mining Sciences*, *45*(3), 376–383.

Allen, A., & Tadesse, G. (2003). Geological setting and tectonic subdivision of the Neoproterozoic orogenic belt of Tuludimtu, western Ethiopia. *Journal of African Earth Sciences*, *36*(4), 329–343.

Alonso, E. E., Pinyol, N. M., Puzrin, A. M., Alonso, E. E., Pinyol, N. M., & Puzrin, A. M. (2010). Earth Dam Sliding Failure: Aznalcóllar Dam, Spain. *Geomechanics of Failures. Advanced Topics*, 129–164.

Altarejos-García, L., Escuder-Bueno, I., Serrano-Lombillo, A., & de Membrillera-Ortuño, M. G. (2012). Methodology for estimating the probability of failure by sliding in concrete gravity dams in the context of risk analysis. *Structural Safety*, *36*, 1–13.

Ankara, H., Çiçek, F., Deniz, İ. T., Uçak, E., & Kandemir, S. Y. (2016). Determination of Slake Durability Index (Sdi) Values on Different Shape of Laminated Marl Samples. *IOP Conference Series: Earth and Environmental Science*, *44*(2), 22006.

Aprilia, F., & Indrawan, I. G. B. (2015). An evaluation of rock slope stability using limit equilibrium analyses. *Journal of Applied Geology*, *6*(2).

Arora, K. R. (2008). *Soil mechanics and foundation engineering (geotechnical engineering) : in SI units*. Standard Publishers PP - Nai Sarak.

ASDSO. (2022). *Gravity Dam Failures. (pp. 1-2)*.

Asfaw, L. M. (1992). Seismic risk at a site in the East African rift system. *Tectonophysics, 209*(1–4), 301–309. https://doi.org/10.1016/0040-1951(92)90038-8

Asfaw, L. M., & Woldeyes, G. (1986). Catalogue of Ethiopian earthquakes, earthquake parameters, strain release and seismic risk. *Geophysical Observatory, Faculty of Science, Addis Ababa University*.

Asfaw, L., Meten, M., & Garo, T. (2022). Leakage and abutment slope stability analysis of Arjo Didesa dam site, western Ethiopia. *Arabian Journal of Geosciences*, *15*(19). https://doi.org/10.1007/s12517-022-10827-7

Asthana, B. N., & Khare, D. (2022). Concrete Gravity Dams. *Recent Advances in Dam Engineering*, 17–72. https://doi.org/10.1007/978-3-030-32278-6_3

ASTM D 2216 (1998). Standard Test Method for Laboratory Determination of Water (Moisture) Content of Soil and Rock by Mass. American society for testing and materials, Conshohocken, PA;19428.

ASTM D 2434 (1994). Standard Test Method for permeability of granular soil. American society for testing and materials, Philadelphia, Pa;19103.

ASTM D 3080 (1998). Standard test method for direct shear test of soils under consolidated drained conditions. Annual Book of Standards, American Society for Testing and Materials, West Conshohocken, PA, Vol. 04.08, pp.339-344.

ASTM D 4318 (1998). Standard Test Method for Liquid Limit, Plastic Limit and Plasticity Index of soils. American society for testing and materials, Conshohocken, PA;19428.

ASTM D 5731 (1995). ASTM standard test method for determination of point load strength index of rocks. American society for testing and materials, vol.04.08, Conshohocken, PA;142-148.

ASTM D6473-10 (2010). ASTM standard test method for determination of water absorption test of rock aggregates. American society for testing and materials

ASTM C 805 (2018), Standard Test Method for Rebound Number of Hardened Concrete, ASTM International, West Conshohocken, PA, 2018, www.astm.org.

ASTM D 854 (1998). Standard Test Method for Specific Gravity of Soils. American society for testing and materials, Conshohocken, PA;19428

Ayalew, L. (1999). The effect of seasonal rainfall on landslides in the highlands of Ethiopia. *Bulletin of Engineering Geology and the Environment*, *58*, 9–19.

Aydin, A. (2009). ISRM Suggested method for determination of the Schmidt hammer rebound hardness: Revised version. *International Journal of Rock Mechanics and Mining Sciences*, *46*(3), 627–634. https://doi.org/10.1016/j.ijrmms.2008.01.020

Aydin, A., & Basu, A. (2005). The Schmidt hammer in rock material characterization. *Engineering Geology*, *81*(1), 1–14. https://doi.org/10.1016/j.enggeo.2005.06.006

Azimian, A. (2016). A new method for improving the RQD determination of rock core in borehole. *Rock Mechanics and Rock Engineering*, *49*, 1559–1566.

Azimian, A., & Ajalloeian, R. (2013). Comparison between Lugeon with secondary permeability index obtained of water pressure test in rock masses. *Electron. J. Geotec. Eng*, *18*, 1603–1612.

Azimian, A., & Ajalloeian, R. (2014). Permeability and groutability appraisal of the Nargesi dam site in Iran based on the secondary permeability index, joint hydraulic aperture and Lugeon tests. *Bulletin of Engineering Geology and the Environment*, *74*(3), 845–859. https://doi.org/10.1007/s10064-014-0675-8

Baghbanan, A., & Jing, L. (2007). Hydraulic properties of fractured rock masses with correlated fracture length and aperture. *International Journal of Rock Mechanics and Mining Sciences*, *44*(5), 704–719.

Barani, H. R. R., Lashkaripour, G., & Ghafoori, M. (2014). A Proposal for Geological Groutability Index (GGI) of Cement Grouting in Rock Foundations. *Indian Journal of Science and Technology*, *7*(2), 95.

Barton, N., & Choubey, V. (1977). The shear strength of rock joints in theory and practice. *Rock Mechanics*, *10*, 1–54.

Barton N, Bandis S (1990) Review of predictive capabilities of JRCJCS model in engineering practice. In: Balkema, AA, (Eds), Proceedings of International Conference on Rock Joints, Leon, Norway

Barzegari, G. (2017). Geotechnical Evaluation of Dam Foundation with Special Reference to In Situ Permeability: A Case Study. *Geotechnical and Geological Engineering*, *35*(3), 991–1011. https://doi.org/10.1007/s10706-016-0155-y

Baylosis, R. B., & Bennett, R. M. (1989). Safety assessment of an existing concrete gravity dam. *Structural Safety and Reliability*, 279–286.

Bekele, T. (1993). *Vegetation Ecology of Remnant Afromontane Forests on the Central Plateau of Shewa, Ethiopia*. Sv. växtgeografiska sällsk..

Berhane, G., Amare, M., Gebreyohannes, T., & Walraevens, K. (2017). Geological and geophysical investigation of water leakage from two micro-dam reservoirs: Implications for future site selection, northern Ethiopia. *Journal of African Earth Sciences*, *129*, 82–93. https://doi.org/10.1016/j.jafrearsci.2016.12.015

Berhane, G., Martens, K., Al Farrah, N., & Walraevens, K. (2013). Water leakage investigation of micro-dam reservoirs in Mesozoic sedimentary sequences in Northern Ethiopia. *Journal of African Earth Sciences*, *79*, 98–110.

Berhane, G., & Walraevens, K. (2013). Geological and geotechnical constraints for urban planning and natural environment protection: a case study from Mekelle City, Northern Ethiopia. *Environmental Earth Sciences*, *69*, 783–798.

Bieniawski, Z. T. (1973). Engineering classification of jointed rock masses. *Civil Engineering= Siviele Ingenieurswese*, *1973*(12), 335–343.

Bieniawski, Z. T. (1979). The geomechanics classification in rock engineering applications. *4th ISRM Congress*.

Bieniawski, Z. T. (1989). *Engineering rock mass classifications: a complete manual for engineers and geologists in mining, civil, and petroleum engineering*. John Wiley & Sons.

Bishop, A. W. (1955). The use of the slip circle in the stability analysis of slopes.

Geotechnique, 5(1), 7–17.

Biswas, A. K., & Tortajada, C. (2001). Development and Large Dams: A Global Perspective. *International Journal of Water Resources Development*, *17*(1), 9–21. https://doi.org/10.1080/07900620120025024

Bowles, D. S., Giuliani, F. L., Hartford, D. N. D., Janssen, J., McGrath, S., Poupart, M., Stewart, D., & Zielinski, P. A. (2007). ICOLD bulletin on dam safety management. *IPENZ Proceedings of Technical Groups*, *33*(2).

Broch, E., & Franklin, J. A. (1972). The point-load strength test. *International Journal of Rock Mechanics and Mining Sciences & Geomechanics Abstracts*, *9*(6), 669–676. https://doi.org/10.1016/0148-9062(72)90030-7

Bruce, D. A., & Dreese, T. L. (2010). Specifications for Rock Mass Grouting. *Proceedings of the Association of State Dam Safety Officials Conference on Dam Safety*.

Bruce, D. A., Dreese, T. L., Harris, M. C., & Heenan, D. M. (2012). Composite cut-off walls for existing dams: theory and practice. In *Grouting and Deep Mixing 2012* (pp. 1248–1264).

Bryson, L. S., Gomez-Gutierrez, I. C., & Hopkins, T. C. (2011). Correlations between durability and geotechnical properties of compacted shales. In *Geo-Frontiers 2011: Advances in Geotechnical Engineering* (pp. 4109–4118).

Budhu, M. (2011). *Soil Mechanics and Foundations* (3rd ed.). JOHN WilEY & SONS, INC PP - New York.

Cabria, X. A. (2015). *Effects of weatherin in the rock and rock mass properties and the influence of salts in the coastal roadcuts in Saint Vincent and Dominica*. University of Twente.

Cai, M., Kaiser, P. K., Uno, H., Tasaka, Y., & Minami, M. (2004). Estimation of rock mass deformation modulus and strength of jointed hard rock masses using the GSI system. *International Journal of Rock Mechanics and Mining Sciences*, *41*(1), 3–19.

Cargill, J. S., & Shakoor, A. (1990). Evaluation of empirical methods for measuring the uniaxial compressive strength of rock. *International Journal of Rock Mechanics and*

Mining Sciences & Geomechanics Abstracts, *27*(6), 495–503. https://doi.org/10.1016/0148-9062(90)91001-n

Carter, J. P., & Kulhawy, F. H. (1988). Analysis and Design of Foundations Socketed into Rock; Report No. *EL-5918*, 158.

Carter, J. P., & Kulhawy, F. H. (1992). Analysis of laterally loaded shafts in rock. *Journal of Geotechnical Engineering*, *118*(6), 839–855.

Chala, E. T., & Rao, K. S. (2021). Evaluation of Weathered Rock Mass Strength and Deformation Using Weathering Indices. *IOP Conference Series: Earth and Environmental Science*, *833*(1), 12194.

Cheng, Y. M., & Lau, C. K. (2014). *Slope stability analysis and stabilization: new methods and insight*. CRC press.

Craig, R. F. (2004). *Craig's soil mechanics*. CRC press.

Das, B. M. (2002). *Soil mechanics laboratory manual*. Oxford University Press PP - New York.

De Hamer, W., Love, D., Owen, R., Booij, M. J., & Hoekstra, A. Y. (2008). Potential water supply of a small reservoir and alluvial aquifer system in southern Zimbabwe. *Physics and Chemistry of the Earth, Parts A/B/C*, *33*(8–13), 633–639.

Deere, D., & Deere, D. (1988). The Rock Quality Designation (ROD) Index. *L. Kirkaldie, Rock Classification Systems for Engineening Purposes*, 91–101.

Deere, D. U. (1967). Discussion on rock classification. *Proceedings of the First Congress of the International Society for Rock Mechanics*, 156–158.

Deere, D. U., & Deere, D. W. (1988). The rock quality designation (RQD) index in practice. *Symposium on Rock Classification Systems for Engineering Purposes, 1987, Cincinnati, Ohio, USA*.

Deere, D. U., & Deere, D. W. (1989). *Rock Quality Designation (RQD) after Twenty Years.* Deere (Don U) Consultant Gainesville Fl.

Deere, D. U., & Miller, R. P. (1966). *Engineering classification and index properties for* *intact rock*. Illinois Univ At Urbana Dept Of Civil Engineering.

Design of Gravity Dams. (1976). A Water Resources Technical Publication, Denver F‘ederal Center, Denver, Colorado 80225. pp(1-586). .

Dhandre, N. M., Kamalasekaran, P. D., & Pandey, P. (2016). Dam parameters monitoring system. *2016 7th India International Conference on Power Electronics (IICPE)*, 1–5.

Duan, Q., & Yang, X. (2014). Experimental studies on gas and water permeability of fault rocks from the rupture of the 2008 Wenchuan earthquake, China. *Science China Earth Sciences*, *57*, 2825–2834.

Duncan, N., & Hancock, K. E. (1966). The concept of contact stress in the assessment of the behaviour of rock masses as structural foundations. *1st ISRM Congress*.

Ellingwood, B., & Tekie, P. B. (2001). Fragility Analysis of Concrete Gravity Dams. *Journal of Infrastructure Systems*, *7*(2), 41–48. https://doi.org/10.1061/(asce)1076-0342(2001)7:2(41)

Engineering Corporation of Oromia, (2022). Finna Bowa Dayole Project Final Feasibility Study and Detail Design Engineering Report (Unpublished report). ECO, Addis Abeba, Ethiopia, 72p.

Ethiopian Construction Design and Supervision Works Corporation, (2022). Bowa Dayole Gravity Dam Project Geotechnical Investigation (Core Drilling) Final Factual Report (Unpublished report). ECDSWC, Addis Abeba, Ethiopia, 65p.

FAO (Food and Agriculture Organization of the United Nations), (2002). Irrigation Manual: Planning, Development Monitoring and Evaluation of Irrigated Agriculture with Farmer Participation, Volume II, Module 7.

Fell, R. (2005). *Geotechnical engineering of dams*. CRC press.

Fell, R., MacGregor, P., Stapledon, D., Bell, G., & Foster, M. (2014). *Geotechnical Engineering of Dams*. CRC Press.

Fookes, P. G., Gourley, C. S., & Ohikere, C. (1988). Rock weathering in engineering time. *Quarterly Journal of Engineering Geology and Hydrogeology*, *21*(1), 33–57.

Foyo, A., Sanchez, M. A., & Tomillo, C. (2005). A proposal for a secondary permeability index obtained from water pressure tests in dam foundations. *Engineering Geology*, *77*(1–2), 69–82.

Gabrielsen, R. H., & Braathen, A. (2014). Models of fracture lineaments—Joint swarms, fracture corridors and faults in crystalline rocks, and their genetic relations. *Tectonophysics*, *628*, 26–44.

Garo, T., & Meten, M. (2021). Engineering geological characterization for evaluation of seepage and geomechanical properties of Chalchal Dam Site, Bale Zone, Southeastern Ethiopia. *Arabian Journal of Geosciences*, *14*(23). https://doi.org/10.1007/s12517-021-08881-8

Ghafoori, M., Lashkaripour, G. R., & Tarigh Azali, S. (2011). Investigation of the geological and geotechnical characteristics of Daroongar Dam, Northeast Iran. *Geotechnical and Geological Engineering*, *29*, 961–975.

Gouin, P. (1970). Seismic and gravity data from Afar in relation to surrounding areas. *Philosophical Transactions for the Royal Society of London. Series A, Mathematical and Physical Sciences*, 339–358.

Gupta, A. S., & Seshagiri Rao, K. (2000). Weathering effects on the strength and deformational behaviour of crystalline rocks under uniaxial compression state. *Engineering Geology*, *56*(3–4), 257–274. https://doi.org/10.1016/s0013-7952(99)00090-3

Gurocak, Z., & Alemdag, S. (2012). Assessment of permeability and injection depth at the Atasu dam site (Turkey) based on experimental and numerical analyses. *Bulletin of Engineering Geology and the Environment*, *71*, 221–229.

Gurocak, Z., Alemdag, S., & Zaman, M. M. (2008). Rock slope stability and excavatability assessment of rocks at the Kapikaya dam site, Turkey. *Engineering Geology*, *96*(1–2), 17–27.

GWP (2010). Global water security Global Water Partnership Secretariat. (Drottninggatan 33, SE-111 51 Stockholm, Sweden).

Haeri, S. M., Khosravi, A., Garakani, A. A., & Ghazizadeh, S. (2017). Effect of soil structure and disturbance on hydromechanical behavior of collapsible loessial soils. *International Journal of Geomechanics*, *17*(1), 4016021.

Haile, T., & Atsbaha, S. (2014). Electrical resistivity tomography, VES and magnetic surveys for dam site characterization, Wukro, Northern Ethiopia. *Journal of African Earth Sciences*, *97*, 67–77. https://doi.org/10.1016/j.jafrearsci.2014.03.023

Hailu, M. B. (2020). Modeling assessment of seepage and slope stability of dam under static and dynamic conditions of Grindeho Dam in Ethiopia. *Modeling Earth Systems and Environment*. https://doi.org/10.1007/s40808-020-01006-2

Haines, A., Terbrugge, P. J., & Carrieri, G. (1991). Preliminary estimation of rock slope stability using rock mass classification systems. *7th ISRM Congress*.

Haramy, K. Y., & DeMarco, M. J. (1985). Use of the Schmidt hammer for rock and coal testing. *The 26th US Symposium on Rock Mechanics (USRMS)*.

Hariri, A. M. A., & Saouma, V. (2014). Quantitative failure metric for gravity dams. *Earthquake Engineering & Structural Dynamics*, *44*(3), 461–480. https://doi.org/10.1002/eqe.2481

Hedayati, H., Lashkaripoor, G. R., Ghafoori, M., & Saba, A. A. (2012). The analysis of engineering properties of the rock mass of Ghordanloo dam site, NE Iran. *International Journal of Emerging Technology and Advanced Engineering*, *2*(9), 17–27.

Hedayati Talouki, H., Lashkaripour, G. R., Ghafoori, M., & Saba, A. A. (2015). Assessment and presentation of a treatment method to seepage problems of the alluvial foundation of Ghordanloo dam, NE Iran. *Journal of the Geological Society of India*, *85*(3), 377–384.

Helfer, F., Lemckert, C., & Zhang, H. (2012). Impacts of climate change on temperature and evaporation from a large reservoir in Australia. *Journal of Hydrology*, *475*, 365–378. https://doi.org/10.1016/j.jhydrol.2012.10.008

Hocking, G. (1976). A method for distinguishing between single and double plane sliding of tetrahedral wedges. *International Journal of Rock Mechanics and Mining Science*, *13*(Analytic).

Hoek, E., & Bray, J. D. (1981). *Rock slope engineering*. CRC press.

Hoek, E., Marinos, P., & Benissi, M. (1998). Applicability of the Geological Strength Index (GSI) classification for very weak and sheared rock masses. The case of the Athens Schist Formation. *Bulletin of Engineering Geology and the Environment*, *57*, 151–160.

Holtz, R. D., & Schuster, R. L. (1996). Stabilization of soil slopes. *Landslides Investigation and Mitigation, Eds. Turner AK and Schuster, RL, Special Report*, *247*.

Houlsby, A. C. (1991). *Construction and design of cement grouting: a guide to grouting in rock foundations* (Vol. 67). John Wiley & Sons.

Hudson, J. A., & Priest, S. D. (1979). Discontinuities and rock mass geometry. *International Journal of Rock Mechanics and Mining Sciences & Geomechanics Abstracts*, *16*(6), 339–362. https://doi.org/10.1016/0148-9062(79)90001-9

Hutchinson, N. N. (1977). Assessment of the effectiveness of corrective measures in relation to geological conditions and types of slope movement. *Bulletin of the International Association of Engineering Geology-Bulletin de l'Association Internationale de Géologie de l'Ingénieur*, *16*(1), 131–155.

ISRM. (1978). International society for rock mechanics commission on standardization of laboratory and field tests: Suggested methods for the quantitative description of discontinuities in rock masses. *International Journal of Rock Mechanics and Mining Sciences & Geomechanics Abstracts*, *15*(6), 319–368. https://doi.org/10.1016/0148-9062(78)91472-9

Jordá-Bordehore, L. (2017). Stability assessment of natural caves using empirical approaches and rock mass classifications. *Rock Mechanics and Rock Engineering*, *50*, 2143–2154.

Justin-Visentin, E., Nicoletti, M., Tolomeo, L., & Zanettin, B. (1974). Miocene and pliocene volcanic rocks of the addis ababa-debra berhan area (ethiopia). Geo-petrographic and radiometric study. *Bulletin Volcanologique*, *38*, 237–253.

Kanik, M., & Ersoy, H. (2019). Evaluation of the engineering geological investigation of the

Ayvali dam site (NE Turkey). *Arabian Journal of Geosciences*, *12*(3). https://doi.org/10.1007/s12517-019-4243-1

Karaman, K., Ercikdi, B., & Kesimal, A. (2013). The assessment of slope stability and rock excavatability in a limestone quarry. *Earth Sciences Research Journal*, *17*(2), 169–181.

Kasim, F., & Lah, W. (2008). Compaction parameters' estimation for ground improvement. *Improvement & Stabilization. Penerbit University Technology Press. Johor*, 1–26.

Katz, O., Reches, Z., & Roegiers, J.-C. (2000). Evaluation of mechanical rock properties using a Schmidt Hammer. *International Journal of Rock Mechanics and Mining Sciences*, *37*(4), 723–728. https://doi.org/10.1016/s1365-1609(00)00004-6

Kazmin, V. (1972). Geology of Ethiopia (explanatory note to geological map of Ethiopia 1: 2000, 000). *Report, Ministry of Mines, Geological Survey of Ethiopia, Addis Ababa, Ethiopia*.

Kirkaldie, L. (1988). *Rock classification systems for engineering purposes*.

Krahn, J. (2004). Stability modeling with SLOPE/W. *An Engineering Methodology: First Edition, Revision*, *1*(396), 70.

Lamplmair, S., Zeman, O., & Voit, K. (2021). Factors Influencing the Load-Bearing Capacity of Rock as Base Material for Post-Installed Anchors. *Materials*, *14*(18), 5130.

Lancellotta, R. (2008). *Geotechnical engineering*. CRC Press.

Lane, E. W. (1935). Security from Under-Seepage-Masonry Dams on Earth Foundations. *Transactions of the American Society of Civil Engineers*, *100*(1), 1235–1272. https://doi.org/10.1061/taceat.0004655

Liu, Y.-C., & Chen, C.-S. (2007). A new approach for application of rock mass classification on rock slope stability assessment. *Engineering Geology*, *89*(1–2), 129–143.

Ljubomir, T. (2014). *Dams and Appurtenant Hydraulic Structures, 2nd edition*. CRC Press.

Louis, C. L. (1974). Introduction to rock hydraulics. *BULL BRGM*, *III*, *4*.

Malkawi, A. I. H., & Al-Sheriadeh, M. (2000). Evaluation and rehabilitation of dam seepage problems. A case study: Kafrein dam. *Engineering Geology*, *56*(3–4), 335–345. https://doi.org/10.1016/s0013-7952(99)00117-9

Manna, B., Rawat, S., Zodinpuii, R., & Sharma, K. G. (2014). Effect of surcharge load on stability of slopes-testing and analysis. *Electronic Journal of Geotechnical Engineering*, *19*, 3397–3410.

Marinos, P. G., Marinos, V., & Hoek, E. (2007). THE GEOLOGICAL STRENGTH INDEX (GSI): A CHARACTERIZATION TOOL. *Proceedings of the International Workshop on Rock Mass Classification in Underground Mining*, *9498*, 87.

Marinos, P., & Hoek, E. (2000). GSI: a geologically friendly tool for rock mass strength estimation. *ISRM International Symposium*.

Martt, D. F., Shakoor, A., & Greene, B. H. (2005). Austin Dam, Pennsylvania: The sliding failure of a concrete gravity dam. *Environmental and Engineering Geoscience*, *11*(1), 61–72. https://doi.org/10.2113/11.1.61

McCartney, M. P., & Menker Girma, M. (2012). Evaluating the downstream implications of planned water resource development in the Ethiopian portion of the Blue Nile River. *Water International*, *37*(4), 362–379.

Mengesha, T., Tadiwos, C., & Workineh, H. (1996). Geological map of Ethiopia. *Bulletin of the Ethiopian Institute of Geological Survey*, *3*.

Morelli, G. L. (2015). Variability of the GSI index estimated from different quantitative methods. *Geotechnical and Geological Engineering*, *33*(4), 983–995.

Morgenstern, N. R. u, & Price, V. E. (1965). The analysis of the stability of general slip surfaces. *Geotechnique*, *15*(1), 79–93.

Murthy, V. (2003). *Principles of soil mechanics and foundation engineering, New Delhi: UBS Publisher's Distributors Pvt*. Ltd.

Naabil, E., Lantei Lamptey, B., Kouadio, K., & Annor, T. (2020). Climate Change Impact on Water Resources; The case of Tono Irrigation Dam in Ghana. *Hydrology*, *8*(4), 69. https://doi.org/10.11648/j.hyd.20200804.12

Nohara, D., Miki, H., & Hori, T. (2011). Long-term reservoir operation considering large-scale meteorological conditions well-correlated with basin precipitation. *Disaster Prevention Research Institute-Kyoto University*.

Norrish, N. I., & Wyllie, D. C. (1996). Landslides: Investigation and Mitigation. Chapter 15-Rock slope stability analysis. *Transportation Research Board Special Report*, *247*.

Öge, İ. F. (2017). Assessing rock mass permeability using discontinuity properties. *ISRM European Rock Mechanics Symposium-EUROCK 2017*.

Ogunsola, N. O., Olaleye, B. M., & Saliu, M. A. (2017). Effects of weathering on some physical and mechanical properties of Ewekoro Limestone, South-western Nigeria. *Int. J. Eng. Appl. Sci*, *4*(11), 257336.

Özsan, A., & Akın, M. (2002). Engineering geological assessment of the proposed Uruş Dam, Turkey. *Engineering Geology*, *66*(3–4), 271–281. https://doi.org/10.1016/s0013-7952(02)00047-9

Palmstrom, A. (1982). The volumetric joint count—a useful and simple measure of the degree of rock mass jointing. *International Association of Engineering Geology. International Congress. 4*, 221–228.

Palmstrom, A. (2005). Measurements of and correlations between block size and rock quality designation (RQD). *Tunnelling and Underground Space Technology*, *20*(4), 362–377.

Palmström, A. (1995). Characterizing rock burst and squeezing by the rock mass index. *International Conference in Design and Construction of Underground Structures*, *10*(10).

Palmström, A. (1996). Characterizing rock masses by the RMi for use in practical rock engineering: Part 1: The development of the Rock Mass index (RMi). *Tunnelling and Underground Space Technology*, *11*(2), 175–188.

Pan, Y., Wu, G., Zhao, Z., & He, L. (2020). Analysis of rock slope stability under rainfall conditions considering the water-induced weakening of rock. *Computers and Geotechnics*, *128*, 103806.

Pantelidis, L. (2009). Rock slope stability assessment through rock mass classification systems. *International Journal of Rock Mechanics and Mining Sciences*, *46*(2), 315–325.

Park, D., & Oh, J. (2018). Permeation grouting for remediation of dam cores. *Engineering Geology*, *233*, 63–75.

Park, H., & West, T. R. (2001). Development of a probabilistic approach for rock wedge failure. *Engineering Geology*, *59*(3–4), 233–251.

Paulay, T., & Priestley, M. J. N. (2009). *Seismic design of reinforced concrete and masonry buildings*. Wiley & Sons PP - New York.

Popescu, M. E. (2002). Landslide causal factors and landslide remediatial options. *3rd International Conference on Landslides, Slope Stability and Safety of Infra-Structures*, 61–81.

Qi, P., & Dashui, G. (2019). Reconstruction and Reinforcement New Techniques for Masonry Gravity Dams Upstream Anti-seepage Panels. *IOP Conference Series: Earth and Environmental Science*, *304*(052020). https://doi.org/10.1088/1755-1315/304/5/052020

Qureshi, M. U., Al-Mawali, K., & Khan, K. M. (2013). Using RQD to estimate the in-situ permeability of discontinuous sedimentary rock. *Proceedings of the 5th International Young Geotechnical Engineers' Conference*, 447–450.

Qureshi, M. U., Khan, K. M., Bessaih, N., Al-Mawali, K., & Al-Sadrani, K. (2014). An empirical relationship between in-situ permeability and RQD of discontinuous sedimentary rocks. *Electronic Journal of Geotechnical Engineering*, *19*, 4781–4790.

Raghuvanshi, T. K. (2019). Plane failure in rock slopes–A review on stability analysis techniques. *Journal of King Saud University-Science*, *31*(1), 101–109.

Ramamurthy, T. (2004). A geo-engineering classification for rocks and rock masses. *International Journal of Rock Mechanics and Mining Sciences*, *41*(1), 89–101.

Ranjan, G., & Rao, A. S. R. (2005). *Basic and Applied Soil Mechanics*. Wiley Eastern Ltd PP - New Delhi.

Rastegar Nia, A., Lashkaripour, G. R., & Ghafoori, M. (2017). Prediction of grout take using rock mass properties. *Bulletin of Engineering Geology and the Environment*, *76*, 1643–1654.

Richards, L. (1992). Slope stability and rockfall problems in rock masses. In *Engineering in rock masses* (pp. 209–230). Elsevier.

Rocscience (2004a) Dips 6.0, http://www.rocscience.com/software/ dips.

Rocscience (2004b) RocData 3.0, http://www.rocscience.com/software/rocdata

Rocscience (2004c) RocPlane 2.0, http://www.rocscience.com/software/rocplane

Rocscience (2004d) Swedge 4.0 http://www.rocscience.com/software/ swedge

Rusnak, J., & Mark, C. (2000). *Using the point load test to determine the uniaxial compressive strength of coal measure rock*.

Sadeghiyeh, S. M., Hashemi, M., & Ajalloeian, R. (2013). Comparison of permeability and groutability of Ostur dam site rock mass for grout curtain design. *Rock Mechanics and Rock Engineering*, *46*, 341–357.

Sharma, S., Raghuvanshi, T., & Sahai, A. (1999). An engineering geological appraisal of the Lakhwar dam, Garhwal Himalaya, India. *Engineering Geology*, *53*(3–4), 381–398.

Shen, J. M. (1998). Soil suction in relation to slope stability: a summary of research carried out in Hong Kong in 1978–1997. *Proceeding of the Annual Seminar on Slope Engineering in Hong Kong*, 93–99.

Shirzad, M., & Nikkhah, M. (2021). Numerical analysis of evaluation of static and seismic bearing capacity of foundations on rock masses. *Innovative Infrastructure Solutions*, *6*, 1–11.

Shukla, S. K., & Hossain, M. M. (2011). Stability analysis of multi-directional anchored rock slope subjected to surcharge and seismic loads. *Soil Dynamics and Earthquake Engineering*, *31*(5–6), 841–844.

Singh, B., & Goel, R. K. (2011). *Engineering rock mass classification*. Elsevier.

Singh, T. N., Kainthola, A., & Venkatesh, A. (2011). Correlation Between Point Load Index and Uniaxial Compressive Strength for Different Rock Types. *Rock Mechanics and Rock Engineering*, *45*(2), 259–264. https://doi.org/10.1007/s00603-011-0192-z

Sissakian, V. K., Adamo, N., & Al-Ansari, N. (2020). The role of geological investigations for dam siting: Mosul Dam a Case Study. *Geotechnical and Geological Engineering*, *38*(2), 2085–2096.

Snow, D. T. (1968). Rock fracture spacings, openings, and porosities. *Journal of the Soil Mechanics and Foundations Division*, *94*(1), 73–91.

Solomon G., Tesfaye Sh., and Yewubnesh B., (2010), The Geology of Seladingay and Part of Debre Berhan Subsheets (NC37-11/C&J), Geological Survey of Ethiopia, Geohazards Investigation Core Process. Addis Abeba, Ethiopia. Page 1-39.

Spencer, E. (1967). A method of analysis of the stability of embankments assuming parallel inter-slice forces. *Geotechnique*, *17*(1), 11–26.

Standard, E. B. C. (n.d.). EBCS-8 (1995): design of structures for earthquake resistance. *Addis Ababa: Ministry of Works and Urban Development*.

Stille, H., & Palmström, A. (2003). Classification as a tool in rock engineering. *Tunnelling and Underground Space Technology*, *18*(4), 331–345. https://doi.org/10.1016/s0886-7798(02)00106-2

Su, H., Hu, J., & Wen, Z. (2013). Service life predicting of dam systems with correlated failure modes. *Journal of Performance of Constructed Facilities*, *27*(3), 252–269.

Terzaghi, K., Peck, R. B., & Mesri, G. (1967). Soil Mechanics in Engineering Practice, John Wiley & Sons. *Inc., New York*, 232–254.

Terzaghi, K., Peck, R. B., & Mesri, G. (1996). *Soil mechanics in engineering practice*. John wiley & sons.

Thermann, K., Gau, C., & Tiedemann, J. (2006). Shear strength parameters from direct shear tests–influencing factors and their significance. *The Geological Society of London*, *484*, 1–12.

Tiruneh, M., & Ababa, A. (2005). *Reservoir Operational Planning Of Irrigation Dams For*

Micro-Hydropower Development. M. Sc. Thesis, Civil Engineering Department, AAU.

Tzamos, S., & Sofianos, A. I. (2007). A correlation of four rock mass classification systems through their fabric indices. *International Journal of Rock Mechanics and Mining Sciences*, *44*(4), 477–495.

Umoren, U. N., Edet, A. E., & Ekwere, A. S. (2016). Geotechnical assessment of a dam site: A case study of Nkari dam, Southeastern Nigeria. *Journal of Earth Sciences and Geotechnical Engineering*, *6*(2), 73–88.

Uromeihy, A., & Barzegari, G. (2007). Evaluation and treatment of seepage problems at Chapar-Abad Dam, Iran. *Engineering Geology*, *91*(2–4), 219–228. https://doi.org/10.1016/j.enggeo.2007.01.012

USBR. (1977). *Design Criteria for Concrete Arch and Gravity Dams*. Office of Design and Construction Engineering and Research Center. Denver, Colorado 80225. pp.(1-40), No. 19.

Vaskou, P., de Quadros, E. F., Kanji, M. A., Johnson, T., & Ekmekci, M. (2019). ISRM Suggested Method for the Lugeon Test. *Rock Mechanics and Rock Engineering*, *52*(10), 4155–4174. https://doi.org/10.1007/s00603-019-01954-x

Wahlstrom, E. (2012). *Dams, Dam Foundations, and Reservoir Sites*. Elsevier.

Wang, M., & Wan, W. (2019). A new empirical formula for evaluating uniaxial compressive strength using the Schmidt hammer test. *International Journal of Rock Mechanics and Mining Sciences*, *123*, 104094.

Warner, J. (2004). Plugging the GAP Working with Buzan: The Ilisu Dam as a security issue. *Occasional Paper*, *67*.

Weaver, K. D. (1991). *Dam foundation grouting*.

Wickham, G. E., Tiedemann, H. R., & Skinner, E. H. (1972). Support determinations based on geologic predictions. *N Am Rapid Excav & Tunnelling Conf Proc*, *1*.

Wieland, M. (2008). Large dams the first structures designed systematically against earthquakes. *The 14th World Conference on Earthquake Engineering*, 12–17.

Wieland, M. (2014). Seismic hazard and seismic design and safety aspects of large dam projects. *Perspectives on European Earthquake Engineering and Seismology*, *1*, 627–650.

Wyllie, D. C., & Mah, C. (2004). *Rock slope engineering*. CRC Press.

Yagiz, S. (2008). Predicting uniaxial compressive strength, modulus of elasticity and index properties of rocks using the Schmidt hammer. *Bulletin of Engineering Geology and the Environment*, *68*(1), 55–63. https://doi.org/10.1007/s10064-008-0172-z

Yang, B., & Elmo, D. (2022). Why Engineers Should Not Attempt to Quantify GSI. *Geosciences*, *12*(11), 417.

Yaşar, E., & Erdoğan, Y. (2004). Estimation of rock physicomechanical properties using hardness methods. *Engineering Geology*, *71*(3–4), 281–288. https://doi.org/10.1016/s0013-7952(03)00141-8

Yoon, W. S., Jeong, U. J., & Kim, J. H. (2002). Kinematic analysis for sliding failure of multi-faced rock slopes. *Engineering Geology*, *67*(1–2), 51–61.

ZainAlabideen, K., & Helal, M. (2016). Determination of the safe orientation and dip of a rock slope in an open pit mine in Syria using kinematic analysis. *Al-Nahrain Journal for Engineering Sciences*, *19*(1), 33–45.

Zaruba, Q., & Mencl, V. (1976). *Chapter 13 - Engineering Geological Investigations for Hydraulic Structures, Developments in Geotechnical Engineering. : Vol. 10. pp(360*. Elsevier. https://doi.org/10.1016/B978-0-444-99877-4.50018-5.

Zaruba, Q., & Mencl, V. (2014). *Landslides and their control*. Elsevier.

Zhang, S., Wang, G., Wang, C., Pang, B., & Du, C. (2014). Numerical simulation of failure modes of concrete gravity dams subjected to underwater explosion. *Engineering Failure Analysis*, *36*, 49–64.

APPENDIXES

Appendix 1: Rock Rating System (After Bieniawski, 1989)

Parameters		Ranges of Values						
Strength of intact material	PLSI (MPa)	>10	4-10	2-4	1-2	For the low range, uniaxial compression test is preferred		
	UCS(MPa)	>250	100-250	50-100	25-50	5-25	1-5	<1
Rating		**15**	**12**	**7**	**4**	**2**	**1**	**0**
(RQD) (%)		90-100	75-90	50-75	25-50	<25		
Rating		**20**	**17**	**13**	**8**	**3**		
Spacing of Discontinuities		>2m	0.6-2m	200-600mm	60-200mm	<60mm		
Rating		**20**	**15**	**10**	**8**	**5**		
Condition of Discontinuities		Very rough surfaces Not continuous (No separation) Unweathered wall rock	Slightly rough surfaces Separation < 1mm Slightly weathered walls	Slightly rough surfaces Separation < 1mm Highly weathered walls	Slickensided surfaces Gouge < 5mm thick Separation1-5mm, continuous	Soft gouge >5mm thick Separation >5mm		
Rating		**30**	**25**	**20**	**10**	**0**		
Groundwater condition		Completely dry	Damp	Wet	Dripping	Flowing		
Rating		**15**	**10**	**7**	**4**	**0**		
RMR rating		100 - 81	80 -61	60 – 41	40 - 21	< 21		
Rock Class		I	II	III	IV	V		
Classification		**Very Good Rock**	**Good Rock**	**Fair Rock**	**Poor Rock**	**Very Poor Rock**		

Appendix 2: Right Abutment Rock mass Permeability from Discontinuity features (Snow, 1965 and Louis, 1974)

RADS-1					
S NO	**$g(m/s^2)$**	**e(m)**	**S(m)**	**$\mu(m^2/s)$**	**$K(m/s^2)$**
1	9.81	0.009	0.34	0.000001	9.34835E-06
2	9.81	0.0054	0.52	0.000001	3.66743E-06
3	9.81	0.0049	0.63	0.000001	2.7468E-06
4	9.81	0.006	0.48	0.000001	4.4145E-06
5	9.81	0.0083	0.56	0.000001	5.23434E-06
6	9.81	0.0078	0.12	0.000001	2.29554E-05
7	9.81	0.01	0.21	0.000001	1.68171E-05
8	9.81	0.05	0.35	0.000001	5.04514E-05
9	9.81	0.15	0.06	0.000001	0.0008829
10	9.81	0.18	0.08	0.000001	0.00079461
RADS-2					
1	9.81	0.0071	0.15	0.000001	1.67162E-05
2	9.81	0.0046	0.13	0.000001	1.24964E-05
3	9.81	0.0083	0.2	0.000001	1.46561E-05
4	9.81	0.0078	0.24	0.000001	1.14777E-05
5	9.81	0.001	0.3	0.000001	1.1772E-06
6	9.81	0.0052	0.165	0.000001	1.11299E-05
7	9.81	0.0034	0.075	0.000001	1.60099E-05
8	9.81	0.009	0.18	0.000001	0.000017658
9	9.81	0.0021	0.19	0.000001	3.90335E-06
10	9.81	0.0049	0.135	0.000001	1.28184E-05

Appendix 3: Left Abutment Rock mass Permeability from Discontinuity features (Snow, 1965 and Louis, 1974)

LADS-1					
S NO	**g (m/s^2)**	**e(m)**	**S(m)**	**μ(m^2/s)**	**K(m/s^2)**
1	9.81	0.071	0.55	0.000001	4.55897E-05
2	9.81	0.0076	0.48	0.000001	5.5917E-06
3	9.81	0.008	0.39	0.000001	7.24431E-06
4	9.81	0.0015	0.52	0.000001	1.01873E-06
5	9.81	0.001	0.15	0.000001	2.3544E-06
6	9.81	0.0048	0.06	0.000001	2.82528E-05
7	9.81	0.056	0.35	0.000001	5.65056E-05
8	9.81	0.0065	0.25	0.000001	9.18216E-06
9	9.81	0.0035	0.2	0.000001	6.1803E-06
10	9.81	0.046	0.4	0.000001	4.06134E-05
LADS-2					
1	9.81	0.008	0.055	0.000001	5.13687E-05
2	9.81	0.015	0.15	0.000001	0.000035316
3	9.81	0.024	0.2	0.000001	4.23792E-05
4	9.81	0.005	0.8	0.000001	2.20725E-06
5	9.81	0.009	0.1	0.000001	3.17844E-05
6	9.81	0.049	0.45	0.000001	3.84552E-05
7	9.81	0.003	0.35	0.000001	3.02709E-06
8	9.81	0.03	0.25	0.000001	4.23792E-05
9	9.81	0.034	0.145	0.000001	8.28099E-05
10	9.81	0.002	0.075	0.000001	9.4176E-06

Appendix 4: Left Abutment (Bearing capacity determination input parameters) according to Bowles (1996)

Depth (m)	RQD (%)	Rock Mass Quality	Depth Range (m)	Rock Unit ID	Average RQD		UCS_{av} (MPa)	Lithological Unit
					%	In decimal values		
0-1	0	Very Poor	0.0-7.0	ABR**1	17.69	0.1769	51.33	Gray, medium strength, fresh to slightly weathered, highly fractured basaltic rock.
1-3	12	Very Poor						
3-4	26	Poor						
4-4.7	0	Very Poor						
4.7-5.4	43	Poor						
5.4-6	0	Very Poor						
6-6.7	33	Poor						
6.7-7.0	27.5	Poor						
7.0-10.0	85	Good	7.0-25.10	ABR**2	89.81	0.8981	48	Gray, strong, fresh, massive basaltic rock.
10.0-12.0	76	Good						
12.0-14	97.5	Excellent						
14-16.5	92	Excellent						
16.5-19.6	92	Excellent						
19.6-20.0	100	Excellent						
20.0-23.10	89	Good						
23.10-25.10	87	Good						

Appendix 5: Right Abutment (Bearing capacity determination input parameters) according to Bowles (1996)

Depth (m)	RQD (%)	Rock Mass Quality	Depth Ranges(m)	Rock unit ID	RQD_{av}		UCS_{av}(MPa)	Lithological Unit
					%	In Decimal Values		
0.0-1.10	85	Good	0.0-25.10	ABR*	93.073	0.93073	65.05	Gray, strong, fresh, massive basaltic rock
1.10-4.0	92.6	Excellent						
4.0-5.5	100	Excellent						
5.5-8.7	92.6	Excellent						
8.7-10.40	89	Good						
10.40-12.50	96.6	Excellent						
12.50-15.50	100	Excellent						
15.50-18.0	96	Excellent						
18.0-20.40	89	Good						
20.40-23.40	95	Excellent						
23.40-25.10	88	Good						

Appendix 6: River Center (Bearing capacity determination input parameters) according to Bowles (1996)

Depth (m)	RQD (%)	Rock Mass Quality	Depth Range (m)	Rock Unit ID	RQD %	RQD Decimal	UCS$_{av}$ (MPa)	Lithological Unit
0-1.4	0	Very poor	0.0-4.20	ABR1	49.8	0.498	81.91	Slightly to highly fractured, fresh to moderately, medium to very strong basaltic rock.
1.40-3.0	72	Fair						
3.0-4.20	66	Fair						
4.20-6.0	75	Good	4.20-6.0	TU1	74.3	0.743	0.2	Reddish to light gray, slightly welded , weak tuff
7.8-9.0	95	Excellent	6.0-16.55	TU2	65	0.65	0.7525	Light gray, slightly welded, weak tuff
9.0-10.10	52	Fair						
10.10-13.0	34	Poor						
13.0-14	73	Fair						
14.0-17.10	61	Fair	16.55-18.0	ABR2	35.5	0.355	0.70	Dull to light gray, weak to medium strength, altered basaltic rock
17.10-19.0	10	Very Poor	18.0-23.10	TU3	36.3	0.363	2.59	Dull to light gray, unwelded to slightly welded tuff
19.0-21.40	85	Good						
21.40-23.10	14	Very Poor						

Appendix 7: Unit Weight Laboratory test data sheets.

Sample Station (BH-ID)	**RSS**	**LARS**	**RARS**
Mass of dry rock sample (gm)	233.0	257.0	430.0
Mass of saturated rock sample (gm)	238.30	258.20	431.00
Mass of water (gm)	5.30	1.20	1.0
Water Initial Volume (cm^3)	500.00	500.00	500.00
Water Final Volume (cm^3)	650.00	590.00	625.00
The volume of rock sample (cm^3)	150.00	90	150.00
Saturated density(g/ cm^3)	1.589	2.86	2.87
Saturated unit weight, (kN/m^3)	**15.58**	**28.05**	**28.16**
Dry Density (g/ cm^3)	**1.55**	**2.856**	**2.87**
Dry unit weight, (kN/m^3)	**15.02**	**28.01**	**28.15**
RSS = Reservoir Rock Sampling Station, RARS = Right Abutment Rock Sample, LARS = Left Abutment Rock Sample			

Appendix 8: Degree of Jointing and Weathering with respect to the RQD value according to Deere and Deere (1988).

RQD values (%)	**Degree of Jointing and Weathering**
10-50	Weathered and Jointed bedrock
<50	Highly jointed
50-75	Moderately jointed
>75	Relatively sound to sound

Appendix 9: Water content determination test data sheets.

Natural Moisture Content of Soil samples									
S. No.	Soil Sample Code	Depth(m)	Cont. Code	Weight of cont. +wet soil(g)	Weight of container+ oven dried soil(g)	Weight of water(g)	Weight of dry soil(g)	Weight of container(g)	Natural moisture content(%)
1.	LBSS-1	0.0-1.0	FD	154	138.1	15.9	112.4	25.8	14.1
2.	LBSS-2	1.0-1.70	IB	162.1	146.8	15.4	123.6	23.2	12.4
3.	RBSS-1	0.0-1.0	RE	108	97.3	10.7	70.7	26.6	15.2
Natural Moisture Content of Soil samples (Data sources: ECO, 2022)									
1.	SO/75/99	0.0-1.0	209	128.5	138.1	8.3	95.1	25.2	8.7
2.	SO/76/99	0.0-1.0	10	128.5	146.8	15.3	86.8	26.4	17.6
3.	SO/77/99	0.0-1.0	L33	109.4	103.	5.7	77.5	26.6	7.3
LBSS-1= Left Bank Soil Sample-1, LBSS-2= Left Bank Soil Sample-2, RBSS-1= Right Bank Soil Sample-1, SO/75/99= Pit 1 Right Upper Bank, SO/76/99= Pit 1 Right Bank, SO/77/99 = Pit 1 Left Bank									

Appendix 10: Summary of Laboratory Test Results of rock core samples from boreholes.

BHID	Sample Depth (m)	Specific Gravity			Water absorption (%)	Unit Weight (gm/cc)	Porosity(%)	Point Load (Mpa)	UCS (Mpa)	Slake Durability, %
		Bulk	SSD	Apparent						
BH-1	5.50-6.00	2.42	2.43	2.44	0.26	2.43	0.82	4.00	95.90	97.8
	13.00-13.30	2.91	2.92	2.93	0.18	2.92	0.68	3.28	78.64	100
	20.60-20.90	2.83	2.88	2.97	4.71	2.94	4.71	0.85	20.50	100
BH-2	3.30-3.55	2.83	2.83	2.84	0.17	2.83	0.07	3.41	81.91	99.04
	5.60-6.00		2.54			1.51		0.01	0.20	
	8.35-8.80		2.38			1.92		0.01	0.17	
	20.00-20.36		2.44			1.78		0.01	0.16	
BH-3	7.00-7.30	2.82	2.83	2.86	0.42	2.80	1.40	2.14	51.33	100
	16.40-16.65	2.61	2.62	2.63	0.10	2.60	0.76	2.80	67.24	99.04
	23.10-23.40		2.66			2.61		1.20	28.76	

Appendix 11: Point load index test data sheets.

Sr. No.	Sample ID (BH)	Depth [m]	W1, mm	W2, mm	Wav, mm	D, mm	De, mm	F, kN	Is, Mpa	Is(50), Mpa	UCS, Mpa
1	RSS	-	125	163.0	144.0	110.0	44.3	4.81	2.45	2.32	55.68
2	LARS	-	90	107.0	98.5	112.0	118.55	57.72	4.11	6.06	145.44
3	RARS	-	83	130	106.5	102.0	117.64	57.72	4.17	6.12	146.88

Appendix 12: Schmidt hammer rebound values data sheets.

Schmidt Hammer Test Survey Station											**Schmidt Hammer Rebound Average**
Reservoir Area											
Station 1	20	24	29	27	20	22	24	18	26	28	25.4
Station 2	27	22	28	25	23	25	26	22	23	26	25.7
Left abutment											
Station 1	43	45	52	49	56	47	52	41	48	51	49.9
Station 2	35	47	36	32	46	48	41	52	42	46	46
Right Abutment											
Station 1	45	56	39	54	52	37	46	56	50	46	51.3
Station 2	44	52	45	57	49	56	46	54	47	43	51.6

Appendix 13: Atterberg Limit test data sheets and Atterberg curve.

LBSS-1

	LIQUID LIMIT			PLASTIC LIMIT		Free Swell	
Test No	1	2	3	1	2	Initial Reading (A)	
Container No.	8	11	10	21	20	Final Reading (B)	
Number of blows	33	26	17	_	_	Difference (C)=B-A	
Wt. of Wet soil + con (g)	47.00	48.20	49.9	26.22	26.2	Free Swell (C/A)*100 %	
Wt. of Dry soil + con (g)	37.2	38.30	39.10	24.82	24.9	Shrinkage Limit (Linear)	
Wt. of container (g)	21.2	22.5	22.1	21.00	21.30		
Wt. of water (g)	9.8	9.9	10.8	1.40	1.3	Initial Reading (A)	
Wt. of Dry soil (g)	16	15.8	17	3.82	3.6	Final Reading (B)	
Moisture Content (%)	61.25	62.66	63.53	36.65	36.11	Difference (C)=B-A	
Ave. Moisture Content (%)	62.48			36.38		Shrinkage (C/A)*100 %	

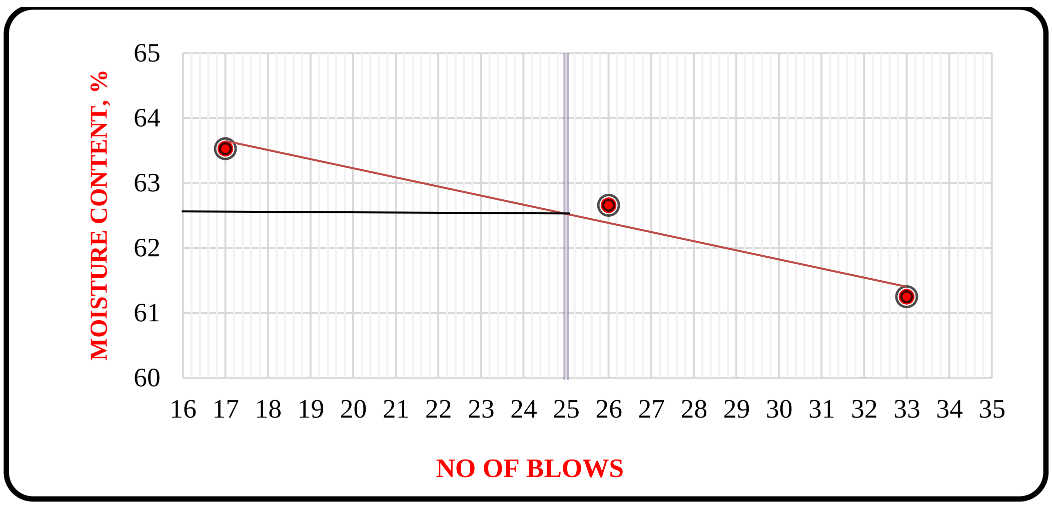

LBSS-2

	LIQUID LIMIT			PLASTIC LIMIT		Free Swell	
Test No	1	2	3	1	2	Initial Reading (A)	
Container No.	E39	25	61	21	9+5	Final Reading (B)	
Number of blows	33	26	17	_	_	Difference (C)=B-A	
Wt. of Wet soil + con (g)	45.50	49.10	50.2	28.45	26.94	Free Swell (C/A)*100 %	
Wt. of Dry soil + con (g)	38.3	39.70	41.20	27.46	26	Shrinkage Limit (Linear)	
Wt. of container (g)	22.93	20.16	23	24.37	23.12		
Wt. of water (g)	7.2	9.4	9	0.99	0.94	Initial Reading (A)	
Wt. of Dry soil (g)	15.37	19.54	18.2	3.09	2.88	Final Reading (B)	
Moisture Content (%)	46.84	48.11	49.45	32.04	32.64	Difference (C)=B-A	
Ave. Moisture Content (%)	48.13			32.34		Shrinkage (C/A)*100 %	

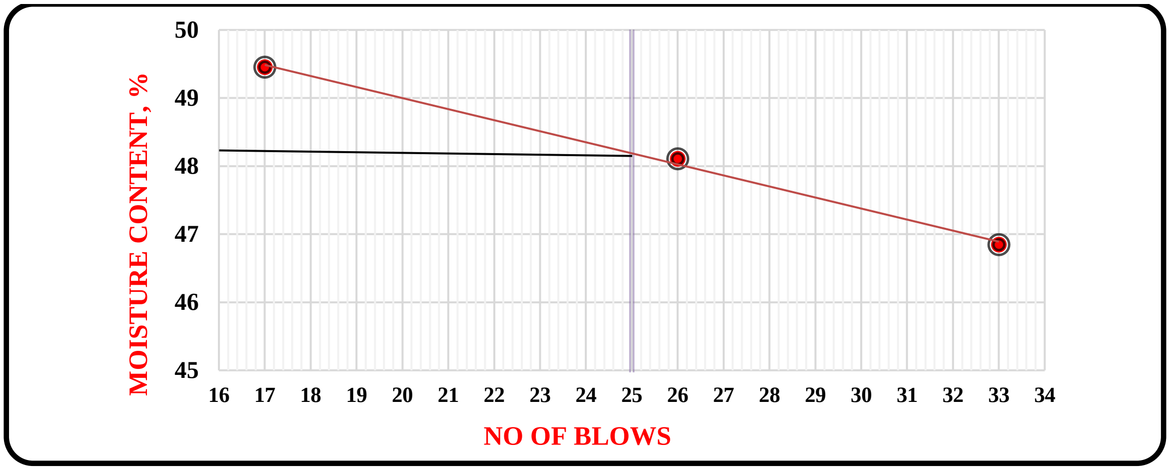

RBSS-1

	LIQUID LIMIT			PLASTIC LIMIT		Free Swell	
Test No	1	2	3	1	2	Initial Reading (A)	
Container No.	8	12	15	22	25	Final Reading (B)	
Number of blows	34	28	19	_	_	Difference (C)=B-A	
Wt. of Wet soil + con (g)	46.82	44.77	46.19	25.33	25.38	Free Swell (C/A)*100 %	
Wt. of Dry soil + con (g)	36.77	36.55	37.20	23.87	23.94	Shrinkage Limit (Linear)	
Wt. of container (g)	20.12	23.12	22.73	20.00	20.00		
Wt. of water (g)	10.05	8.22	8.99	1.46	1.44	Initial Reading (A)	
Wt. of Dry soil (g)	16.65	13.43	14.47	3.87	3.94	Final Reading (B)	
Moisture Content (%)	60.36	61.21	62.13	37.73	36.55	Difference (C)=B-A	
Ave. Moisture Content (%)	61.23			37.14		Shrinkage (C/A)*100 %	

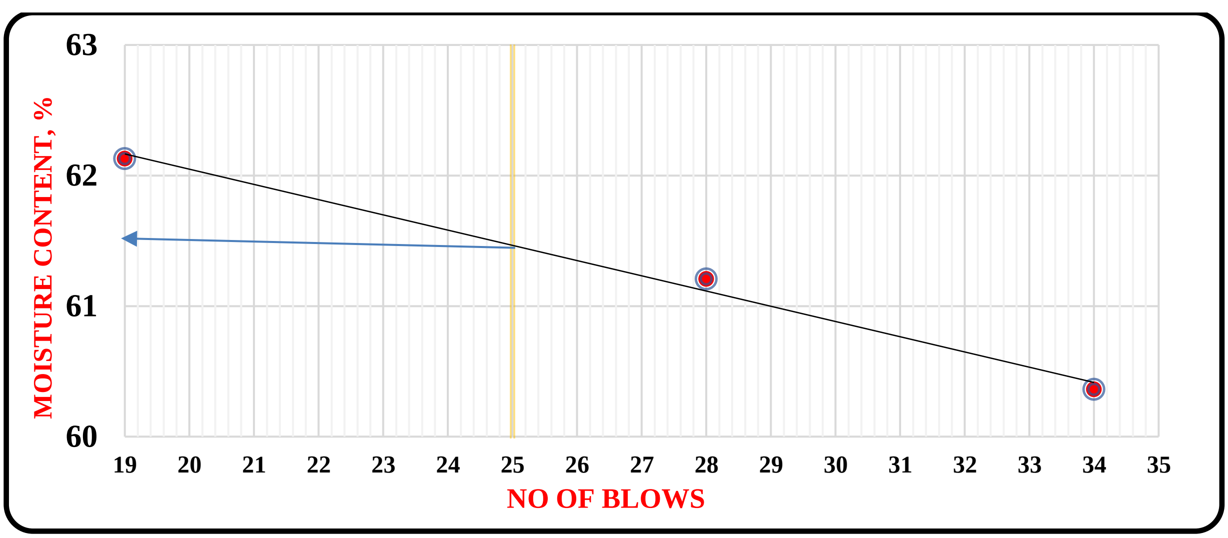

Appendix 14: Rock Mass Strength Determination RocData Software Input and Output data parameter.

Analysis of Rock/Soil Strength using RocData

SW*

Hoek-Brown Classification
intact uniaxial compressive strength = 146.88 MPa
GSI = 56 mi = 25 Disturbance factor = 0.7

Hoek-Brown Criterion
mb = 2.228 s = 0.0017 a = 0.504

Mohr-Coulomb Fit
cohesion = 7.917 MPa friction angle = 32.97 deg

Rock Mass Parameters
tensile strength = -0.112 MPa
uniaxial compressive strength = 5.913 MPa
global strength = 29.146 MPa
modulus of deformation = 9181.49 MPa

Analysis of Rock/Soil Strength using RocData

MW*

Hoek-Brown Classification
intact uniaxial compressive strength = 146.88 MPa
GSI = 52 mi = 25 Disturbance factor = 0.7

Hoek-Brown Criterion
mb = 1.789 s = 0.0010 a = 0.505

Mohr-Coulomb Fit
cohesion = 7.305 MPa friction angle = 31.12 deg

Rock Mass Parameters
tensile strength = -0.078 MPa
uniaxial compressive strength = 4.378 MPa
global strength = 25.885 MPa
modulus of deformation = 7293.12 MPa

Analysis of Rock/Soil Strength using RocData

SW**

Hoek-Brown Classification
intact uniaxial compressive strength = 145.44 MPa
GSI = 42 mi = 25 Disturbance factor = 0.7

Hoek-Brown Criterion
mb = 1.033 s = 0.0002 a = 0.510

Mohr-Coulomb Fit
cohesion = 5.845 MPa friction angle = 26.57 deg

Rock Mass Parameters
tensile strength = -0.031 MPa
uniaxial compressive strength = 2.001 MPa
global strength = 18.916 MPa
modulus of deformation = 4101.22 MPa

Analysis of Rock/Soil Strength using RocData

MW**

Hoek-Brown Classification
intact uniaxial compressive strength = 145.44 MPa
GSI = 36 mi = 25 Disturbance factor = 0.7

Hoek-Brown Criterion
mb = 0.743 s = 0.0001 a = 0.515

Mohr-Coulomb Fit
cohesion = 5.072 MPa friction angle = 23.91 deg

Rock Mass Parameters
tensile strength = -0.018 MPa
uniaxial compressive strength = 1.226 MPa
global strength = 15.591 MPa
modulus of deformation = 2903.44 MPa

Appendix 15: Joint Shear Strength Determination RocData Software Input and Output data parameter.

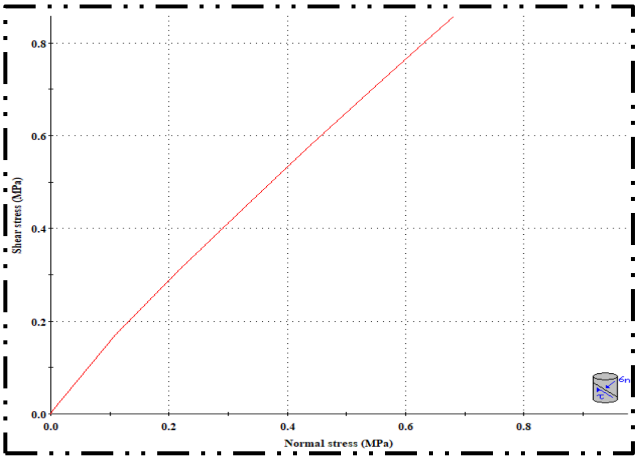

RAJS1

Barton-Bandis Criterion
base friction angle (phib) = 36.5 MPa
joint roughness coefficient (JRC) = 7
joint compressive strength (JCS) = 93.5 MPa

Mohr-Coulomb Fit
cohesion = 0.048 MPa friction angle = 49.70 deg

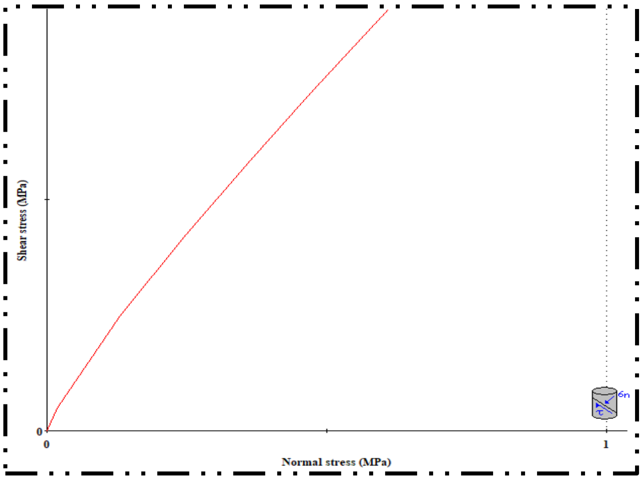

RAJS2

Barton-Bandis Criterion
base friction angle (phib) = 36.5 MPa
joint roughness coefficient (JRC) = 9
joint compressive strength (JCS) = 93.5 MPa

Mohr-Coulomb Fit
cohesion = 0.087 MPa friction angle = 52.97 deg

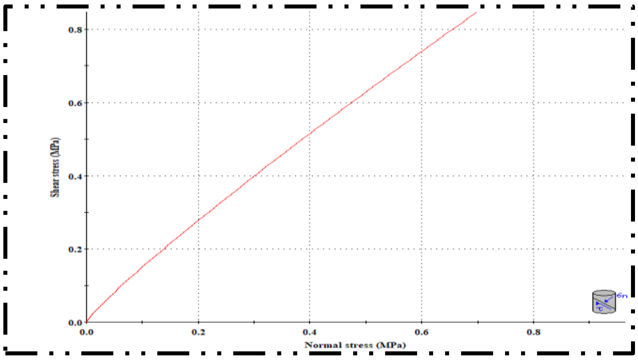

LAJS1

Barton-Bandis Criterion
base friction angle (phib) = 36.5 MPa
joint roughness coefficient (JRC) = 7
joint compressive strength (JCS) = 69.5 MPa

Mohr-Coulomb Fit
cohesion = 0.046 MPa friction angle = 48.84 deg

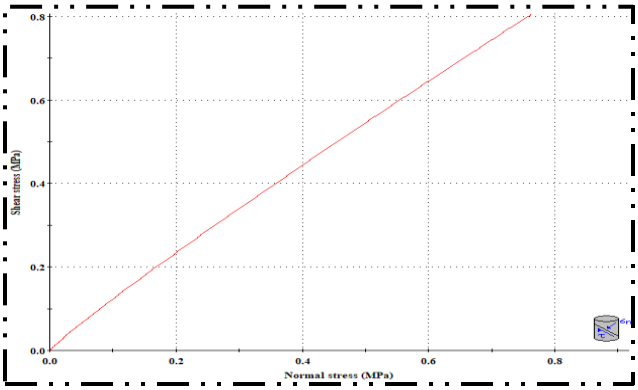

LAJS2

Barton-Bandis Criterion
base friction angle (phib) = 36.5 MPa
joint roughness coefficient (JRC) = 5
joint compressive strength (JCS) = 78.5 MPa

Mohr-Coulomb Fit
cohesion = 0.026 MPa friction angle = 45.73 deg

Appendix 16:Permeability values according to Terzaghi et al. (1967) and ISRM (1981)

Term	Discontinuity Spacing Interval (m)	Permeability class of rock mass	Coefficient of Permeability, K (m/s)
Very closely to extremely closely spaced discontinuities	< 0.2	Highly permeable	10^{-2} - 1
Closely to moderately widely spaced discontinuities	0.2 – 0.6	Moderately permeable	10^{-5} – 10^{-2}
Widely to very widely spaced discontinuities	0.6 – 2.0	Slightly permeable	10^{-9} – 10^{-5}
No discontinuities	> 2	Effectively impermeable	< 10^{-9}

Appendix 17: Coefficient of Permeability and Permeability Class of soils according to (USBR, 1987)

Coefficient of Permeability(mm/sec)	Permeability Class
Greater than 10^{-3}	Previous
10^{-5} to 10^{-3}	Semi-pervious
Less than 10^{-5}	Impervious

Appendix 18: Classification of strength of rock according to Deere and Miller, (1966)

Unconfined Compressive Strength (UCS) (MPa)	Strength of the Rocks
Over 224	Very High Strength
112-224	High Strength
56-112	Medium Strength
28-56	Low Strength
Less than 28	Very Low Strength

Appendix 19: Determined bearing capacity factors according to Bell (2007).

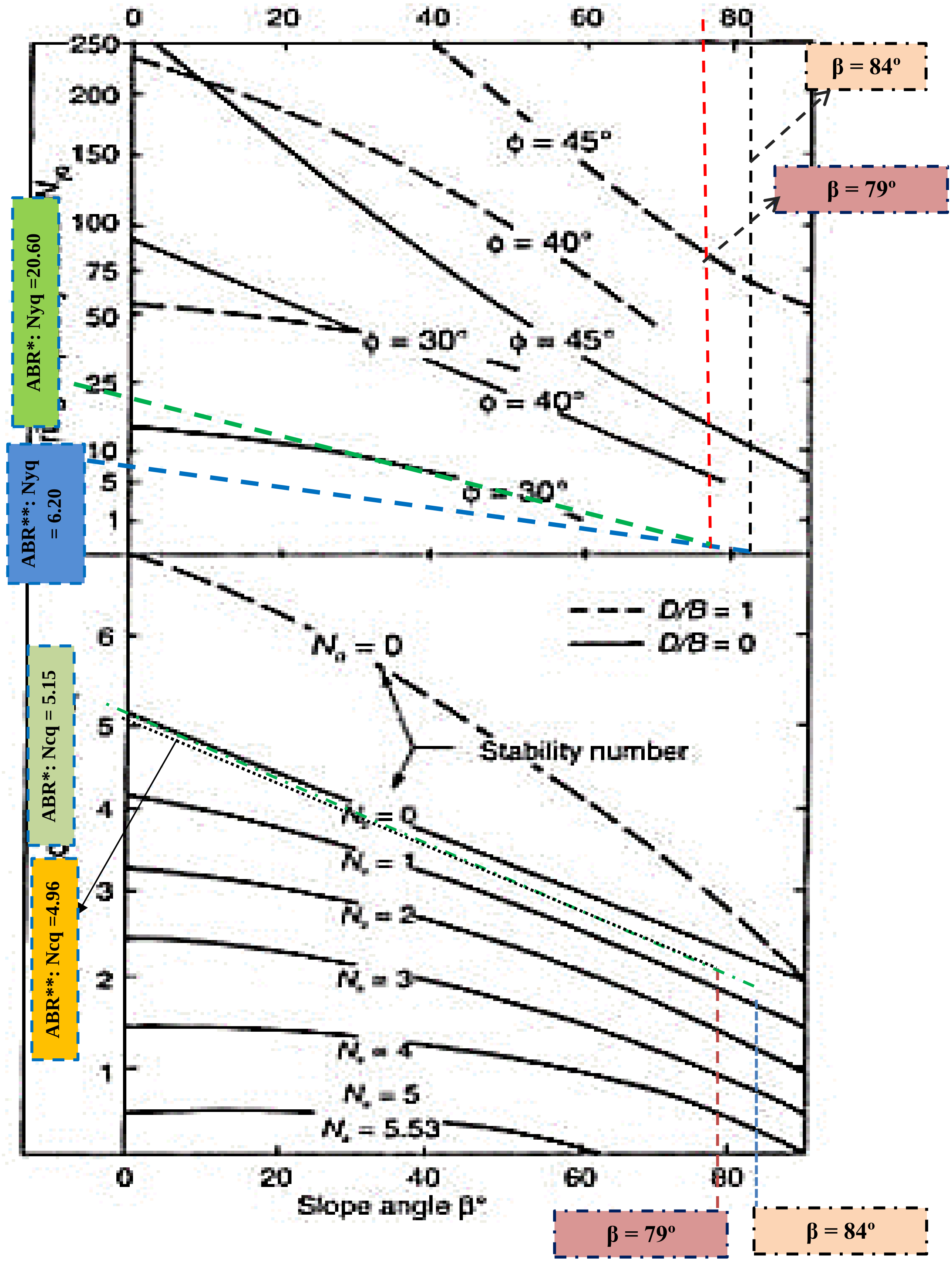

Appendix 20: Sieve Analysis of the Soil samples from the Reservoir area

a) Sieve Analysis of Soil Sample from Left Bank of the Reservoir at the depth of 0.0-1.0m (LBSS-1).

Sieve Size(mm)	Weight retained (g)	Percent of weight retained (g)	Cumulative % weight retained	Cumulative Percent Passing
75	0	0.00	0.00	100
63	0	0.00	0.00	100.00
50	0	0.00	0.00	100.00
37.5	0	0.00	0.00	100.00
25	0	0.00	0.00	100.00
20	0.0	0.00	0.00	100.00
12.5	0.0	0.00	0.00	100.00
10	7.6	1.52	1.52	98.48
4.75	11.32	2.27	2.27	96.21
2	9.71	1.95	4.22	94.26
0.425	26.3	5.27	9.49	88.99
0.075	25.45	5.10	14.59	83.89
Pan				
Total	498.7			

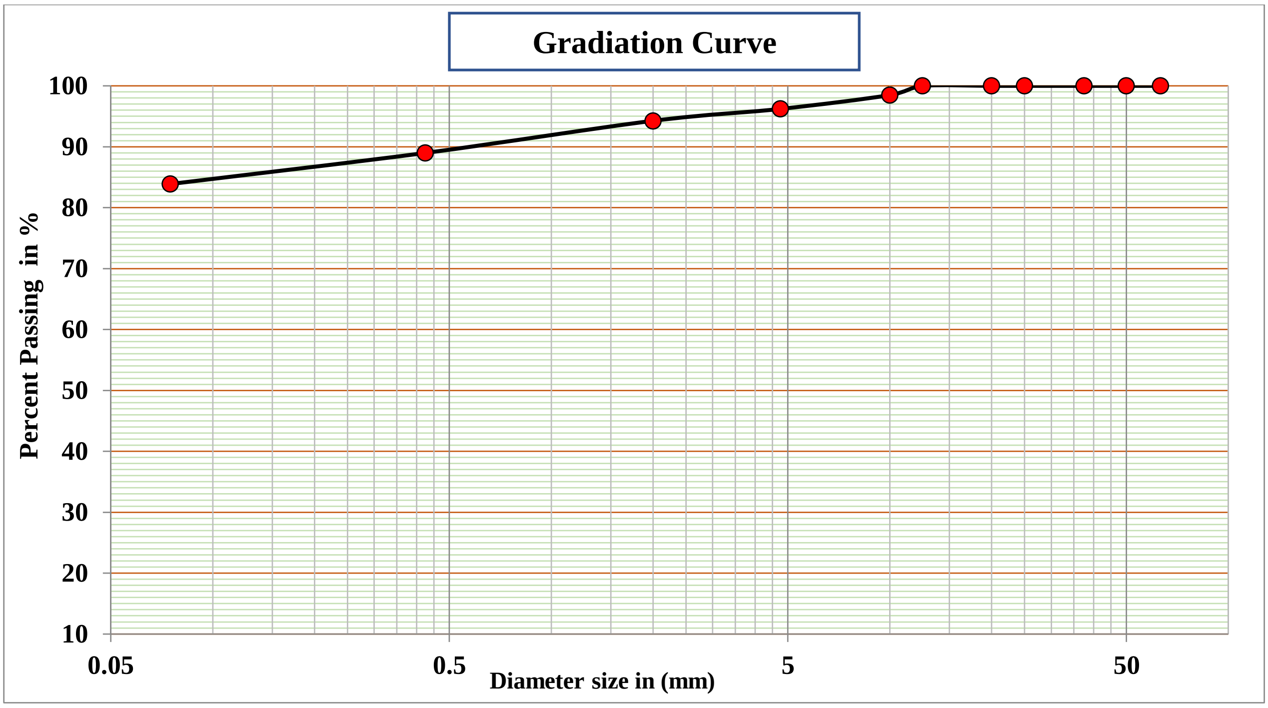

b) Sieve Analysis of Soil Sample from Left Bank of the Reservoir at the depth of 0.0-1.70m (LBSS-2).

Sieve Size , mm	Weight Retained	Percent of Retained	Cumulative . % Passing	Percent of Passing
75	0	0.00	0.00	100
63	0	0.00	0.00	100.00
50	0	0.00	0.00	100.00
37.5	0	0.00	0.00	100.00
25	40.58	7.21	7.21	92.79
20	29.5	5.24	12.45	87.55
12.5	21.1	3.75	16.20	83.80
10	21.4	3.80	20.00	80.00
4.75	99.02	17.59	30.04	62.41
2	123.52	21.94	51.98	40.47
0.425	98.26	17.45	69.43	23.02
0.075	40.03	7.11	76.54	15.91
Pan				
Total	562.97			

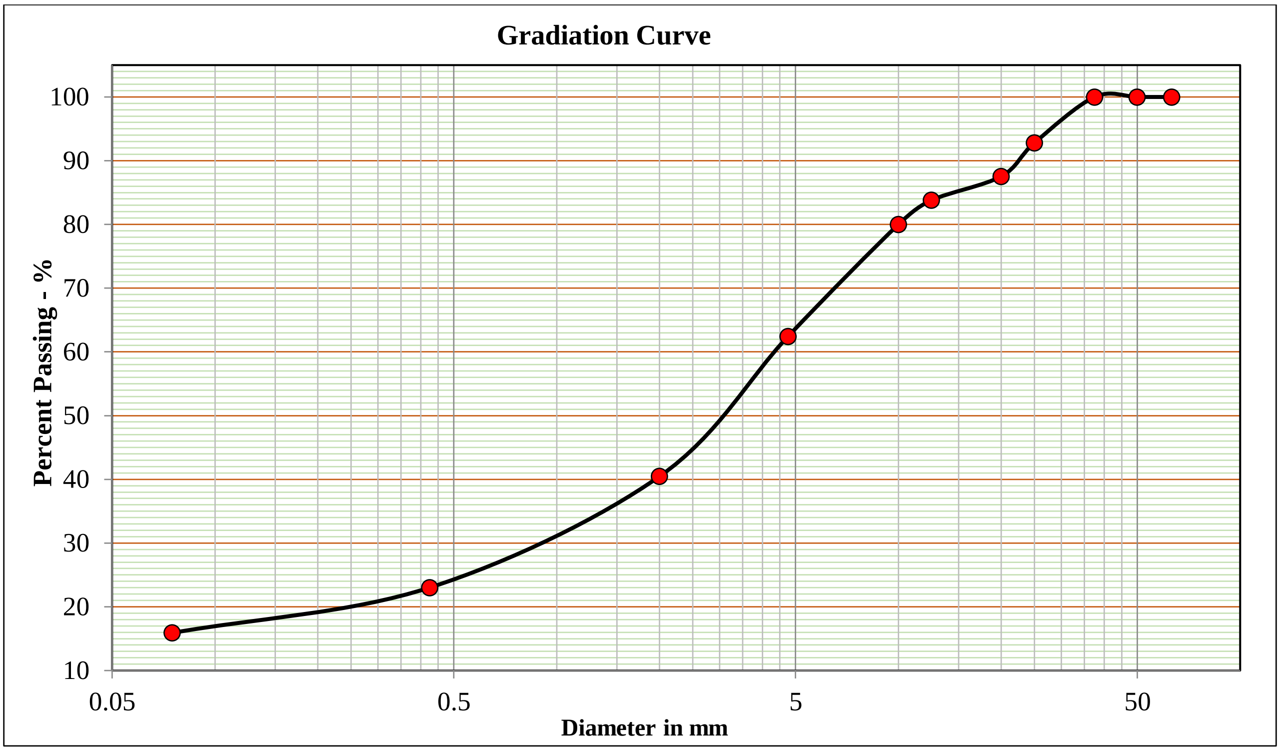

c) Sieve Analysis of Soil Sample from Right Bank of the Reservoir at the depth of 0.0-1.0m (RBSS-1).

Sieve Size(mm)	Weight retained (g)	Percent of weight retained (g)	Cumulative % weight retained	Cumulative Percent Passing
75	0	0.00	0.00	100
63	0	0.00	0.00	100.00
50	0	0.00	0.00	100.00
37.5	0	0.00	0.00	100.00
25	0	0.00	0.00	100.00
20	0.0	0.00	0.00	100.00
12.5	0.0	0.00	0.00	100.00
10	0.0	0.00	0.00	100.00
4.75	0	0.00	0.00	100.00
2	1.72	0.48	0.48	99.52
0.425	18.78	5.23	5.71	94.29
0.075	18.26	5.09	10.80	89.20
Pan				
Total	358.76			

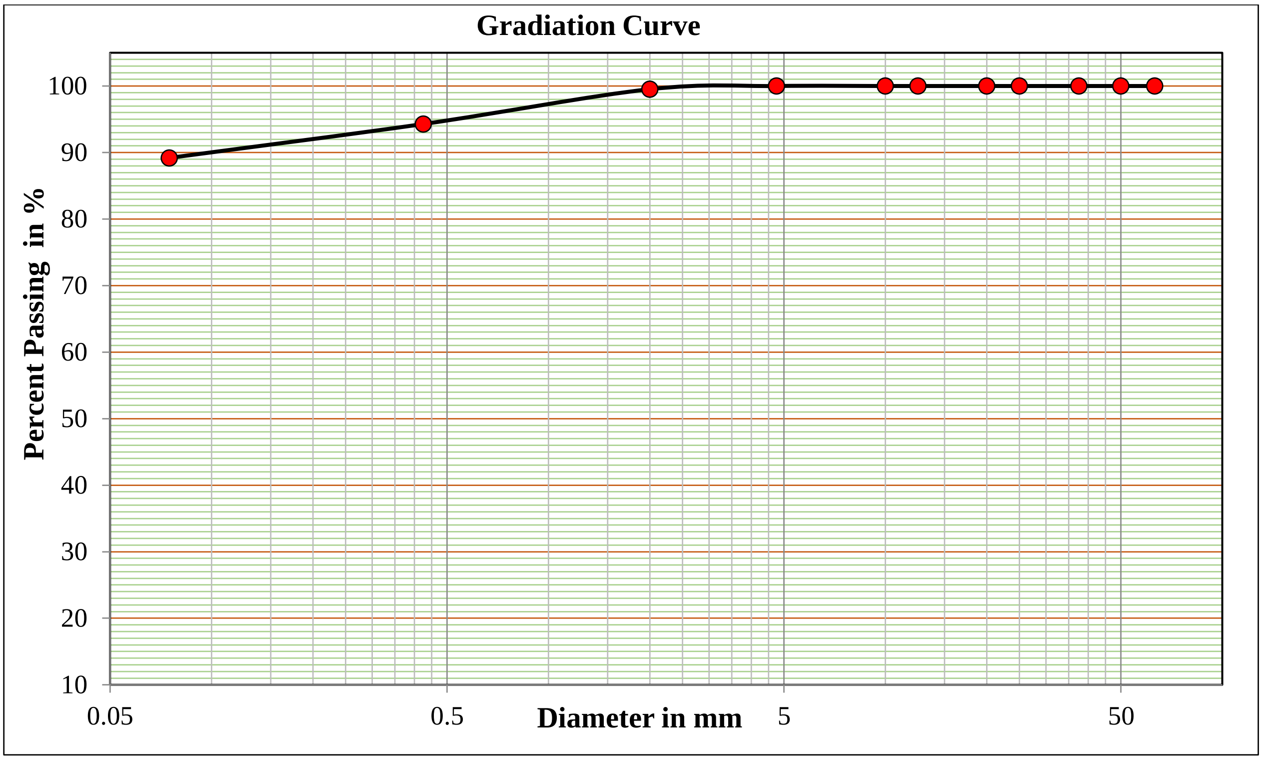

Research Fund Acknowledgement

This research thesis was funded by Adama Science and Technology University under the grant number of ASTU/SM-R/705/23, Adama, Ethiopia.